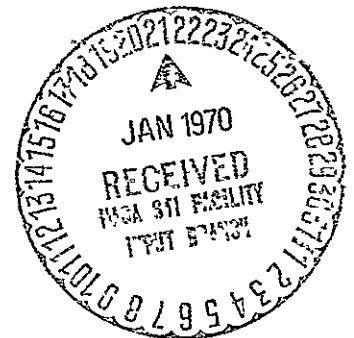


2-P

NAS 8-20396  
GEORGE C. MARSHALL  
SPACE FLIGHT CENTER

# STUDY OF CRACK INITIATION PHENOMENA ASSOCIATED WITH STRESS CORROSION OF ALUMINUM ALLOYS

FINAL SUMMARY REPORT



FACILITY FORM 602

N70-28089	(THRU)
(ACCESSION NUMBER)	
306	(CODE)
(PAGES)	
CR-102474	17
(NASA CR OR TMX OR AD NUMBER)	(CATEGORY)

ALCOA RESEARCH LABORATORIES  
NEW KENSINGTON, PA



## NOTICE TO USERS

Portions of this document have been judged by the Clearinghouse to be of poor reproduction quality and not fully legible. However, in an effort to make as much information as possible available to the public, the Clearinghouse sells this document with the understanding that if the user is not satisfied, the document may be returned for refund.

If you return this document, please include this notice together with the IBM order card (label) to:

Clearinghouse  
Attn: 152.12  
Springfield, Va. 22151



ALUMINUM COMPANY OF AMERICA  
Alcoa Research Laboratories  
Physical Metallurgy Division  
New Kensington, Pennsylvania

STUDY OF CRACK-INITIATION PHENOMENA  
ASSOCIATED WITH STRESS CORROSION  
OF ALUMINUM ALLOYS

Contract Number - NAS8-20396  
Control Numbers - DCN 1-6-54-01113 (1F)  
DCN 1-7-54-20093 (1F)  
DCN 1-8-54-10220 (1F)

October 6, 1969

FINAL SUMMARY REPORT

Authors

M. S. Hunter  
W. G. Fricke, Jr.

Contributors

H. Gilcher  
R. W. King  
D. L. McLaughlin  
J. J. Ptasienski  
D. L. Robinson  
D. O. Sprowls  
J. D. Walsh

## TABLE OF CONTENTS

	<u>Page</u>
Foreword	
Abstract.....	i
Introduction.....	1
Scope of Investigation.....	2
Materials.....	2
Procedure and Results.....	4
Effect of Metallurgical Structure.....	4
Characterization of Material.....	5
Light Microstructure.....	5
Alloy 2219.....	6
Alloy 7075.....	8
Alloy X7375.....	10
Alloys 7079-T6 and 7039-T6.....	10
Electron Microstructure.....	11
Phase Identification.....	15
Microprobe Analyses.....	17
Corrosion of Unstressed Specimens.....	19
Light Microscopy.....	20
Electron Microscopy.....	23
Stressed Specimen.....	25
Corrosion of Stressed Specimens.....	27
Light Microscopy.....	27
Alloy 2219.....	27
Alloy 7075.....	29
Alloy X7375.....	33
Alloy 7079.....	33
Alloy 7039.....	33
Electron Microscopy.....	34
Microprobe Investigations.....	36
Corrosion Films.....	<u>37</u>
Fracture Surfaces.....	37

## TABLE OF CONTENTS

	<u>Page</u>
Electron Fractography.....	40
Methods.....	40
Fracture Surfaces - Transmission Microscopy.....	41
Fracture Surfaces - Scanning Microscopy.....	43
Evolution of Grain Boundaries.....	44
Composition.....	45
Microstructure.....	47
Stress Corrosion Behavior.....	48
Corrosion of Thin Films.....	50
Calculations of Grain Boundary Composition.....	51
Grain Orientation.....	57
Effect of Stress.....	59
Stress Level.....	59
2219 Alloy.....	59
7075 Alloy.....	59
7079-T6 Alloy.....	61
7039-T6 Alloy.....	61
Stressing Direction.....	62
Effect of Surface Roughness.....	65
Individual Topographical Irregularities.....	66
Pre-Corrosion.....	68
Mechanical Roughness.....	69
Effect of Surface Film.....	70
Effect of Environment.....	74
Screening Tests.....	74
7075-T651 Alloy.....	75
2219-T37 Alloy.....	76
2219-T87 and 7075-T7351.....	77
Supplemental Tests in pH 2 Solutions.....	78
Electrolytes Containing Certain Cations and Alkaline Solutions at pH 11-11.5.....	79

## TABLE OF CONTENTS

	<u>Page</u>
Selected Environments.....	81
7075-T6 and 2219-T37.....	82
7075-T73 and 2219-T87.....	84
7039-T6.....	85
Effect of Pre-corrosion.....	88
Effect of Stress.....	88
Electrochemical Effects.....	89
7075 Alloy.....	92
7039-T6 Alloy.....	96
Acoustic Emission.....	98
Discussion of Cracking Mechanisms.....	101
Summary and Conclusions.....	105
References.....	109
Tables	
Figures	

## FOREWORD

This report was prepared by Aluminum Company of America under contract NAS8-20396 entitled "Study of Crack-Initiation Phenomena Associated with Stress Corrosion of Aluminum Alloys" for the George C. Marshall Space Flight Center of the National Aeronautics and Space Administration. The work was administered under the technical direction of the Astronautics Laboratory, Materials Division of the George C. Marshall Space Flight Center with Mr. J. G. Williamson acting as contracting officer's representative.

A number of Alcoa Research Laboratories personnel made significant contributions to this work. Mr. D. L. McLaughlin conducted some of the light microscope investigations. Mr. J. J. Ptasienski conducted the remainder of the light microscope examinations, the electron transmission examinations of corroded thin films and some of the electrochemical measurements. Mr. R. W. King also assisted with the electrochemical measurements. Mr. D. L. Robinson contributed the thin-foil transmission micrographs showing alloy structure and the electron microscope phase identification. Mr. D. O. Sprowls and Mr. J. D. Walsh supervised and conducted the environmental screening tests. Mr. H. Gilcher assembled and operated the equipment used in acoustic emission studies.

This report has been reviewed and approved by Mr. H. Y. Hunsicker, Chief of Physical Metallurgy Division, Alcoa Research Laboratories. The section on Effect of Environment has also been reviewed and approved by Dr. J. L. Brandt, Chief of Chemical Metallurgy Division, Alcoa Research Laboratories.

ABSTRACT

An investigation has been made of stress-corrosion crack initiation phenomena in thick plate of 2219, 7075, X7375, 7079 and 7039 alloys with emphasis on the short-transverse direction. Techniques used included light and electron microscopy, electron fractography, x-ray and electron diffraction, the electron microprobe and acoustic emission monitoring. A number of effects were evaluated including those of structure and structural evolution, grain orientation, stress level and direction, surface roughness and pre-corrosion, surface film, and environment.

The prime requisites for initiation of cracking were a combination of a particular environment, a grain boundary region susceptible to selective attack in that environment and the presence of tensile stress. Cracking was promoted by the presence of long, continuous crack-susceptible paths oriented perpendicular to the stress direction, by high stress levels and by large differences in orientation between the grains adjoining the crack-susceptible boundary regions. Dislocations, dispersoids, zone-type precipitates and microconstituent particles had no intrinsic effect on crack initiation. Boundary precipitate particles did not affect initiation, although in 2219, 7075 and 7079 alloys, their formation generated the crack-susceptible paths adjacent to boundaries.

Stress level affected only the rates of initiation and propagation. Stressing direction was very important because of the rapid crack propagation when boundaries were largely perpendicular to the stress. With 2219-T37 and 7075-T6, both longitudinal and short-transverse stresses initiated cracks rapidly in appropriate environments, but cracks propagated rapidly only with short-transverse stress. Scratches and mechanical or corrosion pits had no affect on crack initiation, and mechanical surface abrasion had only a temporary effect on crack development. The effects of intergranular pre-corrosion could not be judged accurately because corrosion crevices widened by stress had the appearance of stress-corrosion cracks. Surface films delayed but did not prevent crack initiation. Environment, along with localized composition and structure at boundaries, determined whether cracking would occur and controlled the rates of initiation and propagation.

Acoustic emission monitoring disclosed that energy bursts are generated by sudden mechanical crack propagation but not by crack initiation or propagation by stress-corrosion.

In the course of the work, new methods for electron fractographic examination were developed. Also, a means was devised for simulating metallurgical conditions within grains and in depleted boundary regions so that electrochemical relationships can be measured.

## INTRODUCTION

The stress-corrosion cracking of high-strength aluminum alloys imposes limitations in the design and use of certain alloys and tempers in components and structures that must be subjected to stress under corrosive conditions. Much effort has been expended in analyzing the stress-corrosion process, and a number of very ingenious and well-documented mechanisms have been proposed to explain this phenomenon. These proposed mechanisms have been so many and varied, however, that one can only conclude that it is highly unlikely that all can be operative at the same time and, therefore, that each may apply only with certain rather specific combinations of material, stress and environment.

In analyzing the stress-corrosion mechanism in high strength aluminum alloys, the majority of past work has been devoted to the testing of various alloys in various environments, and to the determination of failure times and threshold stresses. Under this contract, however, a different approach has been taken by focusing attention on the initiation of stress-corrosion cracks. Crack initiation is perhaps the most important stage in stress-corrosion cracking because if failure is to occur, a crack must first initiate, and if a crack does initiate, failure almost certainly will result if conditions conducive to cracking are maintained.

## SCOPE OF INVESTIGATION

The broad objective of this investigation has been to develop a better understanding of the mechanisms of stress corrosion of commercial high-strength aluminum alloys by a comprehensive analysis of factors which might affect crack initiation. Major emphasis was placed on the influence of metallurgical structure on crack initiation, including thorough analyses of microstructures, determination of where and how cracks initiate on a microscopic scale, observation of the development of microstructures during fabrication, and estimation of potential relationships that could exist in crack-susceptible regions. Other factors evaluated were the effects of stress level and direction, of surface roughness, of surface film, and of environment. In achieving these objectives, a wide variety of techniques were used, including light microscopy, transmission (and to a limited extent scanning) electron microscopy, x-ray and electron diffraction, electron microprobe analysis, electrochemical measurements, and acoustic emission monitoring. Much of the work was of the searching, probing type, in an endless search for new approaches to the analysis of crack initiation. As a result, a few sections of this report contain relatively little conclusive information and are primarily indicative of paths that might profitably be followed by future investigators.

## MATERIALS

The alloys used in this investigation were of three main types, 2219 representing the Al-Cu type of high-strength



alloy, 7075 and 7079 representing the Al-Zn-Mg-Cu type, and 7039 representing the Al-Zn-Mg type. These alloy types differ in the compositions of their dispersoid and precipitate phases, the electrochemical potentials of their precipitating phases and, therefore, the solution potentials of solute-depleted regions. In addition, limited work was done with X7375 alloy which is similar to 7075 alloy but contains no chromium. This alloy was used to evaluate the effects of grain shape because, lacking chromium, it recrystallized to an equiaxed structure on heat treatment.

The alloys were obtained as plant-fabricated plate having a thickness of two inches or more. This form was selected because of the inferior stress-corrosion resistance of certain tempers associated with structural directionality and the inability to obtain a rapid quench with thick sections. Also, thick plate has a specific and predictable directionality of structure, permitting tests of specimens stressed short transversely with respect to the microstructure. The 2219 alloy plate was 4" thick and the 7075 alloy plate was 3" thick. Confirming tests on these alloys were made with 2.5" thick plate. The thickness of the 7079 alloy plate was 6" and that of 7039 and X7375 alloy plate was 3".

The 2219 alloy plate was received in the stress-corrosion-prone T351 and T37 tempers, portions being precipitation heat treated in the laboratory to the stress-corrosion-resistant T851 and T87 tempers by treatments of 18 hours at 350 F and 24 hours at

325 F respectively. The 7075 alloy plate was solution heat treated at 870 F in the laboratory, quenched in cold water and aged four days at room temperature before being precipitation heat treated 24 hours at 250 F for the T6 temper and 6 hours at 225 F plus 24 hours at 325 F for the T73 temper. The 7079 alloy plate was plant solution heat treated at 830 F, spray quenched, stretched, and precipitation heat treated 48 hours at 240 F to the T651 temper. The 7039 plate was solution heat treated at 870 F, quenched in cold water, aged four days at room temperature, and precipitation heat treated 8 hours at 225 F + 16 hours at 300 F to the T6 temper. With the X7375 alloy plate the treatments used were those applied to 7075 alloy. Lacking chromium, X7375 does not age as rapidly as 7075 alloy and, therefore, immunity to stress-corrosion cracking after application of the two-step precipitation heat treatment was not expected. For crack initiation studies, this was inconsequential. The composition, tensile properties and other characteristics of the plate materials are given in Tables I-VIII. All materials are typical for the respective alloys and tempers.

All tests and examinations related to structure and crack initiation were made at locations one-inch below the surface of the plate and at least one-inch away from any edge exposed during the quench. This was done to be in a region of relatively slow cooling during quenching, and to obtain materials cooled at about the same rate regardless of plate thickness.

#### PROCEDURE AND RESULTS

##### Effect of Metallurgical Structure

A major concern of this contract was the relationship between crack initiation and metallurgical structure. The work in

this category was divided into nine interrelated sections, each logically following its predecessors. First, the microstructure of the plate materials was characterized thoroughly by light and electron microscopy, x-ray and electron diffraction, and the electron microprobe. Next, the initiation and progress of corrosion in the absence of stress was observed microscopically to define the existing anodic sites and electrochemical relationships. Then, the initiation and early growth of cracks was followed by light and electron microscopy and fracture surfaces were examined by electron fractography and the microprobe. In addition, attempts were made to follow corrosion and crack initiation directly by transmission electron microscopy. Other investigations related to metallurgical structure included a study of the manner in which the crack-susceptible paths in 7075 alloy were generated, calculations of compositional gradients in boundary regions based on diffusion data, and attempts to relate crystallographic orientation to crack initiation tendencies.

### Characterization of Material

#### Light Microstructure

In analyzing and recording light microstructures, sections were taken in the longitudinal (YZ) and transverse (XZ) planes\* and were prepared by conventional metallographic procedures. By examining these mutually perpendicular planes, the directionality of structure and grain shape, as well as the constituent and precipitate phases, were seen. The arrays of microconstituent

---

\*Based on convention that X is transverse to the rolling direction, Y is the rolling direction, and Z is the thickness direction.

particles were observed on as-polished surfaces at 500 diameters magnification. General microstructure, directionality, and grain shape were apparent at 100X magnification after etching with Keller's etch. The finer structures were seen on etched specimens at a magnification of 500 diameters. In all micrographs of etched specimens, the precipitate particles appear larger than actual size because of the exaggerating effect of the etch.

The micrographs selected to illustrate microstructures in this report are of longitudinal (YZ) sections only. These are adequate to define the structures acted upon by the short-transverse and longitudinal stresses that were used in the contract work. Full sets of micrographs have appeared in the Quarterly Reports under this contract.

#### Alloy 2219

The light microstructures of 2219 alloy plate in the T351 and T37 tempers were the same because the higher amount of cold work applied after quenching to produce the T37 temper does not alter the microstructure. These tempers are characterized by high grain contrast (Fig. 1) because of the high amount of copper in solid solution. At low magnification (Fig. 1 - top), indications of the dendritic ingot structure remain, and the grains are somewhat elongated in the rolling direction. At higher magnification (Fig. 1 - bottom), boundary precipitate particles are apparent, and "white boundaries," indicating matrix depletion in boundary regions, are evident. These structural features are the result of precipitation which occurred during the quench on selected grain boundaries. In the as-polished condition (Fig. 2), the constituent arrays and some larger boundary precipitate particles are seen,

with the constituent particles generally aligned in the rolling direction.

Very definite changes in light microstructure resulted from the precipitation heat treatments. In the T851 temper, produced by aging the T351 temper at 350 F, the grain contrast is reduced considerably (Fig. 3) because of the decrease in copper in solid solution that accompanied precipitation. Also tracteries of slip plane precipitation are apparent as a streaking or cross-hatching of most grains. This slip plane precipitation is revealed most clearly at high magnification (Fig. 3 - bottom), where the general matrix precipitate, grain boundary precipitate and depleted boundary regions characteristic of this temper can be seen.

The structure of the T87 temper, produced by precipitation heat treating the T37 temper at 325 F, differed in two respects from that of the T851 temper. Copper depletion of the matrix was greater, as indicated by the lower grain contrast after etching (Fig. 4 - top). In addition, the matrix precipitation in the T87 temper was distributed generally and was not aligned along slip planes (Fig. 4 vs. Fig. 3). The changes in light microstructure were confined to the fine structures, because the constituent particles and large boundary precipitates are not affected by artificial aging.

The higher power examination of etched specimens (Figs. 1, 3 and 4) indicated that at least two types of microconstituents were present and were common to all tempers. Those present in the greatest number and having a dark appearance are primarily the insoluble iron-bearing phase  $\text{Cu}_2\text{FeAl}_7$ . The rounded particles, fewer in number and retaining a white appearance, are

probably particles of the copper-bearing phase  $\text{CuAl}_2$ . This phase is soluble in aluminum but, because of the high copper content of 2219 alloy, which exceeds the solubility limit, the presence of undissolved particles of this phase is entirely normal.

#### Alloy 7075

The general microstructures of the 7075 alloy plate were similar in both the T6 and T73 tempers, and consisted of aggregations of irregularly shaped grains, highly elongated in the rolling direction (Fig. 5 - top). These grains consisted of clusters of grain fragments and apparently represented the fragmented and distorted remains of grains originally present in the ingot or new grains that may have formed by dynamic recrystallization during the early stages of hot rolling. It appears that, as these grains were deformed during fabrication, some of the grain boundaries were extensively broken and their continuity was destroyed. Others, however, maintained their identity and are apparent in the structure of the final product. Considering the forces at work during fabrication of the plate, fragmentation of a grain boundary would be related to its angle with respect to the rolling direction. Those initially oriented at a high angle to the rolling direction would tend to be broken and dispersed, whereas those initially parallel to the rolling direction would tend to be elongated rather than broken. It is believed that this accounts for the fact that in the final product the most prominent boundaries are generally those parallel to the rolling direction.

The fragmented grain structure, certain of the precipitate structures and the extreme elongation of boundaries

in the 7075 alloy plate are shown at higher magnification in Fig. 6. In both the T6 and T73 tempers, considerable grain and fragment boundary precipitate is apparent, the majority occurring on grain boundaries. This precipitate was also present in the W temper, indicating that it developed during the quench. In the T6 temper (Fig. 6 - top) there is only a minor speckling of the matrix, whereas in the T73 temper (Fig. 6 - bottom), matrix precipitation is more extensive. This difference was related to the amount and size of matrix precipitation, as will be discussed during consideration of electron microstructures.

On the basis of their etching characteristics, the microconstituents in 7075 alloy were primarily of two types,  $\text{Cu}_2\text{FeAl}$ , from the iron impurity and  $\text{Mg}_2\text{Si}$ . The microconstituent volume fraction was less in 7075 alloy than in 2219 alloy, with the result that the constituent clusters were smaller and not as continuous in 7075 alloy. There was the usual constituent alignment in the direction of rolling (Fig. 5 - bottom).

Another microstructural feature, observed primarily on longitudinal sections, consisted of tiny voids between pairs of constituent particles (Fig. 5 - bottom). These voids develop during fabrication when pairs of contiguous microconstituent particles are separated or when individual particles are fractured. Even though the matrix is flowing plastically, it is unable to conform immediately to the contour of the separated particles and occupy the space between them. The result is a void. Such voids can be of importance during mechanical fracture because they constitute sites for formation of some of the dimples

observed by electron fractography. Their effect on stress corrosion is probably very small, however, since cracking in aluminum alloys follows an intergranular path, while constituent particles and clusters are not generally situated on grain boundaries.

#### Alloy X7375

In contrast to the structure of 7075 alloy, which had an unrecrystallized, highly-elongated structure, the X7375 alloy plate was completely recrystallized and consisted of equiaxed grains (Fig. 7). No difference was apparent between the T6 and T73-type tempers either at low or high light microscope magnifications. The precipitate structure of X7375 alloy consisted of strings of particles along grain boundaries (Fig. 7), the particles having developed during quenching. Constituent structures of X7375 alloy consisted of particles of  $\text{Cu}_2\text{FeAl}_7$  and  $\text{Mg}_2\text{Si}$ , with only slight directionality.

#### Alloys 7079-T6 and 7039-T6

The light microstructures of the 7079-T6 and 7039-T6 plate materials resembled very closely that of 7075 alloy. Both were substantially unrecrystallized and consisted of fragmented grains elongated in the rolling direction (Fig. 8 - top and Fig. 9 - top). The extent of structural elongation and the degree of constituent alignment (Fig. 10) were in proportion to the thickness of the plate, being much less in the 7079-T6 plate than in the other materials because this item was six inches thick. Both alloys had considerable boundary precipitate, both on primary boundaries and on fragment boundaries (Figs. 8 - bottom and 9 - bottom).



### Electron Microstructures

In characterizing the structure of the plate materials, the electron microscope was used to examine the finest microstructural features including dislocations, dispersoids and precipitates, employing magnifications of from 20,000 to 100,000X.

The fine structure of the 2219-T351 plate was characterized by a relatively small number of dislocations and a few comparatively large precipitate particles on boundaries (Fig. 11). The dislocations were undoubtedly generated during the stretching of the plate because their density was that expected for the 1.5-3% stretch. The large precipitate particles on boundaries were formed during quenching and correspond to those seen in the light microstructure (Fig. 1).

The electron microstructure of the 2219-T37 plate reflected the higher degree of cold work as compared to the T351 temper. The T37 structure was characterized by dense forests of dislocations such as those seen in Fig. 12.

Examinations of the precipitation heat treated tempers of 2219 plate revealed clearly the details of the precipitate structures indicated in the light micrographs. In the T851 temper, the matrix had a densely packed array of interlocking precipitate plates (Fig. 13) with well-defined crystallographic alignment. In addition to this matrix precipitation, there were many small boundary precipitate particles which formed or grew during the precipitation heat treatment, and Mn-bearing dispersoid particles previously developed during ingot preheating.

The structure of the 2219-T87 plate was also characterized by a dense matrix precipitate of interlocking plates (Fig. 14). These plates appear to be finer and more numerous than those in the T851 temper, which would be expected from the greater amount of cold work and the lower aging temperature. The size and shape of the plates and the more uniform distribution of dislocations which provided the sites for their nucleation explain the more uniform and general precipitation apparent under the light microscope (Fig. 4).

In comparing the electron microstructures of the T351 and T851 tempers, it was noted that dislocations had been eliminated by the precipitation heat treatment. From this, and the fact that stress-corrosion cracking is virtually eliminated by precipitation heat treating, it might be concluded that the improved behavior resulted from elimination of the dislocations. It should be pointed out, however, that the precipitation treatment also led to pronounced matrix depletion and the development of extensive matrix precipitate. It is much more likely that these latter major structural changes, rather than elimination of dislocations, per se, brought about the improvement in stress-corrosion behavior.

Structures of 7075 alloy in all tempers were characterized by numerous E-phase ( $\text{Cr}_2\text{Mg}_3\text{Al}_{18}$ ) dispersoid particles scattered throughout the structure (Figs. 15-18). In addition, there were a number of relatively large boundary precipitate particles, apparently developed during quenching. In the W temper (Fig. 15), dislocations were present, but their number was quite small because of the relatively slow quench

that the material had received. These dislocations were fairly evenly scattered throughout the matrix and no concentrations in grain boundary regions were observed. The dislocations were generally quite long, which is a characteristic of those formed during moderately slow quenching, and almost all were pinned to the E-phase dispersoid particles.

Precipitation heat treating to the T6 temper had no noticeable effect on the dispersoid or dislocation structures (Fig. 16 vs. Fig. 15). This treatment, however, developed a very fine zone-type precipitate in the matrix as well as some fine grain boundary precipitate (Fig. 17 vs. Fig. 15). No depleted boundary regions were observed in this temper.

The extended, high-temperature precipitation treatment to develop the T73 temper did not alter the dispersoid structure but completely eliminated the dislocations and produced more advanced precipitate structures (Fig. 18 vs. Figs. 15-17). The precipitate particles on grain boundaries were increased in number and size, the matrix zone-type precipitates grew appreciably, and some M' or M-phase precipitates ( $\text{MgZn}_2$ ) developed. Occasional depleted boundary regions were observed in the T73 temper.

The electron microstructures of X7375 alloy were illustrated and described in detail in the First Annual Report on this contract but, since this alloy was used only to evaluate effects of grain shape and recrystallization, this information is not included in this report.

The electron microstructure of the 7079-T6 plate was similar in most respects to that of the 7075-T6 alloy plate.

Numerous E-phase ( $\text{Cr}_2\text{Mg}_3\text{Al}_{18}$ ) dispersoid particles were scattered throughout the structure, with certain areas having a high concentration of particles, and others being almost dispersoid-free. Numerous precipitate particles were present on boundaries, including large particles developed during quenching and much finer particles formed during precipitation heat treatment. Within the matrix, there was a moderate number of dislocations, a large percentage of which were pinned by the E-phase dispersoid particles. Also present in the matrix was a multitude of fine zone-type precipitates. These were randomly distributed except at some boundaries where narrow (200-300 Å) precipitate-free regions were apparent. Transmission structures of the 7079-T6 plate are shown by Figs. 19-20.

The structure of the 7039-T6 plate was also similar to that of 7075-T6 alloy. E-phase dispersoids were fairly numerous and unevenly distributed, two distinct sizes of boundary precipitates were apparent, and some dislocations were present in the matrix. Precipitate-free regions were similar to those in 7079-T6, although possibly somewhat wider (250-400 Å). Transmission structures of the 7039-T6 plate at two magnifications are shown by Figures 21-22.

Considering the possible metallurgical nature of the precipitate-free boundary regions, they could be free of precipitate because they were depleted in solute by diffusion to the boundary and formation of the fairly extensive grain boundary precipitate. On the other hand, these regions may be free of precipitate because they are depleted in vacancies which

assist the development of zone-type precipitate. In either case, these regions would be different from the remainder of the grain, both mechanically and electrochemically. They could be weaker mechanically, and thus selectively more susceptible to mechanical rupture, either because they contain less solute or because they do not have the strengthening effect of the zone-type precipitation. From the electrochemical standpoint, these regions could be a selective anodic path either because they are depleted in copper by diffusion or because they are not depleted in zinc because precipitation did not occur.

#### Phase Identification

To further characterize the plate materials, the phases present were identified by x-ray and electron diffraction and by the electron microprobe. The results confirmed those deduced from the light and electron microscope examinations.

The 2219 alloy plate contained the phases  $\text{CuAl}_2$  ( $\theta$ ),  $\text{Cu}_2\text{FeAl}_7$ , and  $\theta'$ , which is a coherent transition precipitate of  $\text{CuAl}_2$  composition. The  $\text{CuAl}_2$  ( $\theta$ ) represented undissolved particles, and the  $\text{Cu}_2\text{FeAl}_7$  represented insoluble Fe-bearing phase, both of which were apparent in the light microstructure. The  $\theta'$  phase was present in a very small amount in the T351 and T37 tempers and presumably represented a few particles formed during the quench. This phase was present in large amounts in the T851 and T87 tempers, and corresponded to the large number of densely packed platelets that were evident in the electron microstructure.

The 7075 alloy plate contained the phases  $\text{Mg}_2\text{Si}$ ,  $\text{Cu}_2\text{FeAl}_7$ , E-phase ( $\text{Al}_{12}\text{Mg}_2\text{Cr}$  or  $\text{Al}_{18}\text{Mg}_3\text{Cr}_2$ ), and M-phase [ $\text{MgZn}_2$

or possibly a phase of the form  $\text{Mg}(\text{Zn,Cu,Al})_2$ ]. The  $\text{Mg}_2\text{Si}$  was present in a very small amount as undissolved constituent particles. The  $\text{Cu}_2\text{FeAl}_7$  represented insoluble iron-bearing constituent particles, and the Cr-bearing E-phase was the dispersoid developed by solid state precipitation during ingot preheating. The M-phase was also present in relatively small amount and, in the T6 temper plate, apparently represented the large particles on boundaries that developed during quenching. In the T73 temper, the greater amount of M-phase presumably consisted of additional boundary precipitate particles and the larger particles developed within grains by the higher temperature precipitation treatment. The coherent precipitate,  $\text{M}'$ , was probably also present in 7075, particularly in the T73 temper, but diffraction effects from this more complex structure tend to be obscured by the diffraction lines from the M-phase.

The phases present in 7079-T6 and 7039-T6 were similar and consisted of  $\text{Mg}_2\text{Si}$ ,  $(\text{Fe,Mn,Cu})\text{Al}_6$ ,  $\text{Al}_{12}(\text{Fe,Mn})_3\text{Si}$ , and E-phase ( $\text{Al}_{12}\text{Mg}_2\text{Cr}$  or  $\text{Cr}_2\text{Mg}_3\text{Al}_{18}$ ). These phases can be matched with features observed in the microstructure. The  $\text{Mg}_2\text{Si}$  represents undissolved Mg combined with Si, and the Fe-bearing constituents are the combination products with this insoluble impurity element. Both of these are apparent in light microstructures. The E-phase particles are the relatively fine dispersoid particles resolved only in the electron microstructure, and represent high temperature precipitation of this phase during preheating.

In interpreting the electron microstructures of the 7XXX alloys used in this contract, the intermediate-sized dispersoid particles have been described as E-phase. This was based on the

fact that these dispersoids were present only in alloys containing Cr and the x-ray diffraction analysis that observed major amounts of E-phase in these alloys. This interpretation, however, is contrary to statements made in the literature and in reports on other contracts that the particles in question are  $\text{MgZn}_2$  (M-phase).

Selected area electron diffraction analyses were made to identify the intermediate-sized dispersoid in the 7075-T6, 7079-T6 and 7039-T6 plate. This work proved conclusively that the dispersoid particles were predominantly E-phase ( $\text{Cr}_2\text{Mg}_3\text{Al}_{18}$ ). Some M-phase particles were identified but these were definitely in the minority. Electron micrographs of E-phase and M-phase particles, and the corresponding diffraction patterns of the area within the dotted square, are shown in Figs. 23-24.

#### Microprobe Analyses

The electron microprobe was also used to evaluate the homogeneity of the solid solution matrix in 7075-T6 plate and, in particular, to search for compositional variations in grain boundary regions. Homogeneity was checked by making step-scans at five-micron intervals along straight lines in the short-transverse direction. In 7075-T6, localized variations were found for Mg, Cu and Zn, the variations being of a periodic nature, with elemental compositions differing somewhat between grains that appeared dark after a metallographic etch and those that appeared light (Fig. 25). The most pronounced variation was in Mg, the point-to-point values ranging from 2.16 to 2.59% and tending to be higher in dark-etching grains. Copper varied from 1.35 to 1.46% and changed inversely to Mg. Variations in

Zn were from 5.67 to 5.88% and tended to change in the same direction as Mg, but were less pronounced than the Mg and Cu variations. It is doubtful that the compositional variations within the matrix had any direct effect on crack initiation.

The solid solution matrix of the 2219-T351 plate had a uniform copper content of 5.7%, the maximum solubility for the solution heat treating temperature used. No differences related to location or etched appearance were detected, the latter depending solely on orientation.

The search for compositional differences near grain boundaries was made in the hope of detecting depleted boundary regions that could be anodic sites for crack initiation. To enlarge the effective width of any such region, the path of the probe trace was oriented at a very low angle to the boundary. Thus, although the beam was translated 2 microns per step along the direction of the scan, this amounted to only a fraction of a micron in a direction perpendicular to the boundary. This is essentially the method J. B. Clark used to detect depleted zones in Al-Ag alloys<sup>(1)</sup>.

The results of one such scan with 7075-T6 are presented in Fig. 26. Eight measurements in the vicinity of the grain boundary showed significantly lower Mg than in the grain bodies on either side. Cu and Zn also show apparent depletion. There is one high analysis for Cu exactly on the boundary. Conceivably, this could be evidence of a grain boundary precipitate, although coincident high Mg and Zn would be expected if the particle were M-phase.

Analyses across other boundaries, however, did not confirm in detail the results with this boundary. Depleted zones,



if present, were in most cases narrower than the ones shown. Sometimes depletion of Zn was more pronounced than that of Mg and it was often uncertain whether there was any localized depletion of Cu. Thus, the microprobe showed some evidence for depleted zones in the vicinity of at least some grain boundaries but did not produce definite proof of their existence.

#### Corrosion of Unstressed Specimens

As part of the groundwork for the crack initiation studies, the initiation and progress of corrosion in the absence of stress was observed using light microscopy. Specimens from the longitudinal (YZ) plane of the various plate materials were polished metallographically and were exposed to a corrosive environment while under constant observation with the light microscope. The metallographic finish was selected because it produces a film-free surface suitable for microscopic examination. The environment selected for all alloys except 7039-T6 was an aqueous solution of 1M NaCl + 0.21M AlCl<sub>3</sub>, adjusted to pH 1.0 with HCl. This solution had been used in other contract work,<sup>(2)</sup> and was chosen because it developed corrosion and stress-corrosion cracking at the proper rate for continuous observation and recording. The results obtained in this solution were representative of the behavior of the materials in more conventional environments, because the types of attack matched those of the corrosion test per MIL-H-6088D, and cracking tendencies matched those in the 3.5% NaCl alternate immersion test. The solution chosen for 7039-T6 was an aqueous solution of 0.5N NaCl + 0.5N Na<sub>2</sub>CrO<sub>4</sub>.

adjusted to pH 2 with HCl. This change was required because cracks did not initiate in 7039-T6 in the NaCl-AlCl<sub>3</sub> solution.

To record the initiation and progress of corrosion, areas were selected after an initial brief corrosion exposure, and successive micrographs were made of this same area. A comparison of continuous and interrupted exposures showed that, although the progress of corrosion was slower in the interrupted exposure, the initiation sites and path of corrosion were the same in both. Since the delay times during the taking of micrographs could not be kept constant, the exposure times on the illustrative micrographs cannot be used to judge corrosion rates.

#### Light Microscopy

The initiation and progress of corrosion were similar in 2219-T351 and 2219-T37 alloys, both being susceptible to intergranular attack in the absence of applied stress. Corrosion started at discrete points on grain boundaries and spread along these boundaries until a well-defined intergranular network of corrosion had developed. In the absence of applied stress, this network indicated continuous anodic paths on or adjacent to boundaries. A series of micrographs illustrating the development of the intergranular network in the T3-type tempers of 2219 alloy is shown in Fig. 27 and Fig. 29 - top.

The sequences of corrosion in the precipitation heat treated tempers of 2219 alloy (T851 and T87) were similar but differed greatly from that in the T351 and T37 tempers. The majority of the corrosion in the precipitation heat treated tempers began at or adjacent to the CuAl<sub>2</sub> and Cu<sub>2</sub>FeAl<sub>7</sub> microconstituent

particles. This indicates that the particles were cathodic to the matrix, as would be expected. In addition to the pitting attack, some corrosion of grain boundary segments was noted, but this attack developed only on portions of widely scattered boundaries and appeared to be very shallow. This was not unexpected because precipitation heat treatment of this alloy does not completely eliminate intergranular attack although it substantially eliminates stress-corrosion cracking. A series of micrographs illustrating the typical development of unstressed corrosion in the precipitation heat treated tempers of 2219 alloy is shown in Fig. 28 and Fig. 29 - bottom.

With 7075-T6 plate, the first corrosion was a random speckling of the matrix and localized attack in short segments of grain boundaries. As the exposure continued, the localized boundary attack extended and attack also developed at the boundaries of the fragments within grains. This indicates that both grain boundaries and fragment boundaries are anodic, and are about equally anodic, to the solid solution matrix. The initiation and progress of corrosion of the 7075-T6 plate are shown by Fig. 30 and Fig. 32 - top.

Corrosion of the 7075-T73 plate was of the cubic pitting type, initiating primarily at random sites in the matrix. The pits increased in size with continued exposure and frequently developed in straight lines, as if following particular crystallographic planes. There were no indications of anodic regions in this temper. The progress of corrosion in the 7075-T73 plate is shown by Fig. 31 and Fig. 32 - bottom.

Unstressed corrosion of the X7375-T6 alloy plate developed as a speckling of the matrix and an outlining of the grain structure by discrete pits and crevices along boundaries (Fig. 33 - top). The latter is indicative of anodic boundary regions. With the X7375 alloy plate in the T73-type temper, unstressed corrosion was primarily of the intergranular type, but was combined with cubic pitting of the type observed in 7075-T73 alloy (Fig. 33 - bottom).

The unstressed corrosion of 7079-T6 plate was similar to that of 7075-T6 with intergranular attack initiating first on grain boundaries and later on fragment boundaries. As corrosion progressed, some matrix pitting occurred and nests of inter-fragmentary attack developed along the sides of the intergranular fissures produced earlier. Thus it appears that both the grain boundaries and fragment boundaries were anodic to the remainder of the grains, and that the grain boundaries were slightly anodic to the fragment boundaries. Features of the unstressed corrosion of 7079-T6 are shown in Fig. 34.

With 7039-T6 exposed unstressed to the NaCl-Na<sub>2</sub>CrO<sub>4</sub> solution, only very little corrosion occurred even in relatively long exposure times. The majority of the corrosion that did develop consisted of constituent removal and pits associated with particles or clusters of microconstituents (Fig. 35). In cross section, the corrosion tended to be very shallow and did not follow a selective path, indicating that no anodic paths were present in the absence of stress.

### Electron Microscopy

The details of the unstressed corrosion of the 2219, 7075 and X7375 alloy plate exposed to the NaCl-AlCl<sub>3</sub> solution at pH 1 were investigated using electron microscopy. For this work, the oxide replica technique was used because it has the almost unique ability to reveal the internal surfaces of tiny fissures, crevices and cracks, as well as the surface topography of a specimen. The manner in which the oxide replica reveals structure is shown in Fig. 36. In the formation of the replica, the solution penetrates any cracks or crevices and oxide film is produced on all exposed surfaces. When the metal is removed and the oxide film is examined by electron transmission, the image will have different densities, determined by the thickness of oxide penetrated. With surface features, or structures within the open mouth of a crack or crevice, the electron beam penetrates a single thickness of replica and the image is relatively light. Areas within a crack or crevice appear dark because the electron beam must penetrate three layers of the replica, that on the surface of the specimen plus the films on both surfaces of the crack. The furthest penetration of the dark area represents the corrosion front or crack front.

Examinations of replicas of 2219 alloy unstressed specimens in the T351 and T37 tempers, both of which were susceptible to intergranular attack, revealed a corrosion front which penetrated between grains in a very irregular manner (Fig. 37). The corrosion front developed channels and

crystallographic tunnels along boundaries and often channels of corrosion joined, isolating, at least temporarily, certain portions of the boundary region. As corrosion progressed, grain boundary particles and islands of corrosion products were left behind.

With the 2219-T851 and 2219-T87 plate, the electron microscope examinations showed that the fine speckling corrosion seen with the light microscope consisted of a multitude of cubic pits. Some were aligned along grain boundaries, tending to define the grain structure in certain regions, but there was no significant boundary penetration. In the matrix, the pits were scattered at random but were aligned in the direction of the precipitate platelets developed during precipitation heat treatment, which were also apparent in the replicas. Figure 38 shows a typical corrosion pattern.

These examinations also demonstrated the role of certain constituent particles as cathodes, promoting corrosion of the surrounding matrix. Some particles showed a heavy concentration of pits at the particle-matrix interface. Others had pits in a region around the particle, with pit concentration decreasing as the distance from the particle increased (Fig. 39).

Examinations of replicas from corroded 7075-T6 specimens, which were susceptible to intergranular attack, revealed a very irregular corrosion front penetrating along boundaries. The corrosion front had an angular shape and the grain surfaces exposed by the corrosive attack had a faceted appearance (Fig. 40), indicating that corrosion was by a cubic-pitting mode.

Attack of 7075-T73 was not selective but was also by a cubic-pitting mode. Many fine pits were observed in the matrix, as was the case with the precipitation heat treated tempers of 2219 alloy. Also, there were large faceted areas (Fig. 41), which presumably represented the large cubic pits observed with the light microscope. In addition, there was some concentration of pitting on grain boundaries and on fragment boundaries, but this attack did not penetrate to the extent observed with samples in the T6 temper.

While X7375 alloy was not of prime concern to the contract objectives, electron microscope examinations of unstressed corroded specimens provided some excellent illustrations of the devious paths by which intergranular attack can penetrate a boundary region. One of these is shown in Fig. 42, which illustrates the extreme irregularity of a corrosion front, numerous isolated areas, and extensive penetration to the side from a comparatively narrow entrance on a boundary.

#### Stressed Specimen

A special "tuning-fork" type of specimen was designed for this contract (Fig. 43). With this specimen, tensile stress is applied to the outer surface of the base of the fork by bringing together the two legs, and the design is such that the area of maximum stress is comparatively small. This feature facilitated microscopic examination of crack initiation by restricting the area in which cracks were most likely to form. The dimensions of the specimen were selected to permit testing the plate one inch below the surface under short-transverse or

longitudinal stress. With the end of the specimen in the longitudinal plane of the plate, short-transverse stress is applied when the axis of the bolt is perpendicular to the surface of the plate, and longitudinal stress is applied when the axis of the bolt is parallel to the rolling direction.

With a specimen of this type, the stress on the end face is actually of a biaxial nature. Taking this into account, the relationships between deflection and short-transverse stress were determined (Fig. 44). Because of the biaxial stress condition, the stress perpendicular to the major stress was about one quarter of the major stress.

In preparing the specimen for exposure, it was first stressed to an appropriate level. The stressed face was then ground and polished through all but the final metallographic polishing operation. All surfaces except the stressed face were then coated, first with glyptal and then with a beeswax-rosin mixture, to insulate them from the solution when the specimen was exposed. The final polishing operation was then performed, a pre-cut mask was applied to the polished surface, and the specimen was exposed. The opening in the mask was rectangular in shape, about one square centimeter in area, and was located in the approximate center of the mask. This restricted the exposed area to the most highly stressed region of the face, eliminated any edge effects, and provided an area small enough to be examined rapidly under the light microscope. A stressed specimen ready for exposure is shown in Fig. 45.



### Corrosion of Stressed Specimens

Studies of crack initiation in the various contract materials were carried out using both light and electron microscopy of stressed tuning-fork specimens. The investigations described in this section were all made with a short-transverse stress of 75% YS and with exposure to the NaCl-AlCl<sub>3</sub> solution at pH 1 for all alloys except 7039-T6, for which the NaCl-Na<sub>2</sub>CrO<sub>4</sub> solution at pH 2 was used. Tests at other stress levels, with longitudinal stress, and in other environments were made and will be reported in other sections of this report. The methods of preparing specimens, and of continuously observing and recording events have been described previously. The interruptions for micrographs which had delayed the corrosion of unstressed specimens also retarded the resumption of crack growth but did not change the crack path.

At this point in this investigation, the question arose as to what constituted the "crack initiation" stage with which this work was primarily concerned. This stage was arbitrarily chosen to extend from the time the specimen was immersed, through the time when a crack was first visible in the light microscope (about 0.00002"), and until it reached a length of about 0.002", at which point it was still not visible to the unaided eye. In reality, this stage included both initiation and early propagation.

#### Light Microscopy

##### Alloy 2219

In the tests of 2219-T351 and 2219-T37 specimens,

cracks initiated on boundaries oriented normal to the direction of principal tensile stress and, in some cases, at grain junctions. They progressed along boundaries perpendicular to the stress, and proceeded quite rapidly as long as boundaries having this favorable orientation lay in their path. Because of the relatively equiaxed grain structure of 2219 alloy, however, the growing crack would frequently encounter an unfavorable boundary orientation (not perpendicular to stress) and the crack would become stalled. An instance of this is shown in Fig. 46 where a crack developed to a considerable length along a series of favorably oriented boundaries during 12 minutes of exposure and then ceased to grow. As indicated by Fig. 47, which shows the ends of the initial crack at higher magnification, both ends of the crack encountered unfavorable boundary orientation and it became easier to form new cracks along more favorably oriented paths than to extend the original crack.

Cross sections of this same specimen showed that only a few of the cracks observed on the surface penetrated to appreciable depth. Those that did grow selected the grain boundaries most nearly perpendicular to the stress (Fig. 48). The crack illustrated tended to branch at several points, but the resolved stress on these other boundaries was less and the crack sought and found a more favorably oriented path.

The critical effect of grain-boundary orientation is also shown in the high-power light micrograph at the top of Fig. 49. Here two parallel cracks have formed, the lower one along the favorably oriented boundaries of a series of seven

grains. Many other boundaries were present along this crack but development was slight because of insufficient stress across these boundaries.

The constituent particles in 2219 alloy had little or no direct influence on crack initiation as shown by the lower micrograph in Fig. 49. Numerous particles are present in this field, both within grains and on boundaries. The major portion of the crack, however, is along a boundary having only occasional particles. To the lower left, crack development has selected boundaries free of particles and has ignored a boundary containing a number of particles.

In tests of the precipitation heat treated tempers of 2219 alloy, which are resistant to stress-corrosion cracking, a tendency for directional pitting with a few short intergranular fissures was noted, but no cracks initiated (Fig. 50).

#### Alloy 7075

In tests of 7075-T6 tuning fork specimens, cracks initiated and developed very rapidly. They were very straight and narrow and were perpendicular to the stress (Fig. 51). They always initiated on grain boundaries (Fig. 52) which, for reasons discussed previously, were always highly elongated in the rolling direction and, therefore, perpendicular to the short-transverse stress. Occasionally cracks initiated at  $Mg_2Si$  constituent particles on boundaries, or at pits developed by dissolution of these particles (Fig. 53 - top) but more often they formed at random boundary sites (Fig. 52 and Fig. 53 - bottom). Since crack initiation time was the same with and without constituent

particles or pits, it was concluded that although pits may act as focal points for crack development, they are not a requirement for crack initiation.

Additional features pertinent to crack initiation in 7075-T6 are seen in Fig. 52, which shows a string of tiny stress-corrosion cracks, the longest of which is only 0.0005". At each end of each minute crack, the localized stress has exceeded the yield strength and caused plastic deformation as indicated by the rumpling of the polished surface seen in the upper micrograph. The lower micrograph shows that the crack initiated on a boundary between grains showing a difference in etching coloration and therefore having considerably different orientations. This suggests that the relative orientation of adjoining grains may affect crack initiation on their mutual boundary.

Cross sections of 7075-T6 specimens in which dominant cracks had developed showed clearly how cracks propagate in their early stages. With a typical crack observed in this manner (Fig. 54), development occurred almost entirely along boundaries, and generally along those boundaries oriented most nearly normal to the short-transverse stress. As it progressed, the crack came to boundary junctions and branches started to form, but each time the most favorable boundary orientation was selected for propagation. Near the midpoint of the crack, a fairly large branch formed toward a group of constituent particles. It could not be established whether this branch stopped because of the particles or because of an unfavorable boundary orientation, but it is

apparent that the particles were not harmful. In certain regions the crack was not continuous on the polished section, the crack apparently having sought a favorable boundary orientation above or below the plane of polish.

To obtain further insight into crack initiation in 7075-T6, simultaneous observations of initiation and propagation were made on the longitudinal (YZ) and transverse (XZ) surfaces of tuning-fork specimens. In preparing the specimens for this type of exposure, both the end face and one side face were metallographically polished in the usual manner, both surfaces were masked off except for a narrow band adjacent to their mutual edge, and exposure was then conducted in the usual manner. Cracks initiated primarily at the exposed edge and progressed both along the most highly stressed end face (Fig. 55) and along the side surface (Fig. 56) where stress would decrease as the crack became deeper. Cracks initiated on grain boundaries and progressed along such boundaries in the manner noted in observations of the end face only.

Occasionally, cracks would form on portions of a boundary on the two exposed faces very close to their mutual edge and would progress away from the edge. This developed very high stress on the unfractured metal at the edge, and mechanical fracture would occur. This mechanical fracture did not follow the boundary on which the stress-corrosion cracks had initiated. Thus, examinations of the surface of such a fracture might indicate that the crack had started transgranularly and had then sought an intergranular path. Actually, the sequence of events

was reversed and the transgranular portion of the fracture did not occur first and was produced by a mechanical rather than a stress-corrosion mechanism. It is believed that this was the case in the region shown in Figs. 55 and 56. While the majority of the cracking is definitely intergranular, the fracture appears to be transgranular (or perhaps interfragmentary) at the corner.

This examination also provided additional evidence of the necessity of favorably oriented, susceptible paths for stress-corrosion crack propagation. In the area shown in Figs. 55 and 56, the crack initiated and developed rapidly during the first ten minutes of exposure. In the next ten minutes, however, very little propagation was noted, even though there were no major neighboring cracks, the development of which would relieve the stress. Metallographic etching disclosed that the crack had developed along a favorably oriented boundary between grains having different orientation. The crack had stalled when it reached the end of one of these grains, even though favorably oriented paths along grain and fragment boundaries were still available. Thus, relative orientation on the two sides of a boundary may influence crack initiation, either as a separate factor or as it influences the corrosion susceptibility of the boundary path.

Stressed specimens of 7075-T73 alloy did not develop cracks. Corrosion was of the cubic-pitting type and showed no directionality with respect to either the direction of stress or the directionality of microstructure (Fig. 57).

### Alloy X7375

With stressed specimens of X7375-T6 alloy, cracks initiated quite rapidly at random sites on grain boundaries perpendicular to the stress. They propagated along the boundaries of the large recrystallized grains, seeking series of favorably oriented boundaries (Fig. 58), and were widest on boundaries oriented normal to the stress (Fig. 59a). When unfavorably oriented boundaries were encountered, plastic deformation occurred at the crack tip because of localized high stress (Fig. 59b).

In the T73-type temper, X7375 developed large cubic pits and a broad intergranular attack (Fig. 59c & d), similar to that of unstressed specimens (Fig. 33). There was no indication of stress-corrosion cracking or of any effect of stress on corrosion, in spite of the fact that failures were encountered in the stress-corrosion tests of this material.

### Alloy 7079

Crack initiation in 7079-T6 plate was similar to that of 7075-T6 plate described previously. Cracks initiated and propagated on boundaries perpendicular to the stress, some initiating at  $Mg_2Si$  particles (Fig. 60) but others originating elsewhere in similar times (Fig. 61). In certain regions, where cracks ceased growing because of local stress relief from the passage of larger cracks nearby, interfragmentary attack, typical of unstressed corrosion, developed beside the cracks and within adjoining grains (Fig. 61).

### Alloy 7039

In the investigation of crack initiation phenomena with 7039-T6 alloy, it was originally intended to use the

NaCl-AlCl<sub>3</sub> solution at pH 1 that was used with all other alloys. In tests with two lots of 7039-T6 plate and with short transverse stresses of both 75% YS and 90%, however, no cracks initiated although considerable general corrosion occurred. Since experience has shown that a large amount of general corrosion often reduces the tendency for stress-corrosion, it was concluded that the NaCl-AlCl<sub>3</sub> solution at pH 1 was inappropriate for this investigation. In its place, a solution of 0.5N NaCl + 0.5N Na<sub>2</sub>CrO<sub>4</sub> adjusted to pH 2 with HCl was used.

In the NaCl-Na<sub>2</sub>CrO<sub>4</sub> solution, with short-transverse stress of 75% YS, cracks initiated on grain boundaries and only at Mg<sub>2</sub>Si constituent particles or pits from which these particles had been dissolved (Figs. 62 and 63). Cracks initiated and propagated on grain boundaries perpendicular to the stress and associated themselves with constituent particles only when they were on boundaries (Fig. 64). This association of crack initiation with Mg<sub>2</sub>Si constituent particles in 7039-T6 is contrary to observations with all other alloys, where constituent particles played only an incidental part in crack initiation.

#### Electron Microscopy

Electron microscope examinations were made of cracks in specimens selected from those described in the previous section of this report. The oxide replica technique was used because, as described previously, these replicas are capable of revealing topographical features within a crack or crevice, as well as on a surface. These examinations confirmed the results of light microscope examination and, in addition, revealed other features of crack initiation.



In 7075-T6, cracks initiated and propagated on grain boundaries but not on fragment boundaries. Some cracks appeared to initiate at M-phase particles on boundaries but, more often, initiation occurred at boundary sites not associated with any microstructural feature. Cracks frequently originated at multiple locations along a boundary and the embryonic fissures joined to make a larger crack. A crack that has initiated on a grain boundary and has penetrated beneath the specimen surface is shown in Fig. 65. The veining of the walls of the crack may represent fragment boundaries or the boundaries of a polygonized structure, the evolution of which is discussed in a later section of this report. An embryonic crack, just starting to penetrate a boundary, is shown in Fig. 66. The raggedness of the crack front and the progress of the crack sideways as well as inwards are apparent. Along some boundaries, frequently ahead of cracks growing laterally, strings of pits were observed (Fig. 67). The lighter parts of these markings appear to be pits generated by the dissolution of boundary precipitate particles. The darker parts are where corrosion is entering the boundary region or where a stress-corrosion crack is developing.

With 7075-T73 samples, similar pits resulting from dissolution of boundary particles, and shallow boundary penetration from these pits were observed. Since this temper did not develop cracking, it can be concluded that these pits are not a prime cause of crack initiation and may not even be a particularly important factor.

Similar examinations of stressed 2219-T351 and X7375-T6 specimens revealed features similar to those observed

with 7075-T6. Cracks initiated at boundaries and, in X7375, at particles on boundaries. Crack penetration was highly irregular, occasionally by-passed certain small areas temporarily, proceeded sideways along grain surfaces, and left markings on grain faces which were either boundary particles or pits resulting from dissolution of such particles. Typical crack penetration of 2219-T351 is shown in Fig. 68. Cubic-type crack penetration and boundary penetration from pits in X7375-T6 are shown in Fig. 69.

With 7079-T6, cracks initiated as fine scale attack of the boundary, possibly starting at precipitate particles, and frequently at polygon boundaries representing the junction of dispersoid-lean regions with regions of average structure (Fig. 70). Cracking proceeded downward along the boundary region developing a veined appearance similar to that observed with 7075-T6. The crack front was always very irregular since it apparently propagated by dissolving new metal along narrow tendrils in a crystallographic mode (Fig. 71).

With 7039-T6 specimens, stressed and exposed to the NaCl-Na<sub>2</sub>CrO<sub>4</sub> solution at pH 2, the attack that constituted the start of cracking tended to initiate on polygon boundaries in dispersoid-lean regions. Crack initiation in this alloy was investigated more extensively with specimens exposed to the atmosphere, which will be described in a later section of this report.

#### Microprobe Investigations

In addition to its use in characterizing compositional variations in the plate materials, the microprobe was evaluated

in two other ways as a means of investigating crack initiation.

#### Corrosion Films

To relate crack initiation to the surface films or reaction products developed during a corrosion exposure, stressed 7075-T6 specimens were exposed to the NaCl-AlCl<sub>3</sub> solution at pH 1 until cracks initiated. At this period the exposed surface was still relatively clean except for a few speckled patches of surface film.

Electron beam scanning pictures showed an uneven distribution of oxygen and chlorine on the surface, with none in clean areas, small amounts in the speckled film areas, and considerably larger amounts at the stress-corrosion cracks. Quantitative step-scans across a number of small cracks gave values between the extremes shown in Figs. 72 and 73. The actual values may have been considerably higher than those shown because the electron beam could not be confined wholly to the crack. The crack corresponding to Fig. 72 was a very narrow crack, whereas that for Fig. 73 was comparatively wide. In the latter crack, the oxygen and chlorine levels were lower and the aluminum concentration was closer to that of Al<sub>2</sub>O<sub>3</sub>.

This work indicates that stress-corrosion cracking in 7075-T6 involves the formation of an oxide-type corrosion product containing chlorine, possibly as an absorbed chloride. The microprobe technique holds promise for the investigation of stress-corrosion phenomena.

#### Fracture Surfaces

Another attempted application of the microprobe to crack initiation was in the analysis of fracture surfaces. It

was reasoned that if stress-corrosion cracking proceeds through a grain boundary zone depleted in alloying elements, and the zone is not completely consumed by corrosion, remnants of the zone will be found on the faces of the fracture. Microprobe analysis of the fracture faces would then show the composition of the zone if the depth of analysis was confined to small enough dimensions.

This technique was applied to a 7075-T6 specimen which had been broken open to expose the surface of a relatively large stress-corrosion crack. After mechanically flattening the fracture surface to minimize roughness effects, comparative analyses were made of the stress-corrosion and tensile portions of the fracture. Analyses with a wide analytical spot showed what appeared to be significant differences in Mg and Zn but not in Cu. To obtain statistically significant data, 40 separate analyses were made on each of the two types of fracture with the beam focused to a fine analytical spot. Histograms showing the distribution of the various analyses are shown in Fig. 74. Weibull analyses of the results showed that the values for Zn and Mg were different whereas those for Cu and Cr were not. Numerically, the stress-corrosion fracture showed 0.26% less Zn and 0.03% less Mg than the tensile fracture.

A boundary region depleted in Zn and Mg is not unexpected because of the relatively high diffusion rates of these elements and the fact that precipitation on grain boundaries had occurred. Such a situation however would not support an electrochemical theory of stress-corrosion cracking because a

region depleted in zinc would be cathodic to the matrix and would not be corroded preferentially. On the other hand, it must be remembered that (1) any anodic region might have been completely corroded away during the cracking process and (2) the penetration of the microprobe beam may have been much greater than the depth of the region involved in stress-corrosion cracking.

Differences in composition between fracture surfaces produced by stress-corrosion and by mechanical means were also found with 2219-T37 alloy, but for a different reason. With the microprobe spot defocused to cover a relatively large area, a stress-corrosion fracture analyzed 6.91% Cu and 0.25% Mn, as compared to 9.98% Cu and 0.42% Mn for a tensile fracture. The fact that the copper contents are much higher than the amount present in the alloy indicates that the number of Cu-bearing constituent particles is inordinately high in the mechanically fractured area. When analyses obviously from constituent particles were discarded, both areas analyzed about 5.87% Cu and 0.23% Mn.

This points out that the difference in analysis between the two fracture regions was due not to a difference in matrix composition but to a difference in the number of constituent particles on the fracture surface. This agrees with other electron microscope observations which have indicated that tensile fracture in 2219-T37 occurs preferentially through constituent particle clusters while stress-corrosion fractures show no such inclination and include relatively few particles.

## Electron Fractography

### Methods

Two improved replica methods were developed for investigating crack initiation in tuning-fork specimens by electron fractography. These were particularly useful because they permitted precise differentiation between the stress-corrosion and mechanically fractured regions on a fracture surface. In both methods, the first step was to form a relatively thick (22 volt) oxide replica. The specimen was then broken open by squeezing the legs in a vise, exposing a fracture surface having oxide-covered stress-corrosion cracks and a bare tensile fracture surface. In the one method, a second oxide replica was then formed on the fracture surface at 15 volts. Because of the lower forming voltage, oxide was formed only on surfaces developed by the mechanical fracturing. This oxide appeared lighter in the electron microscope because it was thinner.

The second forming, moreover, repaired damage to the original oxide film and permitted differentiation of topographical features developed during the stress-corrosion test from those developed mechanically during final fracturing of the specimen. An example of the use of this technique is shown by Fig. 75.

In the second method, an evaporated carbon film was substituted for the second oxide film. Application of the carbon at an angle, or using chromium shadowing, also showed whether the various features were above or below the general fracture surface. An illustration of the combination oxide-carbon replica technique is shown by Fig. 76.

The oxide-carbon replica method was useful also for visual and light microscope examinations of fractures because of a color difference between the two regions. The stress-corrosion portion of the fracture, having both oxide and carbon films, was a bluish-gray color which contrasted strongly with the brown color of the mechanically produced surface which had only the carbon film. At a glance one could tell the number and depth of stress-corrosion cracks present. Under the light microscope the difference in color showed unequivocally which type of fracture was being examined.

#### Fracture Surfaces - Transmission Microscopy

Electron fractographic examinations provided additional information regarding crack initiation in 7075-T6 and 2219-T37 stressed short transversely and exposed to the NaCl-AlCl<sub>3</sub> solution at pH 1. In 7075-T6, the stress-corrosion fracture had a finely faceted appearance with a network of furrows (Fig. 77). This configuration apparently represented the surfaces and boundaries of either the polygonal grain fragments seen in the light microscope or the relatively equiaxed polygons observed in the electron microscope in dispersoid-lean regions. Except for the irregularity of the small facets, the stress-corrosion crack surfaces were quite flat, with relatively few branches, indicating that the cracks confined themselves to as planar an interface as the polygon boundaries would allow. Constituent and dispersoid particles were frequently seen but there was no indication that either interacted with the crack.

There were some areas within the stress-corrosion fracture which showed the dimpled appearance characteristic of tensile rather than stress-corrosion fracture. These were generally quite small and apparently represented either (1) regions that had fractured mechanically after having been bypassed by branches of the growing stress-corrosion crack or (2) areas that had not cracked during the test but were produced during the subsequent mechanical fracture. Other than these small areas, no indications were seen that plastic deformation played a significant part in crack initiation or propagation.

The tips of stress-corrosion cracks had fine-scale irregularities, sometimes cubic, but more generally rounded (Fig. 78). This and other features of the crack front were the same as those seen in examinations of surface oxide replicas. Beyond the stress-corrosion crack front there was usually a flat, rather featureless area representing the initial rapid tensile or "pop-in" failure produced when the specimen was being broken open. Beyond this region was the dimpled fracture appearance characteristic of tensile failure (Fig. 79). Each dimple was associated with a tiny dispersoid particle, indicating the strong interaction of this type of particle with tensile fracture, but not with stress-corrosion fracture.

Similar examinations of 2219-T37 specimens showed that unlike the 7075-T6 failures, where the deepening stress-corrosion crack followed a network of polygonal fragments between unrecrystallized grains, cracks in 2219-T37 followed relatively



planar boundaries between recrystallized grains. At high magnification the fracture surfaces had a finely etched appearance apparently produced by the corrosion associated with stress-corrosion cracking. In a few areas, the micro-roughness of the fracture surface was in the form of fine parallel lines (Fig. 80). This is perhaps an etching effect, but might be the remnants of slip steps and, hence, evidence for plastic deformation occurring in the stress-corrosion zone. Small rectangular constituent particles were commonly found lying on the stress-corrosion face of 2219 fractures, but there was no evidence that they contributed to the fracture.

There was ample evidence that the stress-corrosion cracks in 2219-T37 proceed in a very irregular manner rather than on a broad front. There were many islands within the stress-corrosion area that failed in a tensile manner, and at the ends of cracks, there were often spade-like tendrils advancing in front of the main crack beneath the surface (Fig. 81).

#### Fracture Surfaces - Scanning Microscopy

During the demonstration of a scanning electron microscope (SEM), examinations were made of the fracture surface of one specimen each of 7075-T6 and 2219-T37 that had been stressed short transversely to 75% YS, exposed to the NaCl-AlCl<sub>3</sub> solution at pH 1 until stress corrosion cracks initiated, and then fractured mechanically. While both the stress-corrosion and mechanical fracture areas were examined and were described in the Eleventh Quarterly report, only the former will be described here.

In the 7075-T6 specimen, the surface of the stress-corrosion fracture was comparatively smooth and featureless (Fig. 82). Surfaces of individual grains were visible and constituent particles left by the advancing stress-corrosion crack were evident. In certain areas between grains, markings characteristic of tensile fracture were present, presumably developed when a bridge between two approaching cracks was broken mechanically as a result of localized stress concentration.

In the stress-corrosion region of the 2219-T37 sample, the fracture had a somewhat faceted surface, presumably representing grain faces exposed by the stress-corrosion crack (Fig. 83). In addition, it was noted that in this region a small fragment of metal had pulled away from the main fracture. The sides of this chip were marked by elongated facets, evidently produced by the passage of the stress-corrosion crack. Their appearance suggests that the layers represent the "series of grains having favorably oriented boundaries," which were the crack propagation paths in this alloy.

#### Evolution of Grain Boundaries

Throughout the light microscope phases of this investigation, it has been apparent that stress-corrosion cracks in 7075-T6 initiate preferentially on certain boundaries oriented perpendicularly to the stress. Electron microscopy showed that these boundaries were of two types and that stress-corrosion cracks initiated and propagated on both. One boundary represented the junction of two grains (clusters of fragments) of different orientation. The other type, however, was a region of finite

width, composed of relatively equiaxed polygonal cells, and occurring in regions having a low concentration of E-phase dispersoids. An investigation was made to trace the origin and evolution of this type of boundary region. This was done by following the composition, microstructure and stress-corrosion behavior of an ingot section of 7075 alloy as it was rolled to 2.15" thick plate. In one experiment, an 8" thick ingot section was hot rolled to plate with samples being taken at various thicknesses. In another, a 10" thick ingot section was sawed to a tapered shape so that when it was rolled to plate the amount of reduction by hot rolling would vary linearly from zero at one end to 80% at the other. Changes in degree of microsegregation were determined with samples in the as-fabricated (F) and T6 tempers. All other work was performed on T6 temper samples only.

#### Composition

The electron microprobe was used to study progressive changes in microsegregation as the ingot was rolled to plate of decreasing thickness. In the ingot, the elements Zn, Mg and Cu, being eutectic elements, were found to be more concentrated at the edges of dendrite cells. Chromium, on the other hand, is a peritectic element, and was concentrated more toward the center of the dendrite cells. As the ingot was preheated and reduced by hot rolling the compositional variations in Zn, Mg and Cu were reduced because these elements diffuse readily. Conversely, chromium has a low diffusion rate and microsegregation is not eliminated easily. This effect is shown in Fig. 84 which shows

microprobe composition profiles for Cu and Cr across a dendrite cell in 7075 ingot given a T6 heat treatment.

Data from the microprobe analyses in the two tempers, F (as hot rolled) and T6, are shown graphically in Figs. 85-88. For each element, the lower portion of the figure shows the range of the point-to-point variations, and solid curves denote the average solute content of the matrix. The upper portion of each figure shows the change in segregation coefficient with increasing hot rolling reduction for the two tempers. As this coefficient approaches zero, the degree of homogeneity is increasing.

Preheating and relatively small rolling reduction were sufficient to distribute Cu fairly uniformly in the unheat-treated plate. The approach to uniformity in the elements Zn and Mg, however, was more gradual, increasing as rolling progressed. Heat treating provided a substantial further increase in homogeneity with respect to Zn, Mg and Cu, with the degree of microsegregation in the T6 temper being essentially independent of plate thickness. In the case of Cr, neither fabrication nor thermal treatment affected the range of element distribution in any way, and the range of observed Cr in the final plate was just as great as in the original ingot (Fig. 88). Thus, the low chromium content at dendrite boundaries (Fig. 84) will be present in the final T6-temper plate. Recalling that chromium retards recrystallization (7075 vs. X7375), it would then be expected that the dendrite cell boundaries low in chromium would tend to recrystallize more readily. This has actually been noted in the electron microstructure where dispersoid-free regions have had an equiaxed structure of fine polygons or grains. Thus, it can be concluded that the type of

boundary formed by the highly polygonized cells originated as a dendrite cell boundary in the ingot.

### Microstructure

The changes in microstructure associated with different amounts of reduction by hot rolling followed by heat treatment were examined by transmission electron microscopy. Samples from the plate rolled from the tapered ingot were used.

In the region that had received no reduction, the dispersoid-free regions associated with localized low chromium content were apparent, but no polygonization or development of cells had occurred (Fig. 89). In the portion of the plate reduced 30-40%, the dispersoid-free regions had been elongated significantly and, since there were no dispersoid particles to obstruct dislocation movement, these regions remained relatively dislocation-free. The dispersoid particles in adjoining regions, however, were effective obstacles to dislocation movement and many pinned dislocations were apparent (Fig. 90). Also, and perhaps of greater importance, dispersoids were also obstacles to grain boundary movement.

With reductions of 50-60%, interactions between dislocations had produced low-angle polygon boundaries within the dispersoid-free bands and, to a lesser extent, within the adjoining regions of average dispersoid content (Fig. 91). The polygon boundaries were prevented from penetrating very deeply into the regions of high dislocation density because of the dispersoid obstructions. As a result, the polygon boundaries

along the borders of the dispersoid-free band became more prominent as they accumulated more dislocations (Fig. 92).

These observations defined the evolution of the polygonized, cellular bands found on some boundaries. These bands developed preferentially in regions of low E-phase dispersoid content, which were apparently also low in chromium. These regions could be grain boundaries in the original ingot or, as deduced in the previous section, boundaries of original dendrite cells.

#### Stress Corrosion Behavior

The effect of the different amounts of reduction and the accompanying changes in microstructure on resistance to stress-corrosion cracking were evaluated by stress-corrosion tests of short-transverse specimens stressed to 50% and 75% YS, and exposed to the 3.5% NaCl alternate immersion test. The test results (Table IX) show that resistance to stress corrosion decreases as the percent reduction increases. At 75% YS, all samples failed, but those with reductions of 20% or less had longer failure times. At 50% YS, there was a fairly sharp transition, with all samples failing in relatively short periods when reductions were 40% or more, and most samples not failing in 84 days when reductions were 30% or less.

Similar relationships were noted in the crack initiation times of tuning-fork specimens stressed short transversely to 75% YS and exposed to the NaCl-AlCl<sub>3</sub> solution at pH 1. When the reduction was 35%, cracks initiated in 20 minutes. As the percent reduction increased, crack initiation time decreased

until, at 80% reduction, cracks initiated after only six minutes and propagated rapidly across the specimen.

The relation between stress-corrosion behavior and microstructure was evident from electron microscope examinations of replicas from the tuning-fork specimens. With 25% reduction or less, boundaries were relatively straight, even in regions having few dispersoid particles. Cracking initiated on these boundaries (Fig. 93). With 35% reduction some of these boundaries acquired short branches indicative of the start of cell formation. Cracking initiated on the grain boundaries and on the embryonic cell boundaries (Fig. 94). With 45% reduction many of the boundaries were cellular rather than planar, with the cells lying in dispersoid-lean regions, and preferential attack occurring on polygon boundaries (Fig. 95). The cellular configuration and attack of polygon boundaries was even more pronounced with 80% reduction (Fig. 96).

This investigation of the evolution of the crack-susceptible paths in 7075-T6 plate has shown that stress-corrosion resistance in the short-transverse direction deteriorates with increasing reductions from the ingot. One cause is apparently the development of polygonal structures, having continuous boundary paths, in regions having low E-phase dispersoid content. Another cause is the fact that the more conventional type of boundaries (junction of grains having different orientation) are oriented perpendicularly to the stress, either because they were in this position initially or because they were rotated into this

orientation during fabrication.

#### Corrosion of Thin Films

It was planned to study crack initiation directly by transmission electron microscopy using specimens from 7075-T6 and 7039-T6 plate. The specimens were to be thinned sufficiently for transmission microscopy and were then to be exposed to appropriate media both unstressed and stressed. This technique had been used successfully in pre-contract investigations of corrosion and stress-corrosion phenomena.

Attempts to duplicate this work with the plate materials involved in the contract met with a series of problems that were never completely solved. The primary difficulty was that with all of the usual thinning procedures, the plate materials were attacked selectively, developing configurations that could not have been distinguished from features developed during corrosion exposure. Another major problem was that of stressing the thinned specimens either quantitatively or consistently. No satisfactory method was found.

Near the end of the contract, changes were made to at least demonstrate the capabilities of this approach. An improved thinning process was developed, a change was made from 7075-T6 plate to sheet, and qualitative stressing was employed. Thinning was accomplished by reducing the sheet to .005" by conventional procedures, and performing the final thinning electrochemically in an electrolyte of 67% methanol and 30% nitric acid maintained at a temperature below -20 F. After the specimen had perforated, it



was rinsed first in methanol at -20 F, and then in methanol at room temperature. Specimens for transmission examinations were taken from the edge of the perforation.

Examinations of thinned specimens of 7075-T6 exposed unstressed to the NaCl-AlCl<sub>3</sub> solution at pH 1 revealed a random cubic pitting type of corrosion, apparently not related to any microstructural feature (Fig. 97). When specimens were stressed qualitatively by pressing them lightly against the bottom of a beaker containing the same solution, intergranular stress-corrosion cracks initiated (Fig. 98).

Even with the resolving power of the electron microscope, the exact path taken by the crack was not certain. Precipitate particles lying on the grain boundary itself did not seem to be involved in the cracking process and were by-passed by the crack. This suggests that the crack followed a very narrow band just adjacent to the actual boundary and that the precipitate particles were cathodic to this band. Sometimes the specimen in advance of the crack tip appeared to be thinner near the grain boundary than within the grain body. This suggests that the imposed stress, perhaps aided by the stress concentrating effect of the crack, made the metal in the vicinity of the boundary more electrochemically active so that dissolution in the corroding medium was more pronounced.

#### Calculations of Grain Boundary Composition

The composition of the region adjacent to boundaries, in relation to those of other solid solution regions, boundary

precipitate particles and matrix precipitates, are important to stress-corrosion crack initiation. Little is known about the composition of this region in commercial alloys, however, because analytical methods do not yet have sufficient resolution to selectively analyze the extremely narrow boundary region. In a theoretical approach to crack initiation, calculations of the composition of the boundary region were made for 7075, 2219 and 7039 alloys. These calculations were based on known diffusion rate data and simple assumptions concerning the composition at the actual grain boundary.

During the solution heat treatment of 7075 alloy, essentially all of the Zn, Mg and Cu are in solution at the heat treating temperature. On quenching, however, the solid solution becomes supersaturated in these elements, precipitation occurs, and to different degrees depending on the rate of quench. The rate of cooling between 750 and 550 F is a very important factor affecting the stress-corrosion resistance of certain aluminum alloys.<sup>(3)</sup> When 7075 is quenched through this range at a rate greater than 300 F per second, the alloy is stress-corrosion resistant. When it is cooled at a rate of about 50 F per second or less, it is susceptible. Stated another way, if 7075 remains in the critical temperature range less than one second it is resistant to stress corrosion, while if it remains more than about four seconds it is susceptible.

The model used for the calculations assumes that the structure produced during quenching is the same as would be

produced by holding the metal at 680 F for a similar period. This temperature was selected because it is in the upper portion of the critical range, where changes occur most readily, and because the required diffusion data are available for this temperature.

Because atomic mobility on the grain boundary itself is very high, it can be assumed that nucleation of precipitates begins much more readily there than in the bulk of the grain. The solute removed from solution by the precipitation produces a compositional gradient which favors diffusion of further solvent from within the grain toward the boundary. It is not known, however, exactly how much of each solute element is removed from solution at the boundary.

A reasonable assumption is that the solute contents adjacent to the grain boundary approach the equilibrium solubility limits for the respective elements at 680 F during quenching and approach them much faster than in the bulk of the grain. If it is assumed that equilibrium solubility is attained instantaneously within the grain at the boundary, the calculated diffusion profiles after various periods are as in Fig. 99. Because the solubility for Zn at 680 F is not much lower than that at the solution heat treating temperature, the gradient in Zn is not very steep. The solubility of Cu and Mg are, however, drastically reduced. When solution potentials are calculated from the known effects of these elements, it is seen that there is an anodic peak in the vicinity of the grain boundary due almost exclusively to the loss of Cu to the boundary. The region adjacent to the boundary is significantly anodic to the bulk of the grain and could indeed provide a preferential path for stress-corrosion cracking.

Another factor contributing to the electrochemical relationships in grain boundary regions is the nature and composition of boundary precipitate particles. Since elements depleted from the boundary region appear on the boundary, the relative amounts of these elements on the boundary were calculated. These values, with a listing of precipitate phases that might form, are given in Table X.

To this point, the calculations have utilized only the bulk diffusion rates at 680 F. Diffusion occurs by a vacancy mechanism, however, and the number of vacancies is strongly temperature dependent. During the initial steps of quenching, excess vacancies are present and as they migrate to boundaries in an attempt to establish equilibrium, they assist migration of solute atoms. If each type of solute atom were affected equally, the only effect of vacancy-assisted diffusion would be to widen the solute-depleted zones. Actually, copper atoms trap vacancies more efficiently than do zinc atoms.

Assuming that all excess vacancies are captured by copper atoms, and that diffusion rate is proportional to the number of vacancies, the copper diffusion rate would initially be increased about 6.8 times, decreasing to the normal level as vacancies were annihilated. Under these conditions, the potential gradient in boundary regions would be similar to that in Fig. 100. By comparison with the curves in Fig. 99, it is seen that excess vacancy-enhanced diffusion would increase the extent of solute depletion but would have little effect on the shape of the potential gradient. Actually, since diffusion of all elements is enhanced

by diffusion, the most accurate estimates of potential gradients would be between those in Figs. 99 and 100.

The excess vacancy-enhanced diffusion will also lead to a change in the amount of solute elements at boundaries. One can assume that the diffusion rates are enhanced in proportion to the binding energy of each element for a vacancy. Taking these to be 0.06 ev for Zn, 0.19 ev for Mg, and 0.25 ev for Cu,<sup>(4)</sup> the material deposited at the boundary is seen to be high in Mg, intermediate in Cu, and low in Zn (Table X).

In 2219 alloy, the only element affecting solution potential and free to diffuse is copper. Calculations were made for this alloy using the same assumptions as with 7075, namely, that compositional differences are established at about 680 F, and that compositions adjacent to boundaries reach equilibrium values for this temperature. The calculations indicated that a grain boundary region anodic to the bulk of the grain would be generated during quenching because of the loss of copper to the boundary (Fig. 101). With the longer effective times at the critical temperature resulting from slower quenches, the width of the anodic region would increase.

In the case of 7039, which does not contain copper, the formation of anodic regions by diffusion of copper would not be possible. Because the solubility for Zn and Mg is not much lower at 680 F than at the solution heat treating temperature, the model does not predict a significant variation in composition in the vicinity of grain boundaries after quenching (Fig. 102).

This suggests that if significant composition gradients are established, they develop at temperatures below 680 F.

The next step was to calculate the effects of artificial aging on the depleted boundary regions developed in 7075-T6 during slow quenching. These calculations were based on the solution potentials known to result when the T6 and T73 aging treatments are applied to material of the compositions calculated to be produced during quenching. The computations predicted a shift in compositions and solution potentials in the boundary regions as a result of artificial aging, but indicated that the potential gradients would not be changed appreciably. Thus, anodic boundary regions were indicated not only for the T6 temper which was susceptible to cracking but also for the T73 temper which was not (Fig. 103).

Two possible explanations come to mind to explain the anomalous relation between actual stress corrosion behavior and the potential relationships predicted for the T73 temper. One, based on microstructure, relates to the relatively large precipitate particles developed throughout the grains during T73 aging. Since these particles are M-phase high in zinc, they would provide a multitude of corrosion anodes of equal or more anodic potential than the boundary region depleted in copper. The improvement in resistance to stress-corrosion cracking observed with extensive precipitation in Al-Mg alloys has been attributed to the reduction in current density at anodic boundaries as a result of an increase in the anode/cathode area ratio.<sup>(5)</sup>

The other possible explanation of the anomaly is related to the assumption that the composition at the boundary was that in equilibrium at 680 F, regardless of the rate of quench. This would be only a limiting case and, actually, the approach to the equilibrium value would be governed by rate of quench. This would alter the predictions of compositions in boundary regions which, in turn, would alter the response to artificial aging. It was planned to follow this lead, but time did not permit. This approach, however, appears potentially profitable in explaining stress corrosion behavior.

Another interesting feature of the calculations with 7075-T6 is that the mechanical properties in the boundary region are also probably affected by quench rate. Estimating the yield strengths on the basis of calculated compositions, it can be seen that the boundary may be significantly weaker than the grain body (Fig. 103). This may be important since some theories of stress corrosion envision a mechanical contribution. In addition, concentrations of deformation in a weak boundary region may affect the local solution potentials.

#### Grain Orientation

It was noted frequently, during light microscope observations of crack initiation, that major cracks developed on high-angle boundaries, as judged by the coloration of adjoining grains after metallographic etching. Also, in one instance, a crack propagating along such a boundary stopped growing when it reached the end of one of the grains involved, even though a favorably oriented continuing path was available but between

grains of more nearly similar orientation.

It was planned to explore the effect of the relative orientations of adjoining grains on the tendency for crack initiation on their mutual boundary. Grain orientation was to be determined by using a Kossel camera attachment to the microprobe, which has been promoted as a precise means of determining orientation. Despite numerous attempts to employ this procedure, satisfactory patterns were never obtained, and it was necessary to change to etch-pit techniques for determination of orientation.

The principal difficulty with the etch-pit method was that of the many solutions for producing crystallographically oriented pits in unalloyed aluminum, none produced satisfactory pits with the high strength aluminum alloy plate. An appropriate solution was available for 2219-T37 from work on the effect of surface roughness, however, and toward the end of the contract period, some work was done with this alloy. The results substantiated the microscope observations that boundaries between grains of greatly different orientation tend to be preferred sites for crack initiation. An example is shown in Fig. 104, which shows two etch-pitted grains and a stress-corrosion crack on the intervening boundary. Figure 105 is a stereographic projection showing the orientation of the two grains relative to the boundary. These grains differ rather widely in orientation, the nearest cube poles being  $46^\circ$  apart.

In this example, there was no particular crystallographic relation between the grains that would be conducive to crack initiation other than the rather large difference in



orientation. In the limited number of cases investigated, this has been found to be generally true. This suggests that increasing atomic mis-match at a grain boundary promotes crack formation.

#### Effect of Stress

The effect of stress on crack initiation phenomena was investigated for 2219, 7075, 7079, and 7039 alloys. The tests included evaluations of stress level, stressing direction and in some cases, combinations of the two. The "standard" environments were used, namely, the NaCl-AlCl<sub>3</sub> solution at pH 1 for 2219, 7075 and 7079 alloys, and the NaCl-Na<sub>2</sub>CrO<sub>4</sub> solution at pH 2 for 7039. Certain tests made with 7039-T6 in other environments will be reported in a later section.

#### Stress Level

##### 2219 Alloy

With 2219 alloy a comparison was made between short transverse stresses of 75% and 90% YS, using both the T351 temper that did develop cracks and the T851 temper that did not. With 2219-T351, the number of cracks was fewer at 90% than at 75% (Figs. 106 vs. 46) but the cracks initiated and propagated more rapidly, and initiation sites and propagation paths were the same. At the 90% stress level more localized plastic deformation was visible in the vicinity of cracks.

With 2219-T851, increasing the stress to 90% produced intergranular crevices of the type seen at 75% YS (Fig. 50), but no true cracks initiated.

##### 7075 Alloy

With 7075-T6 at the 90% YS stress level, cracks initiated and propagated very rapidly and considerable plastic

deformation was noted in the vicinity of small cracks (Fig. 107). Initiation sites and propagation paths were the same as at 75% YS. With 7075-T73 only non-directional pitting developed, as was the case at 75% YS (Fig. 57).

In view of the fact that crack initiation times were shorter at the higher stress level, possible quantitative relationships were investigated with 7075-T6 specimens stressed to eight levels between 50 and 90% YS. A semi-logarithmic relationship was found (Fig. 108).

In addition to tests at very high stress levels, crack initiation near the threshold level was also investigated. Specimens from 7075-T6 plate stressed to 20, 15 and 10% YS were used because this material had shown failures at 15% YS in standard tests (Table V). At the 20% and 15% stress levels, cracks initiated in fairly short periods and were readily distinguishable from the intergranular and interfragmentary corrosion that also developed (Figs. 109 and 111).

With the 10% YS stress level, a few cracks formed but it would have been very difficult to distinguish them from crevices of intergranular corrosion except for the fact that they were exclusively oriented perpendicular to the stressing direction (Fig. 110) and were clearly apparent in cross section (Fig. 111). Cracks were much fewer at these lower levels than at the 75% stress level, presumably because cracks developed on only the most susceptible and most favorably oriented boundaries. The crack initiation sites and path and mode of propagation were the same as at the higher stress levels, except that no plastic deformation at crack tips was noted.

### 7079-T6 alloy

In tests of 7079-T6 stressed short-transversely to 90% YS, cracks initiated more rapidly than was the case at 75% YS, but the cracking sites and propagation paths were the same. Cracks initiated on boundaries, and frequently at constituent particles and clusters if they were present on boundaries (Fig. 112). Propagation occurred quite rapidly and along boundaries lying most nearly perpendicular to the stress (Figs. 112 and 113). In the cross section (Fig. 113), these paths were not particularly straight because the 7079-T6 plate was much thicker than the other plate items, and did not have as much structural elongation.

### 7039-T6 Alloy

Tests of 7039-T6 stressed short-transversely included stress levels of 90, 50 and 25% in addition to the 75% stress tests already described. As with the other alloys, cracking time was a function of stress level. Initiation time was a few minutes at 90% YS, several hours at 75% YS, 48 hours at 50% YS, and no cracks developed in 33 days at 25% YS in the NaCl-Na<sub>2</sub>CrO<sub>4</sub> solution at pH 2. Initiation sites and propagation paths were always on boundaries perpendicular to the stress at all stress levels. At the 50% and 75% stress levels, the boundary initiation sites were always at Mg<sub>2</sub>Si particles or at pits from which these particles had been dissolved. At 90% YS, initiation generally but not always occurred at these sites (Fig. 114 and Fig. 115 - top). Also, at this stress level, the ends of comparatively long cracks departed from the boundaries and entered the grains by either an interfragmentary or transgranular path (Fig. 115 - bottom). It was not

established whether these tiny cracks and branches from the main crack were stress-corrosion cracks or mechanical cracks developed by the stress concentration at this location.

To summarize the effect of stress level, crack initiation time and propagation rate were functions of stress level, but initiation sites and propagation paths were always on boundaries perpendicular to the stress. The only difference among alloys was with 7039-T6 alloy which showed a pronounced tendency for initiation at  $Mg_2Si$  particles on boundaries or at pits from which such particles had been dissolved.

#### Stressing Direction

In view of the difference in stress-corrosion behavior frequently encountered between the short-transverse and longitudinal directions of aluminum alloy plate, crack initiation in longitudinally stressed specimens was investigated. Tests were made only on materials that cracked in short-transverse tests. The tests used tuning-fork specimens exposed to the environments used previously for the various alloys.

With 2219 alloy stressed longitudinally, cracks initiated very rapidly and at the same location as in specimens stressed short-transversely, that is, on boundary segments oriented perpendicularly to the stress. These particular boundaries, however, would have blocked the progress of cracks initiated by short-transverse stress. As the exposure continued, the cracks in longitudinally stressed specimens grew very slowly if at all (Fig. 116), because they were blocked by unfavorably oriented boundaries.

With longitudinally stressed 7075-T6 samples, cracks also initiated very rapidly but propagated very slowly (Fig. 117). The cracks that did form were located on grain boundaries but since the grains were highly elongated in the rolling direction, only their ends were highly stressed by longitudinal stresses. In addition, the boundaries below the exposed surface were parallel to the rolling direction (Fig. 118). Thus, crack initiation and growth were doubly difficult, first because there were very few favorably oriented boundaries of appreciable length on the surface and, second, because most of these had an unfavorable orientation below the surface.

The effects of stressing direction were shown quite dramatically by a direct comparison of relatively large areas of stressed specimens at relatively low magnification. With short-transverse stress applied to 2219-T37 (Fig. 119), series of favorably oriented boundaries along the recrystallized grains were available and relatively long cracks developed easily. With longitudinal stress (Fig. 120), however, cracks also developed rapidly but continuity of optimum boundaries was not available and cracks remained short.

This effect was even more pronounced with 7075-T6 alloy because of its highly elongated, unrecrystallized grain structure. With short-transverse stress (Fig. 121), long cracks developed easily along boundaries. With longitudinal stress (Fig. 122), however, very few cracks developed even after long exposure. In this figure, some cracks will be noted parallel to the stressing direction. These were formed under the influence

of the low short-transverse stress associated with the biaxial stress condition. This emphasizes strongly the effect of grain configuration and stressing direction because a relatively low short-transverse stress developed more and larger cracks than a longitudinal stress several times greater in magnitude.

Further evidence of these effects was observed with X7375 alloy which has an almost equiaxed recrystallized structure. With short-transverse stress, cracks formed readily along the boundaries of the large grains (Fig. 123). With longitudinal stress (Fig. 124), boundary orientation was also quite favorable and cracks initiated and developed with almost equal ease.

To determine the effect of stress level with longitudinally stressed specimens, samples of 7075-T6 were exposed with a 90% YS stress. Behavior was identical to that at 75% YS, cracks initiating very rapidly but propagating only with great difficulty.

Electron microscope examinations were made of cracks in longitudinally stressed specimens of 7075-T6 and 2219-T37. Crack initiation and boundary penetration were the same as with short-transverse stress, cracks initiating at random sites on boundaries and propagating along a ragged intergranular front between grains. With the longitudinally stressed specimens, however, a number of cracks initiated on boundaries parallel to, or at a low angle to the stressing direction (Fig. 125). As explained previously, this was associated with the biaxial stress condition in the specimen and the ease of crack initiation under the much lower short-transverse direction stress.

The effect of stressing longitudinally was also investigated with specimens from the 7079-T6 plate using stresses

of 75 and 90% YS. As was the case with 7075-T6 alloy, small cracks initiated rapidly but propagated very slowly because favorably oriented boundary paths were not available.

A comparison was also made of 7039-T6 specimens stressed longitudinally and short-transversely to 75% and 90% YS and exposed to the NaCl-Na<sub>2</sub>CrO<sub>4</sub> solution. Results were different from those with all other alloys in that no cracks initiated with longitudinal stresses in periods up to two months. In contrast, cracks initiated in periods of a few minutes at 90% YS and a few hours at 75% YS with short-transverse stresses. This difference could not be explained because boundary segments perpendicular to the longitudinal stress were available, and the same Mg<sub>2</sub>Si constituents and pits from which these particles had been dissolved were present.

In summary, and with the possible exception of 7039-T6, the effect of stressing direction on stress corrosion behavior is related not to the ability to initiate cracks, but to the ability of cracks to propagate. This, in turn, is controlled by boundary configuration with respect to the stressing direction and the availability of continuous crack-susceptible paths perpendicular to the stressing direction.

#### Effect of Surface Roughness

Investigation of the effects of surface roughness was divided into three phases

1. Individual topographical irregularities
2. Pre-corrosion
3. Mechanical Roughness

### Individual Topographical Irregularities

The effects of both chemically produced and mechanically produced irregularities were evaluated. The former were produced by etch pit techniques and would simulate pits developed during the initial stages of a corrosion exposure. Pits have been claimed to be crack initiation sites generally, and were found to be such sites in 7039-T6 when they developed on boundaries. The etch pits were produced with a basic solution of 100 ml distilled water and 100 ml ethanol saturated with NaCl, to which was added 30 ml each of HCl and HNO<sub>3</sub> for 2219 alloy specimens, and 4cc HF for 7075 and 7039 alloy specimens. The solution temperature was 60°F for 2219, and 45°F for 7075 and 7039. Specimens were held with nichrome tongs to introduce a slight galvanic effect.

In evaluating the effect of etch pits, tests were made with 2219-T37, 2219-T87, 7075-T6 and 7075-T73 specimens exposed to the NaCl-AlCl<sub>3</sub> solution at pH 1, and with 7039-T6 specimens exposed to the NaCl-Na<sub>2</sub>CrO<sub>4</sub> solution at pH 2. Short transverse stress of 75% YS was used.

No evidence was found that the etch pits had any effect on crack initiation with any material. In crack-susceptible alloys, cracks initiated in times similar to those required for unpitted specimens, and no cracks initiated in crack-resistant alloys. When cracks did initiate, they were associated with pits only when the pits were on boundaries. Also, cracks formed in similar periods and in a similar manner on unpitted boundaries. Typical areas on a 2219-T37 specimen are shown in Fig. 126. In the field to the left, only one pit is



associated with a stress-corrosion crack, and this pit is at the end of the crack and does not appear to be its initiation site. In the field to the right of Fig. 126, a crack has progressed through a number of pits on a boundary, but pits on other boundaries have not initiated cracks. It is concluded, therefore, that the pits were not a significant factor in crack initiation.

The mechanically produced irregularities were made with a diamond marker on a metallograph and were of two types. One was a "punch mark," developed by bringing the marker into light contact with the surface of the stressed specimen. The other type consisted of scribe marks developed by establishing contact between marker and specimen surface and then moving the specimen with the microscope stage. Scribe marks of various depths were made both parallel to and perpendicular to the stressing direction. Specimens of 2219-T37 and 7075-T6 were used, with short transverse stress of 75% YS and exposure to the NaCl-AlCl<sub>3</sub> solution at pH 1. Cracking occurred in the same manner as with polished specimens and apparently without regard to the mechanically produced irregularities. Cracks always initiated at boundaries but neither sought out nor avoided the mechanical irregularities. Occasionally a crack initiated within a scribe mark but other cracks formed elsewhere with equal ease. Occasionally a crack would propagate along a scribe mark, but it would do so only when the boundary followed the mark, and would deviate from the mark to follow the boundary. A typical field on a 7075-T6 specimen is shown in Fig. 127. As seen in the upper

micrograph, numerous cracks have formed, all perpendicular to the stressing direction and unaffected by the vertical scribe marks. Two of the cracks appear to have developed from the ends of the horizontal scribe marks. As shown by the lower micrographs, however, the cracks followed boundaries, and were associated with the scribe marks only because the scribe marks were on or close to boundaries. Thus, it is concluded that small, mechanically produced surface irregularities are not a significant factor in crack initiation.

#### Pre-Corrosion

In evaluating the effects of pre-corrosion on crack initiation, tuning-fork specimens of the stress-corrosion-susceptible alloys 2219-T37 and 7075-T6 were exposed unstressed in the NaCl-AlCl<sub>3</sub> solution at pH 1 until well-defined intergranular fissures developed. The specimens were then washed thoroughly, stressed short-transversely and re-exposed to the NaCl-AlCl<sub>3</sub> solution.

The specimens were first examined before the final exposure because difficulty was foreseen in differentiating between intergranular corrosion crevices widened by corrosion and true stress-corrosion cracks. In experiments with 7075-T6 stressed to 90% YS after corrosion, stressing widened the corrosion crevices perpendicular to the stress, and only those perpendicular to the stress. The resulting crevices looked exactly like the stress-corrosion cracks developed by direct exposure of similar specimens (Fig. 128). This is very important because it points out quite strikingly that intergranular corrosion

crevices later widened by stress could be mistaken for stress-corrosion cracks.

The final step in the sequence was to re-expose the samples. This was done with 7075-T6 samples stressed short-transversely to 75% YS. Comparing the same areas before and after the stress-corrosion exposure, it was obvious that the cracks extended quite rapidly by a stress-corrosion mechanism. It was impossible, however, to distinguish between the widened-corrosion-crevice and stress-corrosion portions of the final crack. Two areas, before and after the stress-corrosion exposure are shown in Fig. 129.

#### Mechanical Roughness

In evaluating the effect of fine, mechanically-produced surface roughness, tuning-fork specimens of 2219-T37 and 7075-T6 were taken through the 3-0 metallographic paper grinding operation, some with the grinding marks parallel to the longitudinal direction, and others with the marks parallel to the short-transverse direction of the structure. With unstressed specimens exposed to the NaCl-AlCl<sub>3</sub> solution at pH 1, it was very difficult to observe the corrosion paths (Fig. 130) because (1) the grinding marks were the most prominent features at the high light-microscope magnifications used, and (2) because the plastic deformation associated with the grinding apparently altered the microstructure. With tuning-fork specimens stressed short-transversely to 75% YS, cracking was not observed until a period well beyond that required for obvious cracking in polished specimens (Figs. 131 and 132). When cracks did become visible, it

was impossible to establish their paths because of the gross roughness of the ground surface. The delay in apparent cracking was undoubtedly caused to some degree by the masking effect of the roughness.

Examinations of sections of the specimens showed that cracks were actually well-developed when they were first visible under the microscope, indicating that crack initiation had occurred at an earlier time. The cracks at the ground surface were not of the fine intergranular type but consisted of wide crevices, generally intergranular, from which fine intergranular cracks emanated (Fig. 133). Thus, fine mechanical surface roughening altered crack initiation in a shallow layer at the surface, and may have delayed cracking while this layer was being penetrated. Once this region was breached, however, cracking proceeded in a normal manner.

#### Effect of Surface Film

Investigation of the effects of surface film on crack initiation involved natural films and films produced both electrochemically and chemically. The effects of the natural oxide film were noted throughout the contract work. Natural films that formed between final metallographic polishing and exposure of stressed specimens had a pronounced effect on the time required for crack initiation, making it essential to control very carefully this time interval. Also, interruptions in an exposure for making micrographs delayed the resumption of crack propagation. In no case, however, was there any change in either the sequence of events or the mode of cracking.

In a quantitative evaluation of the effect of natural film on crack initiation, a series of stressed 7075-T6 specimens was prepared and exposed to the atmosphere for various periods prior to exposure in the NaCl-AlCl<sub>3</sub> solution at pH 1. With delay times of 1, 5, 15 and 60 minutes, corresponding times for crack initiation were 1, 7, 19 and 26 minutes. This relationship is strikingly similar to that for the formation of natural films on aluminum. This suggests that, in the absence of film, cracking should start almost instantaneously and that the "incubation period" prior to crack initiation is the time required for the corrosion environment to dissolve or penetrate the film. Support for this hypothesis is the fact that with the specimen in which cracks initiated in seven minutes, no changes in the surface were observed in the first six minutes. From the metallurgical and stress-corrosion viewpoint, it seems quite unreasonable that everything should happen during the seventh minute. On the other hand, it seems very reasonable that six minutes might have been required for the corroding environment to dissolve or penetrate the air-formed film. This, in turn, suggests that the effectiveness of various environments in promoting or preventing stress-corrosion cracking may be controlled, at least in part, by their ability to form or dissolve surface films.

Another phase of this work involved investigation of the effects of different thicknesses of barrier-type oxide formed anodically on 7075-T6 and 2219-T37 alloys. Films were applied in an ammonium tartrate solution at pH 5.5, and thicknesses of 85 (6V), 250 (18V) and 750 Å (54V) were evaluated. During film

formation, the microconstituents and boundary precipitate particles were generally dissolved out, leaving pits of a corresponding size both within the matrix and at boundaries (Fig. 134).

The anodic barrier films delayed crack initiation but not for times proportional to film thickness or for times as long as observed with natural films. The crack initiation mechanism was the same as with as-polished specimens, however, cracks starting either at random sites or at pits on boundaries and progressing along boundaries perpendicular to the stress (Fig. 134). The fact that cracking time was not proportional to film thickness suggests that the film is thinner or weaker than normal at the boundaries. This was confirmed by electron microscope examinations which showed film weakness at boundaries where the precipitate particles had been dissolved out or converted to a porous type of oxide. Similar behavior was noted with the constituent particles and dispersoids but this was not significant because cracks did not initiate at these locations.

Electron microscope examinations were made, using the double-oxide replica technique, to study the effect of barrier oxide films on crack initiation and on the propagation of cracks formed before application of the oxide film. These examinations confirmed the findings from light microscope work in that there appeared to be a delay in crack development which presumably represented the time required for the environment to breach the barrier oxide film. Oxide breakdown occurred more readily at boundaries and at constituents but only the boundary breakdown

led to crack initiation. Boundary pitting through the oxide was associated with crack development but did not appear to be an essential condition for crack initiation.

With cracks existing before application of the first barrier film, some did not propagate, although there was no indication that the oxide film prevented propagation. Other cracks propagated by breaching the oxide and proceeding along the same paths they had followed before the oxide film was applied. With some of these, the breach was small and the crack developed from this location as a focal point, but the majority developed along a fairly broad front (Fig. 135).

The effects of three other films on crack initiation in stressed tuning-fork specimens of 2219-T37 and 7075-T6 were also evaluated. One was a chemically-formed phosphate film applied by boiling for two minutes in a 2%  $\text{NaH}_2\text{PO}_4$  solution at pH 7. Other work at these laboratories has shown that a film of this type can delay or prevent attack of aluminum surfaces. The other two films were of the anodic barrier type and were formed to a thickness of about 250 Å by forming at 18 volts. One was formed in the 2%  $\text{NaH}_2\text{PO}_4$  solution at pH 7, the other in a 3%  $\text{CrO}_3$  solution adjusted to pH 7 with  $\text{NH}_4\text{OH}$ .

With the chemically-formed phosphate film, crack initiation was delayed with 2219-T37 but no effect was noted with 7075-T6, cracks developing very rapidly. With the film formed anodically in the phosphate electrolyte, cracking of 2219-T37 was again delayed appreciably, but crack initiation in 7075-T6 was

about as rapid as without the film. With the anodic film formed in the chromate solution, crack initiation was considerably delayed with both alloys, possibly as a result of inhibition by the chromate ion. With all films, the crack initiation sites and the cracking mechanism appeared to be the same as with samples without the films.

This work led to three conclusions:

1. The presence of the films had no effect on crack initiation sites or the cracking mechanism.
2. The films themselves could delay but could not prevent crack initiation. The delays presumably represented the time required for the corroding environment to breach the surface film.
3. The pits developed during film formation had no noticeable effect on crack initiation sites or the cracking mechanism.

#### Effect of Environment

The evaluation of the effect of environment on crack initiation in high strength aluminum alloys was divided into two sections. First, standard stress-corrosion tests of specimens from 2219 and 7075 alloy plate were conducted in a wide variety of aqueous solutions. From these screening tests, appropriate environments were then selected for further studies involving the observation and analysis of crack initiation.

#### Screening Tests

The materials used in the screening tests were 4" thick 2219-T37 and 2" thick 7075-T651 commercially fabricated plate. Prior tests had shown that these items were susceptible



to stress-corrosion cracking in the 3.5% NaCl alternate immersion test when stressed in the short-transverse direction. Portions of these two plate alloys were precipitation heat treated in the laboratory to the stress-corrosion-resistant 2219-T87 and 7075-T7351 tempers. Short-transverse tensile specimens, 0.125" diameter and 2" long, were machined from each item and were stressed to 75% YS in the "constant-strain" type stressing frame shown in Fig. 136. Stressed and unstressed specimens were exposed to the various solutions in covered dishes containing one liter of solution and maintained at 80-85 F. Tensile tests were made of unstressed specimens at periods corresponding to stressed specimen failures, and of all specimens remaining at the end of the 60-day test.

The test results are summarized in Tables XI-XIV. The specimen performance in representative types of electrolytes is illustrated graphically in Figs. 137-140.

#### 7075-T651 Alloy

Stress-corrosion cracking occurred principally in solutions that caused intergranular attack of both unstressed and stressed specimens. The pH of the solution was an important factor. In neutral solutions, stress-corrosion cracking or acceleration of corrosion due to applied stress occurred only in solutions containing chloride and bromide anions. No stress-corrosion cracking or evidence of stress corrosion was detected in neutral solutions of the following sodium salts: sulfate, nitrate, phosphate, iodide, fluoride and chromate. The propensity for intergranular attack and stress-corrosion cracking in the various solutions was markedly increased when they were acidified .

to pH 2. Under these conditions stress-corrosion cracking occurred in the following additional solutions of the sodium salts: iodide, fluoride, sulfate and acetate (pH 4). No stress-corrosion cracking was encountered with acidified nitrate, phosphate and chromate solutions.

#### 2219-T37 Alloy

Stress-corrosion cracking of 2219-T37 alloy, like 7075-T651 alloy, occurred in aqueous solutions which caused intergranular corrosion. There appeared to be no acceleration of corrosion due to stress in those solutions which did not support intergranular corrosion.

Susceptibility to intergranular corrosion and stress-corrosion cracking was most evident in solutions containing chloride ions, especially when such solutions were acidified to pH 2. Acidification with oxidizing acids or the addition of an oxidizer such as  $H_2O_2$  stimulated intergranular attack in chloride solutions. No stress-corrosion cracking was noted at either pH 2 or pH 7 in sodium salts of such anions as bromide, fluoride, nitrate, sulfate, phosphate, chromate, acetate or bicarbonate. Test results in solutions of the ammonium salts were generally similar to those observed with the sodium salts. There appeared to be a slight tendency for intergranular corrosion to occur in acidified (pH 2) solutions of  $Na_2SO_4$ , but no stress-corrosion cracking or acceleration of attack due to stress was observed in these solutions. The addition of an oxidizer such as  $H_2O_2$  to a solution of  $Na_2SO_4$  caused some susceptibility to stress-corrosion cracking, but the probability of failure in such solutions appeared to be low.

In analyzing the test results obtained in certain of the more aggressive solutions, considerable difficulty was encountered in determining whether failures had resulted from stress-corrosion cracking or from severe localized corrosion. This was particularly true when failure times were long (1-3 weeks), unstressed tensile losses were high, and corrosive attack was of the severe general intergranular type. In such cases, the long failure times may be related to the limited elastic strain energy of the stressing frame, as discussed by Lifka and Sprowls.<sup>(6)</sup> Instances in which there was doubt as to the mode of failure are noted in Tables XI and XII, and were investigated further in supplemental tests described below.

2219-T87 and 7075-T7351

No evidence of stress-corrosion cracking was detected in specimens of either alloy in any of the solutions tested. A few failures occurred in highly corrosive solutions but the type of attack in each was substantially or exclusively pitting. It was concluded that the failures were the result of severe localized corrosion and not stress-corrosion cracking.

The most corrosive solutions were those containing sodium chloride either alone or in combination with other sodium salts and acidified to a pH 2. Severe corrosion with some failures, principally in 2219-T87 specimens, also occurred in the acidic solutions of bromide and iodide anions. Acidic solutions of sulfate anions caused severe corrosion of the 7075-T7351 specimens but only mild corrosion of the 2219-T87 specimens. Acidified solutions of other sodium salts (fluorides, nitrates, chromates and phosphates)

caused only mild corrosion of either alloy. Neutral solutions of the various sodium salts were not highly corrosive and caused no failures. However, the addition of  $H_2O_2$  stimulated corrosion and induced failure of both alloys in a neutral NaCl solution, and 7075-T7351 in a neutral sulfate solution. The only other failures in neutral solutions occurred after 44-60 days exposure, with 7075-T7351 specimens in  $NH_4Cl$  and with both alloys in NaCl plus  $Na_2SO_4$ .

The fact that the corrosion patterns in the acidified chloride solutions were so varied emphasized that visual ratings of corrosion damage can be very misleading. Four samples having greatly different visual ratings, but all having sustained high loss in strength from corrosion are shown in Fig. 141. Cross sections of the samples having the best and worst visual corrosion ratings (Figs. 142-143) reveal the true severity of the corrosion.

#### Supplemental Tests in pH 2 Solutions

In view of the questions regarding failure mode in certain highly acid media, supplemental tests were made. These involved the tensile testing and metallographic examination of specimens removed from test at several intervals. The objective was to determine whether corrosion was accelerated by stress, which is a prime indicator of stress corrosion. The test results are given in Tables XV and XVI.

With 2219-T37 and 7075-T651 alloys in the sodium chloride solutions, the corrosion initiated as fine intergranular attack. The losses in strength of stressed specimens of both alloys were significantly higher than those of corresponding unstressed

specimens (Figs. 144 - top and 145 - top) thereby indicating a marked accelerating effect of stress. It was concluded that the failures in these solutions were the result of stress-corrosion cracking. With 7075-T651 in the acidified sodium sulfate solution, corrosion was primarily of the pitting type, but there was some acceleration of corrosion by stress. Thus, there was still some doubt that the failures were of the stress-corrosion variety.

Corrosion of both 2219-T87 and 7075-T7351 alloys was exclusively pitting. Application of stress did not affect the rate of corrosion of 2219-T87 in the acidified NaCl solution (Fig. 145 - bottom) and only slightly accelerated that of 7075-T7351 in this solution (Fig. 144 - bottom). In the other solutions, no significant effect of stress was noted. This confirmed previous conclusions that the failures were the result of severe localized corrosion rather than stress-corrosion cracking.

Electrolytes Containing Certain Cations  
and Alkaline Solutions at pH 11-11.5

Eight electrolytes were selected for this phase of the screening tests. The solutions involved are listed in Table XVII, together with the results of stress-corrosion tests.

Stress-corrosion cracking of 2219-T37 and 7075-T651 alloy specimens occurred in acidic (pH 2) and neutral (pH 7) solutions of calcium chloride. Failures were also encountered with 2219-T87 and 7075-T7351 specimens, but metallographic examination revealed no evidence of stress-corrosion cracking. Both tempers of each alloy corroded very rapidly in ferric chloride (pH 1.5), cupric chloride (pH 2) and sodium hydroxide (pH 11.5)

electrolytes, but no stress-corrosion failures developed. In the cupric chloride solution, there was an immediate deposition of copper over the entire specimen surface with subsequent rapid attack that necessitated removal of the test specimens after 10-30 minutes exposure.

In the cupric sulfate solution at pH 2, deposition of copper also occurred but corrosion was not as rapid and stress-corrosion cracking developed in 2219-T37. Failures were also encountered with 7075-T651 and T7351 specimens, but metallographic examination revealed no evidence of intergranular attack or stress-corrosion cracking. High tensile losses of unstressed specimens of 7075-T7351 indicate that those failures were due to localized corrosion, but the somewhat lower losses of unstressed specimens of 7075-T651 suggest that stress-corrosion may have been responsible for the failure of the T651 specimens. There is still some doubt about this, however, just as in the case of the  $\text{Na}_2\text{SO}_4$  solution with pH 2 (page 79). Further investigation of the mechanism of these failures is described below in the section on stress-corrosion crack initiation in selected environments.

In the ammonium hydroxide electrolyte (pH 11) stress-corrosion cracking occurred only with the 7075-T651 specimens. In sodium chloride solutions of similar alkalinity (pH 11), stress-corrosion cracking occurred with both the 2219-T37 and 7075-T651 specimens. Failures also occurred with 2219-T87 and 7075-T7351 specimens, but these failures were the result of severe local pitting.

The results of these environmental tests have amply demonstrated that the susceptibility of aluminum alloys to

stress-corrosion cracking depends not only upon the alloy and temper, but also to a high degree upon the environment. It should be cautioned that these screening tests were not prolonged sufficiently that the absence of failures of a given alloy and temper in a specific solution justifies conclusions to the effect that the alloy and temper is immune to stress-corrosion cracking in that solution. Particularly in the less corrosive solutions it is possible that a more extended exposure might result in stress-corrosion cracking. It also is noteworthy that slightly changed test conditions could change the susceptibility of an alloy in a specific solution. For example, Hollingsworth and English<sup>(6a)</sup> found in tests similar to these that 7075-T651 did not stress corrosion crack in 1N NaNO<sub>3</sub> (pH 2) in a 45 day exposure, at 72 or 113 F, but did crack within 20 to 40 days when the temperature was raised to 153 F. Such variations in behavior are by no means peculiar to aluminum alloys, for a similar environmental dependency is well illustrated in the literature for other alloy systems.

#### Selected Environments

From the many solutions evaluated in the environmental screening tests, two groups of five each were selected for crack initiation studies with the light microscope. One group was selected for 7075-T6 and 2219-T37, and included solutions in which both definite and questionable stress-corrosion failures had occurred. The other group, chosen for 7075-T73 and 2219-T87, included three solutions in which acceleration of corrosion by stress had suggested the possibility of stress corrosion, one solution that produced considerable corrosion but no failures, and

one solution producing little corrosion and no failures. Tuning-fork specimens from plate used for previous tuning-fork tests were stressed to 75% YS in the short-transverse direction for these tests. The primary objective was to determine the effect of environment on crack initiation and propagation. A secondary objective was to establish whether certain screening test failures were the result of stress-corrosion cracking or excessive localized corrosion.

7075-T6 and 2219-T37

The solutions selected and the failure times in the screening tests were:

<u>Solution</u>	<u>pH</u>	<u>Adjusted With</u>	<u>Failure Times - Days</u>	
			<u>7075-T651</u>	<u>2219-T37</u>
1N NaAc	4	HAc	4,6,13	---
1N Na <sub>2</sub> SO <sub>4</sub>	2	H <sub>2</sub> SO <sub>4</sub>	39*,40*,47*	OK-60
0.5N NaCl + 0.5N Na <sub>2</sub> CrO <sub>4</sub>	2	HCl	8,10,19	1,1,OK-60
4N NaCl + 0.5N KNO <sub>3</sub>	0.4	HNO <sub>3</sub>	1,1,1	1,1,1
0.5N NaCl + 0.5N Na <sub>2</sub> SO <sub>4</sub>	2	H <sub>2</sub> SO <sub>4</sub>	2,2,3	No Test

\*SCC questionable (Tables XI, XV)

With 7075-T6 in the 1N NaAc solution at pH 4, only slight pitting and no cracking was observed in periods up to six days (Fig. 146) which is in direct contrast to the screening test failures. This anomaly was explained by additional tests which will be described at the end of this section.

In the 1N Na<sub>2</sub>SO<sub>4</sub> solution at pH 2, stressed 7075-T6 sustained general corrosion initially and, after longer periods, developed crevices that proved to be selective attack along grain.



boundaries perpendicular to the stress (Fig. 147). It was concluded that this alloy showed a borderline susceptibility to stress-corrosion cracking in this environment, which is in agreement with tests by Hollingsworth and English<sup>(6a)</sup> involving different temperatures. With 2219-T37 in this environment, some wide, shallow attack at boundaries occurred but no cracks developed. This is in agreement with screening test results.

In the 0.5N NaCl + 0.5N Na<sub>2</sub>CrO<sub>4</sub> solution at pH 2, only pitting attack and no cracking developed during a 21-day exposure, which is contrary to screening test results. This anomaly was also explained by additional tests to be described shortly. With 2219-T37 in this environment, cracks initiated and propagated rapidly along grain boundaries generally perpendicular to the stress (Fig. 148). Initiation sites and propagation paths were the same as in the NaCl-AlCl<sub>3</sub> solution at pH 1.

With the 4N NaCl + 0.5N KNO<sub>3</sub> solution at pH 0.4, both alloys developed intergranular stress-corrosion cracks very rapidly. These cracks initiated at pits and random sites on boundaries perpendicular to the stress and propagated along these same boundaries (Figs. 149-151).

In the 0.5N NaCl + 0.5N Na<sub>2</sub>SO<sub>4</sub> at pH 2, intergranular cracks initiated and propagated on boundaries perpendicular to the stress as typified by the micrographs of the 7075-T6 specimen seen in Figs. 152-153. In this particular area, the preference for crack formation on boundaries between grains of different orientation is again illustrated. As the cracks propagated inward with this specimen, cracks selected grain boundaries perpendicular to the

stress wherever possible, but on rare occasions when such boundaries were not available, the crack would follow an inter-fragmentary path (Fig. 153).

In view of the disagreement between screening and tuning-fork tests of 7075-T6 in the 1N NaAc (pH 4) and 0.5N NaCl + 0.5N Na<sub>2</sub>CrO<sub>4</sub> (pH 2) solutions at 75% YS, additional specimens were run at a stress of 90% YS. Results were the same as at the lower stress, with occasional broad, shallow pitting on boundaries but no cracking. The environmental screening type of test was then repeated using samples from the lot of plate used for the tuning-fork tests. With both environments, no stress-corrosion cracks were encountered, indicating that both the screening and tuning-fork tests were accurate. Since cracking developed in specimens from both lots of material in other environments, including the 3.5% NaCl alternate immersion test, it was concluded that these environments were of the "borderline" type and that further investigation would be required to evaluate fully these alloy-environment combinations.

#### 7075-T73 and 2219-T87

The environments selected for microscope work with 7075-T73 and 2219-T87, and the results of screening tests were:

<u>Solution</u>	<u>pH</u>	<u>Adjusted With</u>	<u>Failure Times* - Days</u>	
			<u>7075-T7351</u>	<u>2219-T87</u>
1N NaCl	2	HCl	18,18,22	54,54,54
1N NaCl	2	H <sub>2</sub> SO <sub>4</sub>	2, 2, 4	8, 9, 9
1N KHF <sub>2</sub>	1.5-2.0	--	OK 60	OK 60
1N NaBr	2	HBr	OK 60	--
1N NaCl	2	CrO <sub>3</sub>	--	16,21,OK 60

\*All failures considered to be the result of severe localized corrosion

With the 7075-T73 and 2219-T87 tuning-fork specimens, only a pitting type of attack developed and nothing even remotely resembling a crack appeared. The attack of the various alloy-environment combinations has been described and illustrated in previous reports on this contract but, since this information is not pertinent to crack initiation, it is not included here. The conclusion drawn from this phase of the work was that the screening test failures with these alloys and environments were the result of excessive localized corrosion and not stress-corrosion cracking.

7039-T6

Although investigation of environmental effects with 7039-T6 was not planned initially, developments during the crack initiation studies led to a very limited study of the effect of environment. The first of these occurred when original plans to test all alloys in the NaCl-AlCl<sub>3</sub> solution at pH 1 were carried out on 7039-T6. Despite the fact that the plate selected had poor resistance to stress corrosion in standard tests, no cracks initiated in tuning-fork specimens. Tests of another lot of plate, judged to have very poor resistance to stress corrosion, yielded similar results, that is, considerable general corrosion but no cracks. It was concluded that this was another instance of the likelihood of cracking decreasing with an increase in the amount of general corrosion. The change was then made to the NaCl-Na<sub>2</sub>CrO<sub>4</sub> (pH 2) solution which produced very little general corrosion but did induce cracking.

To verify the apparent absence of cracking in 7039-T6 in solutions producing severe general corrosion, tuning-fork

specimens stressed short-transversely to 75% YS were exposed to the 4N NaCl + 0.5N KNO<sub>3</sub> solution at pH 0.4. This solution had been highly corrosive to 7075-T6 and 2219-T37 but had produced cracks with extreme rapidity. In the case of 7039-T6, general corrosion occurred but no cracks developed, as was the case with the NaCl-AlCl<sub>3</sub> (pH 1) solution which also produced general corrosion.

The other incident that led to further investigation of environmental effects with 7039-T6 was the fact that stressed specimens awaiting exposure developed cracks in the laboratory atmosphere. Examinations of specimens stressed to 75% YS in the short transverse direction revealed crack initiation in less than a week. Cracks initiated at Mg<sub>2</sub>Si particles situated on grain boundaries and propagated along grain boundaries perpendicular to the stress (Figs. 154-155). No cracks initiated at Mg<sub>2</sub>Si particles that were not on boundaries. This persistent tendency for initiation at Mg<sub>2</sub>Si particles is contrary to the behavior of other 7XXX alloys that also contain such particles.

Electron fractographic examinations of cracks formed in air revealed cubic pitting on the specimen surface and at the start of the crack. This pitting probably occurred after the formation of the crack because the crack surface generally had a faceted appearance (Fig. 156). Some evidence of plastic deformation was observed (Fig. 157). This deformation may represent mechanical blunting of the crack tip, or possibly mechanical crack growth. The stress-corrosion crack front had a finely scalloped appearance, with a series of similar markings nearby (Fig. 158), indicating intermittent crack propagation."

Further environmental effects were noted when additional tests in laboratory atmosphere produced no cracking. The reason was that the laboratory atmosphere had changed with a change in season. With tests run in August, when the laboratory atmosphere was 90-95 F and 50-75% relative humidity, cracks had initiated in about five days. In October, when the laboratory atmosphere was 70-75 F and 25-40% R.H., no cracks initiated in 21 days.

In a brief investigation of other atmospheric effects, samples were run at room temperature (70-75 F) and 100% R.H. Cracks did not develop during a three-week exposure. Next, tests were run at 125 F and 100% R.H. Cracks initiated quite rapidly at constituent particles and propagated along boundaries perpendicular to the stress (Fig. 159). This environment was not satisfactory because condensate caused excessive corrosion of and adjacent to all constituent particles. With the numerous pits, cracks often initiated at several sites along a boundary (Fig. 159) with these cracks later joining to form a major crack.

Finally, atmosphere at 100 F and 90% R.H. was evaluated. This combination proved to be satisfactory for crack initiation studies of 7039-T6. With tuning fork specimens stressed short-transversely to 75% YS, attack of the polished surface was confined to a darkening of the  $Mg_2Si$  particles. Cracks initiated at these particles and propagated along boundaries perpendicular to the stress (Fig. 160), as they had done in all other exposures of this alloy. While the  $Mg_2Si$  particles were focal points for crack initiation, they appeared to have no effect on propagation rate or path.

The results of the environmental tests have demonstrated that environment is a very important factor in determining whether a stress-corrosion crack will form. With combinations of alloy and environment that will initiate a crack, however, the environment has no apparent effect on the crack initiation mechanism, the cracking sites or the propagation paths.

#### Effect of Pre-Corrosion

Since crack initiation in 7039-T6 has occurred at constituent particles that have been attacked by the environment, it might be concluded that the time required for crack initiation was that required to develop a pit by constituent attack. To test this hypothesis, samples that had been exposed to the atmosphere until the  $Mg_2Si$  particles were attacked, were subsequently exposed to the  $NaCl-Na_2CrO_4$  solution at pH 2. Crack initiation time was about the same as with samples that had not been pre-corroded. This indicates that crack initiation time is not merely the time required for pit development. It might also be concluded that the pit is not a prerequisite for cracking, but is merely the preferred site because the stress is somewhat higher at the pit. Such a conclusion is somewhat questionable, however, because cracks in other alloys having  $Mg_2Si$  particles did not initiate at these particles.

#### Effect of Stress

The effect of stress level was also evaluated with 7039-T6 exposed to several indoor atmospheric environments. When no cracks developed at 75% YS in a three week exposure in air at 70-75 F and 100% R.H. other specimens were run at 90% YS. Cracks

initiated in 15 days at the usual sites. With the 125 F and 100% R.H. atmosphere, specimens were exposed at stress levels of 90%, 75% and 50% YS. Crack initiation time was a function of stress level but initiation sites and propagation paths were not affected by stress level. With laboratory air at 100 F and 90% R.H., tests were made at 75%, 50%, 25% and 10% YS. At 75% YS cracks initiated in ten hours and at 50% YS cracking required 50 days, the initiation sites and propagation paths being the same. At the lower stresses, no cracks developed in 90 days.

In tests of 7039-T6 exposed to air at 100 F and 90% R.H., the effect of stressing direction was also evaluated. In the short-transverse direction a stress of 75% YS initiated cracks in ten hours. With similar longitudinal stress, no cracks initiated in 90 days. This again emphasizes the extreme effect of micro-structural configuration with this alloy.

#### Electrochemical Effects

The investigation of electrochemical effects related to crack initiation was not started until the last half-year of the contract and, since an entirely new approach was being taken, much of the program was generated as the work progressed. This combination of circumstances did not permit completion of this phase of the work. Results that were obtained, however, were most informative and confirmed the validity of the approach for investigating crack initiation phenomena.

The traditional approach to the electrochemical measurement of conditions prevailing at and near grain boundaries has been to paint out either the boundary regions or the grain

centers and make measurements of the remaining area. This could not be done with the 7075 and 7039 alloy plate used in this contract because these materials were unrecrystallized, because the boundaries on which cracks initiated were only visible at high microscope magnifications, and because the boundary region involved in cracking was extremely narrow. Therefore, a method was devised for simulating in sheet materials the conditions prevailing within grains and grain boundary regions of 7075-T6 and 7039-T6 plate.

This simulation was made on the basis used in the calculations of grain boundary compositions, namely, that the slower cooling rate prevailing as thick plate is quenched through the critical temperature range permits the diffusion of solute from a region adjoining the boundary and the development of precipitate on the boundary. Assuming that the entire grain is at equilibrium at a heat treating temperature of 870 F, the composition of any solute-depleted boundary region will correspond to equilibrium conditions at some temperature below 870 F. On this basis, compositions corresponding to various degrees of solute depletion in grain boundary regions were obtained by heat treating 0.025" sheet to equilibrium at various temperatures and quenching rapidly to retain the "depleted" conditions. For 7075 alloy, the temperatures selected were 870, 810, 750, 715, 680, 610 and 550, the latter five of which are in the temperature range that is critical during quenching. After quenching, portions of the samples were given the standard T6 and T73 aging treatments to simulate compositions in depleted boundary regions in these tempers. For 7039 samples, heat treating temperatures of 870, 750, 680 and 550 F were used, and only T6 aging was employed.



Solution potential measurements were made of unstressed specimens, and some specimens stressed to 75% YS, in solutions in which cracks did and did not initiate in tuning-fork specimens taken from plate of the same alloys. The solutions used were (1) 1N NaCl + 0.21N AlCl<sub>3</sub> at pH 1, which initiated cracks in 7075-T6, (2) 0.5N NaCl + 0.5N Na<sub>2</sub>CrO<sub>4</sub> at pH 2, which initiated cracks in 7039-T6 but not in 7075-T6, and (3) 0.5N Na<sub>2</sub>CrO<sub>4</sub> at pH 2, which did not initiate cracks in 7039-T6.

In addition to the solution potential measurements, current flow measurements between selected couples were made because current as well as potential difference has a bearing on crack initiation and development. Measurements were made on (1) couples of the same alloy heat treated at different temperatures, both unstressed and stressed, to estimate possible current flow between grains and depleted boundary regions, and (2) stressed and unstressed samples of the same material to determine the effect of stress on potential. The solutions used were those described above for potential measurements.

The preparation of specimen surfaces was the conventional metallographic polish, with the time between polishing and measuring standardized at ten minutes. With unstressed specimens, an electrical lead was percussion welded to the specimen after polishing and the back surface and edges were masked off. Specimens to be stressed were initially cut 1/2" wide by 2" long, and were then cut to a pre-determined length before polishing. A lead was then attached, masking was applied and the specimen was finally sprung into a special plastic fixture.

The plastic fixture was one used for other stress-corrosion contract work conducted at these laboratories<sup>(7)</sup> and is a block of plastic 10" long by 5/8" wide by 1" high with a slot 1.75" long and 1/4" deep cut into one 10" x 5/8" face. The appropriate stress is induced in the specimen by cutting to specific lengths greater than the span of the fixture. The specimen lengths required were calculated from curves derived by Haaijer and Loginow<sup>(8)</sup> for the stressing of bent beam specimens. These curves related stress, modulus, span length and specimen length. Values were taken from these curves and were plotted as the relationship of stress to specimen length for the particular materials and stressing fixture (Fig. 161).

#### 7075 Alloy

The tensile tests of 7075 alloy specimens, which were made primarily as a basis for the stressing of specimens, yielded very interesting information (Table XVIII). Of particular interest were the yield strength values for 7075 which are plotted in Fig. 162. The values for the as-quenched samples show the expected gradual decrease in strength as heat treating temperature is decreased, because of the progressively lower amounts of solute in solution. The samples given T6 aging show a gradual decrease in yield strength with decreasing heat treating temperature down to 715 F, and then an abrupt decrease between this temperature and 680 F. Samples given the T73 aging treatment show a fairly regular decrease in strength with decreasing heat treatment temperature and do not show the abrupt change between 715 and 680 F. This indicates that the amounts of solute in solid solution

at 715 F and above are susceptible to precipitation at 250 F, whereas those in solution at 680 F and below are not. On the other hand, the strengths after T73 aging indicate that the higher aging temperature will induce precipitation with much lower amounts of solute in solution.

Solution potential measurements of 7075 alloy specimens were made without stress and with 75% YS stress. As described above, solutions that did and did not induce cracks in 7075-T6 plate were used. Results are listed in Tables XIX and XX and values for unstressed specimens are plotted in Figs. 163 and 164.

Comparing the values for stressed and unstressed 7075 alloy specimens, differences were either very small or non-existent. Consequently, it does not appear that a change in potential with stress is a significant factor in crack initiation or stress corrosion of 7075 alloy.

Considering the NaCl-AlCl<sub>3</sub> solution potential values and yield strength data on the basis that samples heat treated at lower temperatures represent depleted boundary regions, large differences in both solution potential and in strength between grains and these boundary regions are possible. Assuming that 870 F equilibrium represents grain centers which have not been depleted in solute, and that 680 F equilibrium represents depleted boundary regions, the boundary regions in the T6 temper would be about 115 millivolts anodic to the grains. Also, the yield strength of the depleted regions would be about 30 ksi less than that of the grains. Consequently, an overall stress of 75% YS would apply exceptionally high localized stress to the boundary

region, and could result in plastic flow in this region.

It might be argued that, in the case of plate several inches thick, the equilibrium solute content at the solution heat treating temperature could not be maintained during quenching. In that event, assume the rather extreme case that the solute content of the grains corresponds to that of the 750 F treatment and that of the depleted boundary region is the equivalent of the 680 F treatment. The boundary region would still be over 70 millivolts anodic to the grain and its yield strength would still be over 20 ksi less.

Referring to the NaCl-AlCl<sub>3</sub> solution potential values for the samples given the T73 aging, the situation is different from that with the T6 aging because the change in potential with decreasing temperature of heat treatment is more gradual. Evaluating the examples used with the T6 temper, the combination of 870 F equilibrium conditions for the grains and of 680 F equilibrium conditions for boundary regions indicates a potential difference between grains and boundaries of 40-50 millivolts, which is less than half that with the T6 aging. With the assumption of 750 F conditions for the grains and 680 F conditions for boundaries, the potential difference is only 13-25 millivolts. This lower potential difference undoubtedly contributes to the traditionally superior resistance to stress corrosion of the T73 temper.

Comparing the solution potential values for 7075-T6 in the NaCl-NaCrO<sub>4</sub> solution (Table XX) with those in the NaCl-AlCl<sub>3</sub> solution, as is done in Fig. 164, indicates that, although the potentials differ somewhat in the two solutions, the

changes in potential with heat treating temperature are similar in both. This indicates that the potential difference between grains and depleted boundary regions are the same in both solutions, even though stress-corrosion cracks initiated in one solution but not in the other. Thus, while stress and a selective anodic path may be necessary conditions for crack initiation, the presence of both does not invariably lead to cracking.

To define further the electrochemical conditions associated with crack initiation in 7075 alloy, a variety of current measurements were made. These included current flow between (1) pairs of unstressed samples representing equilibrium at different temperatures, (2) similar selected stressed pairs and (3) pairs of stressed and unstressed samples of the same material.

With the unstressed pairs of 7075-T6 specimens in the NaCl-AlCl<sub>3</sub> solution (Table XXI), the current flow was fairly low when both of the samples were at equilibrium at 715 F or above. When one of the samples represented equilibrium at 680 F or below, currents were from two to five times as large. Also, surprisingly, when one of the samples represented equilibrium at 680 F or below, the currents were higher as the equilibrium temperature of the other member of the couple decreased. This would suggest that, with a badly depleted boundary zone (680 or 610), cracking might be more prone to occur if the remainder of the grain was somewhat depleted.

With 7075-T6 specimens in the NaCl-Na<sub>2</sub>CrO<sub>4</sub> solutions, in which cracks did not initiate, current flow between all pairs (Table XXI) was very low in spite of the relatively large potential

differences between certain of the pairs (Table XX). Thus, the fact that no cracks initiated in this solution is apparently the result of there being almost no corrosion current, possibly because of passivation or film formation.

With 7075-T73 in the NaCl-AlCl<sub>3</sub> solution (Table XXI), currents were comparatively low and did not differ greatly among the various pairs. This is in agreement with the earlier observation that potential differences were also much less than in the T6 temper. These relationships, combined with the fact that a large number of anodic sites are generated during T73 aging, satisfactorily explains the good stress-corrosion resistance of 7075-T73.

Current measurements of selected 7075 alloy stressed pairs gave the results listed at the top of Table XXII. Currents were of the same order as for corresponding unstressed pairs (Table XXI). This indicates that stress would not alter the electrochemical relationship between grains and depleted boundary regions in 7075 alloy.

Current measurements were also made between stressed and unstressed specimens of the same 7075-T6 materials as another test of the effect of stress on potential. As shown in Fig. 165, the steady currents were very low, confirming that stress had no significant effect on potential in this alloy.

#### 7039-T6 Alloy

In the tests simulating grain and grain boundary conditions with 7039 alloy, four of the equilibrium temperatures used

with 7075 alloy were selected. The choice was not particularly fortunate and time did not permit the preparation and testing of samples solution heat treated at other temperatures.

The tensile test values for 7039 alloy specimens (Table XXIII) showed a trend similar to that noted with 7075 alloy in that strength decreased, first gradually and then rapidly, as heat treating temperature was lowered. The transition point was somewhat lower than that for 7075 and the more rapid change appears to be just starting at 680 F.

The solution potentials of unstressed 7039-T6 samples in the  $\text{NaCl-Na}_2\text{CrO}_4$  solution, in which cracks initiated in specimens from plate, showed a similar trend with potential becoming more anodic as solution temperature decreased (Table XX). Similar measurements with stressed specimens gave no indication of any affect of stress on potential. Solution potential values for 7039-T6 in the  $\text{Na}_2\text{CrO}_4$  solution were greatly different from those in the  $\text{NaCl-Na}_2\text{CrO}_4$  solution (Table XX) but no trend with equilibrium temperature was evident.

A few current measurements were made with pairs of 7039-T6 specimens. With unstressed pairs of samples at equilibrium at different temperatures, measured in  $\text{NaCl-Na}_2\text{CrO}_4$  solution, current values were quite low (Table XXII). The lower temperature samples were always anodic and the higher currents were noted when the 550 F sample was one of the pair. Thus, values are in the proper direction for selective anodic solution of a boundary region. The current values are low but crack initiation time with plate samples of this alloy in this solution were comparatively long.

With stressed pairs of 7039-T6 specimens, current flow was very low and in the NaCl-Na<sub>2</sub>CrO<sub>4</sub> solution the higher temperature sample was anodic. This would not be indicative of stress-corrosion cracking.

The current flow measurements between stressed and unstressed samples of the same material gave the results seen in Fig. 166. There is some indication of an effect from the stress but further investigation is required before conclusions can be drawn.

To summarize the investigation of electrochemical effects, the method of simulating grains and depleted boundary regions appears to hold considerable promise for investigating stress-corrosion phenomena, particularly with materials in which these areas cannot be physically isolated. This approach has provided a plausible explanation of the stress-corrosion behavior of 7075 alloy in different tempers and environments. Indications were found that this approach would also explain the behavior of 7039 alloy, although considerably more work is required.

#### Acoustic Emission

In view of the increasing popularity of acoustic emission for monitoring mechanical and stress-corrosion failures in metals,<sup>(9-13)</sup> the initiation and early propagation of stress-corrosion cracks in 7075-T6 and 7039-T6 tuning-fork specimens were followed by this technique. Procedures were similar to those used for microscope observation of crack initiation with the added feature that acoustic emission was monitored simultaneously. This was accomplished by mounting an acoustic



transducer below the microscope stage and placing the beaker containing the specimen and corrodent on the face of the transducer rather than on the microscope stage. The specimens used were of 7075-T6 exposed to the  $\text{NaCl-AlCl}_3$  solution at pH 1 and of 7039-T6 exposed to the  $\text{NaCl-Na}_2\text{CrO}_4$  solution at pH 2, both stressed short transversely to 75% YS.

The equipment used for emission monitoring consisted of (1) a Branson broad band type Z acoustic transducer with a center frequency of 100 kc, (2) a preamplifier having one megohm input impedance to match the transducer, a band width of 1-700 kc, and a gain of 20, and (3) a Tektronix 564 memory oscilloscope. The photographs of the oscilloscope readout did not accurately record the signal amplitude because the signal bursts were too fast for the oscilloscope's memory feature. The signal occurrence rate, however, was accurately recorded. It was initially feared that bubbles, which develop very rapidly during exposure to the  $\text{NaCl-AlCl}_3$  solution, would produce spurious indications. With this particular equipment, however, no noticeable response developed from bubble formation, joining of bubbles, release of bubbles from the specimen surface, or bursting of bubbles at the surface of the corroding solution. Thus, all acoustic bursts apparently came from the specimen itself.

First exposures were of 7075-T6 in the  $\text{NaCl-AlCl}_3$  solution at pH 1. Cracks began to initiate within several minutes, which is characteristic for this combination of alloy and solution, but no acoustic emission was produced as the cracks initiated. The first emission bursts did not appear until a large

number of cracks had formed and the initial cracks had grown considerably. These bursts were initially several minutes apart but their frequency increased as the exposure continued. Representative traces during the latter stages of exposure of a 7075-T6 specimen are shown in Fig. 167. Each trace represents about ten seconds in time so that the photograph shows bursts occurring in a little more than a minute.

With a 7039-T6 specimen exposed to the  $\text{NaCl-Na}_2\text{CrO}_4$  solution, acoustic emission was eventually noted, but only after cracks as seen in the microscope were quite large. The cracks in this alloy were fewer, and even after cracks had grown to considerable size, emission bursts were few and of comparatively low magnitude (Fig. 167).

In simultaneous observations of crack development and acoustic emission, there was an almost total lack of correlation between emission bursts and events observed on the surface of the specimen. Cracks initiated and grew at quite a rapid pace but no emission bursts occurred. The progress of the cracks was generally continuous, however, which would not lead one to expect a sudden energy burst.

The source of the acoustic emission was discovered when it was noted that a large burst was generated when two cracks joined suddenly by mechanical rupture of the metal bridge between their adjoining tips. From this it was deduced that the bursts which were not related to surface events were in all probability caused by small sub-surface mechanical extension of cracks. They could have been generated by the joining of cracks

as observed on the surface or they could have been mechanical rupture of tiny islands of metal isolated by the passage of the stress-corrosion crack front. Such islands of dimpled mechanical rupture have been observed on stress-corrosion fracture surfaces. Regardless of the identity of the events producing the bursts, it was concluded that they were of a mechanical nature and that the true stress-corrosion portion of cracking did not produce acoustic emission.

#### Discussion of Cracking Mechanisms

This comprehensive investigation of crack initiation phenomena is unique in comparison with most stress-corrosion investigations in that attention was focused almost exclusively on the period in the life of a stress-corrosion crack before it is visible to the eye. This provided unusual opportunities for evaluating the effects of structure, topography, stress, film and environment on the initiation and early life of a crack. The information gained yielded a clear picture of the birth of stress-corrosion cracks in the materials investigated and permitted a critical examination of several of the proposed mechanisms for stress-corrosion cracking.

In considering the crack initiation mechanism, it should be remembered that the location specified for examination was within thick plate where rapid cooling from the heat treating temperature cannot be achieved. As a result, with one exception (7039-T6), the materials were either subject to intergranular corrosion and stress-corrosion cracking, or were subject to pitting attack and did not crack.

The factors investigated in connection with stress-corrosion crack initiation and growth can be divided into three categories, those necessary for crack initiation, those assisting or delaying initiation, and those promoting crack propagation. The only factors found to be essential for crack initiation were the combination of tensile stress, an appropriate environment and a particular composition in the grain boundary regions such that these regions would be attacked selectively by the particular environment. This corresponds to the classical electrochemical mechanism of stress corrosion proposed by Dix<sup>(14)</sup> and Mears, Brown and Dix<sup>(15)</sup>. Factors assisting or delaying crack initiation were high stress levels which assisted initiation and surface films that delayed it. Crack propagation was influenced primarily by microstructural configuration and the stressing direction. Cracking was promoted by elongated grain structures which provided long, continuous, crack-susceptible paths and by orientation of these paths perpendicular to the stress. The polygonized structures developed during fabrication in regions of 7XXX alloys having below-average chromium content helped to provide such paths.

With regard to the various mechanisms proposed to explain stress-corrosion of aluminum alloys, Robertson and Tetelman<sup>(16)</sup> and Jacobs<sup>(17)</sup> have stressed the importance of dislocation pile-ups at boundaries in promoting stress-corrosion cracking. No evidence was found in this investigation to support this theory. In 7075-T6 a few dislocations were observed, but these were pinned to E-phase dispersoids and were not piled up at boundaries. Such pile-ups could be generated by plastic

deformation either prior to the test or during crack propagation. With the 75% YS stress used in this investigation, no plastic deformation should occur. Therefore, it is doubtful that dislocations are a pertinent factor in crack initiation.

Logan<sup>(18)</sup> has proposed that formation and rupture of oxide film occurs during stress-corrosion cracking. From the fact that the stressed tuning-fork specimens were metallographically polished after stressing, and the only oxide film present was the natural film formed after polishing, film rupture was not a part of crack initiation. Instead, heavier films delayed crack initiation, indicating that the film was breached chemically and not mechanically.

Hoar<sup>(19)</sup> has expressed the belief that plastic straining of the metal is required for stress-corrosion cracking to continue. Considerable plastic deformation was observed on tuning-fork specimens ahead of a crack, and frequently surface deformation of the polished specimen at a crack tip appeared to define the localized stress field. No evidence was found, however, that such deformation preceded crack initiation. Actually, none would be expected when the stress was well below the yield strength.

Pugh and Jones<sup>(20)</sup> suggest that stress corrosion involves weakened metal in boundary regions, caused by precipitation on boundaries. The calculations of grain boundary composition and the corresponding strengths derived in this investigation would support this hypothesis.

McHardy and Hollingsworth<sup>(7)</sup> have indicated that the first stage in the stress-corrosion cracking of 7075-T6 is the

development of pits which act as stress raisers and lead to the development of intergranular attack and cracking. In tuning-fork specimens of 7039-T6 alloy, cracking generally initiated at pits of microscopic size, developed by the dissolution of  $Mg_2Si$  particles. In 7075-T6 and other alloys which developed cracks, no pits were observed at 500X magnification, although some were seen at electron microscope magnifications. It could not be established whether these extremely fine pits were an integral and necessary part of crack initiation. It seems possible that a crack was about to form and selected the pit as the initiation site only because the localized stress was slightly higher there. This is the case when fatigue cracks develop at extremely shallow grooves.

Summary and Conclusions

1. Stress-corrosion cracks in 2219-T351, 2219-T37, 7075-T6 and 7079-T6 initiated at random sites on grain boundaries. Constituent particles in these alloys did not affect crack initiation. Stress-corrosion cracks in 7039-T6 also initiated only on boundaries, but almost exclusively at pits from which  $Mg_2Si$  particles had been dissolved.
2. Stress corrosion cracks propagated along boundaries, selecting the straightest possible paths perpendicular to the stress. In 2219 alloy, these paths were series of recrystallized grain boundaries. In 7075-T6, 7079-T6 and 7039-T6, the paths were boundaries of two types, (1) boundaries from the ingot or an early stage of hot working that were parallel to the surface of the plate and (2) series of polygonized boundaries that developed during hot working in regions of low E-phase dispersoid contact. Some boundaries of the second type apparently represented dendritic cell boundaries in the ingot.
3. Boundary alignment parallel to the surface of the plate and development of the polygonized structure increased with the percent reduction from ingot to plate and was accompanied by progressive deterioration in resistance to stress-corrosion cracking.
4. Cracks showed a preference for high-angle boundaries, those between grains having considerably different orientation.

5. Dislocations, dispersoids and zone-type precipitates had no apparent effect on crack initiation. The development of M' and M-phase particles within grains of 7075-T73, however, apparently contributed to an improvement in resistance to cracking.
6. Precipitate particles on boundaries had no direct effect on crack initiation. Their formation, however, was accompanied by copper depletion in the region adjacent to boundaries in 2219 and 7075 alloys. This provided the anodic regions in which cracks apparently initiated. Calculations indicated that these regions were probably no more than 1000 A wide.
7. With 2219-T37, 7075-T6 and 7079-T6, stressing direction was of no importance to crack initiation but was highly significant with crack propagation. Cracks initiated with equal ease under longitudinal and short-transverse stress, but propagated readily only with short-transverse stress. This pronounced difference with stressing direction was related directly to boundary orientation relative to stressing direction. This, in turn, was related directly to grain shape, directionality of structure and recrystallization.
8. With 7039-T6, stressing direction was important both to crack initiation and propagation, because no cracks initiated in longitudinally stressed specimens under the test conditions used.



9. Stress level affected crack initiation time (semi-logarithmic relationship), crack propagation rate, and the number of major cracks, but generally had no effect on initiation sites or propagation paths. With 7039-T6 under very high stress, some initiation sites were not at  $Mg_2Si$  particles. Under very high stress, the ends of cracks within the specimen occasionally followed a transgranular path, possibly as a result of mechanical fracture.
10. Even the highest stress levels did not propagate cracks from longitudinal stresses because of highly unfavorable boundary orientation.
11. Chemically produced pits and mechanical scratches did not act as crack-initiation sites.
12. Surface abrasion altered crack initiation but only until corrosion or cracking had breached a very shallow surface layer.
13. Intergranular pre-corrosion in 7075-T6 induced rapid crack initiation, but corrosion crevices widened by stress could not be distinguished from, and could be mistaken for, stress-corrosion cracks.
14. Pre-corrosion of 7039-T6, to produce pits at  $Mg_2Si$  particles, did not alter or accelerate crack initiation.
15. Thin natural, anodic and chemical films delayed but did not prevent or alter crack initiation.

16. In environmental screening tests, stress-corrosion cracking of 2219-T37 and 7075-T651 occurred primarily in chloride solutions and was accelerated by acid pH. No stress-corrosion cracking of 2219-T87 and 7075-T7351 was encountered, the few failures being the result of excessive localized corrosion.
17. With 7039-T6, cracks did not initiate in solutions producing rapid general attack, but did develop in mild environments such as an inhibited chloride solution and laboratory air. Failure times in air were affected by temperature and humidity. Air at 100 F and 90% R.H. was a particularly good environment for initiation studies.
18. Environment determined whether cracks developed, and altered crack initiation time and propagation rate, but had no effect on initiation sites or propagation paths.
19. A method was devised for simulating in separate samples the metallurgical condition within grains and in depleted boundary regions. Electrochemical measurements of such samples have satisfactorily explained the stress-corrosion behavior of 7075-T6 in different tempers and environments.
20. Acoustic emission bursts during stress-corrosion tests were associated with sudden, mechanical crack extensions not considered to be part of the stress-corrosion crack growth. No such bursts were generated at crack initiation or during crack growth by stress corrosion.

REFERENCES

1. J. B. Clark, "Electron Probe Test of Two Theories of "Denuded Zone" Formation in Aged Alloys, Acta Met., 12, 1197-1201 (1964).
2. E. H. Hollingsworth and G. C. English, "Investigation of the Mechanism of Stress Corrosion of Aluminum Alloys," U.S. Navy Bureau of Naval Weapons Contract NOW 64-0170c.
3. Aluminum, Vol. I, ASM, 1967, p. 140.
4. Sprusil and Valvoda, Acta Met., 15, 1269 (1967).
5. E. H. Dix, Jr., W. A. Anderson and M. B. Shumaker, Corrosion 15, No. 2, p. 55 (1959).
6. B. W. Lifka and D. O. Sprowls, "Stress-Corrosion Testing of Aluminum Alloy 7079-T6 in Various Environments," ASTM Symposium on Stress-Corrosion Testing, June 28, 1966.
- 6a. E. H. Hollingsworth and G. C. English, "Investigation of the Mechanism of Stress Corrosion of Aluminum Alloys," Final Report, June 1, 1969, Naval Air Systems Command Contract, N00019-67-C-0481.
7. J. McHardy and E. H. Hollingsworth, "Investigation of the Mechanism of Stress Corrosion of Aluminum Alloys," Bureau of Naval Weapons Contract NOW 65-0327-f (1966).
8. G. Haaijer and A. W. Loginow, Corrosion 21 (4), 105-112 (1965).
9. D. Van Rooyen, "Qualitative Mechanism of Stress Corrosion Cracking of Austenitic Stainless Steels," Corrosion 16, p. 93 (September 1960).
10. W. W. Gerberich and C. E. Hartbower, "Monitoring Crack Growth of Hydrogen Embrittlement and Stress Corrosion Cracking by Acoustic Emission," Conference on Fundamental Aspects of Stress Corrosion Cracking - Ohio State - September 1967.
11. H. L. Dunegan, D. O. Harris and C. A. Tatro, "Fracture Analysis by Use of Acoustic Emission," Engineering Fracture Mechanics, 1, p. 105-122 (1968).
12. P. H. Hutton, "Acoustic Emission in Metals as an NDT Tool," 27th National Conference of the American Society for Non-destructive Testing, October 16-19, 1968, Cleveland, Ohio.

13. P. H. Hutton, "Use of Acoustic Emission to Study Failure Mechanisms in Metal," Metals Engineering and Pressure Vessels and Piping Conference, March 31-April 2, 1969, Washington, D.C.
14. E. H. Dix, Jr., "Acceleration of the Rate of Corrosion by High Constant Stresses," Trans. AIME 137, 11 (1940).
15. R. B. Mears, R. H. Brown and E. H. Dix, Jr., "A Generalized Theory of Stress Corrosion of Alloys," Symposium on Stress Corrosion of Metals, 1944, p. 329. Published jointly by ASTM and AIME.
16. W. D. Robertson and A. S. Tetelman, "A Unified Mechanism for Intergranular and Transgranular Corrosion Cracking." Strengthening Mechanisms in Solids. American Society for Metals, p. 217 (1962).
17. A. J. Jacobs, ASM Trans. Quart. 58, 579 (1965).
18. H. L. Logan, "Film Rupture Mechanism of Stress Corrosion." Journal of Research of the National Bureau of Standards 48, 2, 99 (1952).
19. T. P. Hoar, "Stress Corrosion Cracking," Proceedings Second International Congress on Metallic Corrosion, 1963, National Association of Corrosion Engineers, Houston, Texas, p. 14.
20. E. N. Pugh and W. R. D. Jones, "The Mechanism of Stress Corrosion in a High Purity Al-Zn-Mg Alloy," Metallurgia 63, 3 (1961).

TABLE I

CHARACTERISTICS OF ALUMINUM ALLOY PLATE

<u>Spec. No.</u>	<u>Alloy</u>	<u>Composition %</u>									
		<u>Si</u>	<u>Fe</u>	<u>Cu</u>	<u>Mn</u>	<u>Mg</u>	<u>Cr</u>	<u>Zn</u>	<u>Ti</u>	<u>V</u>	<u>Zr</u>
240236 240237	2219	0.10	0.19	5.8	0.26	0.02	0.00	0.01	0.06	0.11	0.16
295490	7075	0.05	0.08	1.40	0.03	2.51	0.19	6.05	0.05	0.01	0.00
295474	X7375	0.05	0.08	1.38	0.01	2.41	0.00	5.59	0.04	0.00	0.00
235972	7079	0.10	0.20	0.73	0.18	3.71	0.19	4.49	0.05	--	--
314759	7039	0.13	0.19	0.03	0.26	2.88	0.20	4.02	0.03	--	--

TYPE OF ATTACK<sup>(1)</sup>

<u>Spec. No.</u>	<u>Alloy and Temper</u>	<u>Type of Attack</u> <sup>(2)</sup>
240326A	2219-T351	I
240327A	2219-T37	I
240326B	2219-T851	P+SI
240327B	2219-T87	P+SI
295490A	7075-T6	I+P
295490B	7075-T73	P
295474A	X7375-T6	P+I
295474B	X7375-T73	I
235972	7079-T651	P+I
314759	7039-T6	P

ELECTRICAL CONDUCTIVITY OF  
7075 AND X7375 ALLOYS

<u>Spec. No.</u>	<u>Alloy and Temper</u>	<u>Conductivity (% IACS)</u>
295490A	7075-T6	31.9
295490B	7075-T73	40.0
295474A	X7375-T6	32.0
295474B	X7375-T73	38.1

(1) 1" below surface

(2) Six-hour exposure to aqueous solution  
containing 57 g/l NaCl + 10 ml/l 30%  
H<sub>2</sub>O<sub>2</sub> as per MIL-H-6088D

TABLE II

TENSILE PROPERTIES<sup>(1)</sup>

<u>Spec. No.</u>	<u>Alloy and Temper</u>	<u>Direction</u>	<u>Tensile Str. ksi</u>	<u>Yield Str. ksi</u>	<u>Elong. %</u>
240326A	2219-T351	Long.	57.2	41.0	20.0
		Long Trans.	56.9	36.0	19.0
		Short Trans.	52.8	34.0	11.0
240327A	2219-T37	Long	61.3	52.7	14.5
		Long Trans.	61.0	45.7	13.0
		Short Trans.	56.8	44.0	7.0
240326B	2219-T851	Long.	67.7	54.4	11.0
		Long Trans.	67.8	52.6	9.5
		Short Trans.	63.8	51.6	5.5
240327B	2219-T87	Long.	71.1	60.6	9.0
		Long Trans.	70.3	59.1	8.5
		Short Trans.	62.4	57.0	3.0
295490A	7075-T6	Long.	84.7	73.1	10.5
		Long Trans.	82.3	70.7	11.5
		Short Trans.	80.6	67.4	10.0
295490B	7075-T73	Long.	75.2	63.3	12.5
		Long Trans.	73.9	62.4	11.0
		Short Trans.	72.6	60.4	8.0
295474A	X7375-T6	Long.	77.2	70.2	6.0
		Long Trans.	76.8	69.0	6.0
		Short Trans.	73.9	63.1	7.0
295474B	X7375-T73	Long.	75.1	68.2	6.5
		Long Trans.	75.2	69.2	5.5
		Short Trans.	73.3	67.4	6.0

(1) 0.125" diameter specimens with gage length approximately 1" from surface of plate and at least 1" from edge.

TABLE III

SOLUTION POTENTIALS OF ALUMINUM ALLOY PLATE<sup>(1)</sup>Sodium Chloride-Hydrogen Peroxide Solution<sup>(2)</sup>

<u>Spec. No.</u>	<u>Alloy and Temper</u>	<u>Potential (-mv)<sup>(3)</sup></u>
240326A	2219-T351	687
240327A	2219-T37	687
240326B	2219-T851	803
240327B	2219-T87	815
295490A	7075-T6	828
295490B	7075-T73	843
295474A	X7375-T6	827
295474B	X7375-T73	829

Methyl Alcohol-Carbon Tetrachloride Solution<sup>(4)</sup>

<u>Spec. No.</u>	<u>Alloy and Temper</u>	<u>Potential (-mv)<sup>(5)</sup></u>
240326A.	2219-T351	345
240327A	2219-T37	365
240326B	2219-T851	950
240327B	2219-T87	1040

(1) Specimen location 1" below plate surface.

(2) 57 g/l NaCl + 10 ml/l 30% H<sub>2</sub>O<sub>2</sub>.

(3) Steady value vs 0.1 N Calomel Electrode.

(4) 7:3 mixture of MeOH and CCl<sub>4</sub> - Method developed under Contract NAS8-5340.

(5) Thirty-minute value vs saturated Calomel.

TABLE IV

RESISTANCE TO CORROSION AND STRESS-CORROSION CRACKING  
OF SHORT-TRANSVERSE SPECIMENS (1) FROM 4" THICK 2219 ALLOY PLATE

<u>Temper</u>	<u>Unstressed Specimens</u>		<u>Stressed Specimens</u>			
	<u>Days Exposure</u>	<u>% Loss in T.S.</u>	<u>Applied Stress</u>		<u>F/N(2)</u>	<u>Days</u>
			<u>% Y.S.</u>	<u>ksi</u>		
T351	5	0	75	25.5	3/3	3, 3, 5
	10	26	50	17.0	3/3	3, 6, 8
	30	27	25	8.5	2/3	19, 19, (OK 84)
	84	33				
T851	5	6	75	38.7	0/3	OK-84
	10	10				
	30	13				
	84	17				
T37	5	13	75	33	3/3	2, 3, 4
	10	24	50	22	3/3	3, 3, 5
	30	35	25	11	0/3	OK-84
	84	41				
T87	5	4	75	42.7	0/2(3)	OK-84
	10	6				
	30	10				
	84	14				

(1) Specimens 1/8" diameter exposed to 3-1/2% NaCl solution by alternate immersion.

(2) Specimens failed/specimens exposed.

(3) A third specimen failed at 27 days from tensile overload after severe pitting.



TABLE V

RESISTANCE TO CORROSION AND STRESS-CORROSION CRACKING OF  
SHORT-TRANSVERSE SPECIMENS<sup>(1)</sup> FROM 3" 7075 and X7375 ALLOY PLATE

<u>Alloy</u>	<u>Temper</u>	<u>Unstressed Specimens</u>		<u>Stressed Specimens</u>			
		<u>Days Exposure</u>	<u>% Loss in T.S.</u>	<u>Applied Stress</u>		<u>F/N<sup>(2)</sup></u>	<u>Days</u>
				<u>% Y.S.</u>	<u>ksi</u>		
7075	T6	5	6	75	50.5	3/3	2, 4, 4
		10	7	50	33.7	3/3	4, 4, 4
		30	12	25	16.8	3/3	5, 7, 7
		84	9	15	10.1	3/3	7, 7, 7
7075	T73	5	0	75	45.3	0/3	OK-84
		10	1				
		30	2				
		84	2				
X7375	T6	5	0	75	47.3	3/3	3, 5, 6
		10	2	50	31.5	3/3	6, 6, 8
		30	3	25	15.8	3/3	6, 10, 10
		84	2	15	9.5	0/3	OK-84
X7375	T73-type	5	2	75	50.5	3/3	8, 10, 12
		10	4	50	33.7	(3)	---
		30	6	25	16.8	0/3	OK-84
		84	7				

(1) Specimens 1/8" diameter exposed to 3-1/2% NaCl solution by alternate immersion.

(2) Specimens failed/specimens exposed.

(3) 3/3 failed but outside reduced section--mode of failure uncertain.

TABLE VI

CHARACTERISTICS OF ADDITIONAL LOTS OF 2219 AND 7075 PLATE

<u>Spec. No.</u>	<u>Alloy<sup>(1)</sup></u>	<u>Composition, %</u>									
		<u>Si</u>	<u>Fe</u>	<u>Cu</u>	<u>Mn</u>	<u>Mg</u>	<u>Cr</u>	<u>Zn</u>	<u>Ti</u>	<u>V</u>	<u>Zr</u>
323038	2219-T37	0.13	0.24	5.8	0.30	0.01	0.01	0.08	0.08	0.12	0.12
323039	2219-T87										
322720	7075-T651	0.12	0.20	1.78	0.04	2.48	0.20	5.80	0.03	--	--
322721	7075-T7351										

(1) Both tempers of each alloy were from same lot.

<u>Spec. No.</u>	<u>NaCl-H<sub>2</sub>O<sub>2</sub><sup>(2)</sup> Solution Potential<sup>(3)</sup></u>		<u>Electrical Conductivity<sup>(3)</sup> - % IACS</u>		
	<u>Alloy</u>	<u>Potential - mv</u>	<u>Spec. No.</u>	<u>Alloy</u>	<u>Conductivity</u>
323038	2219-T37	639	322720	7075-T651	34.1
323039	2219-T87	812	322721	7075-T7351	41.5

(2) 57 g/l NaCl + 10 ml/l 30% H<sub>2</sub>O<sub>2</sub>.

(3) Specimen location at center of 2.5" plate.

TABLE VII

ADDITIONAL LOTS OF 2219 AND 7075 ALLOY PLATE<sup>(1)</sup>

Spec. No.	Alloy and Temper	Direction	Tensile Properties		
			Tensile Str. ksi	Yield Str. ksi	Elong. %
323038	2219-T37	Long	51.7	43.6	20.0
		Long Trans.	53.2	40.2	14.0
		Short Trans.	52.3	39.0	12.0
323039	2219-T87	Long	68.0	56.0	10.0
		Long Trans.	67.6	55.3	8.0
		Short Trans.	64.8	55.5	5.0
322720	7075-T651	Long	85.8	76.8	9.0
		Long Trans.	81.5	72.3	8.0
		Short Trans.	73.0	67.1	2.0
322721	7075-T7351	Long	73.3	62.0	11.0
		Long Trans.	71.1	60.0	8.5
		Short Trans.	64.9	57.1	4.0

Stress Corrosion Properties <sup>(2)</sup>				
Spec. No.	Alloy and Temper	Stress - % YS	F/N <sup>(3)</sup>	Days
323038	2219-T37	75	3/3	2, 2, 2
		50	3/3	2, 2, 3
		25	3/3	3, 4, 84
		15	2/3	84, 84, OK-84
323039	2219-T87	75	0/3	OK-84
322720	7075-T651	75	3/3	2, 2, 3
		50	3/3	2, 3, 3
		25	3/3	3, 4, 6
		15	3/3	5, 6, 7
322721	7075-T7351	75	0/3	OK-84

(1) Commercially fabricated 2.5" plate

(2) 0.125" dia. short-transverse specimens  
exposed to 3.5% NaCl by alternate immersion

(3) Specimens failed/specimens exposed

TABLE VIII

TENSILE PROPERTIES AND STRESS CORROSION BEHAVIOR  
OF 7079-T651 AND 7039-T6 PLATE

<u>Alloy</u>	<u>Direction</u>	<u>Location</u>	<u>Tensile Properties</u>		
			<u>T.S.-ksi</u>	<u>Y.S.-ksi</u>	<u>Elongation %</u>
7079-T651	Longitudinal	1" below surface	75.9	67.1	12.0
	Long. Trans.	1" below surface	76.5	65.1	8.0
	Short Trans.	1" below surface	74.6	65.5	6.0
7039-T6	Longitudinal	Center	63.2	53.8	16.2
	Long. Trans.	Center	64.2	54.4	12.5
	Short Trans.	Center	63.9	54.6	7.5

Stress Corrosion - Center of Plate - 3.5% NaCl Alt. Imm.

7079-T651 - 0.125" Diameter Specimens

<u>Direction</u>	<u>Stress - % Y.S.</u>	<u>F/N (1)</u>	<u>Days to Fail</u>
Longitudinal	75	2/3	14, 84, OK 84
Short Transverse	50	3/3	5, 12, 13
	25	2/3	21, 21, OK 84
	15	0/3	OK 84

7039-T6 C-Rings - 64% Y.S. Short Transverse

<u>F/N (1)</u>	<u>Days to Failure</u>
9/9	8,8,9,9,9,9,11,13,29

(1) Number failed/number exposed

TABLE IX

EFFECT OF HOT REDUCTION ON  
STRESS CORROSION RESISTANCE OF 7075-T6 PLATE

<u>% Reduction</u>	<u>YS, ksi</u>	<u>Failure Times</u>		<u>Loss TS**</u>
		<u>75% YS</u>	<u>50% YS</u>	
None	63.7	9,11,14 days	(3 NF)*	10%
10	63.2	9,10,13 days	(3 NF)	4%
20	62.6	5, 5, 5 days	9 days (2 NF)	14%
30	62.2	4, 5, 5 days	18 days (2 NF)	17%
40	62.2	4, 4, 4 days	8, 8, 8 days	-
50	62.5	4, 4, 4 days	10,11,13 days	-
60	62.8	4, 4, 4 days	7, 7, 8 days	-
70	63.0	4, 4, 4 days	7, 7, 7 days	-
80	63.6	4, 4, 4 days	5, 5, 5 days	-

Triplicate 1/8" dia. short transverse specimens  
 exposed in 3-1/2% NaCl alternate immersion

\*NF = not failed in 84 days

\*\*Percent loss in apparent tensile strength after corrosion.  
 Average of specimens not failing when corroded at 50% YS.

294942-CW. All specimens from one piece of plate.

TABLE X

CALCULATED RELATIVE AMOUNTS OF ELEMENTS AT  
BOUNDARIES OF SLOWLY QUENCHED 7075 ALLOY

	<u>Amount by Weight</u>	<u>Amount by No. of Atoms</u>
If boundary goes to equilibrium solubility limit, and usual diffusion coefficients apply:		
Zn	1.00	1.00
Mg	3.32	8.97
Cu	1.08	1.11

If boundary goes to equilibrium solubility limit, and only Cu diffusion is assisted by excess vacancy migration:

Zn	1.00	1.00
Mg	3.32	8.97
Cu	2.87	2.95

If boundary goes to equilibrium solubility limit, all diffusion coefficients enhanced in proportion to binding energy with vacancies:

Zn	1.00	1.00
Mg	5.92	16.0
Cu	2.18	2.24

Notes: Relative amounts of each element compared to Zn, taken as 1.00. At boundary, elements can combine with aluminum atoms to form intermetallic phases.

Phases possible:

T (AlCuMg) =  $\text{CuMg}_4\text{Al}_6$ , which is isomorphous with and ranges in composition to

T (AlMgZn) =  $\text{Mg}_3\text{Zn}_3\text{Al}_2$

M (AlMgZn) =  $\text{MgZn}_2$ , which is isomorphous with and ranges in composition to

U (AlCuMg) =  $\text{CuMgAl}$

S (AlCuMg) =  $\text{CuMgAl}_2$ , which cannot contain Zn

TABLE XI

## RESISTANCE TO STRESS-CORROSION CRACKING OF ALUMINUM ALLOYS IN VARIOUS AQUEOUS SOLUTIONS

7075-T651 Alloy - Short-Transverse Tensile Specimens, 0.125" Dia  
Tensile Strength - 79.3 ksi, Yield Strength - 68.3 ksi, % El - 3.0

Solution	Nominal pH	Adjusted With	Actual pH Range	Stressed 75% Y S				Unstressed Specimens			Visual Examination	
				F/N	Days	% Loss in TS <sup>(1)</sup>	Type of Attack <sup>(2)</sup>	Days	% Loss in TS	Type of Attack <sup>(2)</sup>	Film <sup>(3)</sup>	Localized Corrosion <sup>(4)</sup>
Halide Anions												
1N NaCl	2	HCl	2.0-2.4	3/3	3,3,3	--	P + I	3,3	31,40	P + I	--	2b
"	7	NaOH	5.2-7.0	2/3	21,47(OK-50)	0	P + I	21,60	1,0	P	Black	1
1N NaBr	2	HBr	2.0-2.3	3/3	6,10,13	--	--	6,13	20,24	P + IF	Red	2a
"	7	NaOH	5.1-7.0	1/3	15(2 OK60)	6,45	--	15,60	8,15	P	None	1
1N NaI	2	HI	2.0-3.0	3/3	7,12,18	--	--	7,18	12,41	P + IF	None	2a
"	7	HI	5.2-7.0	0/3	OK60	8	--	60	3	P	None	1
1N KHF <sub>2</sub>	2	--	2.0	3/3	5,34,42	--	--	5,42	1,7	P	Red	2a
1N NaF	7	HF	7.0-7.5	0/3	OK60	1	--	21,60	4,1	N A A	None	1
Complex Anions												
1N NaNO <sub>3</sub>	2	HNO <sub>3</sub>	2.0-3.9	0/3	OK60	53	--	21,60	9,22	P	Red	2a
"	7	NaOH	5.0-7.0	0/3	OK60	1	--	21,60	0,0	P	Dull Regions	1
"	9	NaOH	5.3-9.0	0/3	OK60	3	--	21,60	12,6	P	Dull Regions	1
1N Na <sub>2</sub> CrO <sub>4</sub>	2	CrO <sub>3</sub>	2.0	0/3	OK60	0	--	21,60	0	N A A	None	1
"	7	CrO <sub>3</sub>	7.0	0/3	OK60	0	--	21,60	0	N A A	None	1
"	9	NaOH	8.4-9.0	3/3	24,25,32	--	N A A	21,32	0	N A A	None	1
1N Na <sub>2</sub> SO <sub>4</sub>	2	H <sub>2</sub> SO <sub>4</sub>	2.0-2.2	3/3(6)	39,40,47	--	P + I	21,47	13,32	P	Red	3b
"	7	NaOH	5.3-7.0	0/3	OK60	4	--	21,60	0	P	Gray	1
"	9	NaOH	5.8-9.0	0/3	OK60	2	--	21,60	0,0	P	Gray	1
0.5N Na <sub>2</sub> SO <sub>4</sub> + 0.5N NaNO <sub>3</sub>	2	H <sub>2</sub> SO <sub>4</sub>	2.0-2.7	3/3(6)	47,56,60	--	P + IF	21,60	15,41	P + IF	Red	3b
"	7	NaOH	5.0-7.0	0/3	OK60	2	--	21,60	2,3	P	Dull	1
0.5N Na <sub>2</sub> SO <sub>4</sub> + 0.5N Na <sub>2</sub> CrO <sub>4</sub>	2	H <sub>2</sub> SO <sub>4</sub>	2.0	0/3	OK60	25	--	21,60	0,4	P	Gray	2b
"	7	H <sub>2</sub> SO <sub>4</sub>	7.0	0/3	OK60	1	--	21,60	0,1	N A A	None	1
1N NaHCO <sub>3</sub>	9	--	9.0-9.7	0/3	OK60	0	--	21,60	0,0	N A A	Gray	1
1N NaHSO <sub>4</sub>	1	--	1.0	3/3(6)	15,17,20	--	P + I	15,17	40,46	P	Red	3a
1N Na <sub>2</sub> HPO <sub>4</sub>	9	--	8.4-8.5	0/3	OK60	3	--	21,60	12,6	P	Gray	1
1N NaH <sub>2</sub> PO <sub>4</sub>	4	--	4.0-4.2	0/3	OK60	0	--	21,60	0,0	P	Red	1
1N NaH <sub>2</sub> PO <sub>4</sub>	4	H <sub>2</sub> SO <sub>4</sub>	4.0	0/3	OK60	0	--	21	1	--	--	--
1N NaC <sub>2</sub> H <sub>3</sub> O <sub>2</sub>	4	CH <sub>3</sub> COOH	4.0	3/3	4,6,13	--	P	4,13	4,8	P	--	--
Sodium Chloride plus Oxidizing Acids												
1N NaCl	2	HNO <sub>3</sub>	--	3/3	1,1,1	--	P + I	1,1	12,47	P + I	--	2b
"	2	H <sub>2</sub> PO <sub>4</sub>	--	3/3	1,1,2	--	P + I	1,2	54,82	P + I	--	2b
"	2	H <sub>2</sub> SO <sub>4</sub>	--	3/3	1,1,1	--	P + I	1,1	46,57	P + I	--	2b
4N NaCl + 0.5N KNO <sub>3</sub>	0.4	CrO <sub>3</sub>	2.0-2.4	2/3	23,60(OK60)	--	P + IF	21,60	66,68	P + IF	None	1
"	0.4	HNO <sub>3</sub>	--	3/3	1,1,1	--	P + IF	1,1	79,85	P + IF	--	2a
Sodium Chloride plus Complex Anions												
0.5N NaCl + 0.5N NaNO <sub>3</sub>	2	HNO <sub>3</sub>	2.0-3.0	3/3	7,8,9	--	P	7,9	6,7	P + IF	None	2a
"	7	NaOH	5.0-7.0	2/3	60(5), 60(5)(OK60)	2	--	21,60	3,3	P	Dull	2a
0.5N NaCl + 0.5N Na <sub>2</sub> SO <sub>4</sub>	2	H <sub>2</sub> SO <sub>4</sub>	2.0-2.2	3/3(6)	2,2,3	--	P + I	2	42	P	Black	1
"	7	NaOH	5.2-7.0	3/3(6)	14,21,30	--	P + I	14,30	25,35	P	Gray	1
0.5N NaCl + 0.5N Na <sub>2</sub> CrO <sub>4</sub>	2	HCl	2.0	3/3	8,10,19	--	N A A	8,19	0,0	N A A	None	1
"	7	HCl	7.0	2/3	22,26(OK60)	0	--	21,60	0,0	N A A	None	1
Ammonium Salts												
1N NH <sub>4</sub> Cl	7	NH <sub>4</sub> OH	6.5-7.0	3/3	15(5), 15(5), 18	--	P + I	15,18	33,18	P + I	Gray	2b
1N NH <sub>4</sub> NO <sub>3</sub>	7	NH <sub>4</sub> OH	6.2-7.0	0/3	OK60	2	--	21,60	0,0	N A A	None	1
1N (NH <sub>4</sub> ) <sub>2</sub> SO <sub>4</sub>	7	NH <sub>4</sub> OH	6.2-7.0	0/3	OK60	0	--	21,60	8,0	N A A	None	1
1N (NH <sub>4</sub> ) <sub>2</sub> CrO <sub>4</sub>	7	CrO <sub>3</sub>	7.0	0/3	OK60	0	--	21,60	0,2	N A A	None	1
Miscellaneous												
1N NaCl + 10 ml/l 30% H <sub>2</sub> O <sub>2</sub>	5.5	--	--	3/3	3,3,3	--	P + I	3,3	36,41	P + I	--	2b
1N NaCl + 1N AlCl <sub>3</sub>	2	HCl	--	3/3	2,3,3	--	I + IF	2,3	13,31	P + I	--	2b
1N Na <sub>2</sub> SO <sub>4</sub> + 10 ml/l 30% H <sub>2</sub> O <sub>2</sub>	5.8	--	--	3/3	15(5), 15(5), 35(5)	--	--	15,35	0,0	P	Gray	2a
1N Na <sub>2</sub> SO <sub>4</sub> + 1N Al <sub>2</sub> (SO <sub>4</sub> ) <sub>3</sub>	2	H <sub>2</sub> SO <sub>4</sub>	2.0-2.3	1/3(6)	48(2 OK60)	--	P	21,60	15,32	P	Red	3a

## Plate Chemical Composition, Weight Per Cent

Si	Fe	Cu	Mn	Hg	Cr	Ni	Zn	Ti	Ba
09	20	1.62	04	2.63	17	00	5.92	02	001

NOTES (1) Results are the average of tests of those specimens which did not fail, unless more than one value is shown due to divergent results

(2) Type of attack N A A = No Appreciable Attack, P = Pitting, P + I = Pitting Plus Intergranular, P + IF = Pitting Plus Interfragmentary.

(3) Wet surface film observed at termination of maximum exposure in individual solutions

(4) Localized corrosion 1 = negligible, 2 = mild, 3 = severe, a = random, b = directional Ratings based upon appearance after maximum exposure time in each solution

(5) Failure occurred outside the reduced section at the edge of or beneath the cellulose acetate coating used to cover all parts of the stressing frame

(6) Stress-corrosion cracking questionable because of high loss in strength unstressed

TABLE XII

## RESISTANCE TO STRESS-CORROSION CRACKING OF ALUMINUM ALLOYS IN VARIOUS AQUEOUS SOLUTIONS

2219-T37 Alloy - Short-Transverse Tensile Specimens, 0.125" Dia

Tensile Strength - 57.9 ksi, Yield Strength - 44.4 ksi, % El - 8.0

Solution	Nominal pH	Adjusted With	Actual pH Range	Stressed 75% Y S				Unstressed Specimens			Visual Examination	
				F/H	Days	% Loss in TS (1)	Type of Attack (2)	Days	% Loss in TS	Type of Attack (2)	Film (3)	Localized Corrosion (h)
Halide Anions												
1N NaCl	2	HCl	2.0-2.4	3/3	19,19,19	--	I	19	65	I	Red	2b
"	7	NaOH	5.0-7.0	3/3	26,28,33	--	I	26,33	6,40	I	Black	1
1N NaBr	2	HBr	2.0-4.3	0/3	OK-60	18	--	21,60	21,22	P	Red	2a
"	7	NaOH	5.4-7.0	0/3	OK-60	23	--	21,60	13,16	P	Gray	1
1N NaI	2	HI	2.0-4.3	(6)	--	--	--	21	10	P	None	1
"	7	NaOH	5.9-7.0	0/3	OK-60	7	--	21,60	0,4	P	None	2a
1N KHF <sub>2</sub>	2	--	2.0	0/3	OK-60	6	--	21,60	7,8	P	Red	2a
1N NaF	7	HF	7.0-7.6	0/3	OK-60	0	--	21,60	4,4	P	None	1
Complex Anions												
1N NaNO <sub>3</sub>	2	HNO <sub>3</sub>	2.0-3.8	0/3	OK-60	37	--	23,60	11,30	P	Black	3a
"	7	NaOH	5.4-7.0	0/3	OK-60	4	--	23,60	2,4	P	Gray	1
"	9	NaOH	6.7-9.0	0/3	OK-60	5	--	23,60	6,8	P	Gray	1
1N Na <sub>2</sub> CrO <sub>4</sub>	2	CrO <sub>3</sub>	2.0	0/3	OK-60	3	--	22,60	0,0	N A A	None	1
"	7	CrO <sub>3</sub>	7.0	0/3	OK-60	6	--	22,60	1,1	N A A	None	1
"	9	NaOH	8.2-9.0	0/3	OK-60	4	--	22,60	1,2	N A A	None	1
1N Na <sub>2</sub> SO <sub>4</sub>	2	H <sub>2</sub> SO <sub>4</sub>	2.0	0/3	OK-60	20	--	22,60	11,20	P + I	Black	2a
"	7	NaOH	5.5-7.0	0/3	OK-60	1	--	22,60	5,5	P	Gray	1
"	9	NaOH	6.0-9.0	0/3	OK-60	3	--	22,60	0,0	P	Gray	1
0.5N Na <sub>2</sub> SO <sub>4</sub> + 0.5N NaNO <sub>3</sub>	2	H <sub>2</sub> SO <sub>4</sub>	2.0-2.8	0/3	OK-60	36	--	21,60	16,25	P	Red	3a
"	7	NaOH	5.0-7.0	0/3	OK-60	5	--	21,60	4,4	P	Dull	1
0.5N Na <sub>2</sub> SO <sub>4</sub> + 0.5N Na <sub>2</sub> CrO <sub>4</sub>	2	H <sub>2</sub> SO <sub>4</sub>	2.0-2.1	1/3	60(5) (2 OK60)	6,24	--	22,60	8,16	P	Black	2a
"	7	H <sub>2</sub> SO <sub>4</sub>	7.0	0/3	OK-60	0	--	22,60	7,3	N A A	None	1
1N NaHCO <sub>3</sub>	9	--	9.4-9.8	0/3	OK-60	4	--	26,60	5,3	N A A	Gray	1
1N NaHSO <sub>4</sub>	1	--	1.0-1.4	0/3	OK-60	56	--	26,60	27,51	P	Red	3a
1N Na <sub>2</sub> HPO <sub>4</sub>	9	--	8.4-8.7	0/3	OK-60	0	--	26,60	6,3	P	Gray	1
1N NaH <sub>2</sub> PO <sub>4</sub>	4	--	4.2-4.3	0/3	OK-60	1	--	26,60	5,4	P	Black	1
1N NaH <sub>2</sub> PO <sub>4</sub>	4	H <sub>2</sub> SO <sub>4</sub>	4.0	0/3	OK-45	--	--	21	5	--	--	--
1N NaC <sub>2</sub> H <sub>3</sub> O <sub>2</sub>	4	CH <sub>3</sub> COOH	4.0	0/3	OK-45	--	P	21	5	P	--	--
Sodium Chloride plus Oxidizing Acids												
1N NaCl	2	HNO <sub>3</sub>	--	3/3	7,7,7	--	I	7	56	I	Red	2a
"	2	H <sub>3</sub> PO <sub>4</sub>	2.0-2.5	3/3	8,8,8	--	I	8	58	I	Red	2a
"	2	H <sub>2</sub> SO <sub>4</sub>	2.0-3.6	3/3	8,8,8	--	I	8	71	I	Red	2a
"	2	CrO <sub>3</sub>	2.0-2.3	1/3	60(2 OK60)	1,6	I	60,60	10,21	I	None	1
1N NaCl + 0.5N HNO <sub>3</sub>	0.4	HNO <sub>3</sub>	--	3/3	1,1,1	--	I	1	76	I	--	2a
Sodium Chloride plus Complex Anions												
0.5N NaCl + 0.5N NaNO <sub>3</sub>	2	HNO <sub>3</sub>	2.0-3.1	0/3	OK-60	16	--	21,60	5,12	P + I	Red	2a
"	7	NaOH	5.2-7.0	0/3	OK-60	12	--	21,60	4,9	P	Gray	2a
0.5N NaCl + 0.5N Na <sub>2</sub> SO <sub>4</sub>	2	H <sub>2</sub> SO <sub>4</sub>	2.0-3.9	(6)	--	--	--	21	86	I	Red	2a
"	7	NaOH	5.5-7.0	3/3	3,6,18	--	I	3,18	29,30	P	Gray	2b
0.5N NaCl + 0.5N Na <sub>2</sub> CrO <sub>4</sub>	2	HCl	2.0	2/3	1,1(OK60)	4	I	1	10	I	None	2a
"	7	HCl	7.0	2/3	4,3(OK60)	0	N A A	23,60	7,5	N A A	None	1
Ammonium Salts												
1N NH <sub>4</sub> Cl	7	NH <sub>4</sub> OH	6.4-7.0	3/3	19,23,34	--	I	22,34	32,60	I	None	2b
1N NH <sub>4</sub> NO <sub>3</sub>	7	NH <sub>4</sub> OH	6.4-7.0	0/3	OK-60	6	--	22,60	1,1	N A A	None	1
1N (NH <sub>4</sub> ) <sub>2</sub> SO <sub>4</sub>	7	NH <sub>4</sub> OH	6.2-7.0	0/3	OK-60	4	--	22,60	1,2	N A A	None	1
1N (NH <sub>4</sub> ) <sub>2</sub> CrO <sub>4</sub>	7	CrO <sub>3</sub>	7.0	0/3	OK-60	3	--	22,60	4,3	N A A	None	1
Miscellaneous												
1N NaCl + 10 ml/l 30% H <sub>2</sub> O <sub>2</sub>	5.5	--	--	3/3	2,3,3	--	I	2	--	I	--	3a
1N NaCl + 1N AlCl <sub>3</sub>	2	HCl	2.0-3.0	3/3	16,16,16	--	I	16	55	I	Red	3a
1N Na <sub>2</sub> SO <sub>4</sub> + 10 ml/l 30% H <sub>2</sub> O <sub>2</sub>	5.8	--	--	1/3	8 (2 OK60)	7	--	10	8	I	--	2a
1N Na <sub>2</sub> SO <sub>4</sub> + 1N Al(SO <sub>4</sub> ) <sub>3</sub>	2	H <sub>2</sub> SO <sub>4</sub>	2.0	0/3	OK-60	33	--	22,60	15,15	P + I	Black	2a

## Plate Chemical Composition, Weight Per Cent

Si	Fe	Cu	Mn	Mg	Cr	Ni	Zn	Ti	Y	Zr
11	19	6.03	26	02	00	01	02	05	10	16

NOTES (1) Results are the average of tests of those specimens which did not fail, unless more than one value is shown due to divergent results

(2) Type of attack N A A = No Appreciable Attack, P = Pitting, I = Intergranular, P + I = Pitting Plus Intergranular

(3) Wet surface film observed at termination of maximum exposure in individual solutions

(4) Localized corrosion 1 = negligible, 2 = mild, 3 = severe, a = random, b = directional Ratings based upon appearance after maximum exposure time in each solution

(5) Failure occurred outside the reduced section at the edge of or beneath the cellulose acetate coating used to cover all parts of the stressing frame

(6) Stressed data invalidated due to breakdown of protective coating on stressing frame



TABLE XIII

RESISTANCE TO STRESS-CORROSION CRACKING OF ALUMINUM ALLOYS IN VARIOUS AQUEOUS SOLUTIONS  
7075-T7351 ALLOY SHORT TRANSVERSE TENSILE SPECIMENS, 0.125" DIAMETER  
TENSILE STRENGTH-67.6 KSI, YIELD STRENGTH-57.7 KSI, % ELONGATION-6.0

Solution	Nominal pH	Adjusted With	Actual pH Range	Stressed - 75% Y.S.				Unstressed Specimens			Visual Examination		
				F/N(1)	Days	% Loss(2) in T.S.	Type of(3) Attack	Days	% Loss(4) in T.S.	Type of(3) Attack	Film(5)	Localized(6) Corrosion	
Halide Anions													
1N NaCl	2	HCl	2.0 - 4.2	3/3(7)	18,18,22	--	P	18,22	50,60	P	Dark Red	3b	
1N NaCl	7	NaOH	4.8 - 7.0	0/3	OK-60	11	P	21,60	25, 6	P	White	2b	
1N NaBr	2	HBr	2.0 - 4.1	0/3	OK-60	69	P	21,60	30,41	P	Dark Red	2b	
1N NaBr	7	NaOH	4.0 - 7.0	0/3	OK-60	5	P	21,60	6, 9	P	Dull	1	
1N NaI	2	HI	2.0 - 3.4	0/3	OK-60	57	P	21,60	15,23	P	Dull	2b	
1N NaI	7	NaOH	5.8 - 7.4	0/3	OK-60	5	P	21,60	3, 4	P	Dark Gray	1	
1N KHF <sub>2</sub>	2	--	1.5 - 2.0	0/3	OK-60	7	P	21,60	3, 4	P	Red	2a	
1N NaF	7	HF	7.0 - 7.3	0/3	OK-60	0	P	21,60	0, 0	P	None	1	
Complex Anions													
1N NaNO <sub>3</sub>	2	HNO <sub>3</sub>	2.0 - 2.7	0/3	OK-60	14	P	21,60	4,13	P	Gray-Red	2a	
1N NaNO <sub>3</sub>	7	NaOH	4.1 - 7.0	0/3	OK-60	1	P	21,60	12, 1	P	White	1	
1N Na <sub>2</sub> CrO <sub>4</sub>	2	CrO <sub>3</sub>	2.0	0/3	OK-60	0	P	21,60	2, 0	P	None	1	
1N Na <sub>2</sub> CrO <sub>4</sub>	7	CrO <sub>3</sub>	7.0	0/3	OK-60	3	P	21,60	0, 0	P	None	1	
1N Na <sub>2</sub> SO <sub>4</sub>	2	H <sub>2</sub> SO <sub>4</sub>	2.0 - 2.5	0/3	OK-60	53	P(8)	21,60	17,47	P	Dark Red	2b	
1N Na <sub>2</sub> SO <sub>4</sub>	7	NaOH	4.5 - 7.0	0/2	OK-60	1	P	21	0	P	Gray	1	
0.5N Na <sub>2</sub> SO <sub>4</sub> + 0.5N NaNO <sub>3</sub>	2	H <sub>2</sub> SO <sub>4</sub>	2.0 - 3.5	0/3	OK-60	48	P	21,60	13,42	P	Black	2a	
0.5N Na <sub>2</sub> SO <sub>4</sub> + 0.5N Na <sub>2</sub> CrO <sub>4</sub>	2	H <sub>2</sub> SO <sub>4</sub>	2.0 - 2.4	0/3	OK-60	21	P	21,60	1,10	P	Gray	1	
1N NaHSO <sub>4</sub>	1	--	0.9 - 1.0	3/3(7)	33,34,35	--	P	21,35	50,72	P	Dark Red	3b	
1N NaH <sub>2</sub> PO <sub>4</sub>	4	--	4.2 - 4.4	0/3	OK-60	0	P	21,60	2, 0	P	Black	1	
Sodium Chloride Plus Oxidizing Acids													
1N NaCl	2	HNO <sub>3</sub>	2.0 - 4.3	3/3(7)	6,7,8	--	P	6, 8	46,49	P	Gray-Red	2b	
1N NaCl	2	H <sub>2</sub> SO <sub>4</sub>	2.0	3/3(7)	2,2,4	--	P	2, 4	36,54	P	--	2b	
1N NaCl	2	CrO <sub>3</sub>	2.0	3/3(7)	39,42,42	--	P	21	21	P	None	1	
4N NaCl + 0.5N HNO <sub>3</sub>	0.4	HNO <sub>3</sub>	0.4 - 3.5	2/2(7)	19,19	--	P	19	68	P	Gray-Red	3a	
Sodium Chloride Plus Complex Anions													
0.5N NaCl + 0.5N NaNO <sub>3</sub>	2	HNO <sub>3</sub>	2.0 - 3.8	0/3	OK-60	30	P	21,60	10,29	P + SI	Red	2b	
0.5N NaCl + 0.5N NaNO <sub>3</sub>	7	NaOH	4.3 - 7.8	0/3	OK-60	7	P	21,60	1, 4	P	Gray-White	1	
0.5N NaCl + 0.5N Na <sub>2</sub> SO <sub>4</sub>	2	H <sub>2</sub> SO <sub>4</sub>	2.0	3/3(7)	2,4,4	--	P	2, 5	27,55	P + SI	--	1	
0.5N NaCl + 0.5N Na <sub>2</sub> SO <sub>4</sub>	7	NaOH	4.7 - 7.0	1/3(7)	60(2 OK 60)	34	P	21,60	18,16	P	Gray-White	1b	
0.5N NaCl + 0.5N Na <sub>2</sub> CrO <sub>4</sub>	2	HCl	2.0	3/3(7)	48,52,60	--	P	21,60	1, 5	P	None	1	
0.5N NaCl + 0.5N Na <sub>2</sub> CrO <sub>4</sub>	7	HCl	7.0	0/3	OK-60	0	P	21,60	2,12	P	None	1	
Ammonium Salts													
1N NH <sub>4</sub> Cl	7	NH <sub>4</sub> OH	6.2 - 7.0	2/3(7)	44,52(OK 60)	28	P	21,60	24,49	P	White	2b	
Miscellaneous													
1N NaCl + 3 g/l H <sub>2</sub> O <sub>2</sub>	5.5	--	--	3/3(7)	18,22,23	--	P	18,23	43,61	P	Gray-White	2a	
1N NaCl + 1N AlCl <sub>3</sub>	2	HCl	2.0 - 2.8	3/3(7)	7,10,19	--	P	7,19	67,82	P	Red	3b	
1N Na <sub>2</sub> SO <sub>4</sub> + 3 g/l H <sub>2</sub> O <sub>2</sub>	5.8	--	--	2/3(7)	29,31(OK 60)	50	P	21,60	0,23	P	Gray	1b	
1N Na <sub>2</sub> SO <sub>4</sub> + 1N Al <sub>2</sub> (SO <sub>4</sub> ) <sub>3</sub>	2	H <sub>2</sub> SO <sub>4</sub>	2.0 - 2.4	0/3	OK-60	54	P	21,60	16,45	P	Dark Red	2b	

- Notes (1) F/N denotes number of specimens failed over number exposed.  
(2) Results are average of tests of those specimens which did not fail.  
(3) Type of attack. P = pitting, P + SI = pitting plus slight intergranular.  
(4) Results are for tests of individual specimens exposed for the specified period.  
(5) Wet surface films observed at the termination of maximum exposure in the solution.  
(6) Localized corrosion 1 = negligible, 2 = mild; 3 = severe, a = random; b = directional; 1b indicates 1 or 2 local corrosion sites. Ratings are based upon appearance after maximum exposure time in each solution.  
(7) Failures associated with severe corrosion. Microscopic examination revealed no evidence of stress-corrosion cracking.  
(8) Microscopic examination revealed slight evidence of transgranular cracking.

TABLE XIV

RESISTANCE TO STRESS-CORROSION CRACKING OF ALUMINUM ALLOYS IN VARIOUS AQUEOUS SOLUTIONS  
 2219-T87 ALLOY SHORT TRANSVERSE TENSILE SPECIMENS, 0.125" DIAMETER  
 TENSILE STRENGTH-69.5 ksi, YIELD STRENGTH-59.6 ksi, % ELONGATION-4.5

Solution	Nominal pH	Adjusted With	Actual pH Range	Stressed - 75% T.S.				Unstressed Specimens			Visual Examination		
				F/N(1)	Days	% Loss(2) in T S	Type of(3) Attack	Days	% Loss(4) in T S	Type of(3) Attack	Film(5)	Localized(6) Corrosion	
<u>Halide Anions</u>													
1N NaCl	2	HCl	2.0 - 4.2	3/3(7)	5h, 5h, 5h	--	P + SI	21, 5h	51, 66	P + SI	Red	3b	
1N NaCl	7	NaOH	4.9 - 7.0	0/3	OK-60	25	P + SI	21, 60	22, 33	P	Gray	2b	
1N NaBr	2	HBr	2.0 - 4.0	2/3(7)	53, 60(OK60)	6h	P + SI	21, 60	32, 51	P	Light Red	2b	
1N NaBr	7	NaOH	4.2 - 7.0	0/3	OK-60	16	P	21, 60	1h, 12	P + SI	Gray	2a	
1N NaI	2	HI	2.0 - 4.0	3/3(7)	29, 32, 3h	--	P + SI	21	32	P	Dull	2b	
1N NaI	7	NaOH	5.5 - 7.0	0/3	OK-60	5	P + SI	21, 60	8, 9	P + SI	Dull	1	
1N KHF <sub>2</sub>	2	--	1.5 - 2.0	0/3	OK-60	7	P	21, 60	11, 1h	P	Red	1	
1N NaF	7	HF	7.0 - 7.4	0/3	OK-60	6	P	21, 60	8, 9	P	None	1	
<u>Complex Anions</u>													
1N NaNO <sub>3</sub>	2	HNO <sub>3</sub>	2.0 - 2.3	0/3	OK-60	18	P	21, 60	13, 22	P	Light Red	1.	
1N NaNO <sub>3</sub>	7	NaOH	4.0 - 7.0	0/3	OK-60	11	P	21, 60	9, 10	P	Dull	1	
1N Na <sub>2</sub> CrO <sub>4</sub>	2	CrO <sub>3</sub>	2.0 - 2.3	0/3	OK-60	10	P	21, 60	11, 8	P	None	1	
1N Na <sub>2</sub> CrO <sub>4</sub>	7	CrO <sub>3</sub>	7.0	0/3	OK-60	8	P	21, 60	12, 11	P	None	1	
1N Na <sub>2</sub> SO <sub>4</sub>	2	H <sub>2</sub> SO <sub>4</sub>	2.0	0/3	OK-60	21	P	21, 60	3, 11	P	Black	1	
1N Na <sub>2</sub> SO <sub>4</sub>	7	NaOH	4.9 - 7.0	0/2	OK-60	10	P	21, 60	2, 3	P	Gray	1	
0.5N Na <sub>2</sub> SO <sub>4</sub> + 0.5N NaNO <sub>3</sub>	2	H <sub>2</sub> SO <sub>4</sub>	2.0 - 2.4	0/3	OK-60	22	P	21, 60	8, 1h	P	Dark Gray	1	
0.5N Na <sub>2</sub> SO <sub>4</sub> + 0.5N Na <sub>2</sub> CrO <sub>4</sub>	2	H <sub>2</sub> SO <sub>4</sub>	2.0 - 2.5	0/3	OK-60	27	P	21, 60	9, 23	P	Black	1	
1N NaHSO <sub>4</sub>	1	--	0.9 - 1.0	0/3	OK-60	21	P	21, 60	20, 38	P	Dark Red	2a	
1N NaH <sub>2</sub> PO <sub>4</sub>	4	--	4.2 - 4.3	0/3	OK-60	3	P	21, 60	10, 11	P	Black	1	
<u>Sodium Chloride plus Oxidizing Acids</u>													
1N NaCl	2	HNO <sub>3</sub>	2.0 - 4.3	3/3(7)	5, 7, 7	--	P + SI	5, 7	61, 76	P + SI	Red	2b	
1N NaCl	2	H <sub>2</sub> SO <sub>4</sub>	2.0 - 4.0	3/3(7)	8, 9, 9	--	P	8, 9	56, 60	P + SI	Red	3b	
1N NaCl	2	CrO <sub>3</sub>	2.0	2/3(7)	16, 21(OK60)	2h	P + SI	16, 60	8, 75	P	None	1	
4N NaCl + 0.5N KNO <sub>3</sub>	0.4	HNO <sub>3</sub>	0.4 - 3.5	3/3(7)	25, 25, 25	--	P + SI	21, 25	61, 60	P + SI	Gray Red	3a	
<u>Sodium Chloride plus Complex Anions</u>													
0.5N NaCl + 0.5N NaNO <sub>3</sub>	2	HNO <sub>3</sub>	2.0 - 3.2	0/3	OK-60	27	P	21, 60	10, 26	P	Light Red	2a	
0.5N NaCl + 0.5N NaNO <sub>3</sub>	7	NaOH	4.5 - 7.0	0/3	OK-60	15	P	21, 60	6, 18	P	White	2a	
0.5N NaCl + 0.5N Na <sub>2</sub> SO <sub>4</sub>	2	H <sub>2</sub> SO <sub>4</sub>	2.0 - 2.7	3/3(7)	4, 5, 5	--	P + SI	4, 5	54, 58	P + SI	Dark Gray	2a	
0.5N NaCl + 0.5N Na <sub>2</sub> SO <sub>4</sub>	7	NaOH	4.8 - 7.0	1/3(7)	46(2 OK 60)	17	P + SI	21, 60	3, 21	P + SI	Gray	1	
0.5N NaCl + 0.5N Na <sub>2</sub> CrO <sub>4</sub>	2	HCl	2.0 - 2.4	2/3(7)	16, 22(OK 60)	4h	P + SI	16, 60	9, 28	P + SI	None	1	
0.5N NaCl + 0.5N Na <sub>2</sub> CrO <sub>4</sub>	7	HCl	7.0	0/3	OK-60	10	P	21, 60	17, 6	P + SI	None	1b	
<u>Ammonium Salts</u>													
1N NH <sub>4</sub> Cl	7	HCl	6.0-7.0	0/3	OK 60	8	P	21, 60	12, 10	P	None	2a	
<u>Miscellaneous</u>													
1N NaCl + 3 g/l H <sub>2</sub> O <sub>2</sub>	5.5	--	--	3/3(7)	6, 6, 7	--	P + SI	6, 7	72, 67	P + SI	Black	3a	
1N NaCl + 1N AlCl <sub>3</sub>	2	HCl	2.0 - 3.1	3/3(7)	4, 4, 5	--	P + SI	4, 5	70, 85	P + SI	Black	2a	
1N Na <sub>2</sub> SO <sub>4</sub> + 3 g/l H <sub>2</sub> O <sub>2</sub>	5.8	--	--	0/3	OK-60	12	P	21, 60	16, 16	P	None	2b	
1N Na <sub>2</sub> SO <sub>4</sub> + 1N Al <sub>2</sub> (SO <sub>4</sub> ) <sub>3</sub>	2	H <sub>2</sub> SO <sub>4</sub>	2.0 - 2.3	0/3	OK-60	20	P	21, 60	9, 23	P	Black	1	

- Notes (1) F/N denotes number of specimens failed over number exposed  
 (2) Results are average of tests of those specimens which did not fail  
 (3) Type of attack P = pitting, P + SI = pitting plus slight intergranular.  
 (4) Results are for tests of individual specimens exposed for the specified periods  
 (5) Wet surface films observed at the termination of maximum exposure in the solution  
 (6) Localized corrosion 1 = negligible, 2 = mild, 3 = severe, a = random, b = directional, 1b indicates 1 or 2 local corrosion sites Ratings are based upon appearance after maximum exposure time in each solution  
 (7) Failures associated with severe corrosion Microscopic examination revealed no evidence of stress-corrosion cracking

TABLE XV

RESISTANCE TO STRESS-CORROSION CRACKING OF ALUMINUM ALLOYS IN ACIDIC ELECTROLYTES  
 2219-T37 AND 7075-T651 ALLOY SHORT TRANSVERSE TENSILE SPECIMENS, 0.125" DIAMETER

Alloy	Solution	Nominal pH	Adjusted With	Exposure Period	Unstressed Specimens			Stressed 75% YS(1)	
					% Loss(2) in T.S.	Type of(4) Attack	F/N	% Loss(3) in T.S.	Type of(4) Attack
2219-T37	1N NaCl	2	HCl	2 days	27	I	0/2	42	I
				4 days	30	I	0/2	39	I
				8 days	50	P+I	1/2 8 da	71	I
				16 days	66	I	2/2 16 da.	--	I
				24 days	53	P+SI	1/2 17 da.	82	P+SI
				Previous Test(6)	19 days	I	3/3 19 da.	--	I
	1N NaCl	2	H <sub>2</sub> SO <sub>4</sub>	1 day	30	I	0/2	52	I
				2 days	49	I	1/2 2 da	69	I
				4 days	46	I	0/2	63	I+SP
				8 days	69	I	0/2	88	I
				16 days	100(5)	--	2/2 8,10 da	--	I
				Previous Test(6)	8 days	I	3/3 8 da.	--	I
7075-T651	1N NaCl	2	HCl	8 hours	4	I	0/2		I
				16 hours	16	I	2/2 16 hr		I
				32 hours	16	I	1/2 32 hr.		I
				64 hours	25	I	1/2 40 hr		I
				96 hours	33	P	2/2 6,24 hr		I
				Previous Test(6)	3 days	P+I	3/3 3 da.	--	P+I
	1N NaCl	2	H <sub>2</sub> SO <sub>4</sub>	1 hour	0	N.A.A.	0/2	0	N.A.A.
				2 hours	0	N.A.A.	0/2	2	N.A.A.
				3 hours	0	I	1/2 3 hr	18	I
				4 hours	.2	P+I	2/2 4 hr.	--	I
				8 hours	1	P+I	2/2 4 hr.	--	P+I
				24 hours	7	I	2/2 4 hr	--	P+SI
				Previous Test(6)	24 hours	P+I	3/3 1 da	--	P+I
	1N Na <sub>2</sub> SO <sub>4</sub>	2	H <sub>2</sub> SO <sub>4</sub>	4 days	1	P	0/2	3	P
				8 days	3	P	0/2	3	P
				16 days	7	P	0/2	31	P
				24 days	12	P	0/2	18	P
				48 days	21	DP	1/2 34 da	38	DP
				Previous Test(6)	47 days	P	3/3 39-47 da.	--	P+I

- Notes (1) Tensile Properties 2219-T37 alloy - 58 ksi tensile, 44 ksi yield, 8% elongation  
 7075-T651 alloy - 79 ksi tensile, 68 ksi yield, 3% elongation  
 (2) Results shown are for tests of individual specimens  
 (3) Results shown are average of tests of specimens that did not fail in previous tests, all others are for individual specimens  
 (4) Type of attack N.A.A. = no appreciable attack, P = pitting, DP = directional pitting, P + SI = pitting plus slight intergranular; P + I = pitting plus intergranular, I = intergranular, I + SP = intergranular plus slip plane  
 (5) Broke while being placed in testing machine.  
 (6) Detailed results given in Tables XI, XII

TABLE XVI

RESISTANCE TO STRESS-CORROSION CRACKING OF ALUMINUM ALLOYS IN ACIDIC ELECTROLYTES  
2219-T87 AND 7075-T7351 ALLOY SHORT TRANSVERSE TENSILE SPECIMENS, 0.125" DIAMETER

Alloy	Solution	Nominal pH	Adjusted With	Exposure Period	Unstressed Specimens			Stressed 75% Y.S (1)	
					% Loss (2) in T S	Type of (4) Attack	F/N	% Loss (3) in T S	Type of (4) Attack
2219-T87	1N NaCl	2	HCl	3 days	28	DP	0/2	21	DP
				7 days	42	DP	0/2	43	P
				14 days	42	P	0/2	37	P
				21 days	57	P	0/2	61	DP
				Previous Test (5)	54 days	P+SI	3/3 54 da	--	P+SI
	1N NaCl	2	H <sub>2</sub> SO <sub>4</sub>	8 hours	12	P	0/2	7	P
				16 hours	17	P	0/2	13	P
				24 hours	12	P	0/2	13	P
				48 hours	19	P	0/2	19	P
				Previous Test (5)	9 days	P+SI	3/3 8-9 da	--	P
	1N NaCl	2	CrO <sub>3</sub>	7 days	8	N A A.	0/2	6	N A.A
				14 days	22	P	1/2 10 da	7	P
				28 days	19	DP	1/2 18 da.	43	DP
				42 days	23	N A.A.	1/2 35 da	3	P
				Previous Test (5)	60 days	P	2/3 16-21 da	24	P+SI
	1N KHF <sub>2</sub>	1.5	--	7 days	11	P	0/2	11	P
				28 days	2	P	0/2	13	P
				42 days	3	P	0/2	10	P
				60 days	4	P	0/2	1	P
				Previous Test (5)	60 days	P	0/2	1	P
7075-T7351	1N NaCl	2	HCl	7 days	8	P	0/2	10	P
				28 days	27	P	0/2	34	P
				42 days	39	P	0/2	56	P
				60 days	54	DP	1/2 60 da	67	DP
				Previous Test (5)	22 days	P	3/3 18-22 da	--	P
	1N NaCl	2	H <sub>2</sub> SO <sub>4</sub>	1 day	2	P	0/2	3	P
				3 days	8	P	0/2	3	P
				7 days	22	P	0/2	31	P
				10 days	26	P	1/2 10 da.	52	P
				Previous Test (5)	4 days	P	3/3 2-4 da	--	P
	1N NaBr	2	HBr	6 days	2	P	0/2	6	P
				28 days	10	P	0/2	15	P
				42 days	34	P	0/2	23	P
				60 days	43	DP	1/2 50 da	40	DP
				Previous Test (5)	60 days	P	0/3	69	P
	1N KHF <sub>2</sub>	1.5	--	7 days	0	P	0/2	0	P
				28 days	1	P	0/2	2	P
				42 days	2	P	0/2	3	P
				60 days	0	P	0/2	0	P
				Previous Test (5)	60 days	P	0/3	7	P

- Notes** (1) Tensile Properties 2219-T87 alloy - 69 ksi tensile, 60 ksi yield, 4.5% elongation  
7075-T7351 alloy - 62 ksi tensile, 55 ksi yield, 3% elongation  
(2) Results shown are for tests of individual specimens  
(3) Results are average of tests of specimens that did not fail in previous tests, all others are for tests of individual specimens  
(4) Type of attack N A A = no appreciable attack, P = pitting, DP = directional pitting, P+SI = pitting plus slight intergranular  
(5) Detailed results given in Tables XIII, XIV

TABLE AVII

## RESISTANCE TO STRESS-CORROSION CRACKING OF ALUMINUM ALLOYS IN VARIOUS AQUEOUS SOLUTIONS

Short Transverse Tensile Specimens, 0.125" Diameter

Alloy	Solution	Nominal pH	Adjusted With	Actual pH Range	Stressed 75% Y S				Unstressed Specimens			Visual Examination		REMARKS
					F/N <sup>(1)</sup>	Days	%Loss in T S (2)	Type of Attack <sup>(3)</sup>	Days	%Loss in T S (4)	Type of Attack <sup>(3)</sup>	Film <sup>(5)</sup>	Localized Corrosion <sup>(6)</sup>	
2219-T37	1N CaCl <sub>2</sub>	2	HCl	2 0-4 1	3/3	8,11,29	--	I + P	8, 29	52, 75	I + P	Dark Red	3b	Removed from test <sup>(7)</sup>
	1N CaCl <sub>2</sub>	7	HCl	7 0-7 6	3/3	14,26,29	--	P + I	14, 29	30, 36	P + I	Gray	1b	
	1N FeCl <sub>3</sub>	1.5	--	--	0/3	1	--	--	--	--	--	--	--	Removed from test <sup>(7)</sup>
	1N CuCl <sub>2</sub>	2	HCl	2 0-3 4	0/3	30 min	--	I + P	30 min	53	I + P	Copper Deposits	3a	
	1N CuSO <sub>4</sub>	2	H <sub>2</sub> SO <sub>4</sub>	2 0-2 8	3/3	47,55,57	--	I	21, 55	47, 71	I + P	Copper Deposits	3a	Removed from test <sup>(7)</sup>
	1N NaOH	11.5	--	--	0/3	1	--	--	--	--	--	--	--	
	1N NH <sub>4</sub> OH	11	--	10 3-11 0	0/3	OK 60	14	N.A.A	21, 60	16, 16	P	Dark Gray	2a	
	1N NaCl	11	NaOH	9 4-11 0	3/3	4, 4, 4	--	P	4, 21	28, 43	P + SI	Dark Gray	2a	
2219-T87	1N CaCl <sub>2</sub>	2	HCl	2 0-4 2	1/3	36(20x60)	58	P	21, 60	47, 76	P	Red	3b	Stress Corrosion doubtful <sup>(8)</sup>
	1N CaCl <sub>2</sub>	7	HCl	7 0-7 4	3/3	47,47,55	--	P	21, 55	34, 47	P	Gray	2b	Stress Corrosion doubtful <sup>(8)</sup>
	1N FeCl <sub>3</sub>	1.5	--	--	0/3	1	--	--	--	--	--	--	--	Removed from test <sup>(7)</sup>
	1N CuCl <sub>2</sub>	2	HCl	2 0-3 2	0/3	20 min	--	P	20 min	54	P	Copper Deposits	3a	Removed from test <sup>(7)</sup>
	1N CuSO <sub>4</sub>	2	H <sub>2</sub> SO <sub>4</sub>	2 0-3 4	0/3 <sup>(10)</sup>	40	--	--	21	33	P	Copper Deposits	3a	Removed from test <sup>(7)</sup>
	1N NaOH	11.5	--	--	0/3	1	--	--	--	--	--	--	--	
	1N NH <sub>4</sub> OH	11	--	10 6-11 2	0/3	OK 60	21	P	21, 60	14, 20	P	Black	2a	
	1N NaCl	11	NaOH	9 0-11 0	3/3	16,20,42	--	P	16, 42	34, 47	P	Black	1	
7075-T651	1N CaCl <sub>2</sub>	2	HCl	2 0-4 1	3/3	1, 1, 1	--	I + P	1	32	I + P	Black	2b	Removed from test <sup>(7)</sup>
	1N CaCl <sub>2</sub>	7	HCl	7 0-7 8	3/3	14, 26, 27	--	P	14, 27	0, 3	N.A.A.	Gray	1	
	1N FeCl <sub>3</sub>	1.5	--	--	0/3	1	--	--	--	--	--	--	--	Removed from test <sup>(7)</sup>
	1N CuCl <sub>2</sub>	2	HCl	2 0-3 5	0/3	10 min	--	P + SI	10 min	61	P + SI	Copper Deposits	3a	Removed from test <sup>(7)</sup>
	1N CuSO <sub>4</sub>	2	H <sub>2</sub> SO <sub>4</sub>	2 0-2 5	3/3	11,11,14	--	P	11, 14	23, 28	P	Copper Deposits	2a	Stress corrosion questionable <sup>(9)</sup>
	1N NaOH	11.5	--	--	0/3	1	--	P	1	83	P	--	3a	Removed from test <sup>(7)</sup>
	1N NH <sub>4</sub> OH	11	--	10 7-11 3	3/3	3, 3, 4	--	P	3, 21	1, 6	P	Gray-Black	2a	Removed from test <sup>(7)</sup>
	1N NaCl	11	NaOH	9 0-11 0	3/3	4, 6, 7	--	P	4, 7	0, 0	P	Black	1	
7075-T7351	1N CaCl <sub>2</sub>	2	HCl	2 0-4 1	3/3	29,38,50	--	P	21, 50	40, 71	P	Dark Red	3b	Stress corrosion doubtful <sup>(8)</sup>
	1N CaCl <sub>2</sub>	7	HCl	7 0-8 0	0/3	OK 60	44	P	21, 60	26, 32	P	Gray	1b	Removed from test <sup>(7)</sup>
	1N FeCl <sub>3</sub>	1.5	--	--	0/3	1	--	--	--	--	--	--	3a	
	1N CuCl <sub>2</sub>	2	HCl	2 0-3 0	0/3	30 Min	46	P	30 min	43	P	Copper Deposits	3a	Removed from test <sup>(7)</sup>
	1N CuSO <sub>4</sub>	2	H <sub>2</sub> SO <sub>4</sub>	2 0-2 6	3/3	28,28,31	--	P	21, 31	51, 64	P	Copper Deposits	3a	Stress corrosion doubtful <sup>(8)</sup>
	1N NaOH	11.5	--	--	0/3	1	--	--	--	--	--	--	3a	Removed from test <sup>(7)</sup>
	1N NH <sub>4</sub> OH	11	--	11 1-11 2	0/3	OK 60	14	P	21, 60	11, 11	P	Black	2a	Stress corrosion doubtful <sup>(8)</sup>
	1N NaCl	11	NaOH	9 2-11 0	1/3	50(20x60)	33	P	9, 60	9, 23	P	Black	1	

- NOTES (1) F/N denotes number of specimens failed over number exposed
- (2) Results are the average of tests of those specimens which did not fail in test
- (3) Type of attack N.A.A. = No Appreciable Attack, P = Pitting, P + SI = Pitting + Slight Intergranular, P + I = Pitting + Intergranular, I + P = Intergranular + Pitting
- (4) Results are for tests of individual specimens exposed for the specified periods
- (5) Wet surface film observed at the termination of maximum exposure in the solution
- (6) Localized corrosion 1 = negligible, 2 = mild, 3 = severe, a = random, b = directional

- (7) Removed from test due to either severe reduction in cross section or complete dissolution of specimen
- (8) Metallographic examination revealed no evidence of intergranular corrosion or secondary cracking. This and high tensile loss indicate failure was probably due to corrosion
- (8a) Failures associated with severe localized or general pitting, metallographic examination revealed no evidence of secondary cracking.
- (9) Metallographic examination revealed no evidence of intergranular corrosion or secondary cracking, but tensile loss data suggest failure may have been due to stress-corrosion cracking
- (10) Specimens removed from test due to severe corrosion of the specimen and stressing frame at the edge and beneath the cellulose acetate coating used to isolate the stressing frames.

TABLE XVIII

Tensile Properties of 7075 Alloy Sheet Samples  
Quenched Rapidly from Various Temperatures

<u>H.T. Temp.</u>	<u>As Quenched (-W)</u>			<u>T6 Aging</u>			<u>T73 Aging</u>		
	<u>T.S.-ksi</u>	<u>Y.S.-ksi</u>	<u>Elong.-%</u>	<u>T.S.-ksi</u>	<u>Y.S.-ksi</u>	<u>Elong.-%</u>	<u>T.S.-ksi</u>	<u>Y.S.-ksi</u>	<u>Elong.-%</u>
870 F	77.6	49.6	18.0	82.2	72.0	13.0	80.3	71.8	9.2
810	74.6	47.4	17.5	79.6	70.0	12.0	75.4	68.5	10.0
750	69.2	42.3	16.5	74.0	63.6	12.0	69.3	60.2	10.0
715	67.2	39.1	16.5	71.5	61.4	12.0	66.3	56.7	10.5
680	62.3	36.9	13.0	55.6	41.2	11.8	59.7	48.4	10.0
610	48.8	35.0	11.0	48.0	36.4	10.0	44.3	35.4	8.2
550	43.9	36.3	6.5	45.3	37.8	7.0	44.0	37.3	7.0

Solution treatment - One hour at metal temperature from cold-rolled temper.

Aging treatment - As-quenched - about one month at room temperature before testing.

- T6 aged 4 days at room temperature + 24 hours at 250 F

- T73 aged 4 days at room temperature + 6 hours at 225 F + 24 hours at 325 F

Composition - %

<u>Si</u>	<u>Fe</u>	<u>Cu</u>	<u>Mn</u>	<u>Mg</u>	<u>Cr</u>	<u>Zn</u>	<u>Ti</u>
0.11	0.23	1.74	0.07	2.56	0.21	5.51	0.06

TABLE XIX

POTENTIAL MEASUREMENTS OF 7075 ALLOY SPECIMENS  
IN NaCl-AlCl<sub>3</sub> SOLUTION

---

<u>H.T. Temp.</u>	<u>As Quenched (W)</u>	<u>Solution Potentials<sup>(1)</sup></u>			
		<u>T6 Aging</u>		<u>T73 Aging</u>	
		<u>Unstressed</u>	<u>Stressed<sup>(2)</sup></u>	<u>Unstressed</u>	<u>Stressed<sup>(2)</sup></u>
870 F	817	745	742	754	753
810	837	759	760	764	762
750	881	787	787	781	780
715	899	801	-	796	-
680	916	859	859	794	805
610	936	884	892	793	801
550	933	866	873	796	811

(1) Millivolts negative to Saturated Calomel Electrode after five minutes in 1N NaCl + 0.21N AlCl<sub>3</sub> solution at pH 1

(2) 75% YS

TABLE XX

Potential Measurements of 7075-T6 and 7039-T6 Specimens

<u>H.T. Temp.</u>	<u>NaCl-Na<sub>2</sub>CrO<sub>4</sub> Solution<sup>(1)</sup></u>		<u>Na<sub>2</sub>CrO<sub>4</sub><sup>(2)</sup></u>	
	<u>7075-T6<sup>(3)</sup></u>		<u>7039-T6<sup>(4)</sup></u>	
	<u>Unstressed</u>	<u>Stressed<sup>(6)</sup></u>	<u>Unstressed</u>	<u>Unstressed<sup>(5)</sup></u>
870 F	711	710	790	124
810	725	730	-	-
750	755	755	802	68
715	782	-	-	-
680	822	824	822	108
610	869	871	-	-
550	835	828	826	90

(1) Millivolts negative to Saturated Calomel Electrode after 15 minutes in 0.5N NaCl + 0.5N Na<sub>2</sub>CrO<sub>4</sub> at pH 2.

(2) Millivolts negative to SCE in 0.5N Na<sub>2</sub>CrO<sub>4</sub> at pH 2.

(3) 15-minute period

(4) 20-minute period

(5) 30-minute period

(6) 75% YS



TABLE XXI

Current Flow<sup>(1)</sup> (Ma/in<sup>2</sup>) Between Unstressed Pairs7075-T6 in NaCl-AlCl<sub>3</sub> (pH 1)

<u>Versus</u>	<u>Equilibrium at</u>			
	<u>870</u>	<u>810</u>	<u>750</u>	<u>715</u>
810	3.9	---	---	---
750	4.9	4.1	---	---
715	4.3	6.4	1.8	---
680	9.3	10.0	21.5	23.2
610	9.7	12.4	17.9	20.3

7075-T6 in NaCl-Na<sub>2</sub>CrO<sub>4</sub> (pH 2)

<u>Versus</u>	<u>870</u>	<u>810</u>	<u>750</u>	<u>715</u>
810	0.3	---	---	---
750	0.1	0.1	---	---
715	0.1	0.1	0.1	---
680	0.1	0.5	0.4	0.4
610	0.3	0.4	0.4	0.5

7075-T73 in NaCl-AlCl<sub>3</sub> (pH 1)

<u>Versus</u>	<u>870</u>	<u>810</u>	<u>750</u>	<u>715</u>
810	2.5	---	---	---
750	5.8	4.4	---	---
715	6.9	6.3	1.8	---
680	6.9	5.8	3.1	1.7
610	6.3	5.8	3.2	1.5

(1) Lower temperature always anodic

TABLE XXII

Current Flow Measurements

<u>7075 Alloy - Stressed Pairs</u>				
<u>Temper</u>	<u>Solution</u>	<u>Pairs</u>	<u>Ma/in<sup>2</sup></u>	<u>Specimen Anodic</u>
T6	NaCl-AlCl <sub>3</sub>	870 vs 680	13.3	Low Temp.
T6	NaCl-AlCl <sub>3</sub>	750 vs 680	16.1	Low Temp.
T6	NaCl-Na <sub>2</sub> CrO <sub>4</sub>	870 vs 680	0.006	Low Temp.
T73	NaCl-AlCl <sub>3</sub>	870 vs 680	5.8	Low Temp.

7039-T6 Unstressed Pairs<sup>(1)</sup> in NaCl-Na<sub>2</sub>CrO<sub>4</sub> (pH 2)

<u>Versus</u>	<u>Equilibrium at</u>		
	<u>870</u>	<u>750</u>	<u>680</u>
750	0.34	---	---
680	0.22	0.19	---
550	0.50	0.80	0.33

(1) Current in Ma/in<sup>2</sup> -  
lower temperature sample anodic

<u>7039-T6 Alloy - Stressed Pairs</u>			
<u>Solution</u>	<u>Pairs</u>	<u>Ma/in<sup>2</sup></u>	<u>Specimen Anodic</u>
NaCl-Na <sub>2</sub> CrO <sub>4</sub>	870 vs 680	0.014	High Temp.
NaCl-Na <sub>2</sub> CrO <sub>4</sub>	750 vs 680	0.097	High Temp.
Na <sub>2</sub> CrO <sub>4</sub>	870 vs 680	0.069	Low Temp.

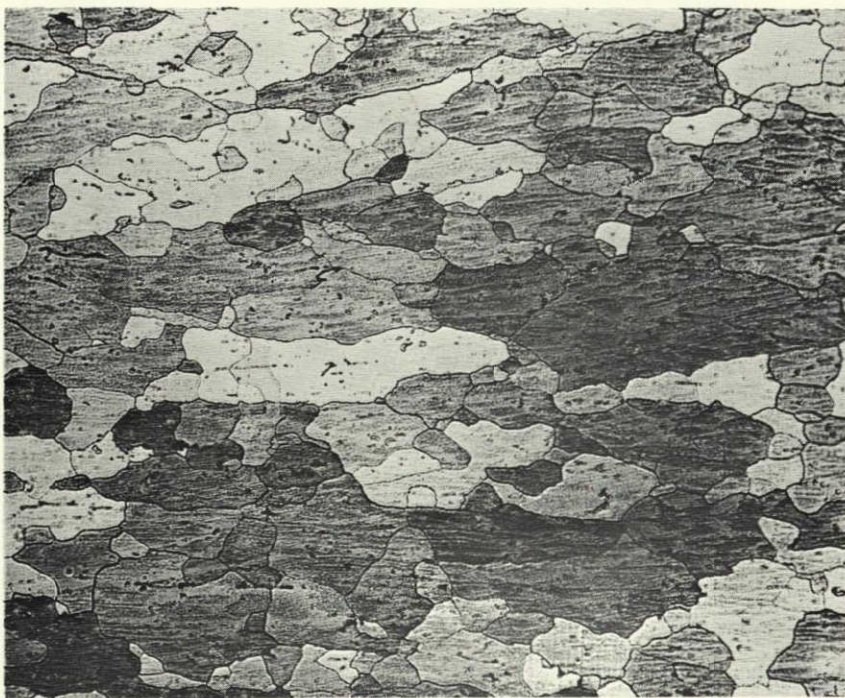
TABLE XXIII

TENSILE PROPERTIES OF 7039 ALLOY SHEET SAMPLES  
QUENCHED RAPIDLY FROM VARIOUS TEMPERATURES

<u>H.T. Temp.</u>	<u>As Quenched (W)</u>			<u>T6 Aging</u>		
	<u>T.S.-ksi</u>	<u>Y.S.-ksi</u>	<u>Elong.-%</u>	<u>T.S.-ksi</u>	<u>Y.S.-ksi</u>	<u>Elong.-%</u>
870 F	60.3	34.8	18.0	65.4	56.4	10.0
750	58.4	33.1	18.5	63.4	54.3	11.0
680	54.8	29.6	17.5	54.1	41.6	10.0
550	38.8	17.2	17.0	37.4	16.8	16.0

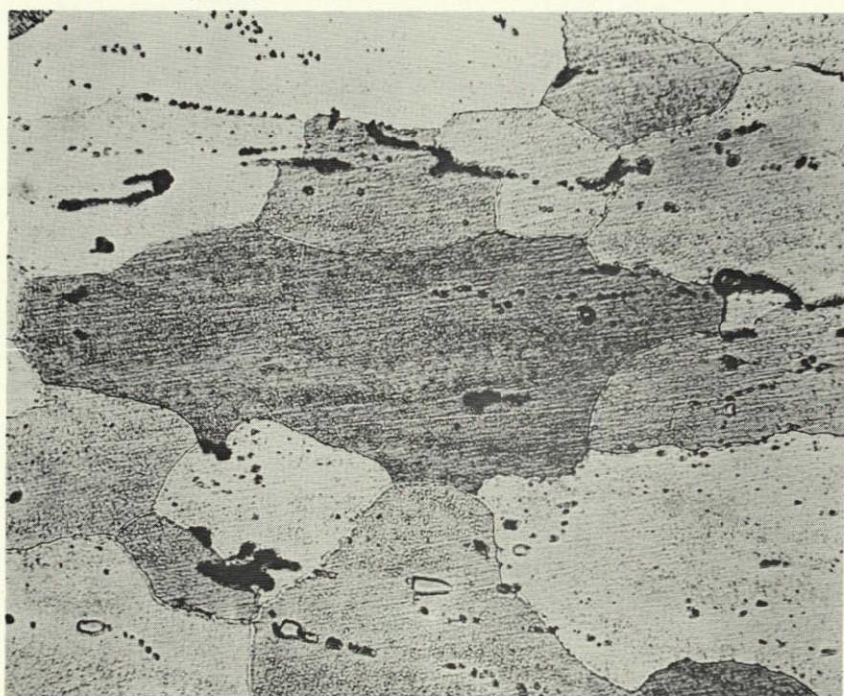
<u>Composition - %</u>							
<u>Si</u>	<u>Fe</u>	<u>Cu</u>	<u>Mn</u>	<u>Mg</u>	<u>Cr</u>	<u>Zn</u>	<u>Ti</u>
0.09	0.14	0.04	0.27	3.06	0.18	3.99	0.01

# FIGURES



Keller's Etch

100X



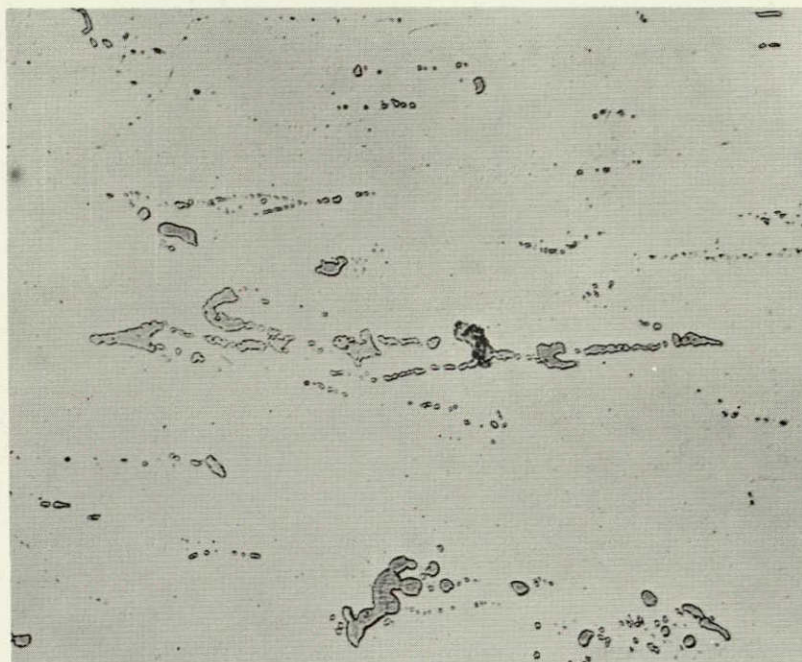
Keller's Etch

500X

Microstructure of longitudinal  
section of 2219-T351 plate.

Figure 1





As Polished

500X

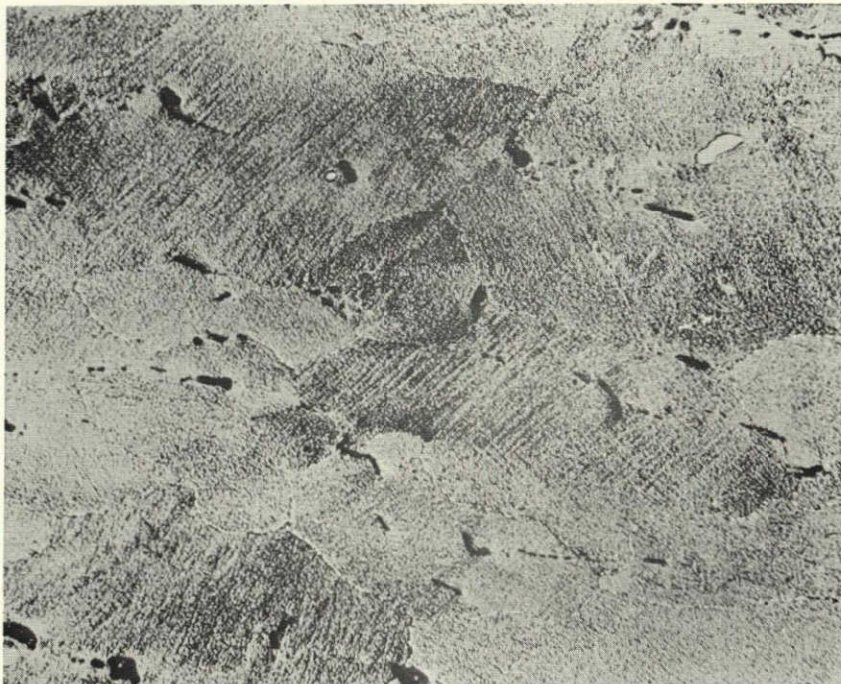
Distribution of micro-constituents  
in longitudinal plane of 2219-T351 plate.

Figure 2



**Kellers Etch**

**100X**



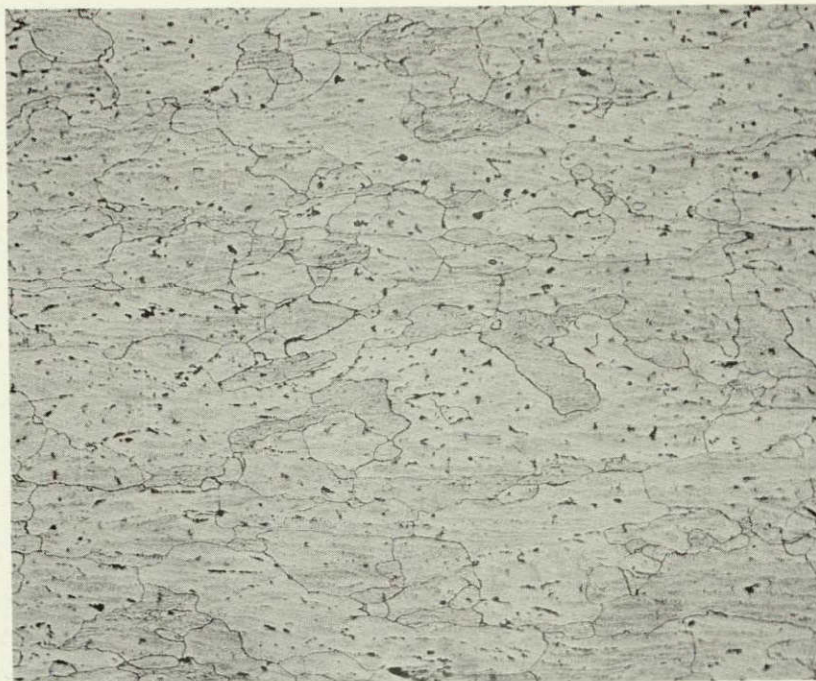
**Keller's Etch**

**500X**

**Microstructure of longitudinal  
section of 2219-T851 plate.**

**Figure 3**

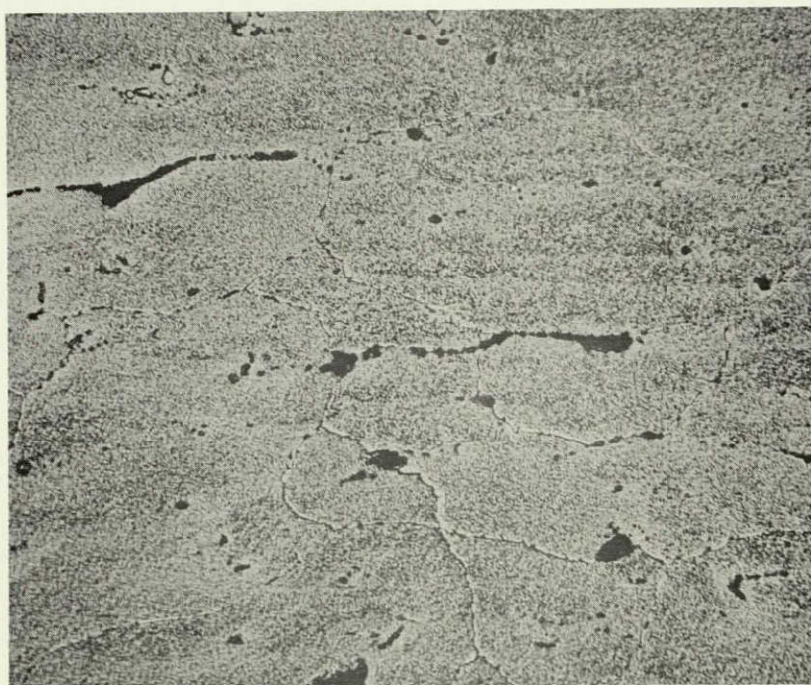




**Keller's Etch**

**100X**

NOT REPRODUCIBLE



**Keller's Etch**

**500X**

**Microstructure of longitudinal  
section of 2219-T87 plate.**

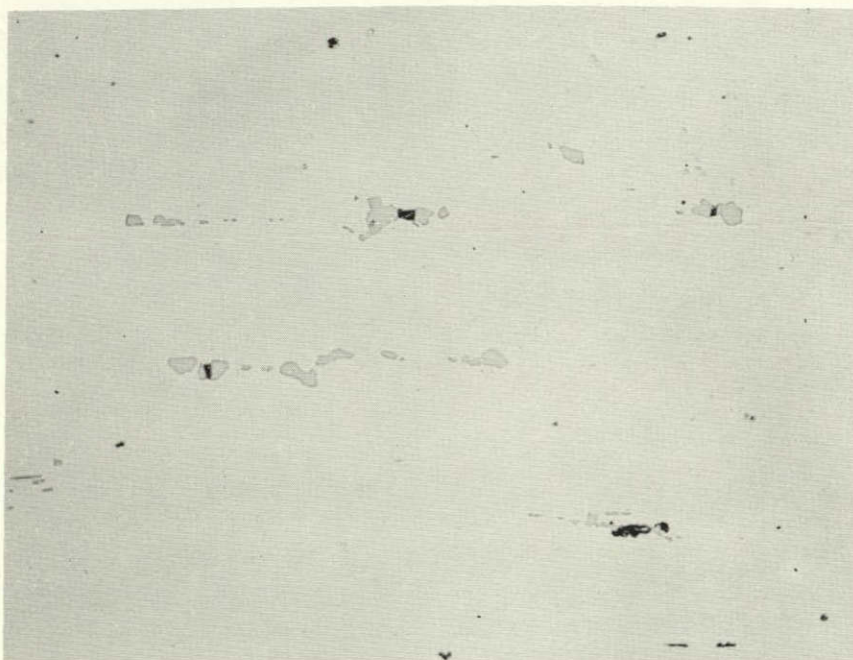
**Figure 4**





Keller's Etch

100X

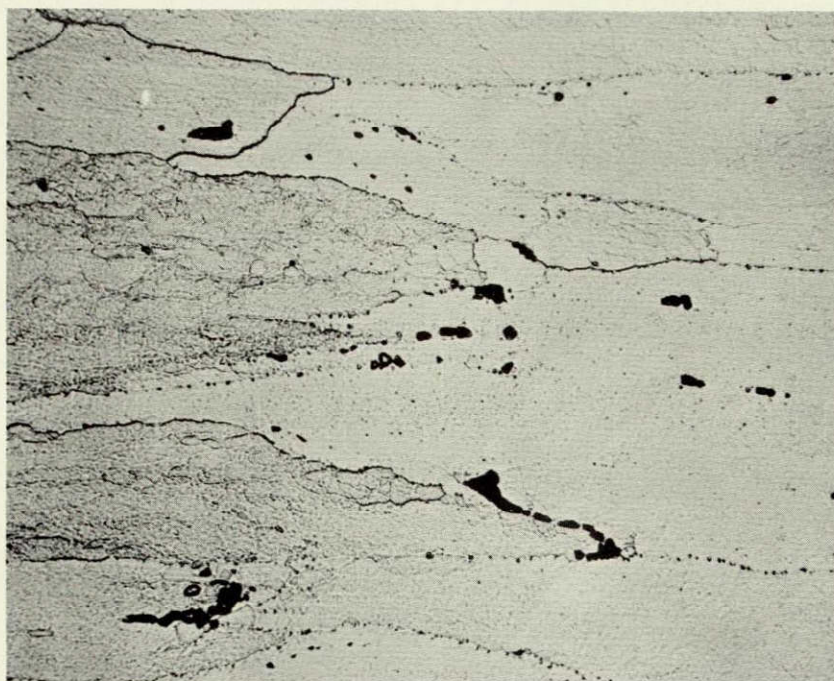


As Polished

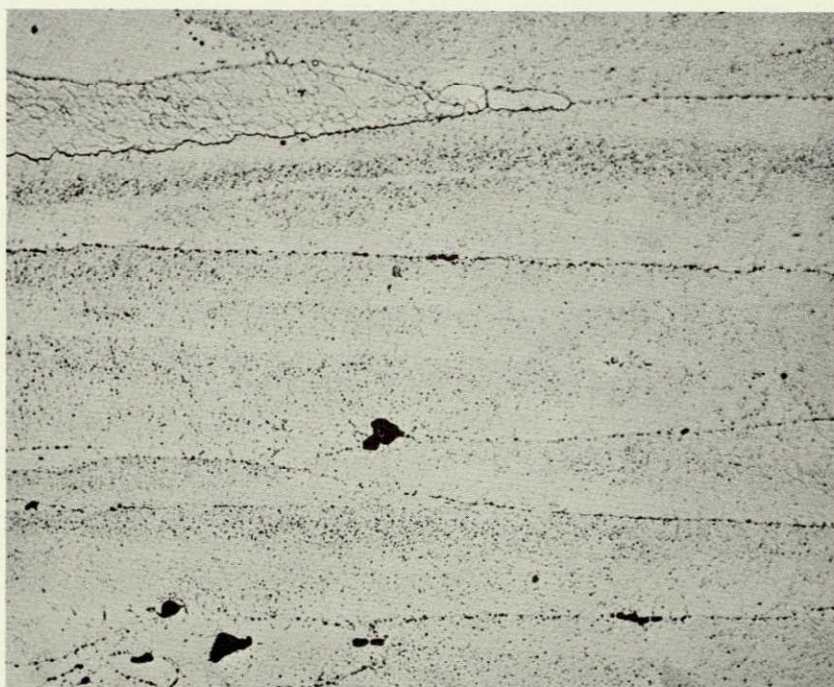
500X

Microstructure (top) and  
constituent distribution (bottom)  
in longitudinal section of  
7075-T6 plate.

Figure 5



7075-T6  
Alloy



7075-T73  
Alloy

Microstructure of longitudinal  
sections of 7075 alloy plate at  
higher magnification.

Figure 6

160141  
160142

NOT REPRODUCIBLE

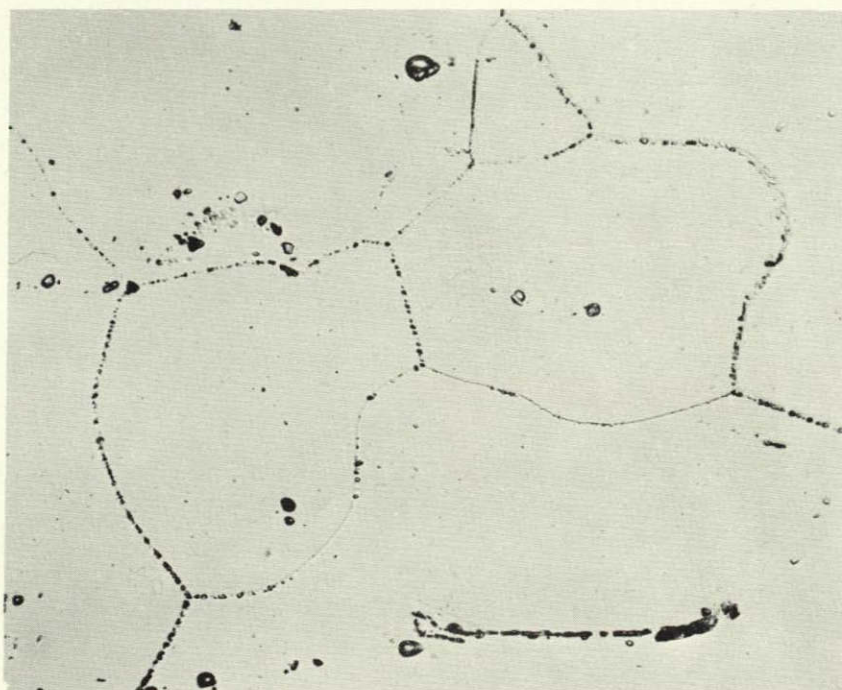




Keller's Etch

100X

X7375-T6



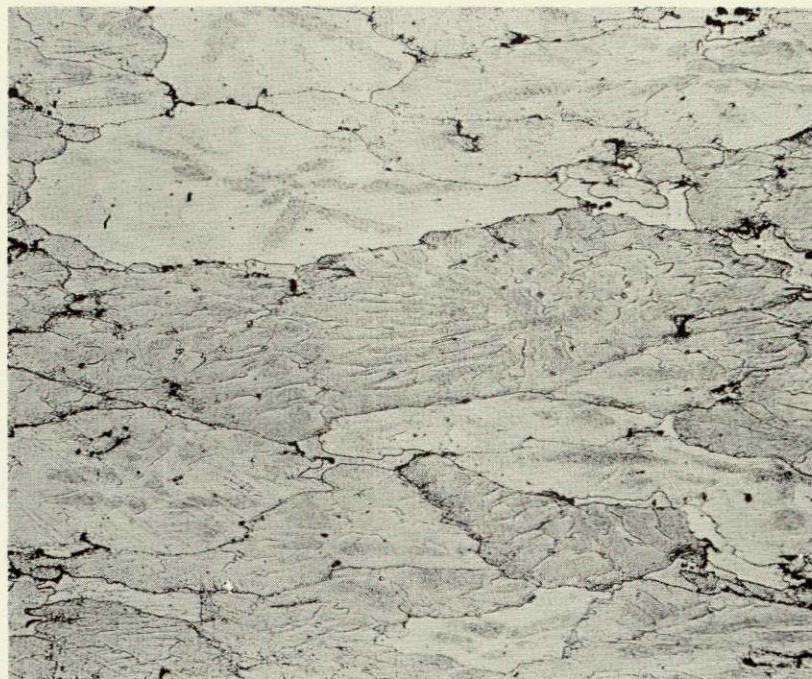
Keller's Etch

500X

X7375-T73 type

Microstructure of longitudinal  
sections of X7375 alloy plate.

Figure 7



Keller's Etch

100X



Keller's Etch

500X

Microstructure of longitudinal  
plane of 7079-T6 plate.

Figure 8





Keller's etch

100X

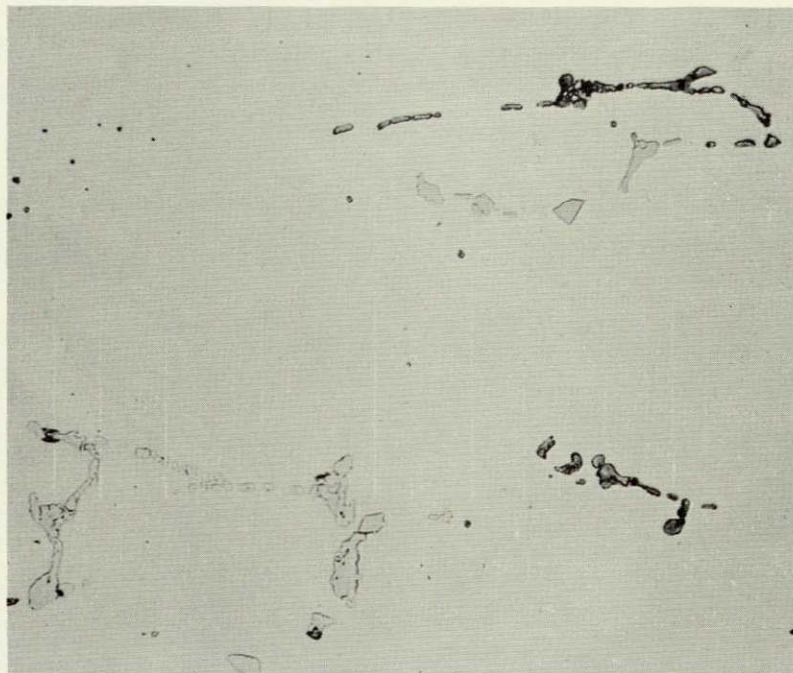


Keller's Etch

500X

Microstructure of longitudinal  
section of 7039-T6 plate.

Figure 9



7079-T6

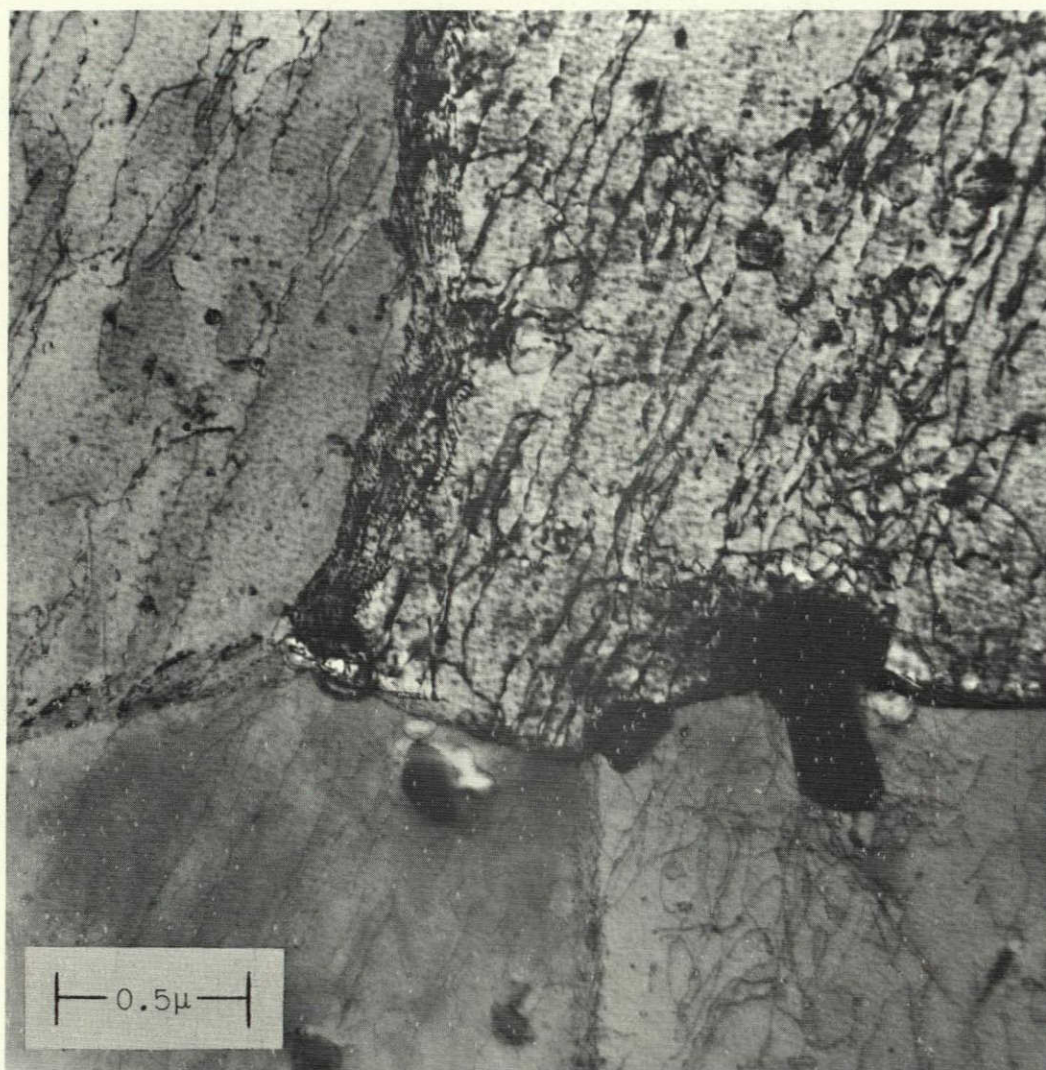


7039-T6

Distribution of microconstituents in longitudinal sections. As Polished (X500)

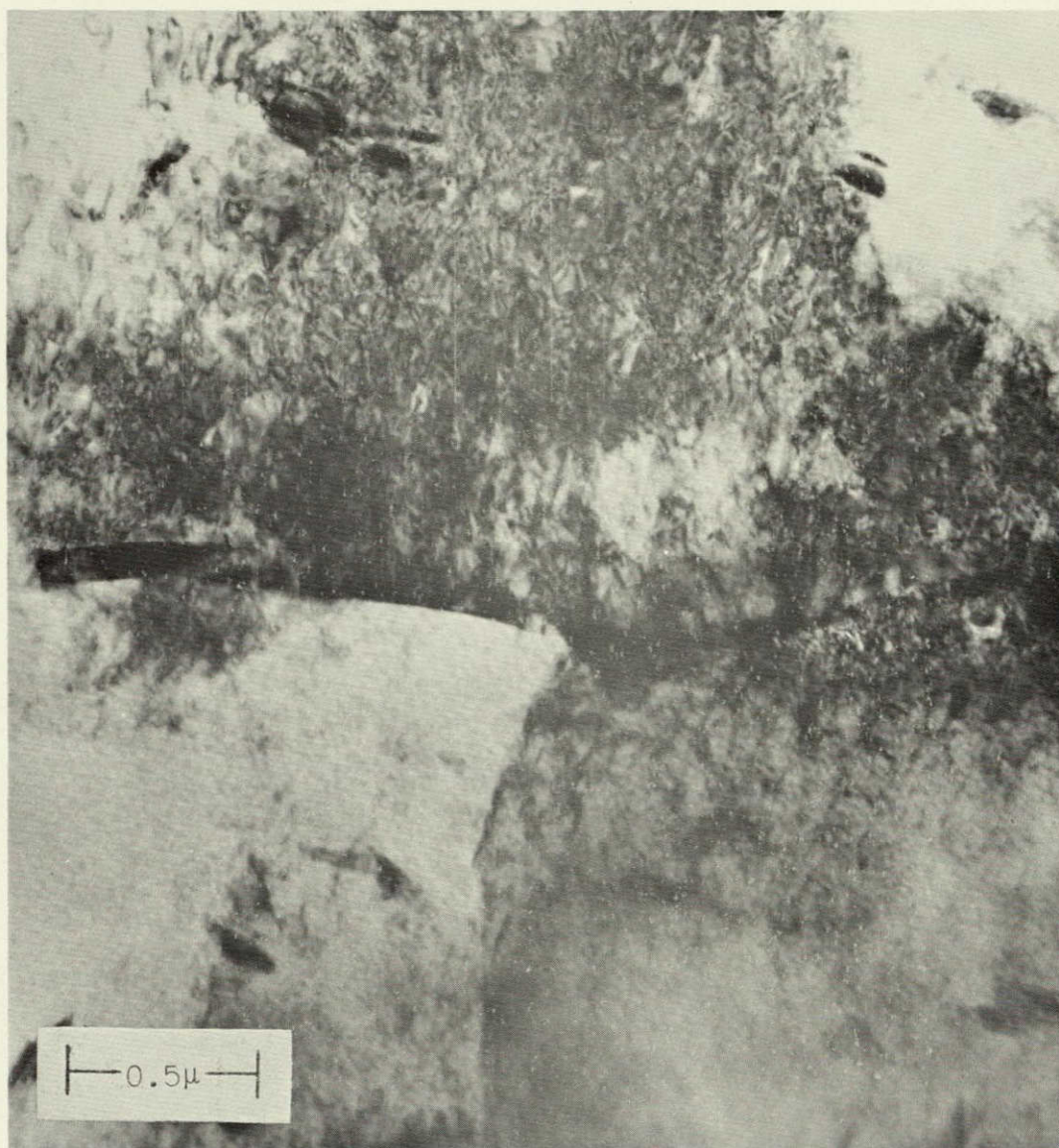
Figure 10





Electron transmission microstructure  
of 2219-T351 plate. (50,000X)

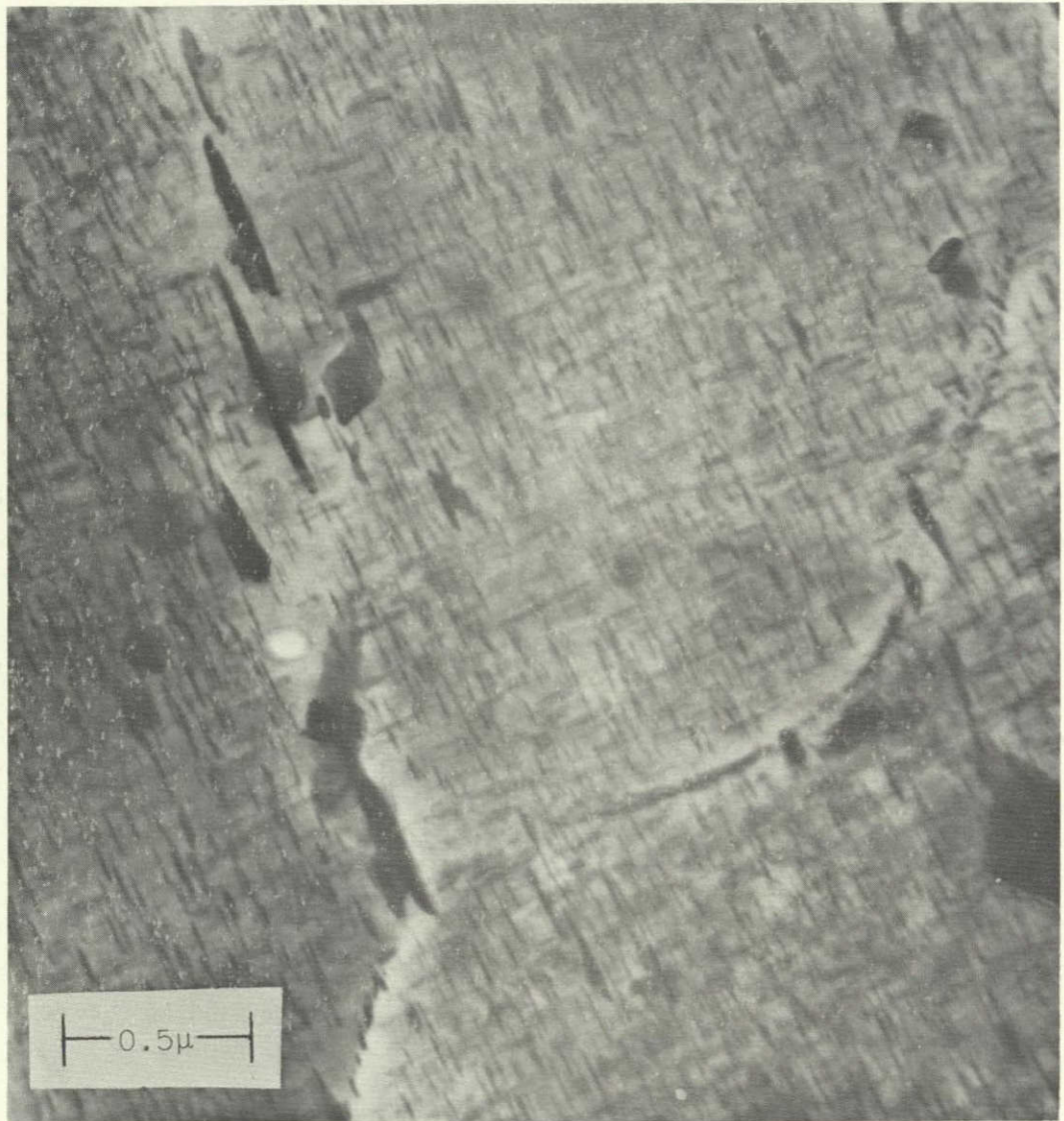
Figure 11



Electron transmission microstructure  
of 2219-T37 plate. (50,000X)

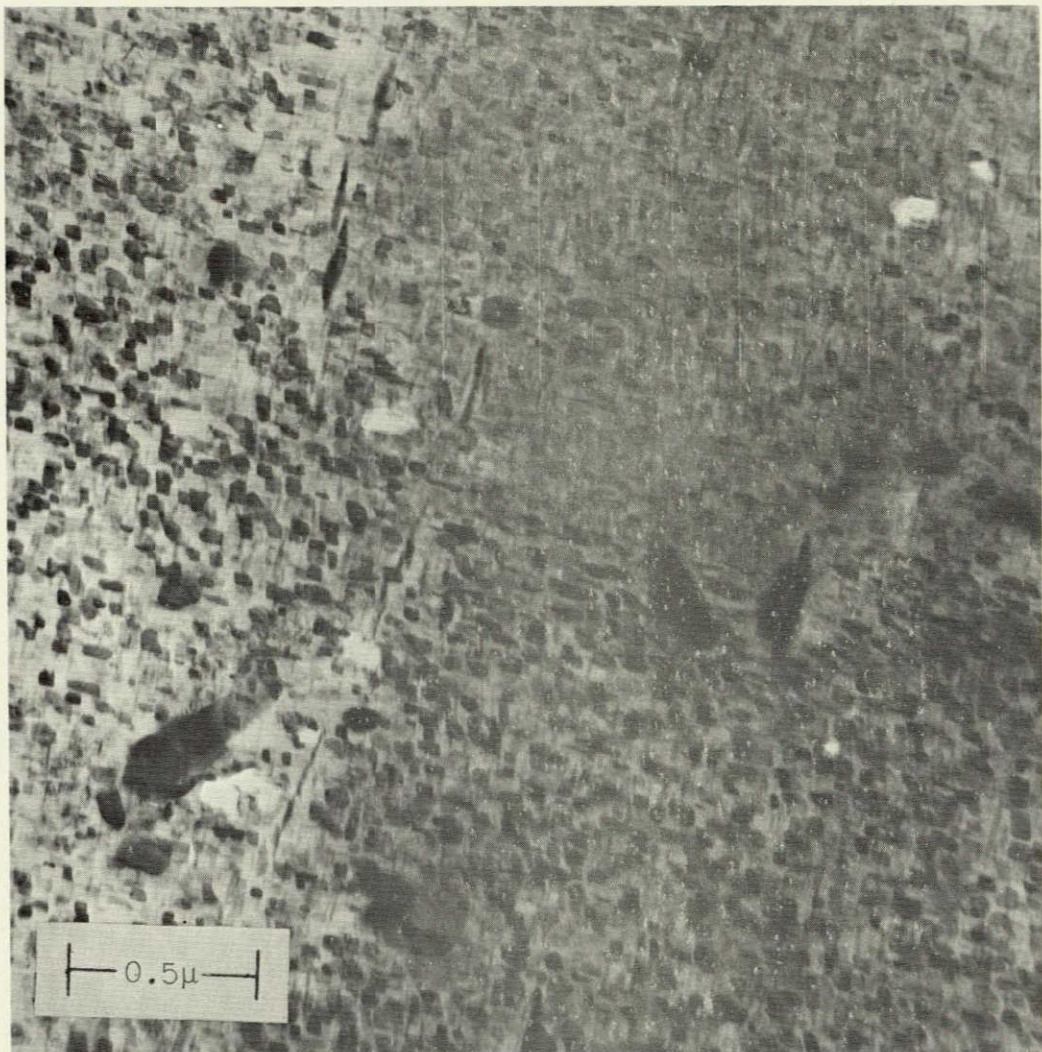
Figure 12





Electron transmission microstructure  
of 2219-T851 plate. (50,000X)

Figure 13

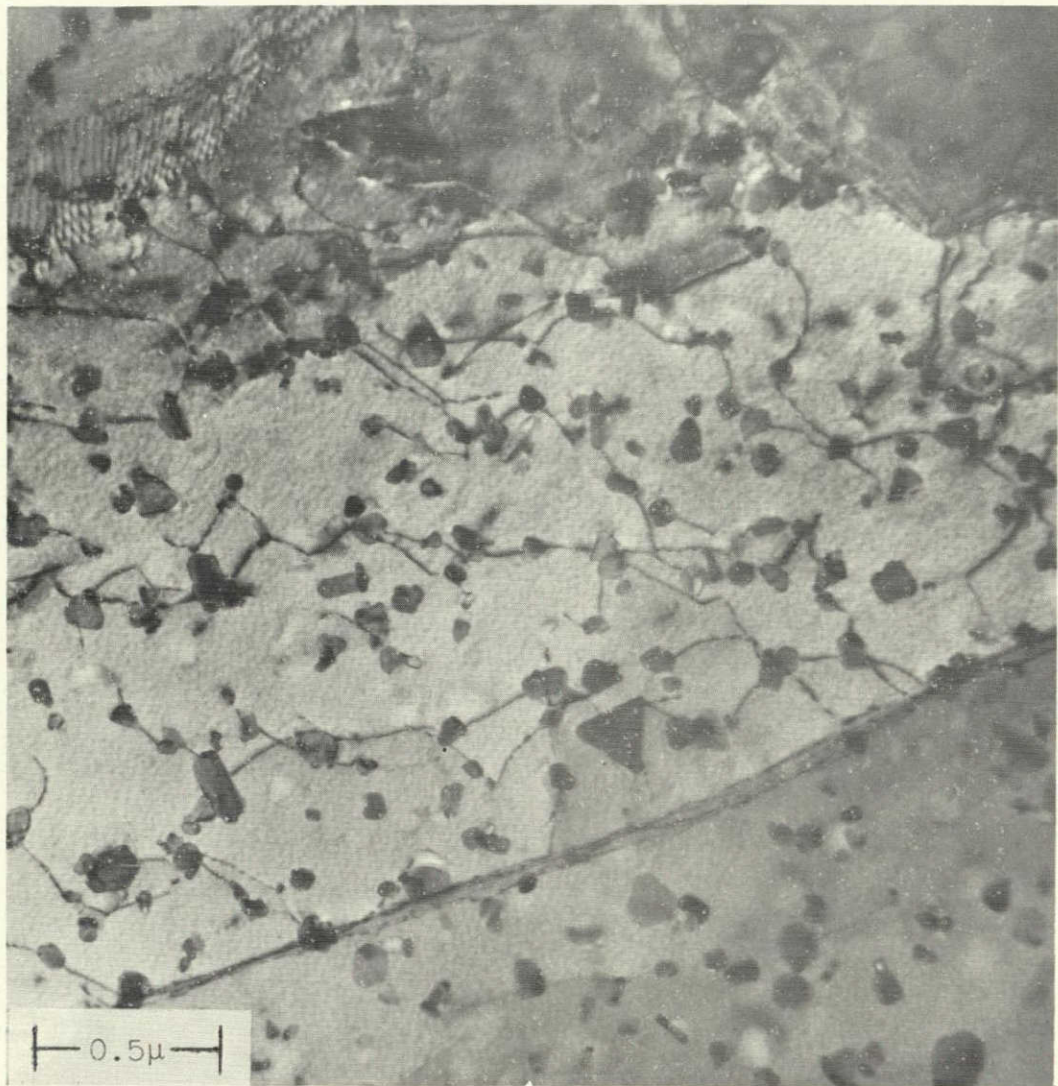


Electron transmission microstructure  
of 2219-T87 plate. (50,000X)

Figure 14

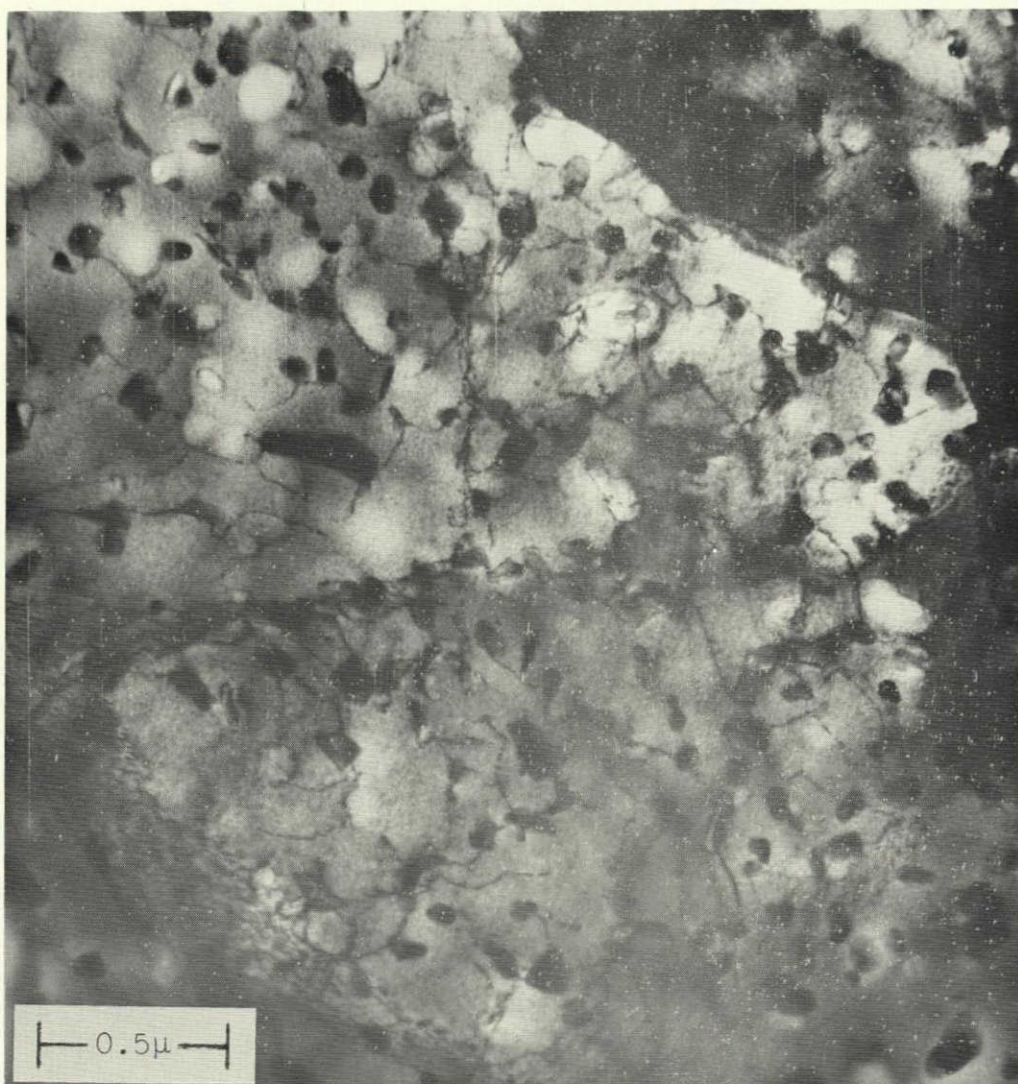
NOT REPRODUCIBLE





Electron transmission microstructure of  
7075 plate in W temper. (50,000X)

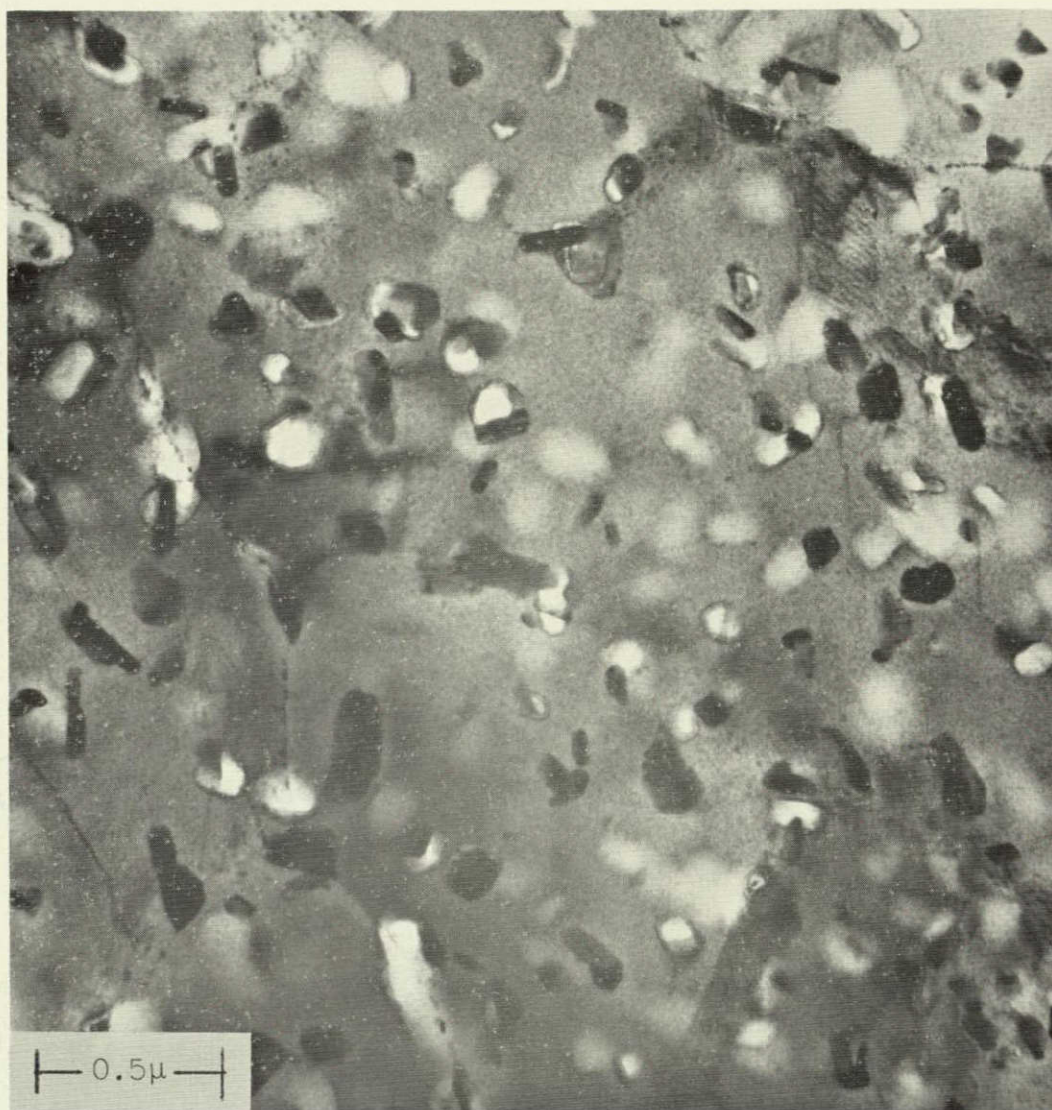
Figure 15



Electron transmission microstructure of  
7075-T6 plate showing dislocation structure.  
(50,000X)

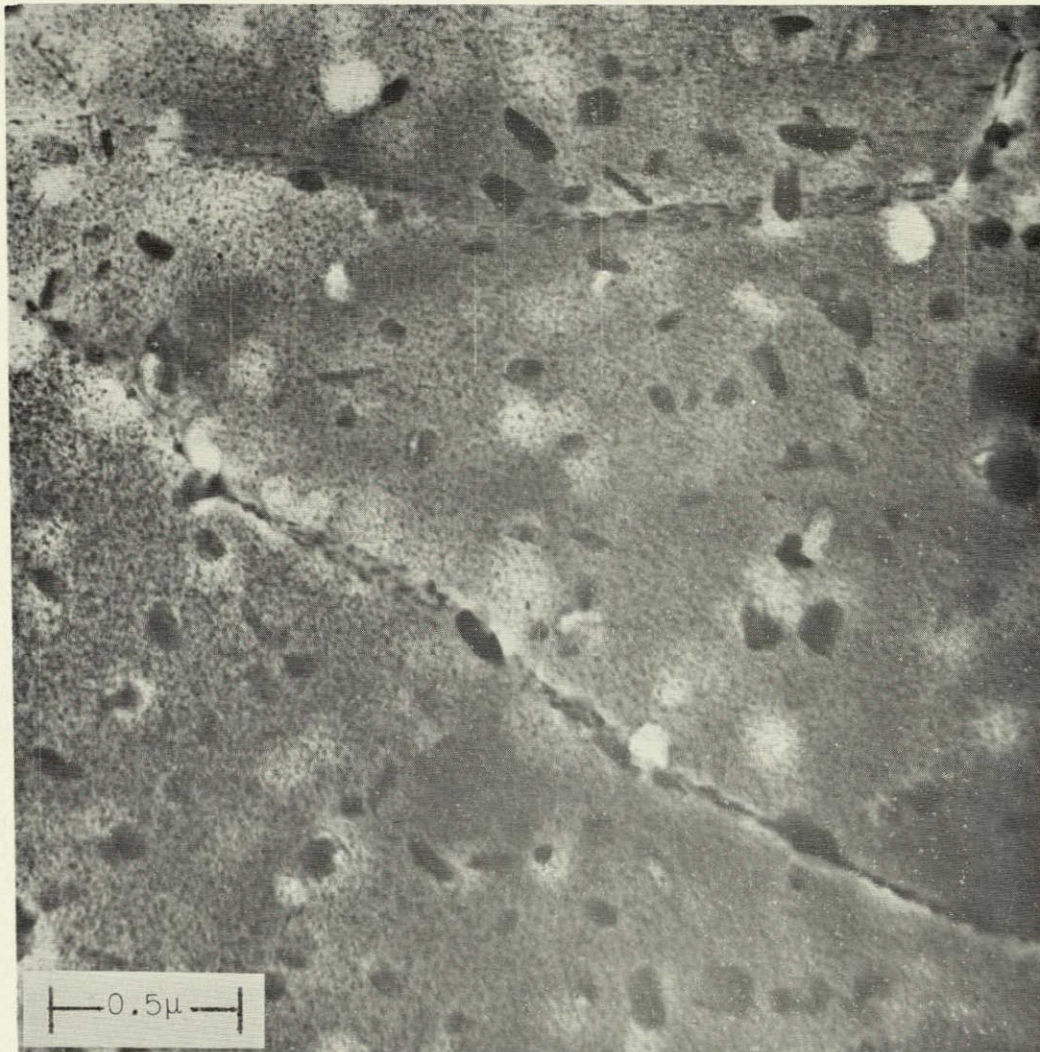
Figure 16





Electron transmission microstructure of 7075-T6 plate showing zone and precipitate structures. (50,000X)

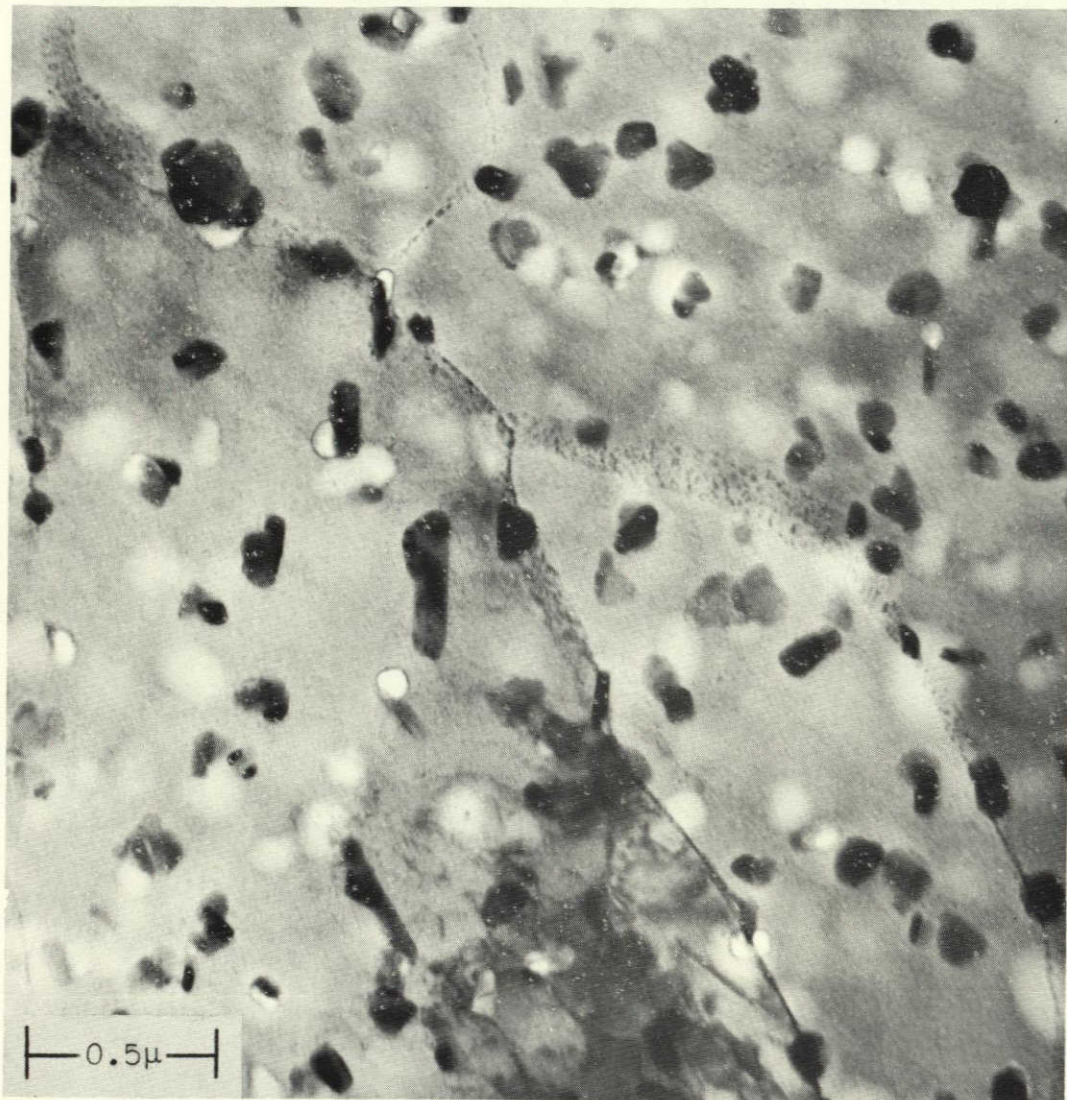
Figure 17



Electron transmission microstructure of  
7075 plate in T73 temper. (50,000X)

Figure 18





Electron transmission microstructure of 7079-T6 plate showing dispersoids, dislocations and precipitates. (50,000X)

Figure 19

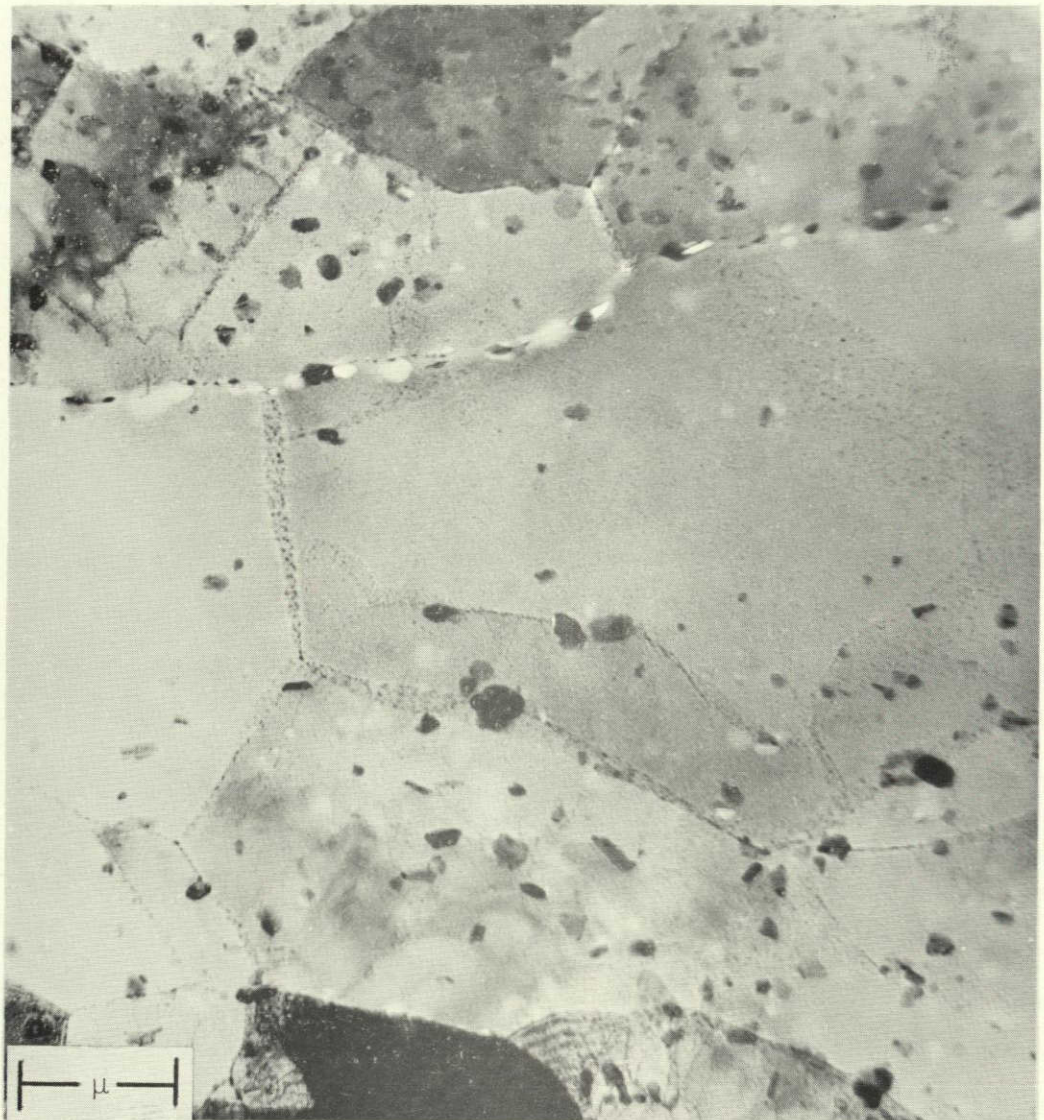


Electron transmission microstructure of 7079-T6 plate in dispersoid-lean region. Two sizes of boundary precipitate, precipitate-free boundary region, and fine zones in matrix are apparent. (50,000X)

Figure 20

NOT REPRODUCIBLE

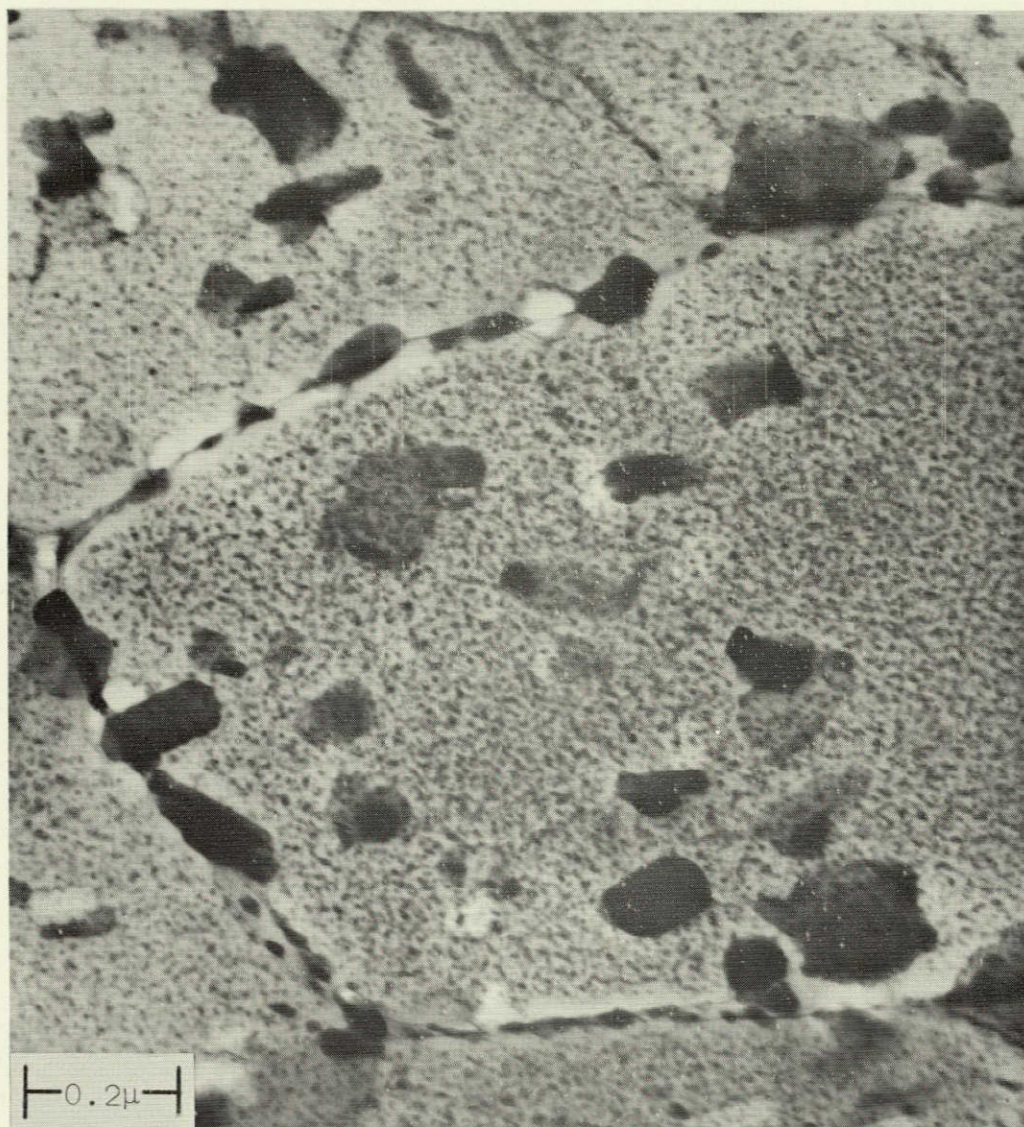




Electron transmission microstructure of 7039-T6 plate showing polygonized structure, dispersoid distribution and occasional dislocations. (20,000X)

Figure 21

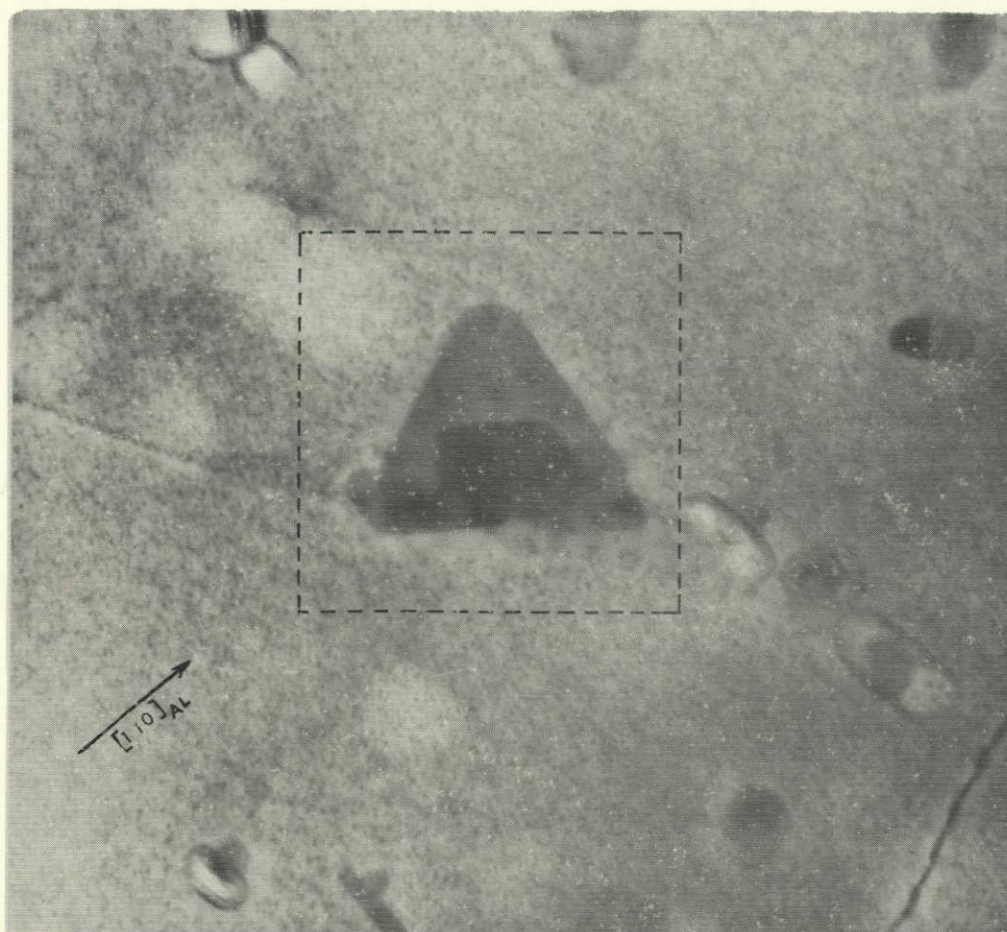




Transmission microstructure of 7039-T6 plate at higher magnification. Note two sizes of boundary precipitate, heavy zone-type precipitate, and precipitate-free boundary region. (100,000X)

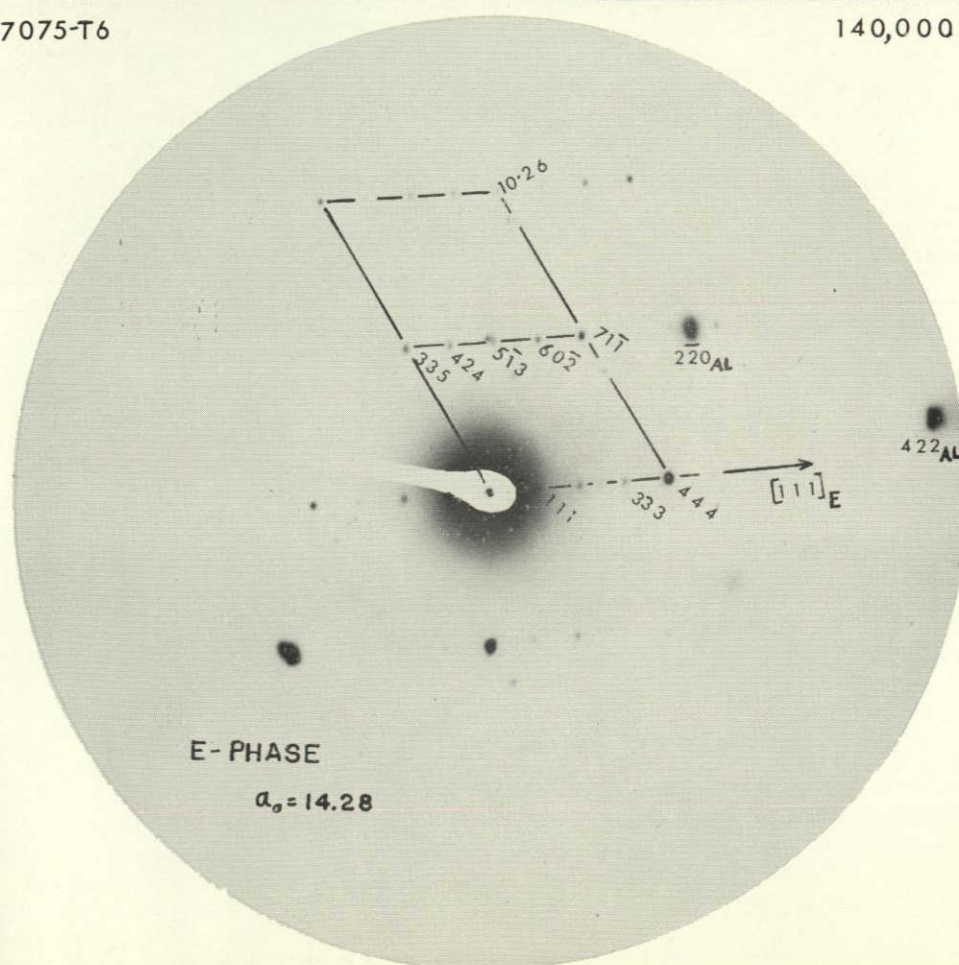
Figure 22





7075-T6

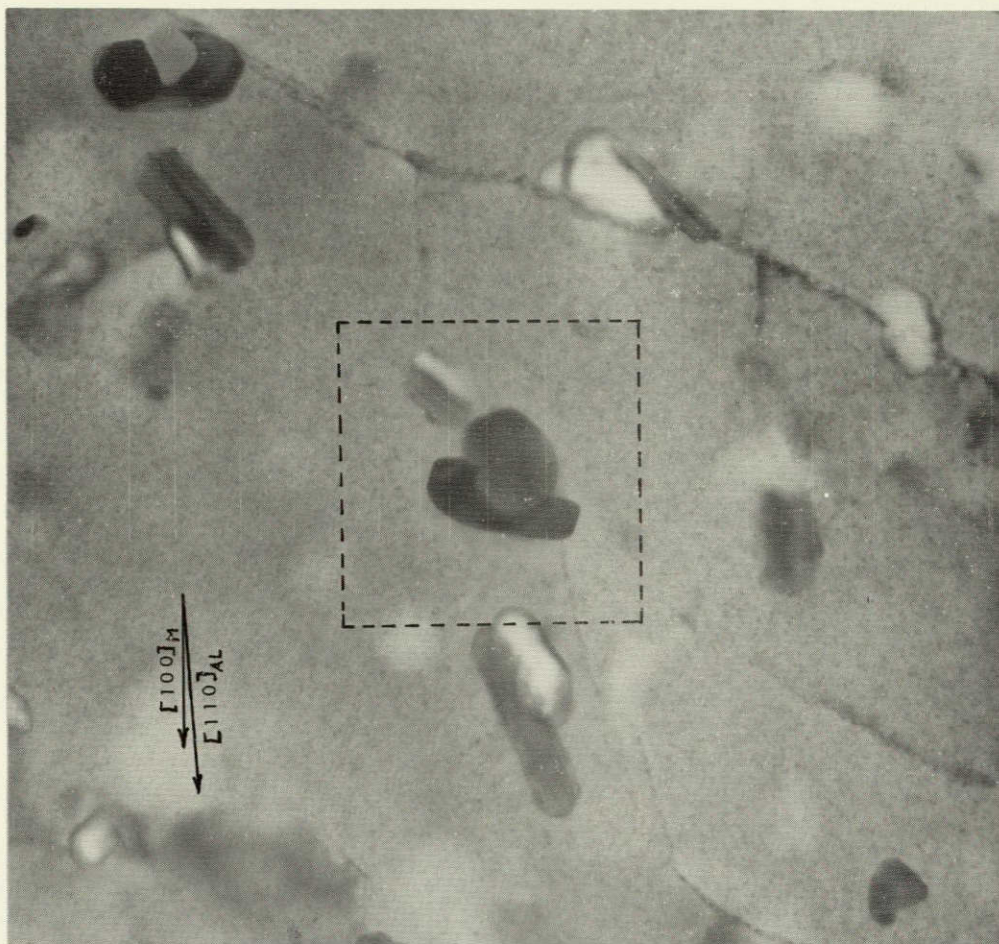
140,000X



Appearance and diffraction pattern of E-phase particle.

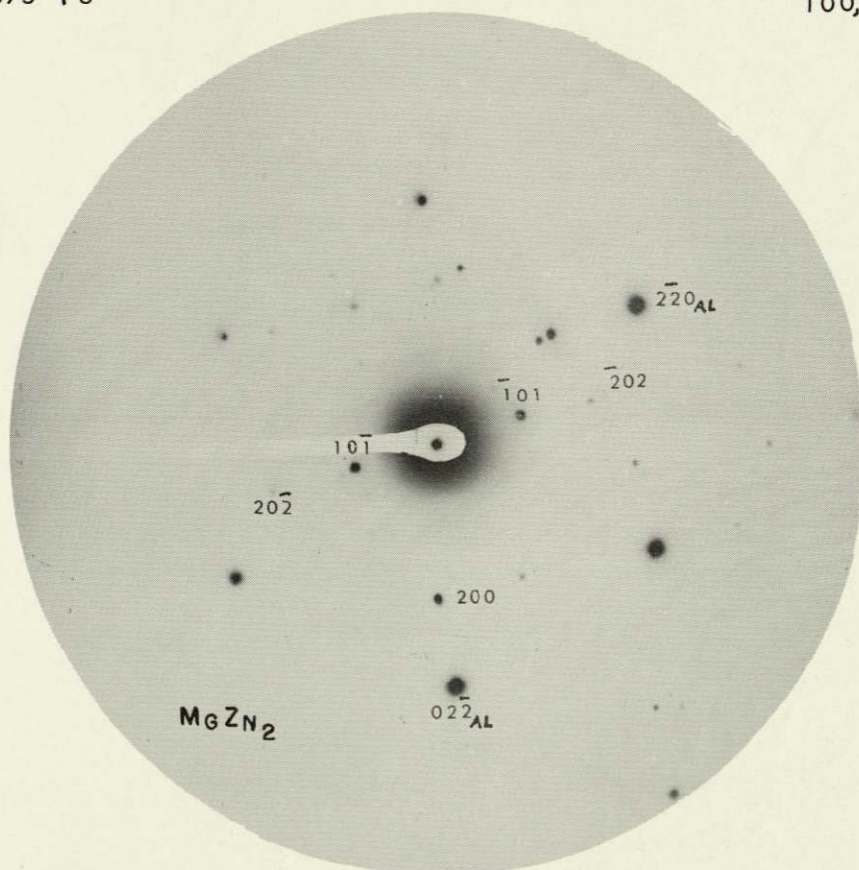
Figure 23





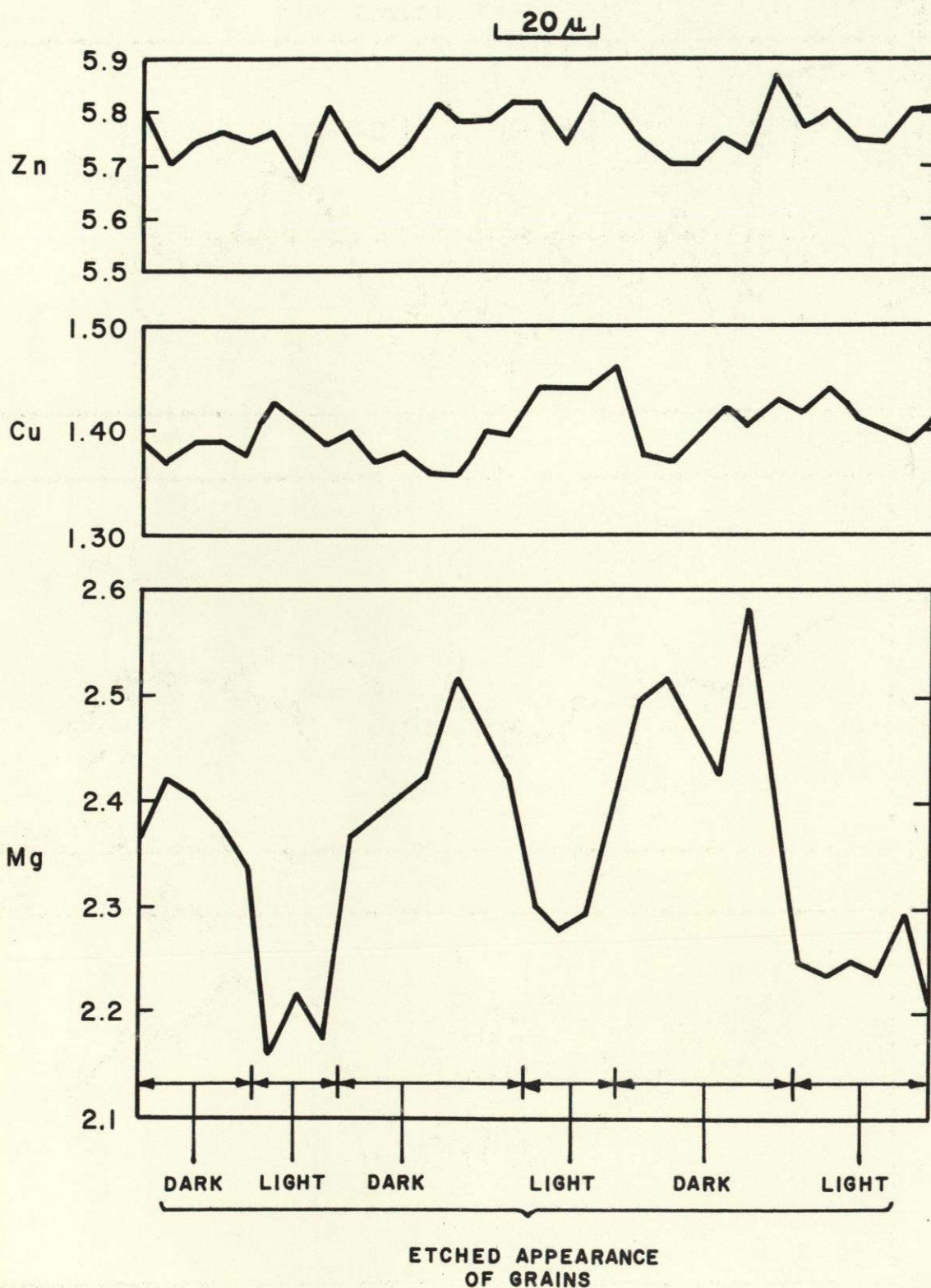
7075-T6

100,000X



Appearance and diffraction pattern of M-phase particle.

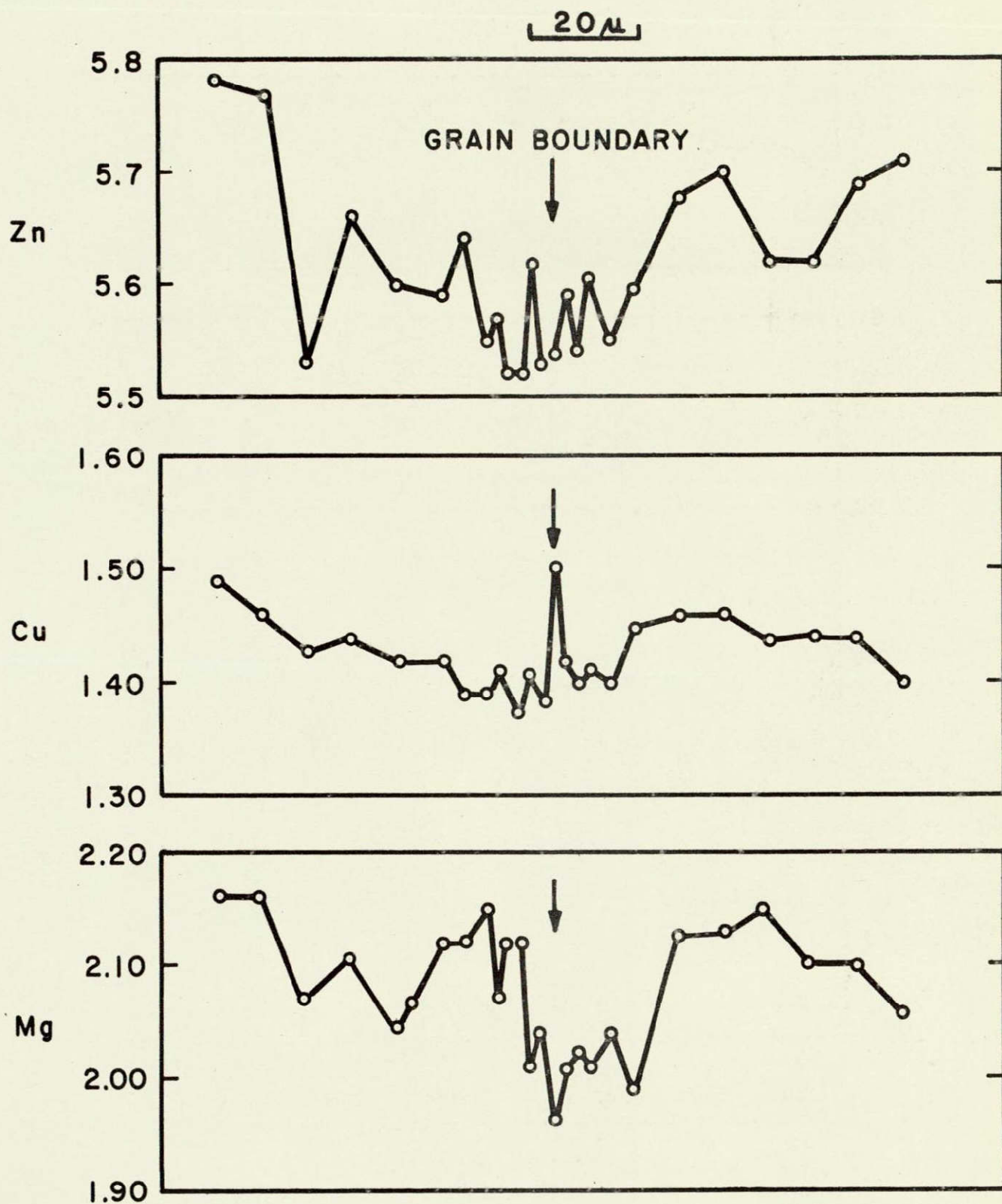
Figure 24



MICROPROBE ANALYSES ACROSS SEVERAL GRAINS  
OF 7075-T6 ALLOY PLATE

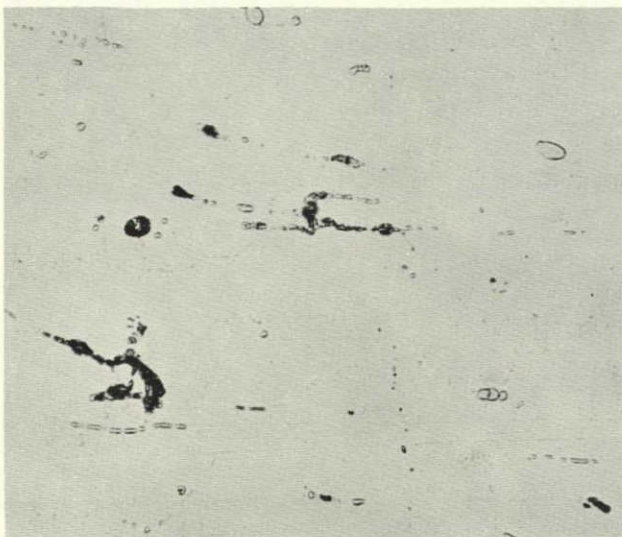
FIGURE 25



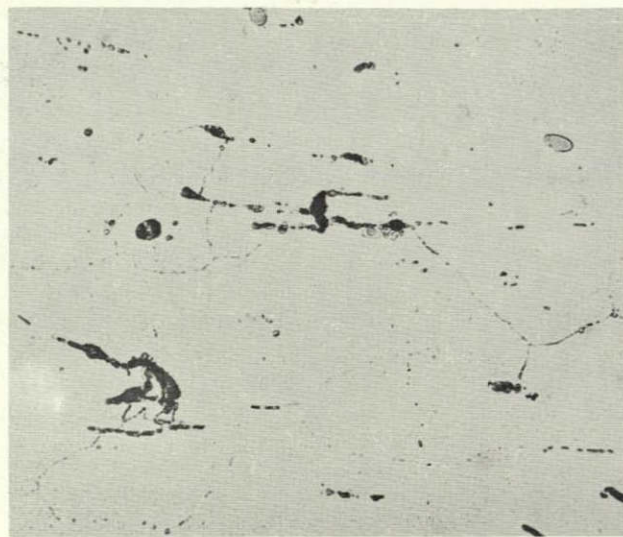


MICROPROBE ANALYSES ACROSS GRAIN BOUNDARY  
OF 7075-T6 ALLOY PLATE

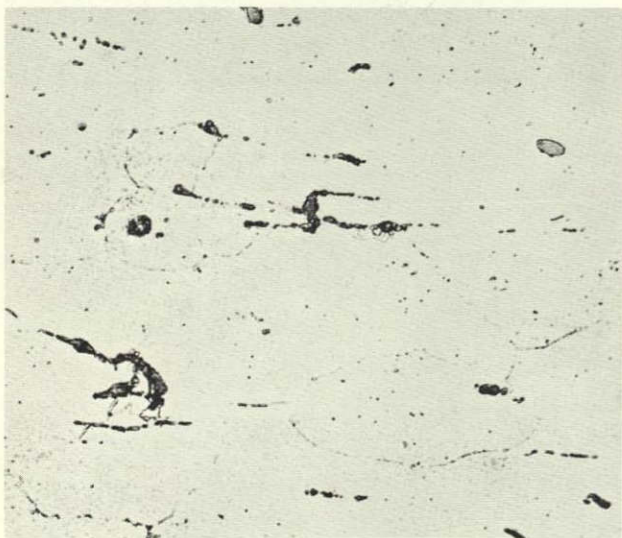
FIGURE 26



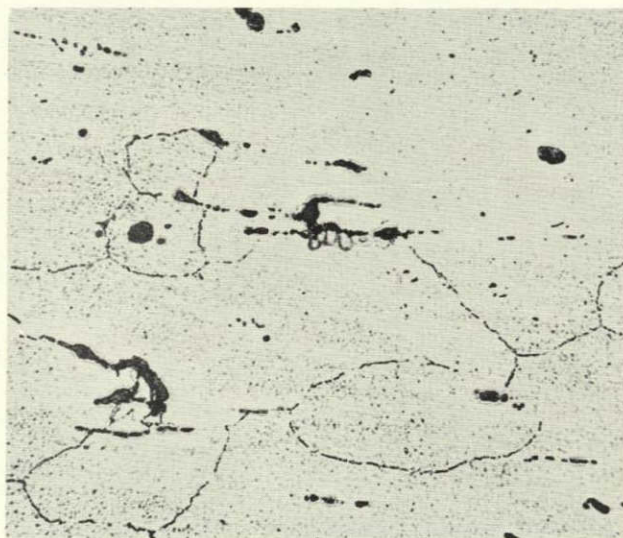
5 Minutes



20 Minutes



30 Minutes



60 Minutes

500X

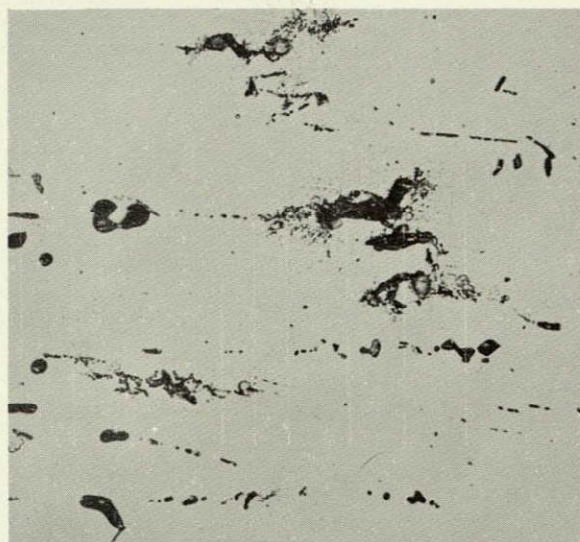
Progressive corrosion of unstressed 2219-T37  
plate in  $\text{NaCl-AlCl}_3$  solution.

Figure 27



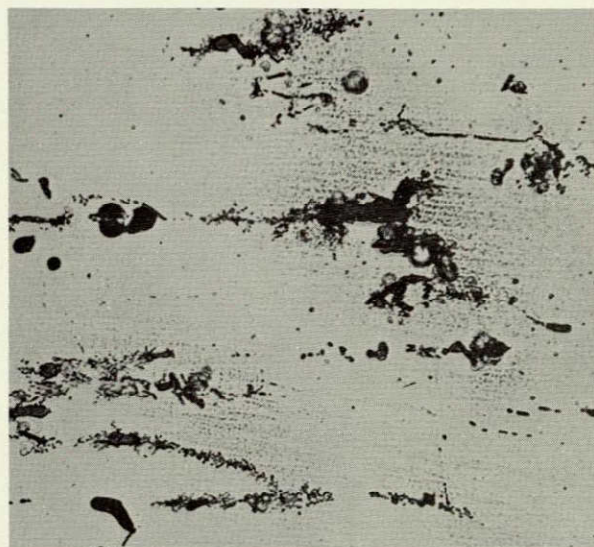


2 Minutes

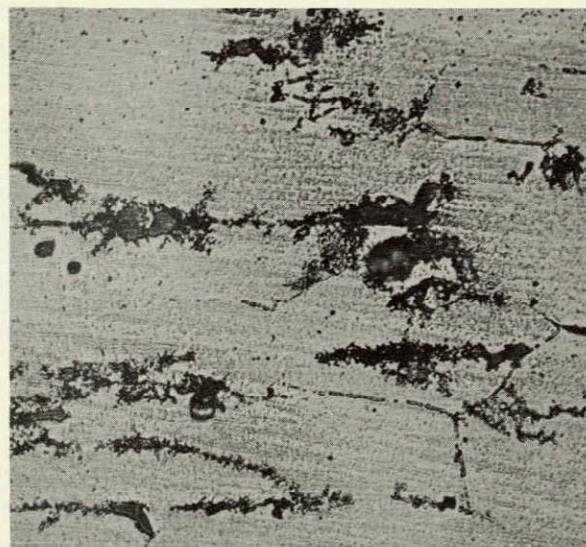


20 Minutes

NOT REPRODUCIBLE



32 Minutes



50 Minutes

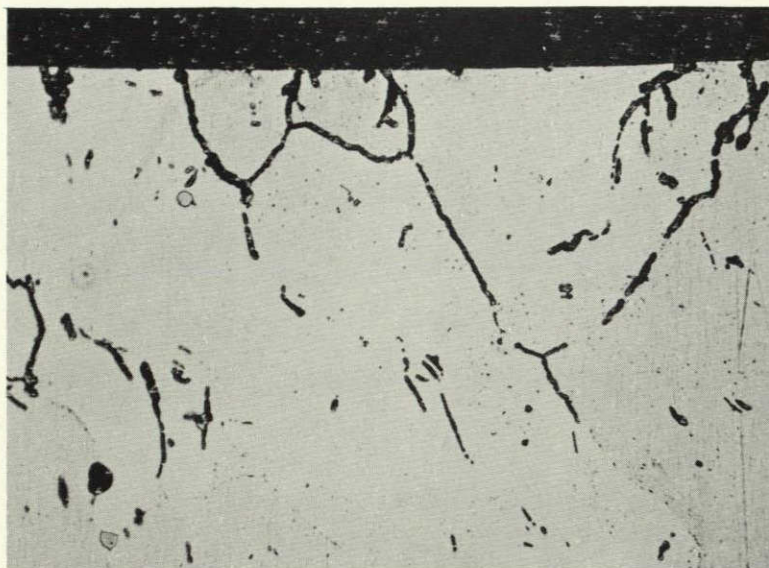
500X

Progressive corrosion of unstressed 2219-T851  
plate in  $\text{NaCl-AlCl}_3$  solution.

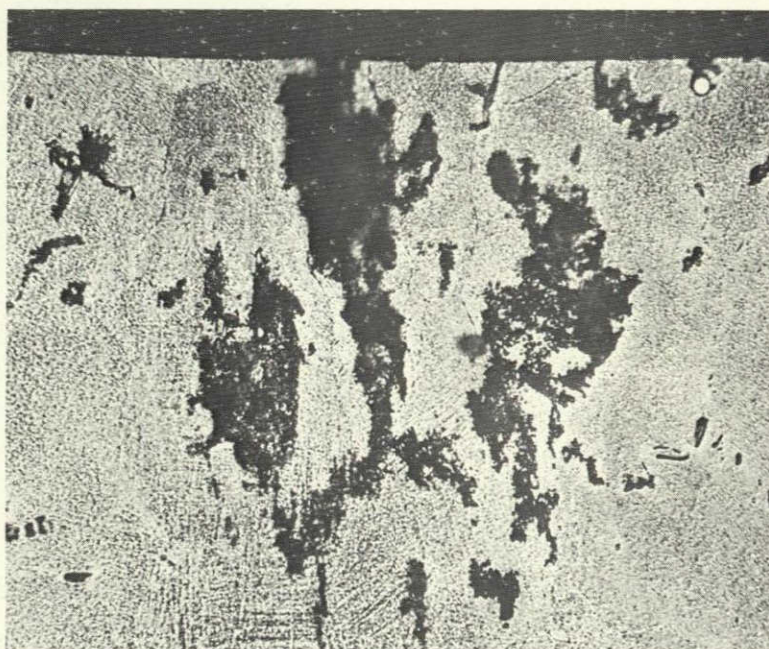
Figure 28

148645  
148651  
148652  
148655





T3-Type Tempers



Precipitation Heat Treated Tempers

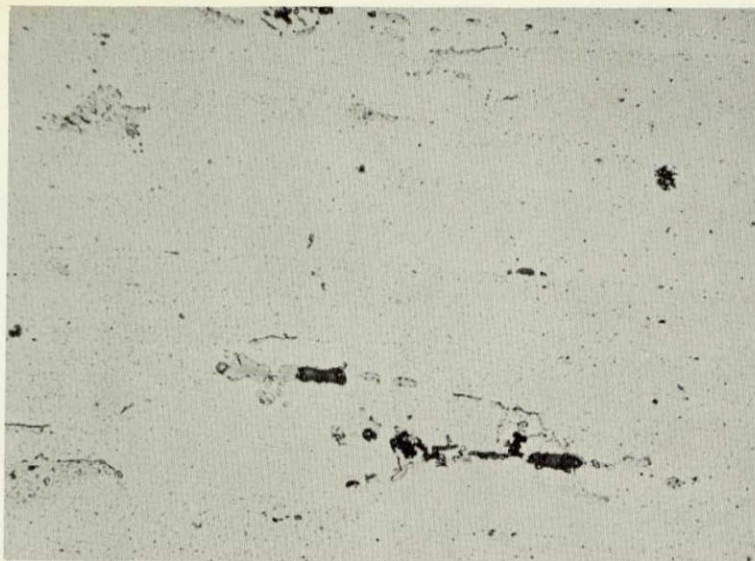
Cross sections illustrating unstressed corrosion of 2219 alloy plate. (X500)

Figure 29

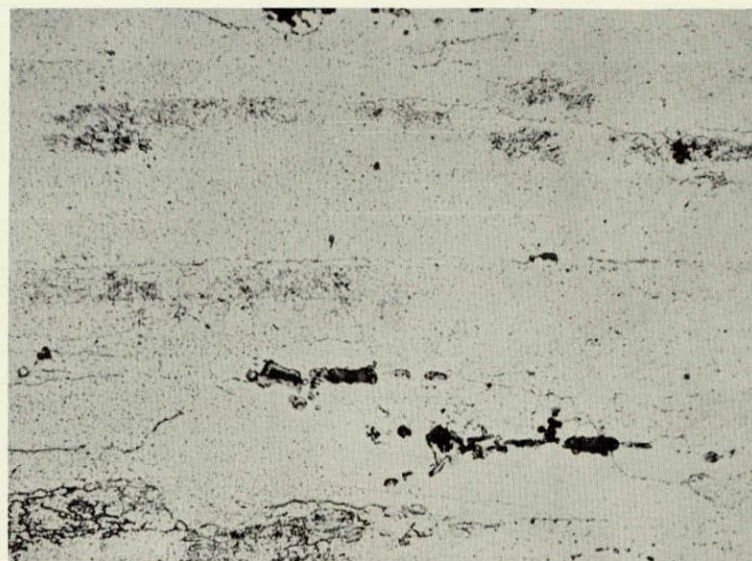


160247  
160248  
160249  
160250

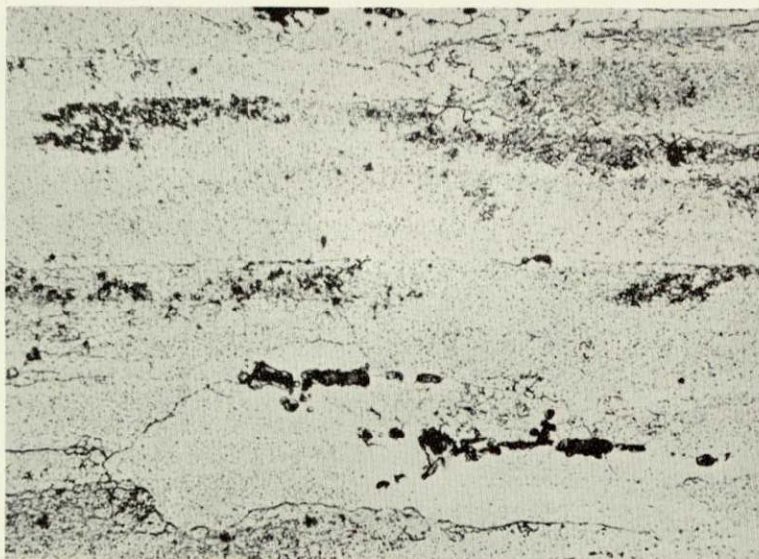
90  
min.



120  
min.



150  
min.



210  
min.



500X

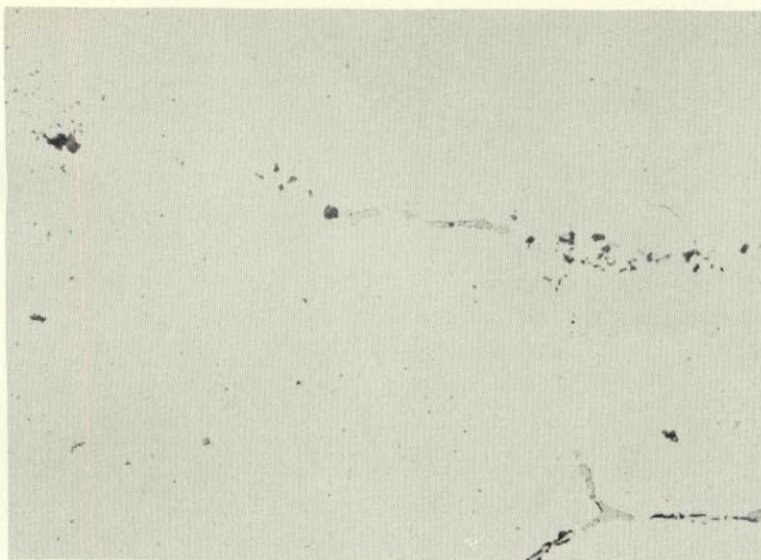
Progressive Corrosion of Unstressed 7075-T6 Plate

Figure 30

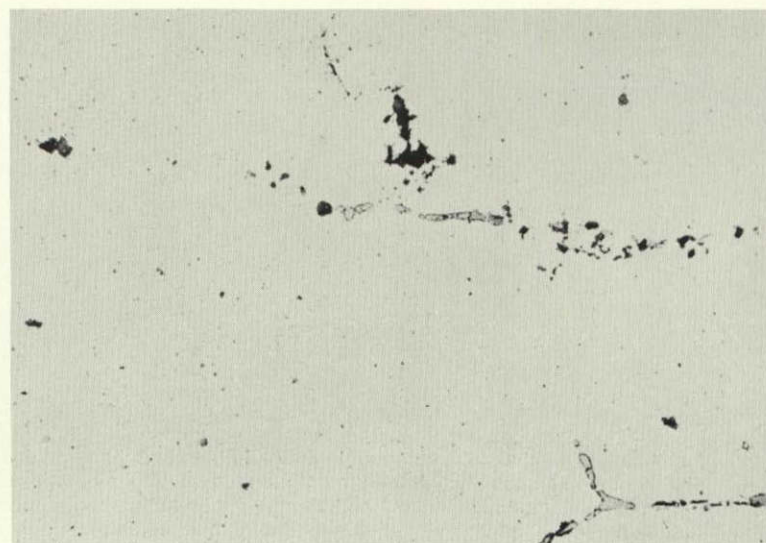


160357  
160360  
160361  
160363

45  
min.



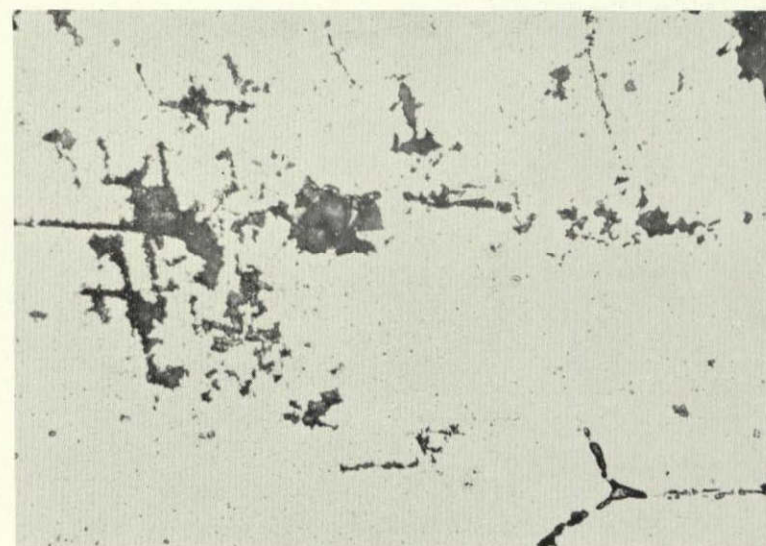
90  
min.



120  
min.



150  
min.



Progressive Corrosion of Unstressed 7075-T73 Plate

500X

Figure 31



T6 Temper

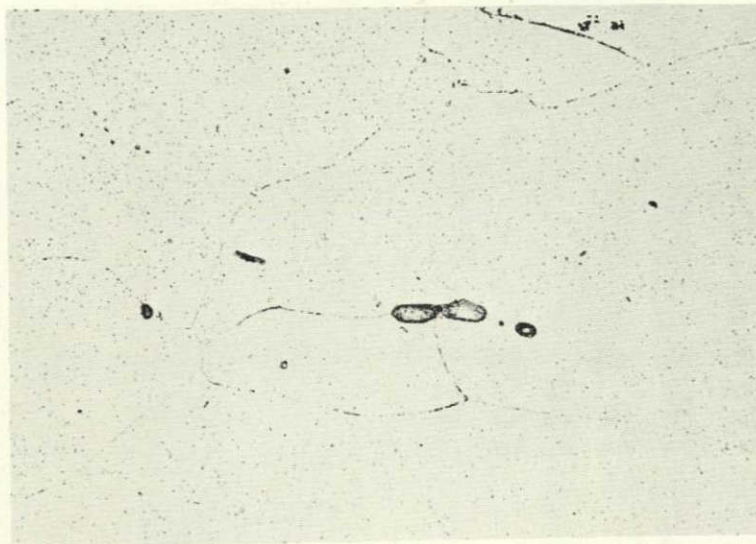


T73 Temper

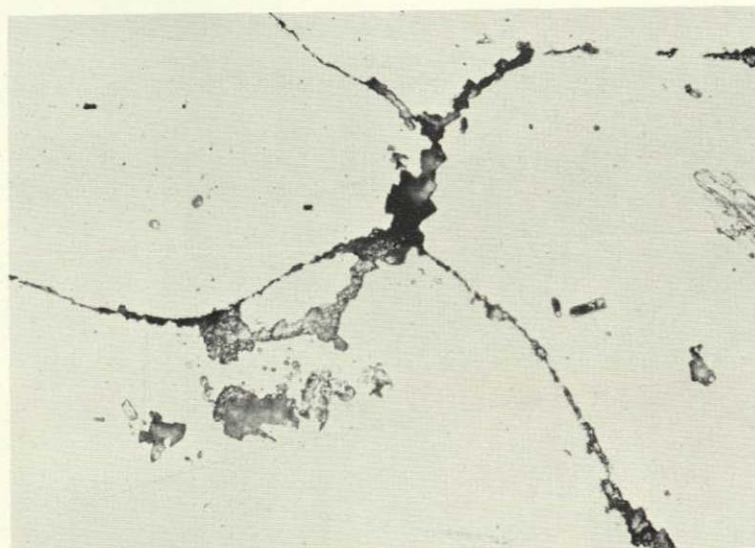
Cross sections illustrating unstressed corrosion of 7075 alloy plate. (X500)

Figure 32





T6 Temper



T73-Type Temper

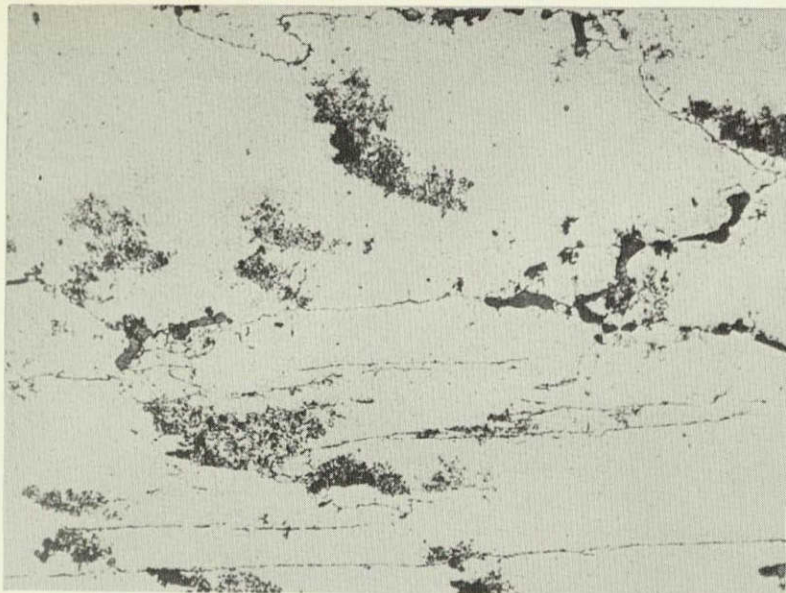
Unstressed corrosion of X7375 alloy plate. (X500)

Figure 33



165723  
165725  
165727  
165729

60 min.



150 min.

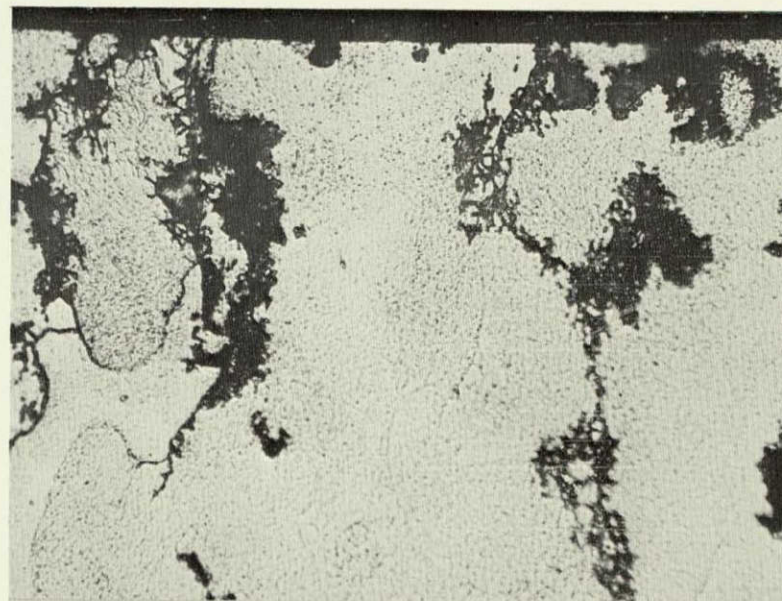


210 min.



210 min.

X-Sect.  
Keller's  
Etch

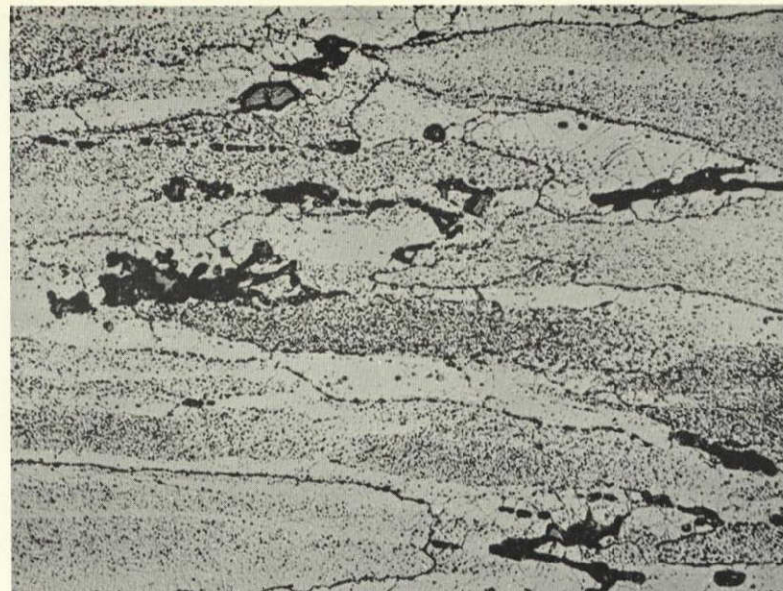


Development of intergranular, interfragmentary and matrix pitting  
attack of 7079-T6 plate exposed unstressed to pH 1 NaCl-AlCl<sub>3</sub> solution (X500).

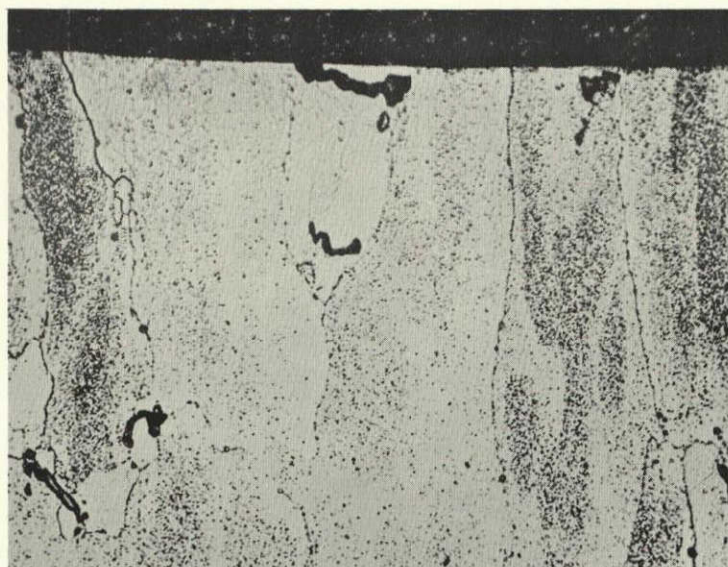


168270  
168271  
168272

19 hrs



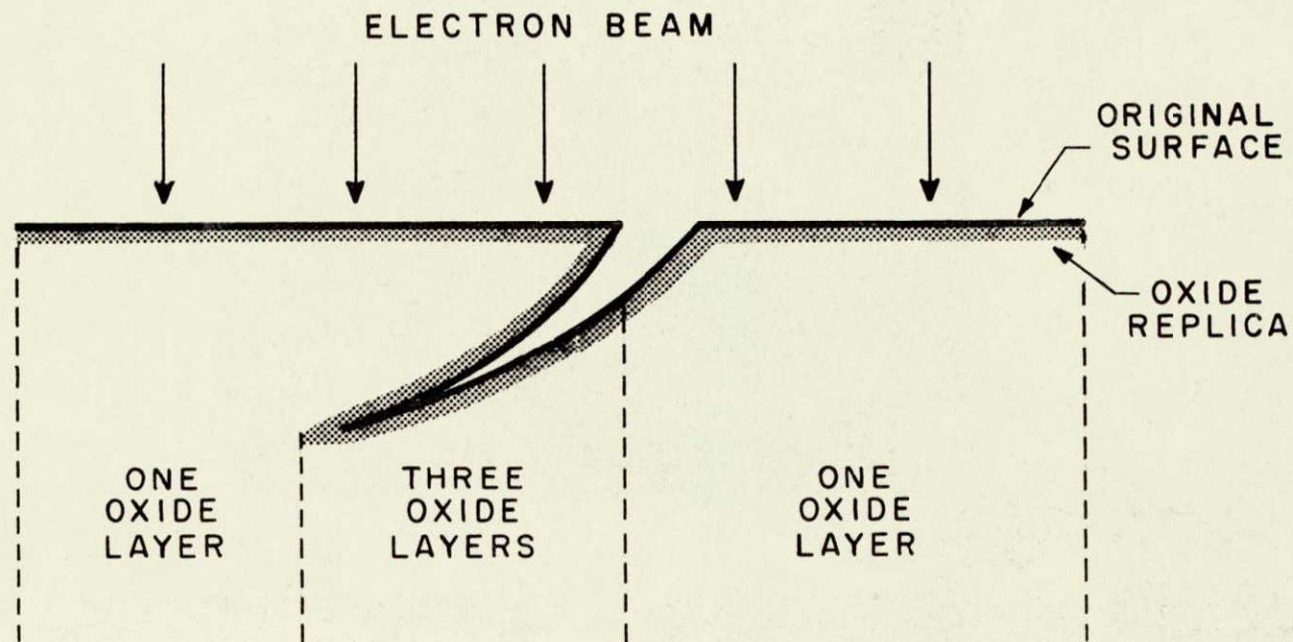
19 hrs  
Keller's  
Etch



19 hrs  
X-Sect.  
Keller's  
Etch

Development of pitting attack in 7039-T6 plate exposed unstressed  
to pH2 solution of 0.5N NaCl + 0.5N Na<sub>2</sub>CrO<sub>4</sub> (X500).

Figure 35



EXAMINATION OF STRESS CORROSION CRACKS AND CORROSION  
CREVICES BY ELECTRON MICROSCOPY USING OXIDE REPLICAS

FIGURE 36



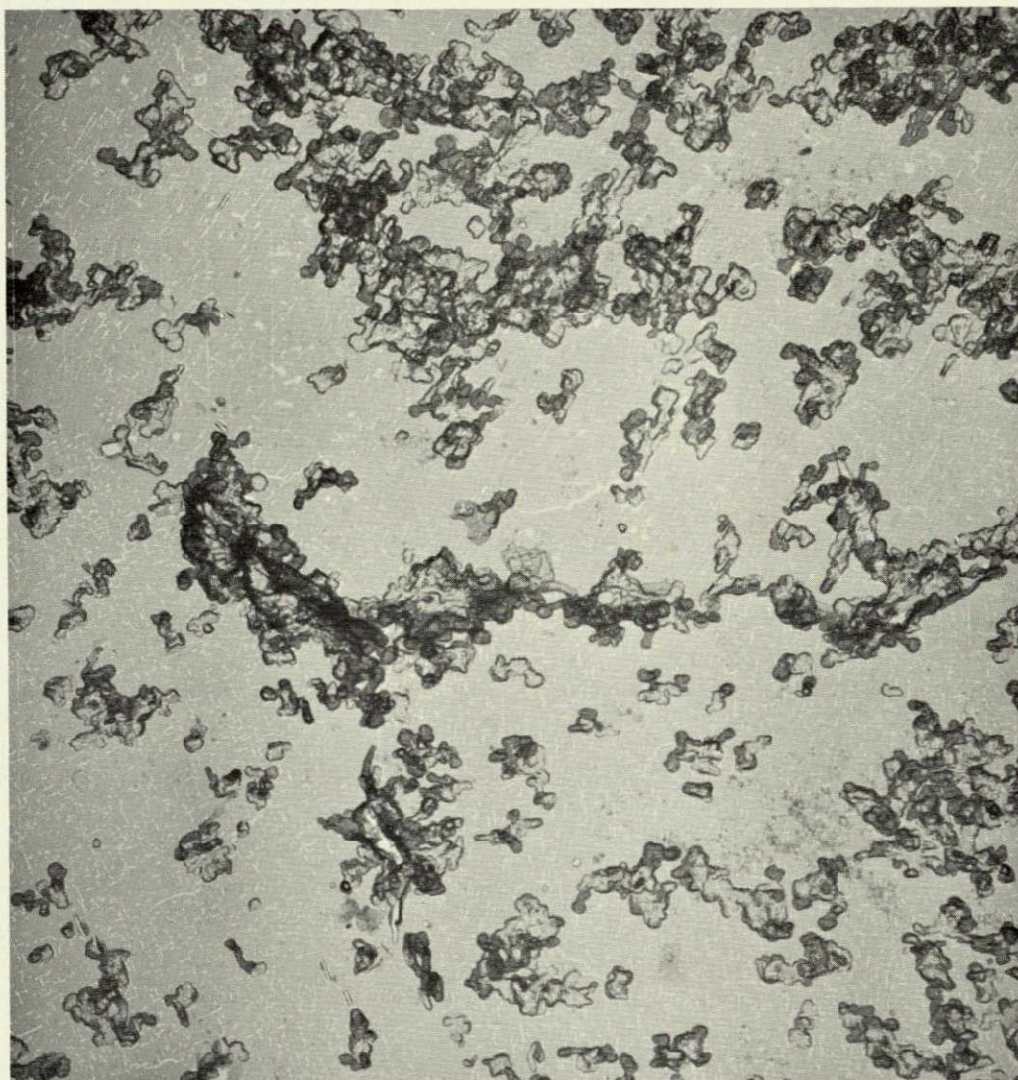


Oxide Replica

5000X

Penetration of intergranular attack in  
unstressed specimen of 2219-T351 alloy

Figure 37



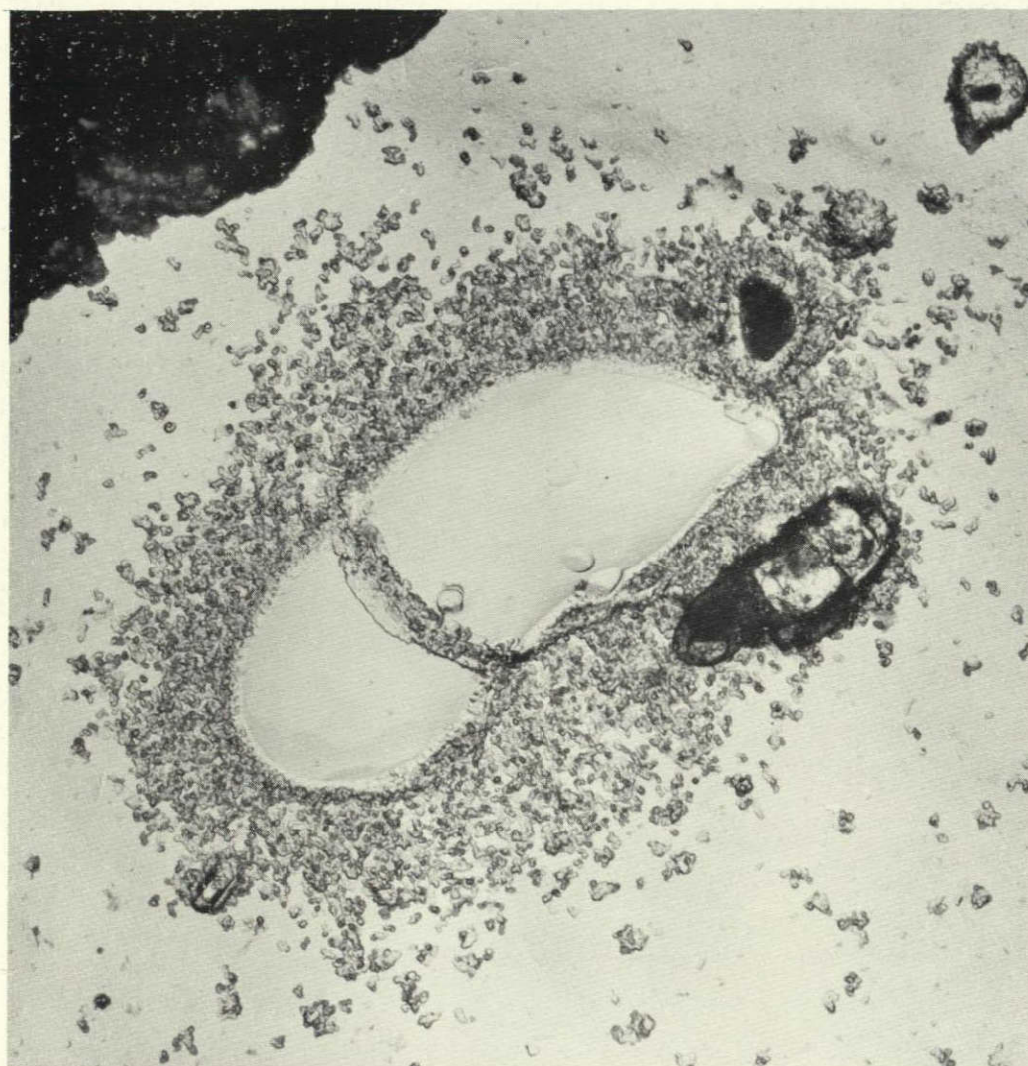
Oxide Replica

20,000X

Unstressed Corrosion of 2219-T851 Plate.  
Note cubic pitting with some concentrations  
on boundary. White markings represent  
precipitate plates.

Figure 38



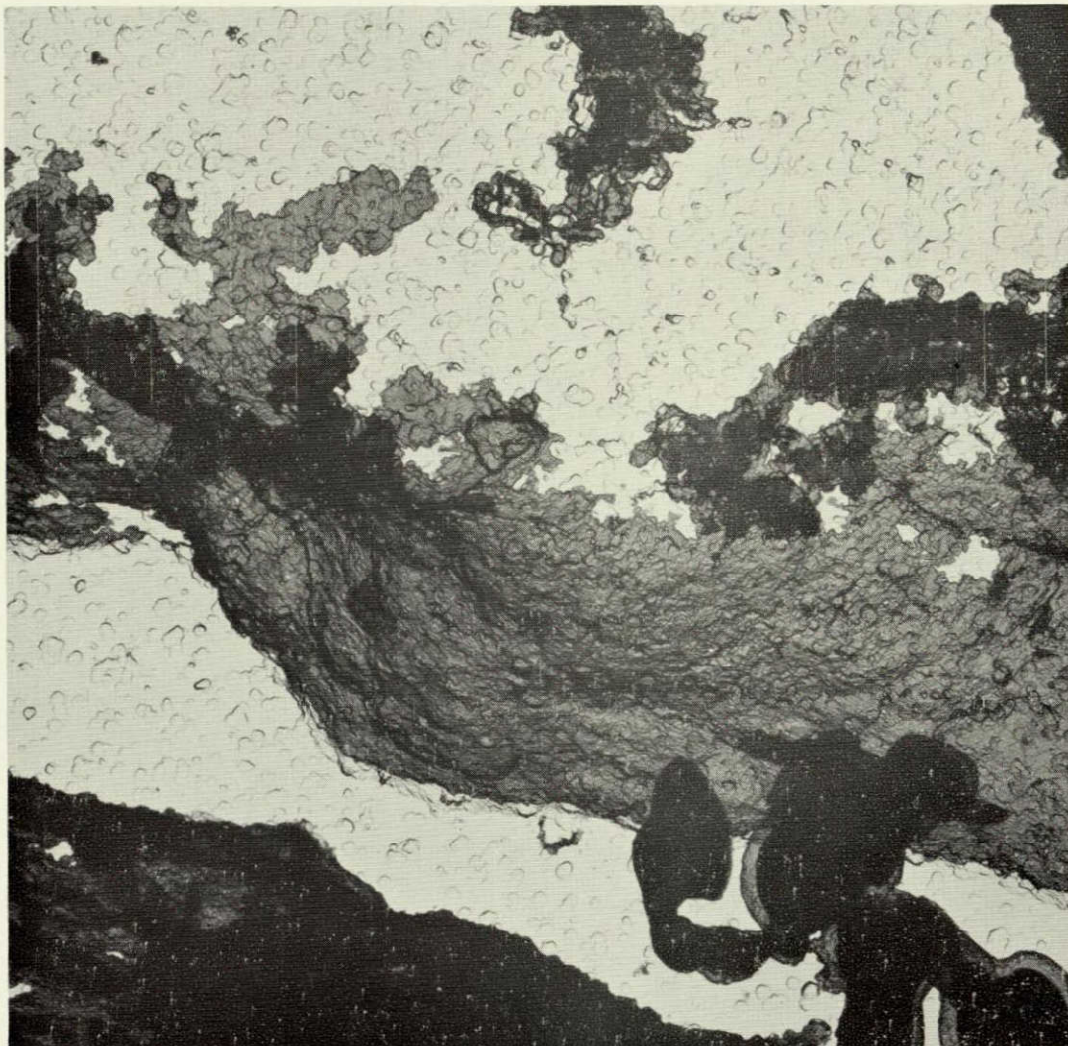


Oxide Replica

5,000X

Cubic pitting surrounding constituent  
particle in 2219-T87 plate

Figure 39



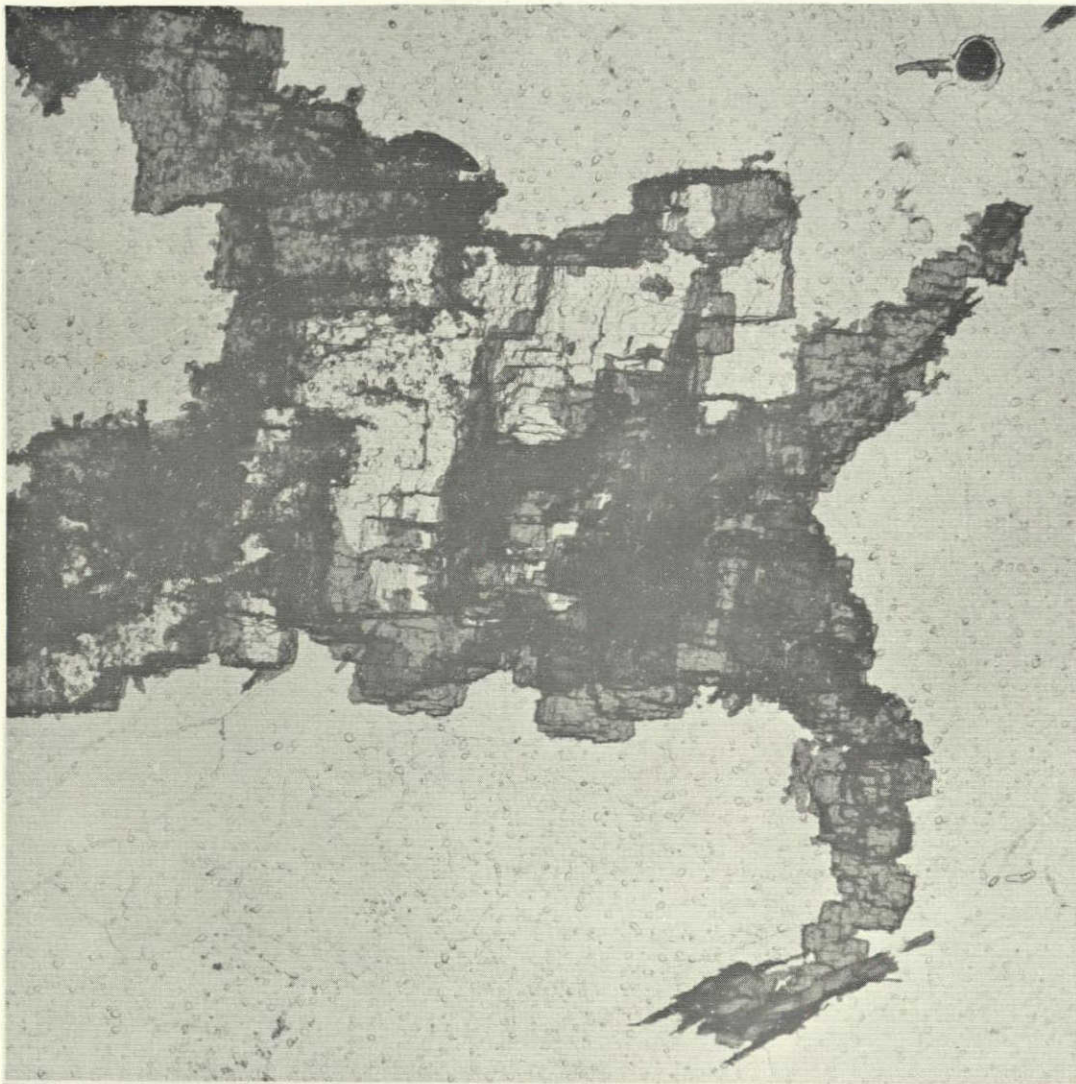
Oxide Replica

5,000X

Intergranular penetration along boundary  
of unstressed 7075-T6 specimen. Note  
angular shape of corrosion front and of  
grain faces, indicating cubic pitting mode

Figure 40



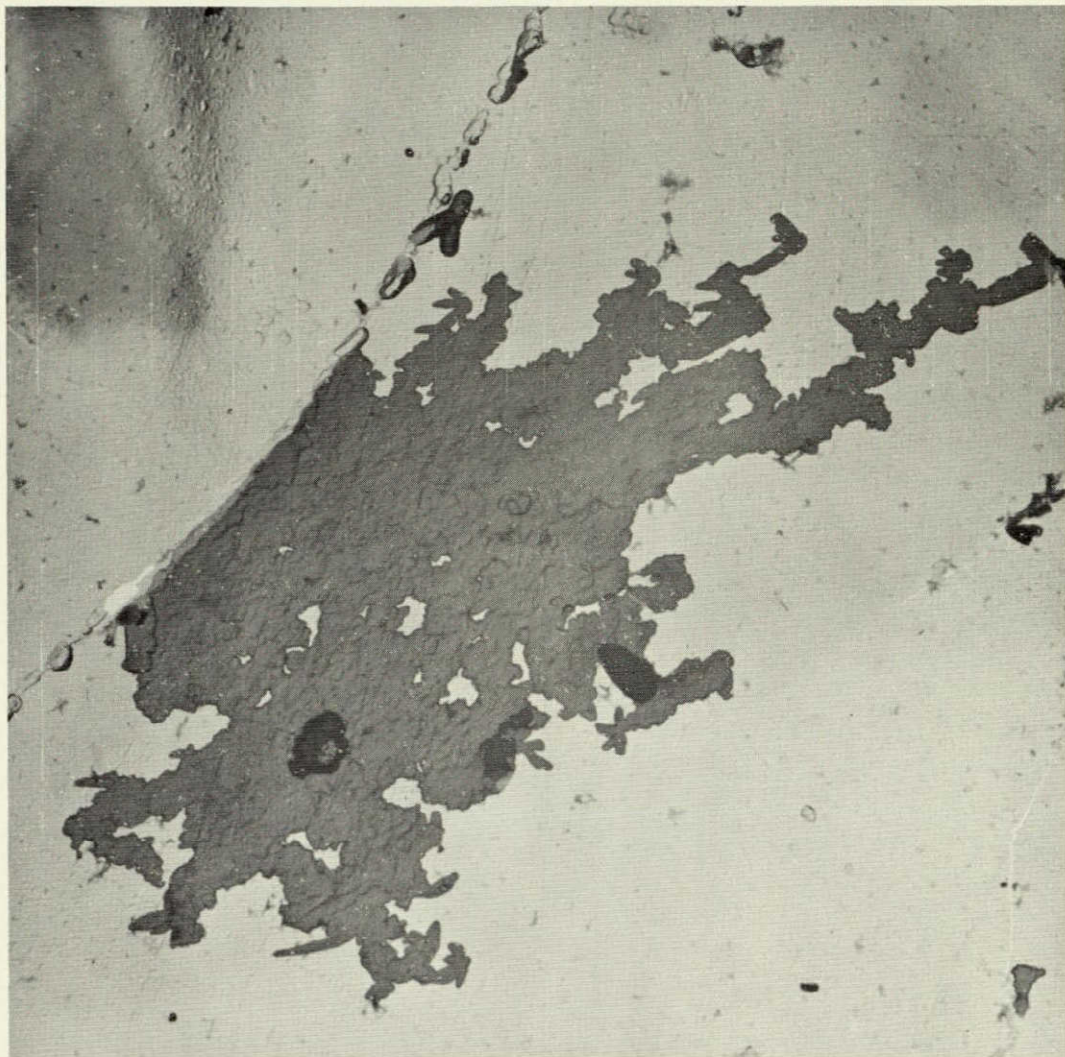


Oxide Replica

2,000X

Cubic pitting characteristic of unstressed  
corrosion of 7075-T73 plate

Figure 41



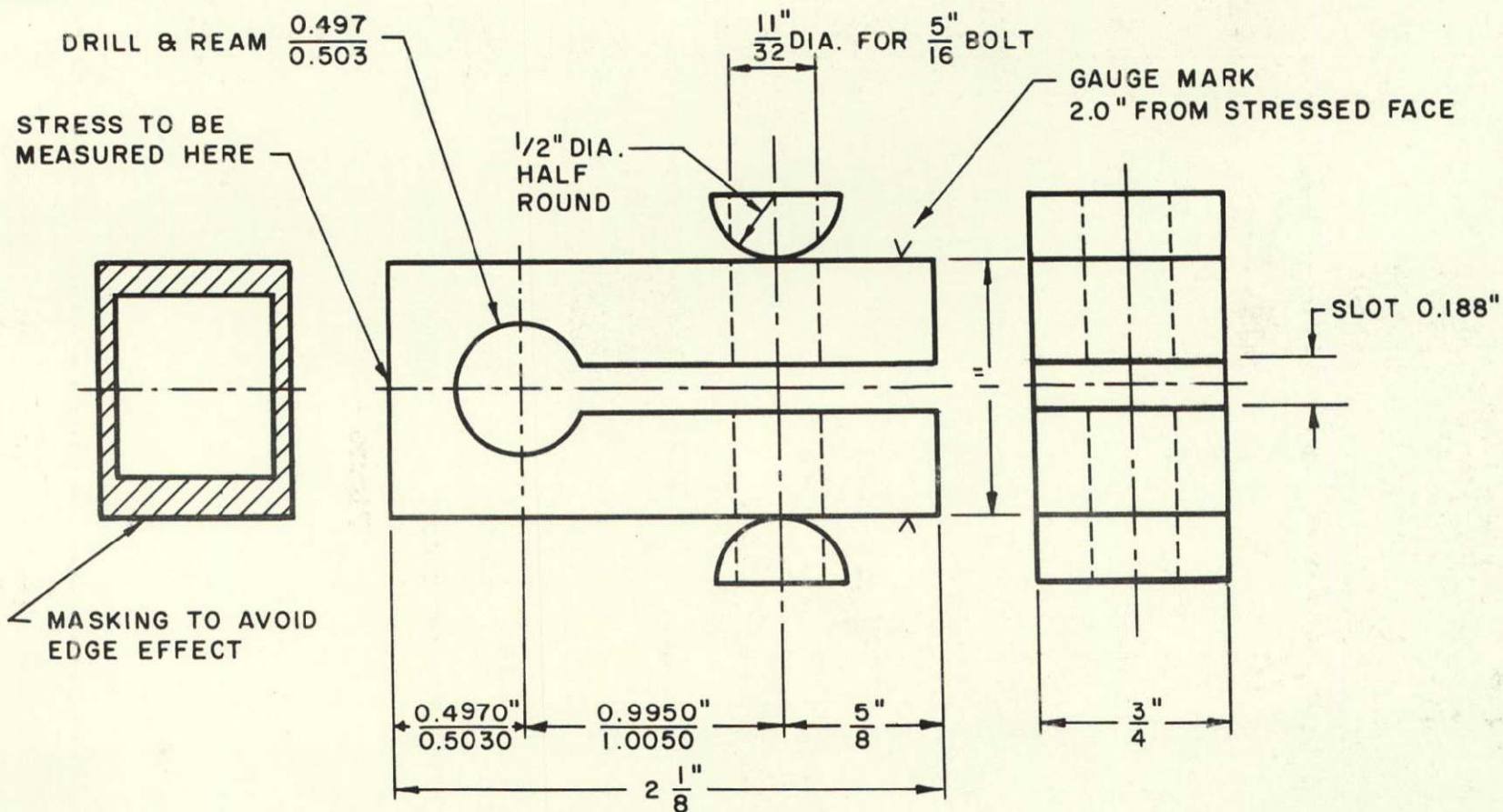
Oxide Replica

5,000X

Intergranular penetration in unstressed X7375-T6

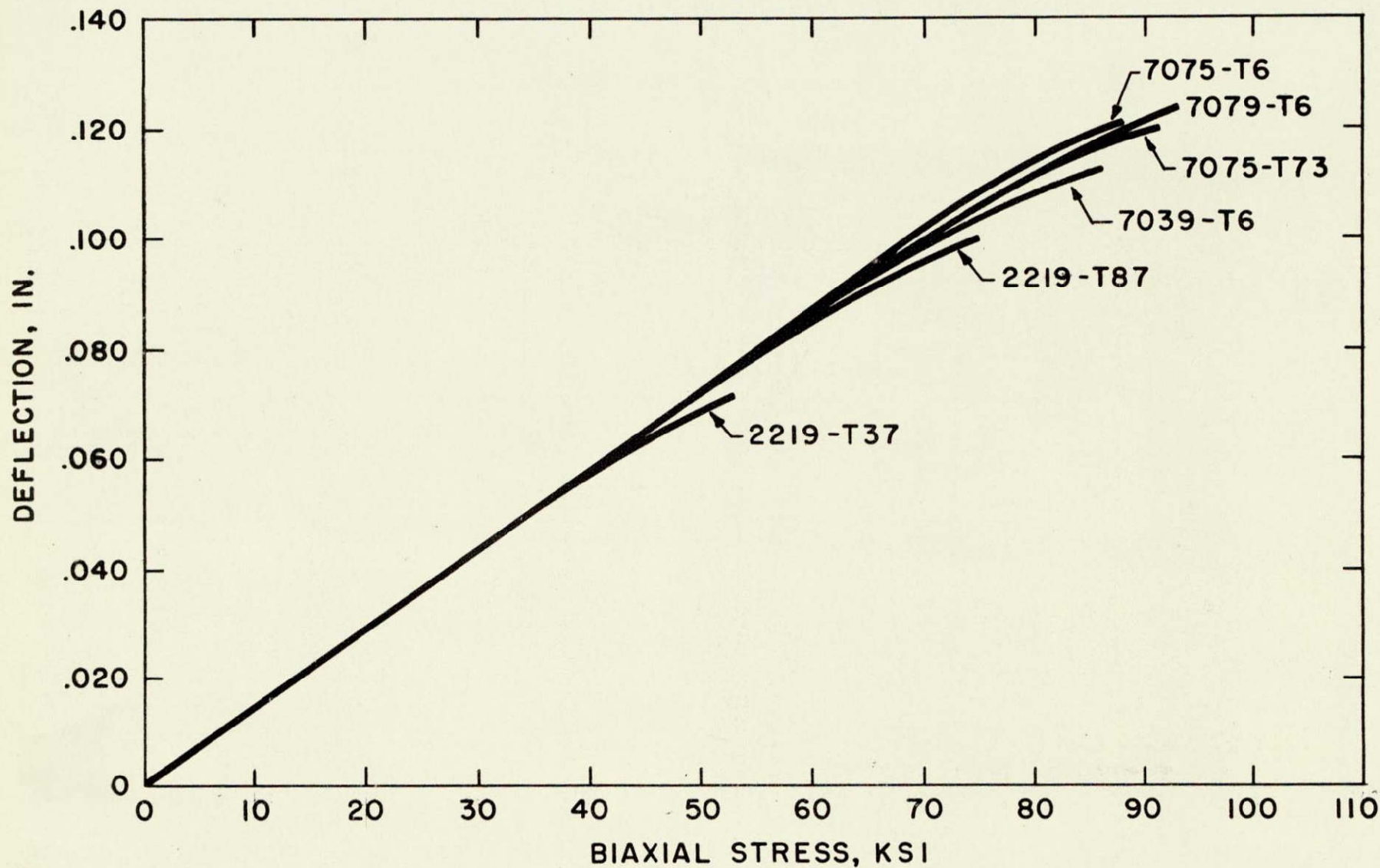
Figure 42





STRESS - CORROSION CRACK INITIATION SPECIMEN

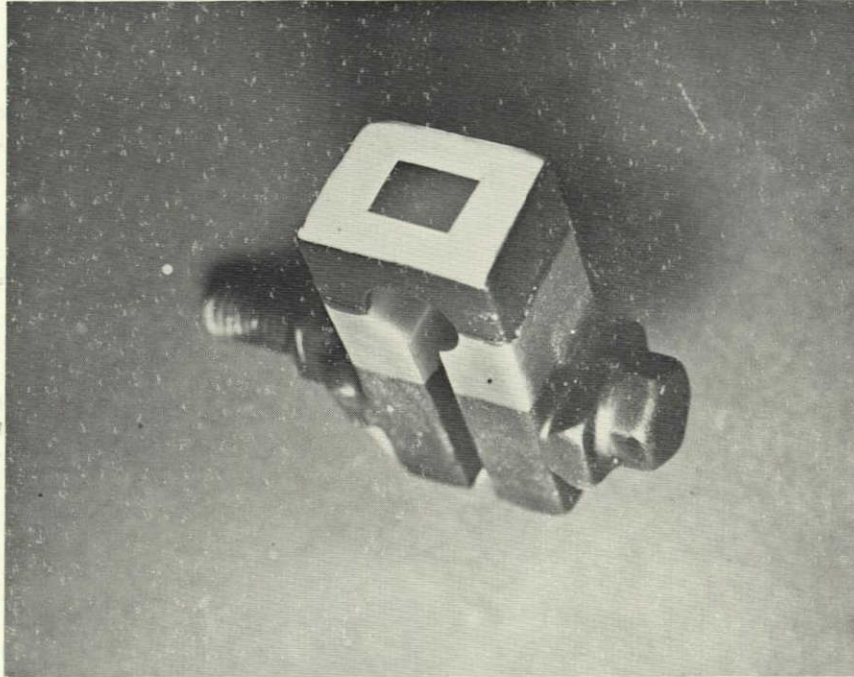
FIGURE 43



RELATION BETWEEN DEFLECTION AND SHORT-TRANSVERSE STRESS IN  
STRESS CORROSION TEST SPECIMEN

FIGURE 44





Stress Corrosion Test Specimen  
Prepared for Exposure

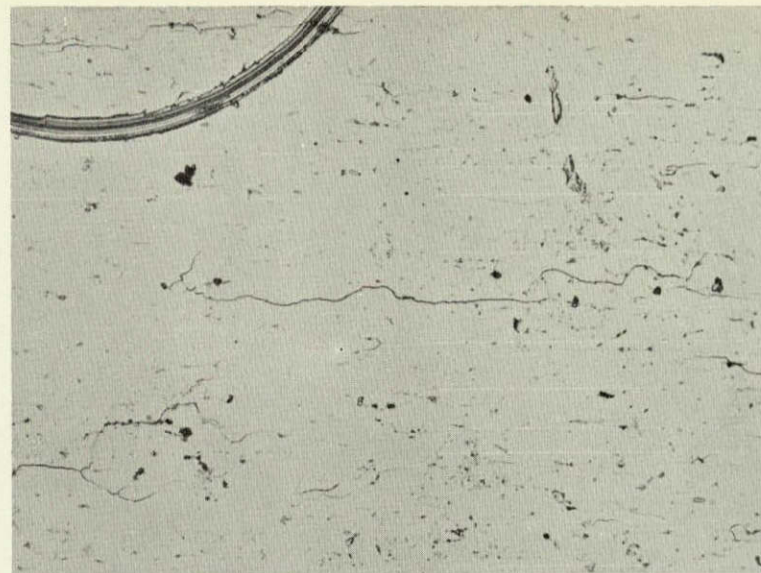
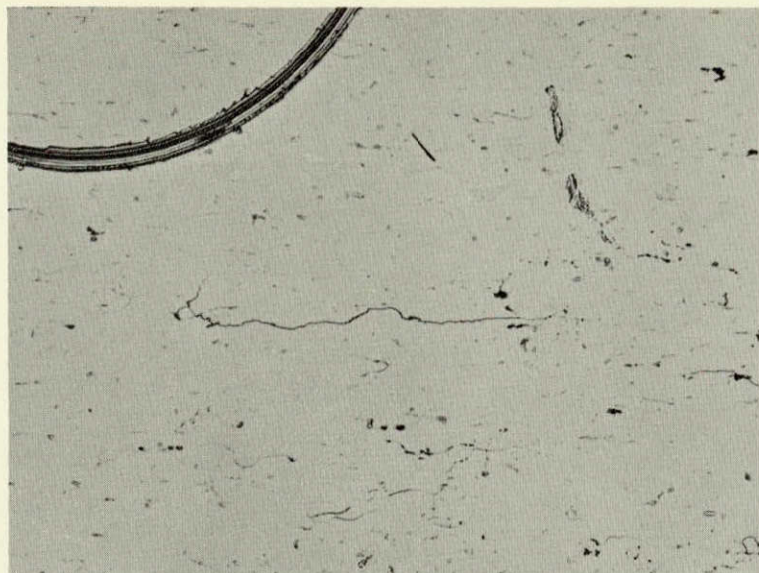
Figure 45

161209  
161216  
161235  
161242

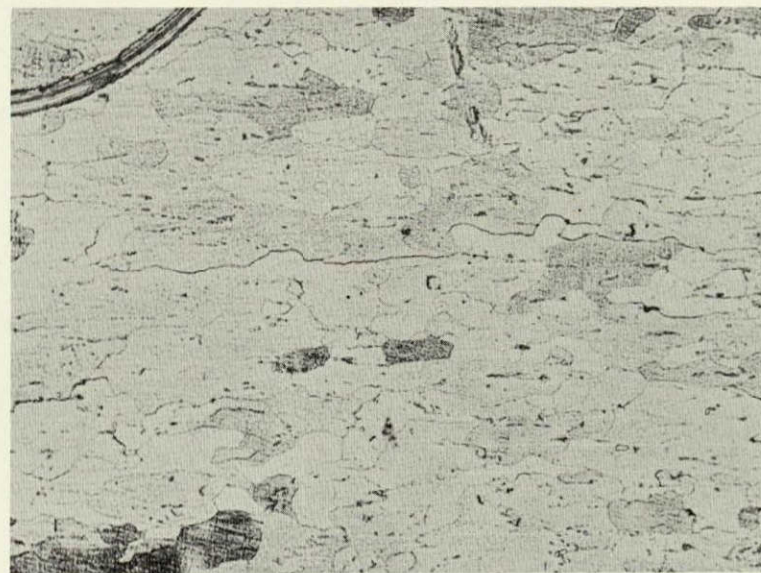
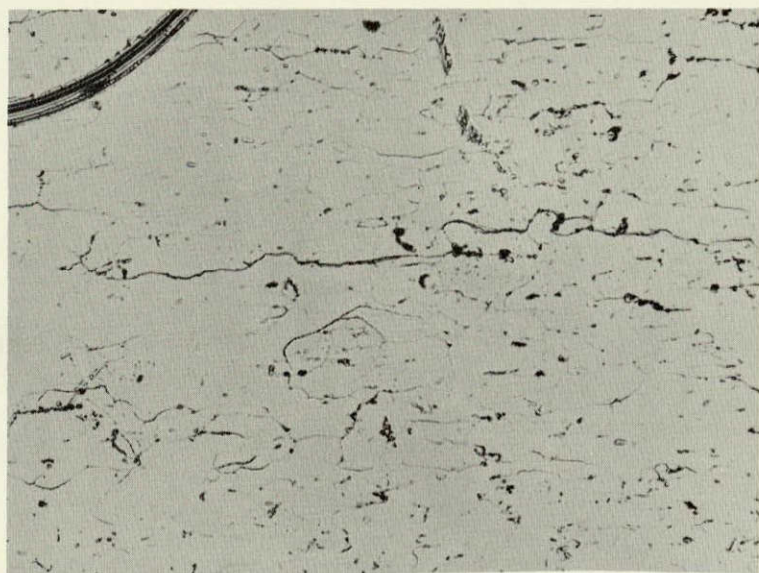
12  
min.

↑  
STRESS  
↓

30  
min.



22  
min.



30  
min.  
Keller's  
Etch

Development of stress corrosion cracks on surface of 2219-T37  
stressed to 75% YS in short transverse direction (X100)

Figure 46

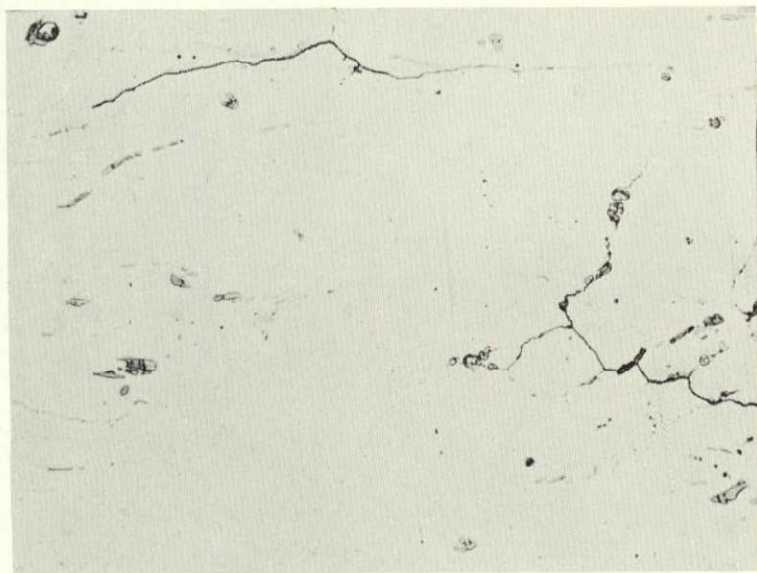
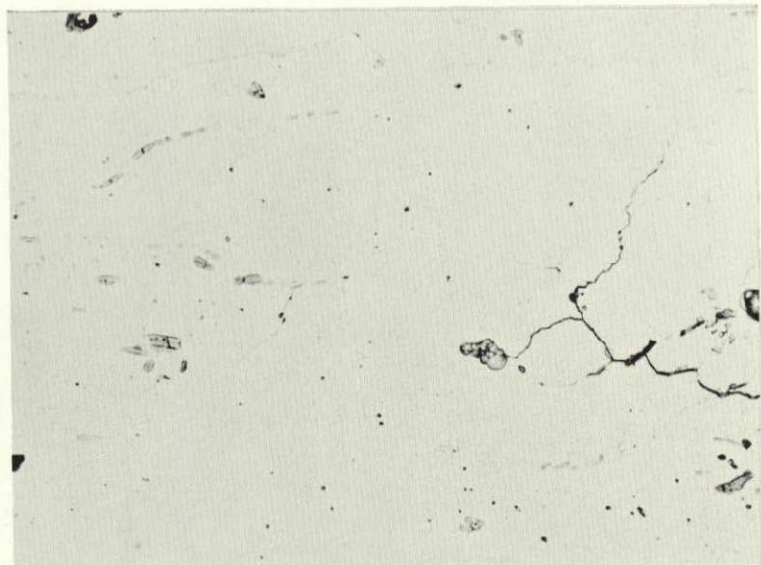


161212  
161236  
161243  
161244

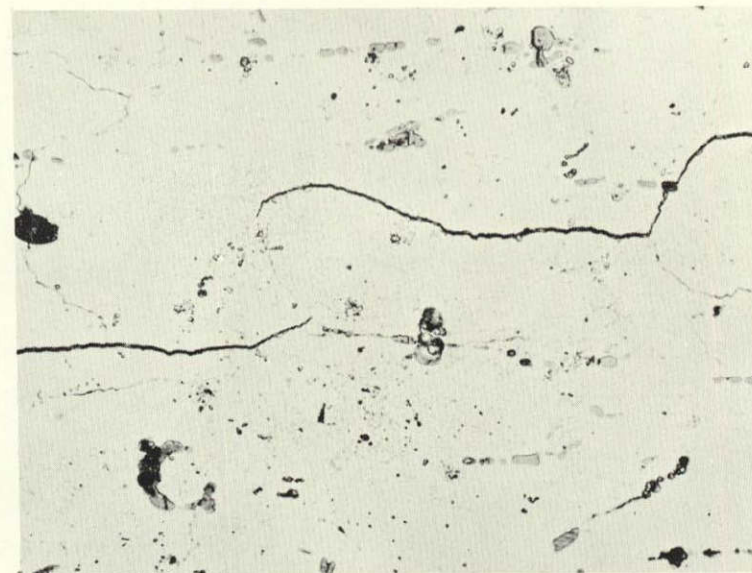
22  
min.

↑  
STRESS  
↓

30  
min.



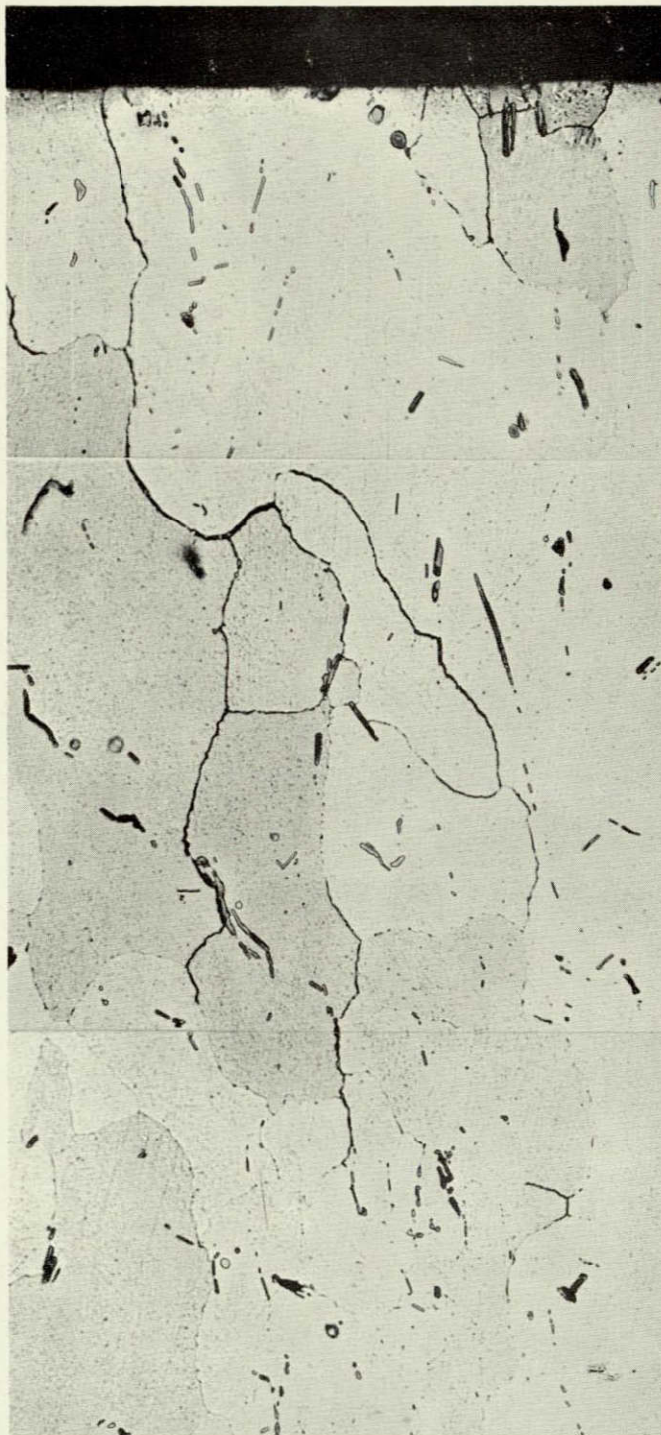
12  
min.



22  
min.

Ends of cracks seen in Fig. 46 at higher magnification (X500)

← STRESS →

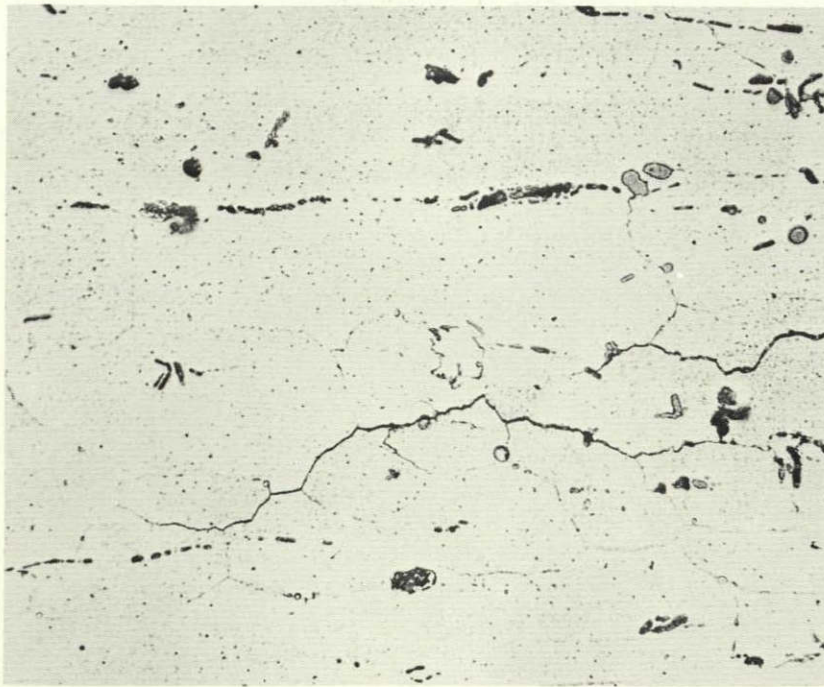


Penetration of stress corrosion  
crack after 30-minute exposure  
of 2219-T37 specimen stressed  
short transversely to 75% YS.  
(X500) Keller's Etch

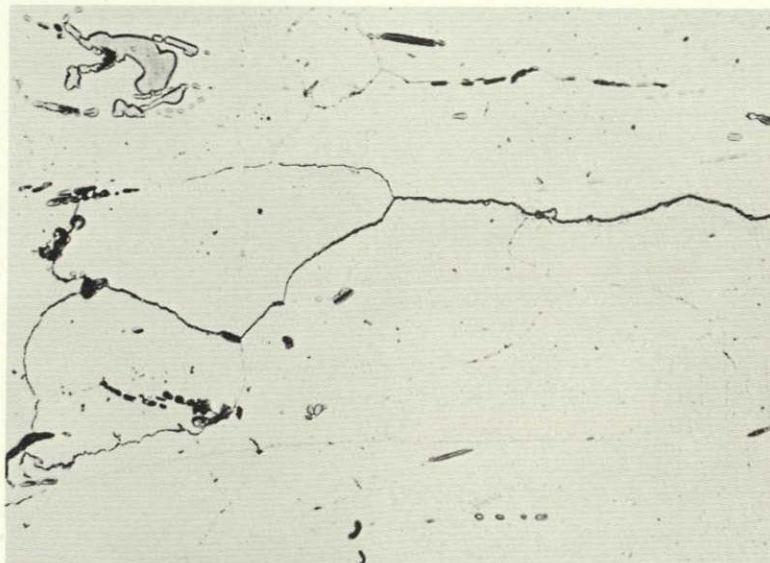
Figure 48



↑ Stress ↓



Selection of favorably oriented boundaries by propagating crack.



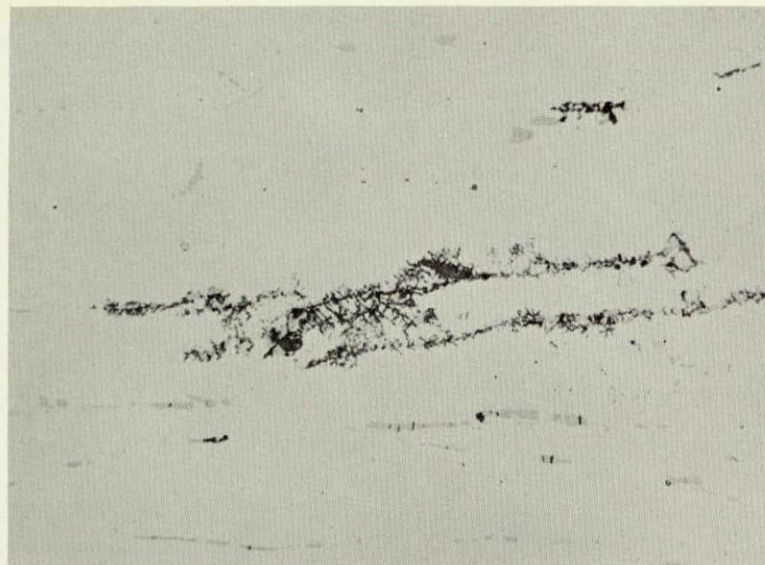
Cracks avoiding microconstituent particles.

Crack development in 2219-T351 stressed short transversely to 75% Y.S. (X500)

Figure 49

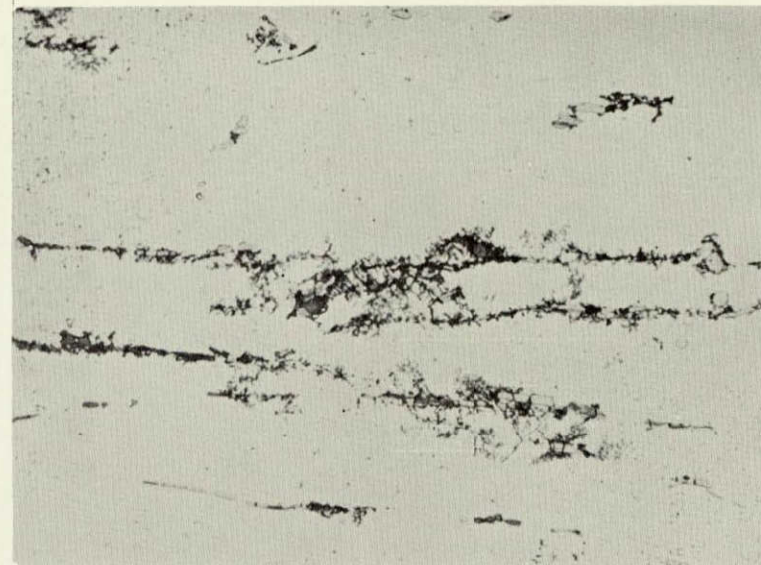


5  
min.

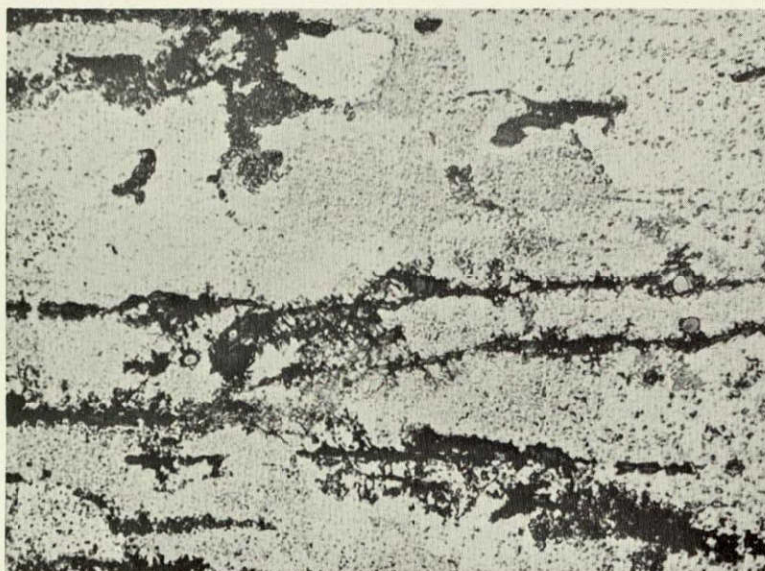


Stress  
↑  
↓

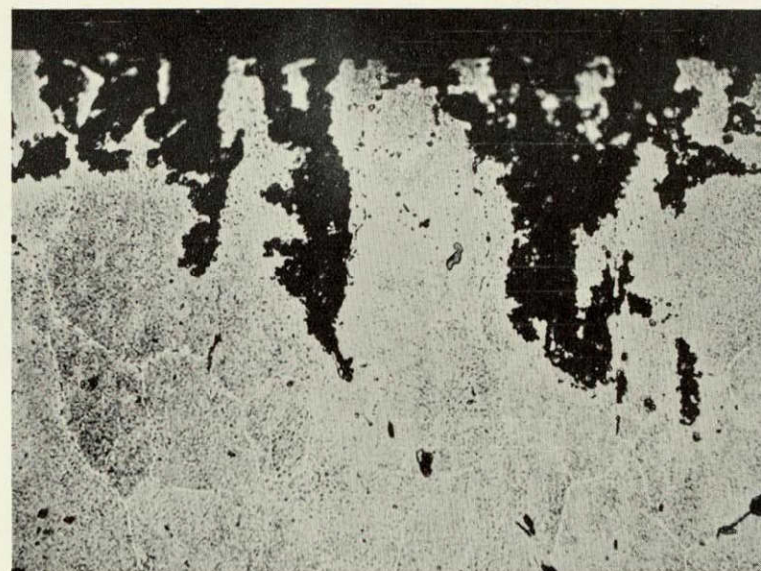
30  
min.



90  
min.



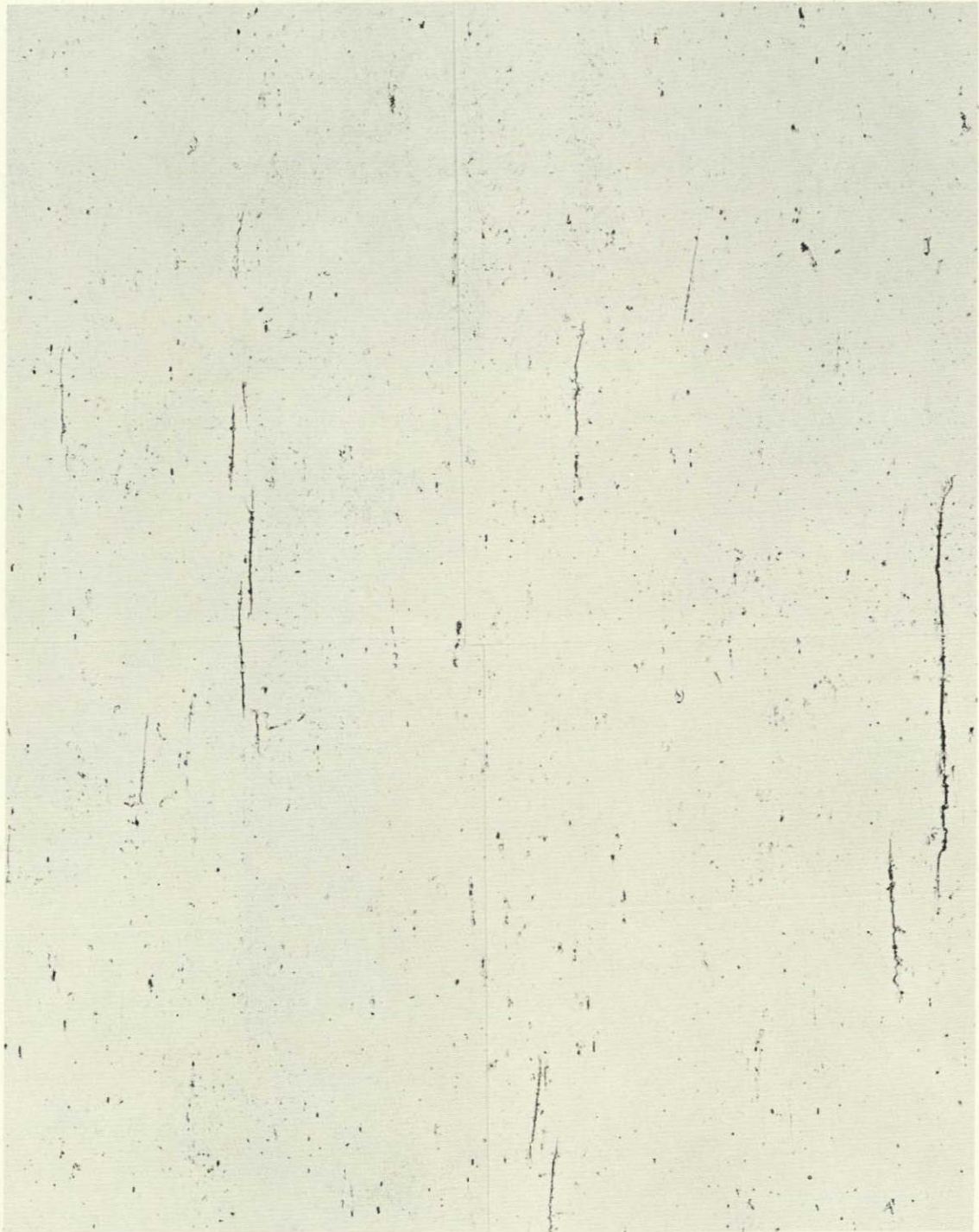
90  
min.  
X-Sect.



Directional attack perpendicular to stress in 2219-T87  
stressed to 75% YS in short transverse direction. (X500)



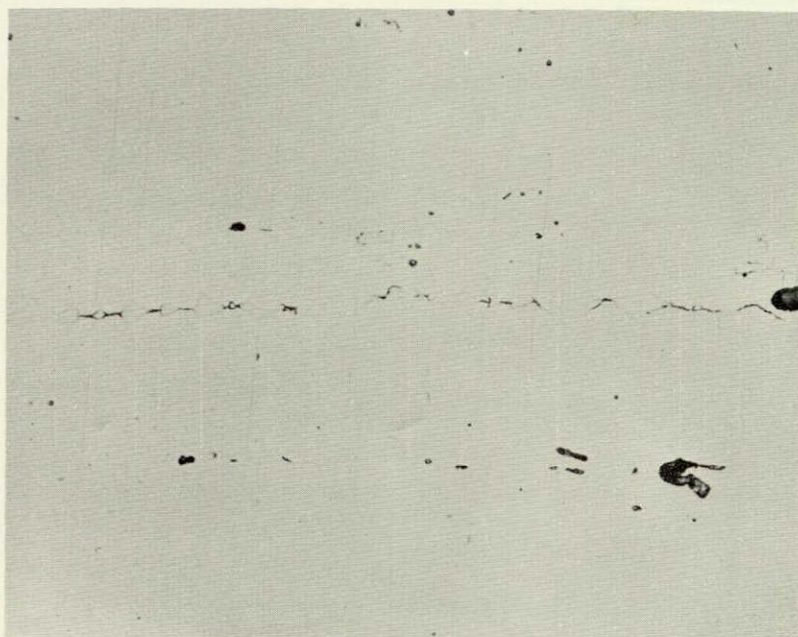
← Stress →



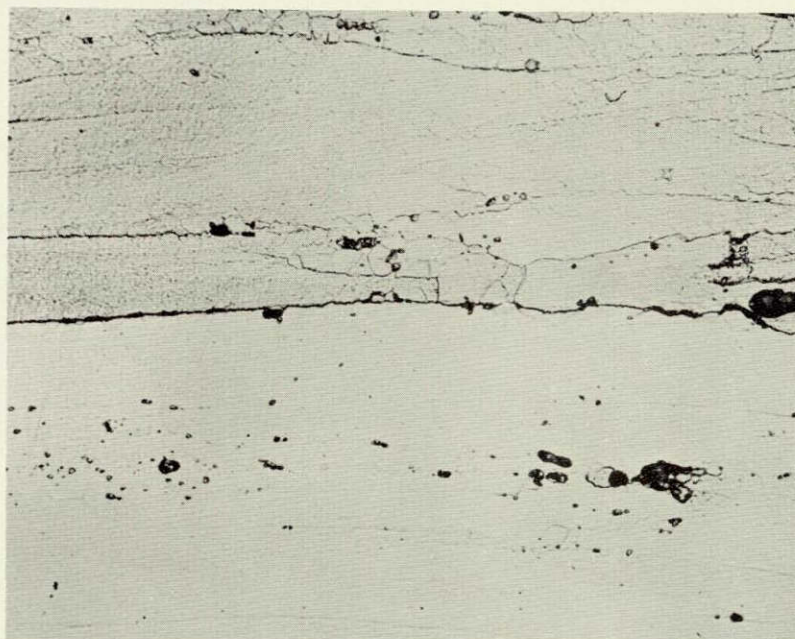
Crack initiation in 7-minute exposure of 7075-T6.  
Stressed short transversely to 75% Y.S. (X100)

Figure 51

↑ Stress ↓



As Corroded



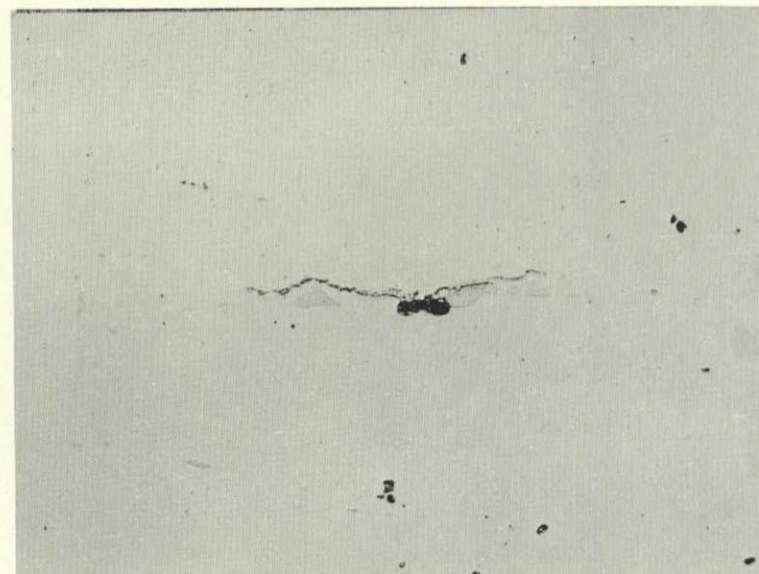
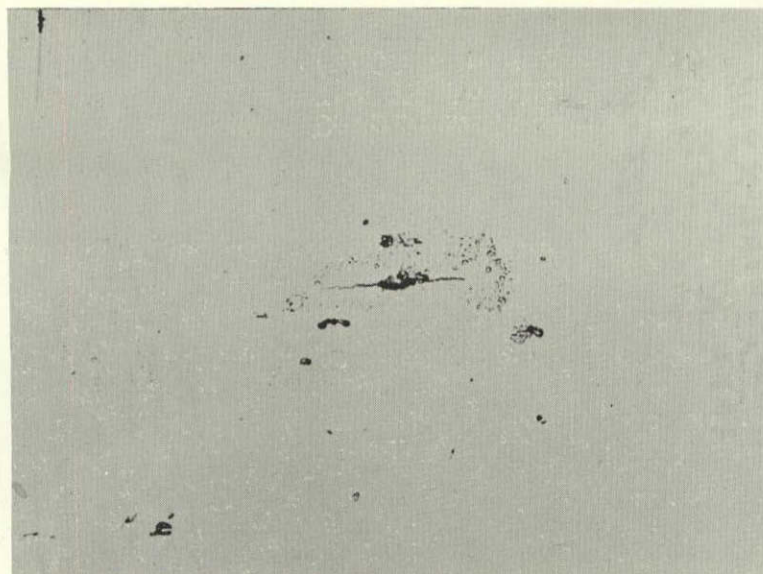
Keller's  
Etch

Crack initiation on boundary of 7075-T6  
stressed 75% YS short transversely. (X500)

Figure 52



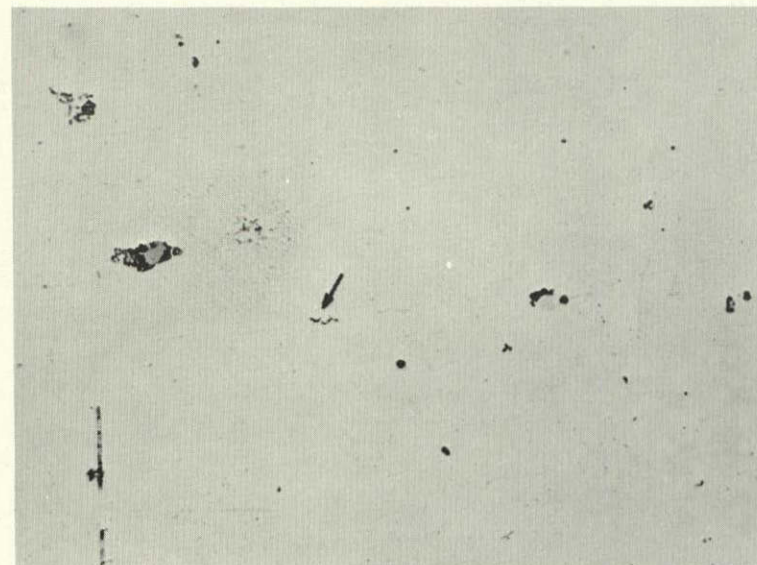
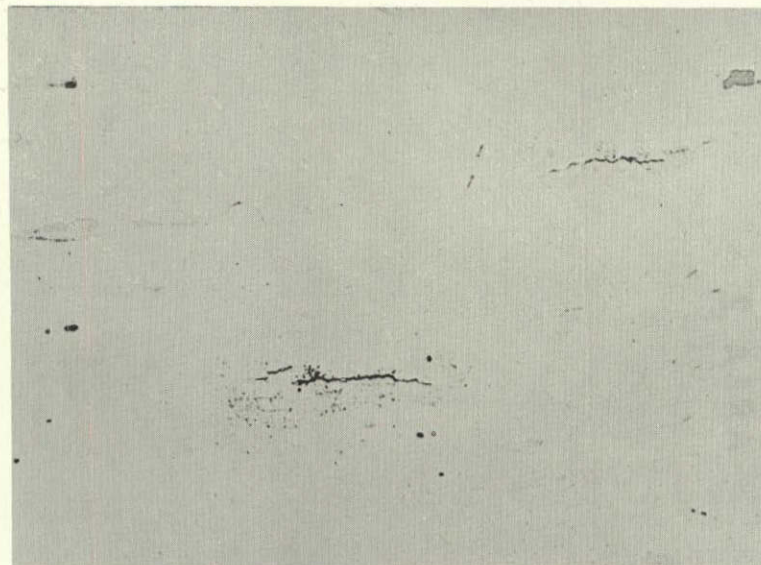
(a)



(b)

↑  
STRESS  
↓

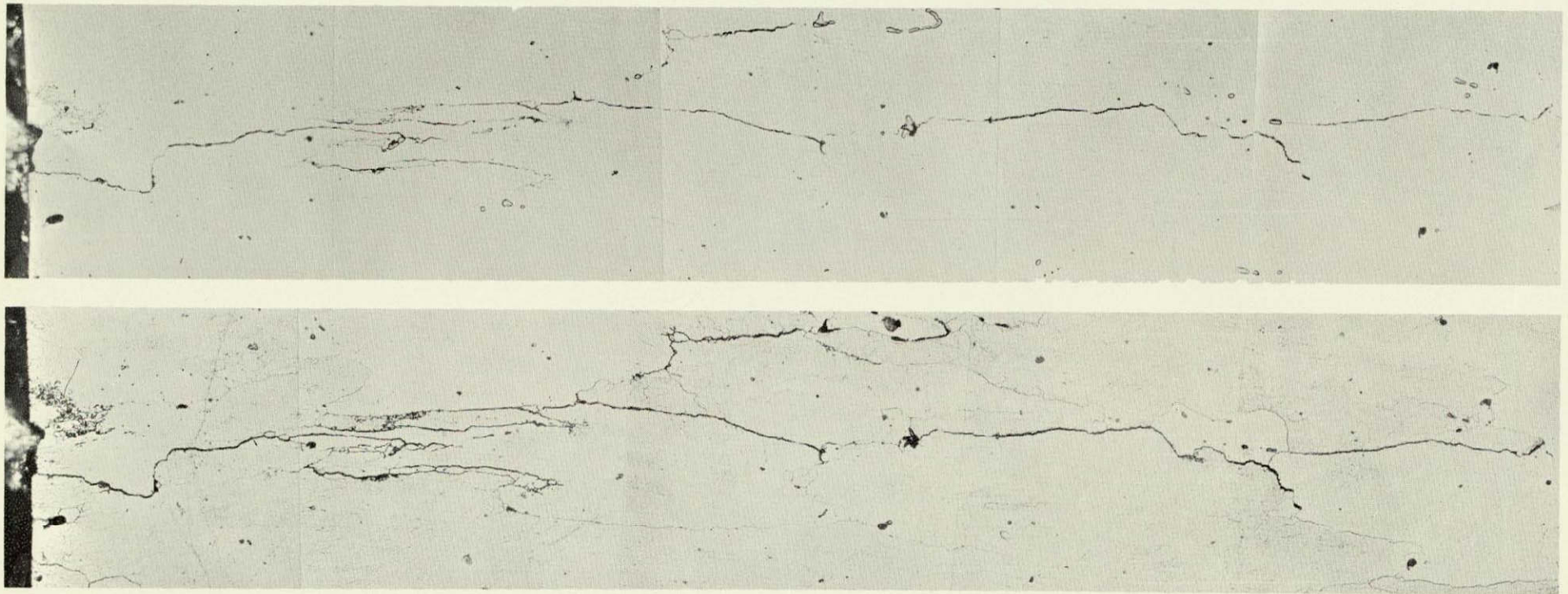
(c)



(d)

Embryonic cracks after 7-minute exposure on surface of  
7075-T6 stressed short transversely to 75% YS (X500)

— STRESS —



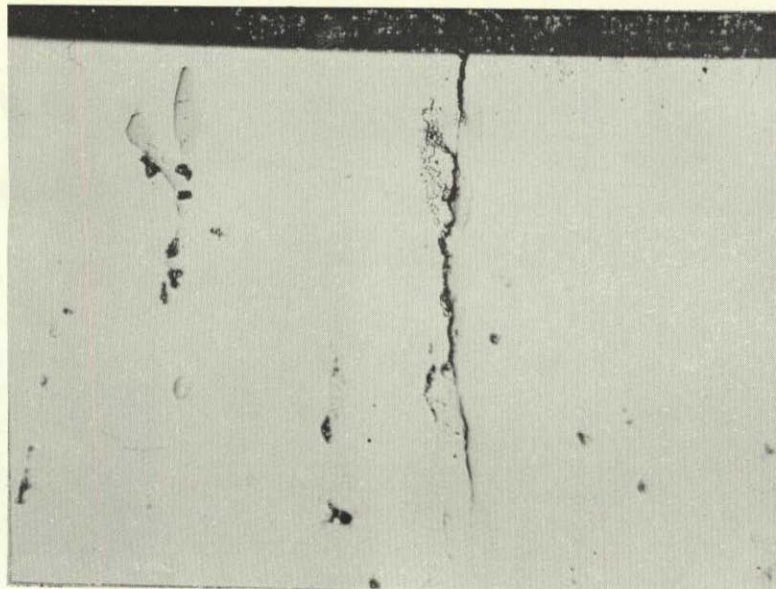
Development of stress corrosion crack in 7075-T6 stressed to 75% YS in short transverse direction and exposed 105 min. (X500 - reduced 1/3). Upper - as polished. Lower - Keller's Etch

Figure 54

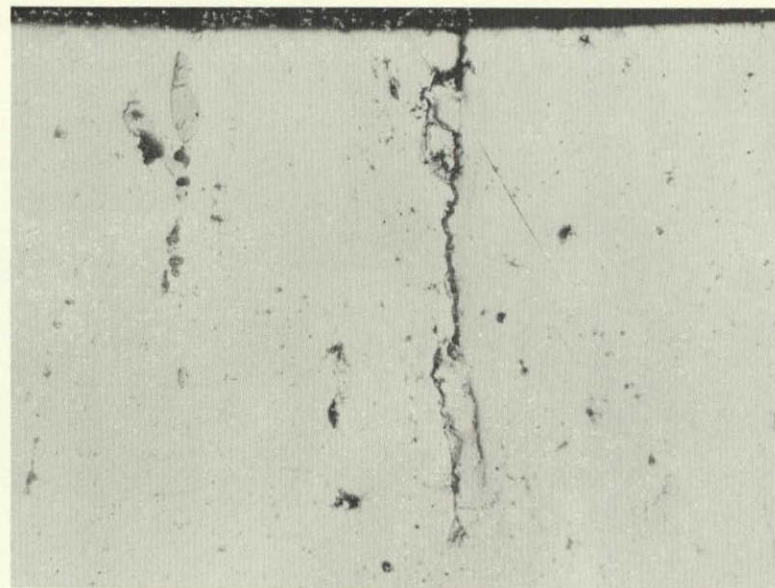


164602  
164607  
164608

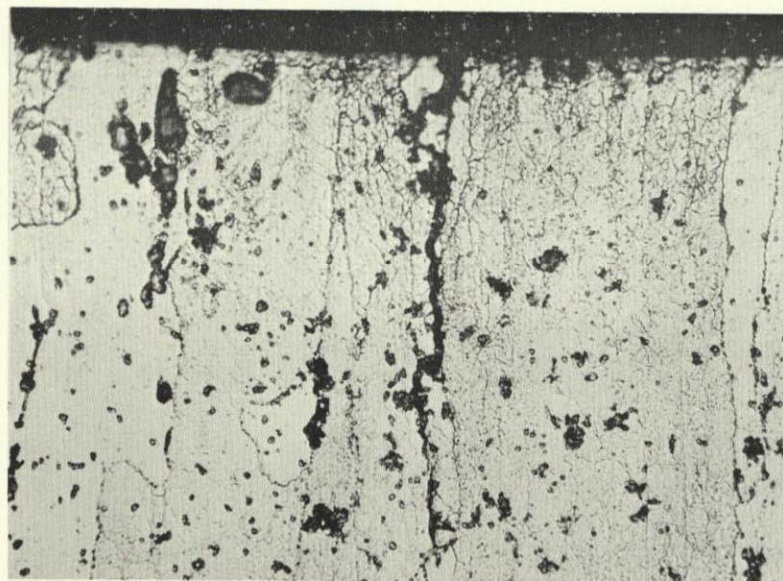
10 min.



20 min.



← STRESS →

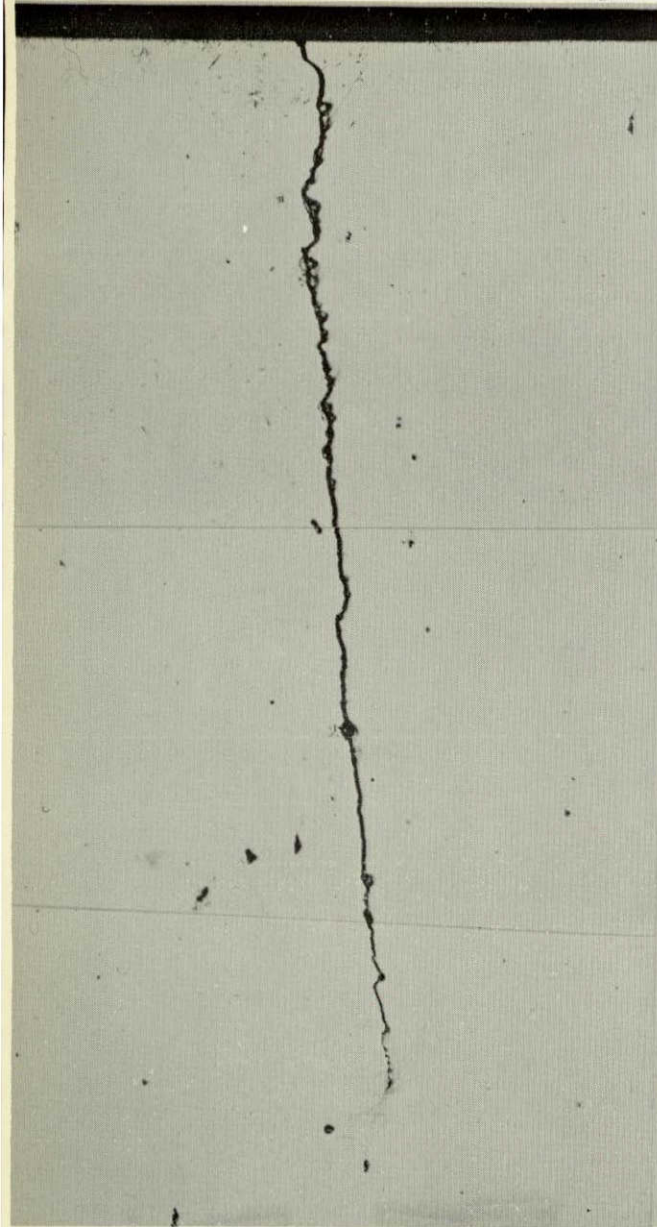


20 min. - Keller's Etch

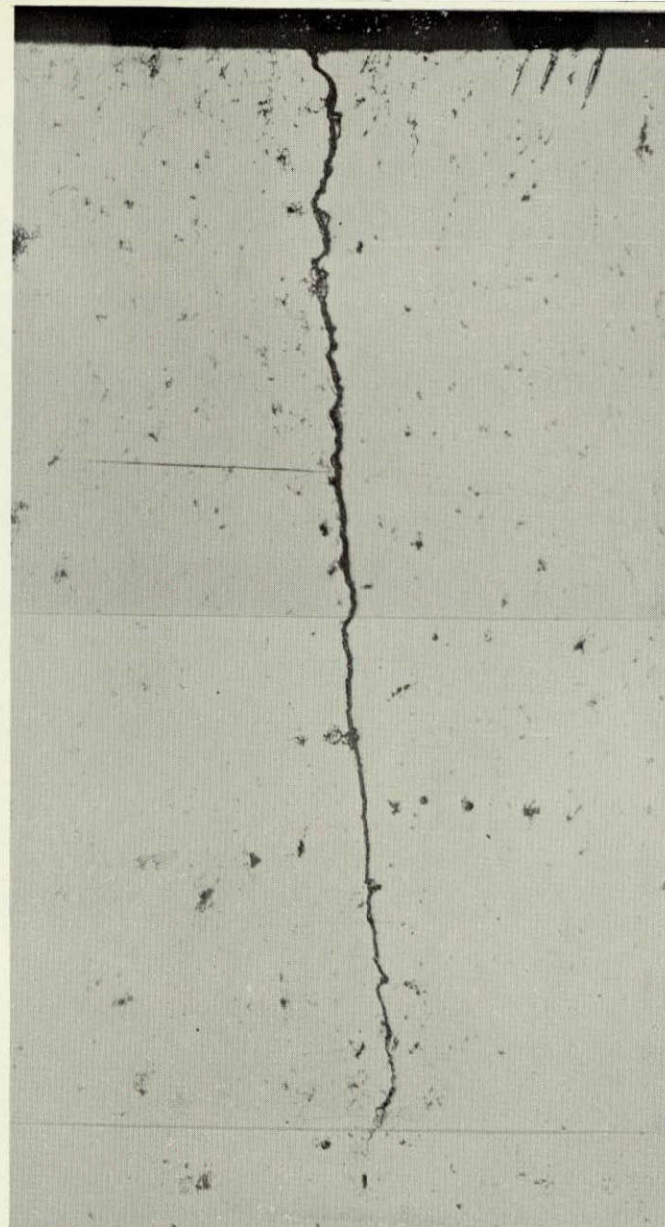
Crack initiation on end face - 7075-T6 stressed short transversely to 75% YS (X500)  
(See Figure 56 for matching side surface of same specimen)

Figure 55



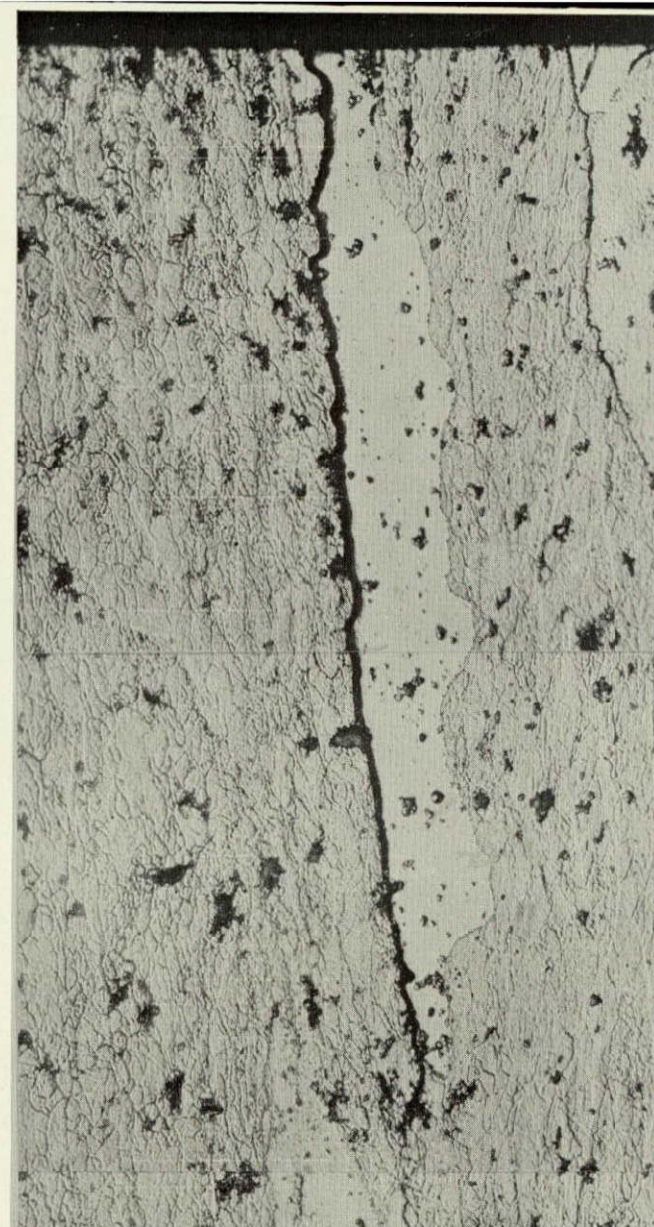


10 min.



20 min.

← STRESS →



20 min.  
Keller's Etch

Crack initiation on side face - 7075-T6 stressed short transversely to 75% YS (X500)  
(See Figure 55 for matching end surface of same specimen)

Figure 56

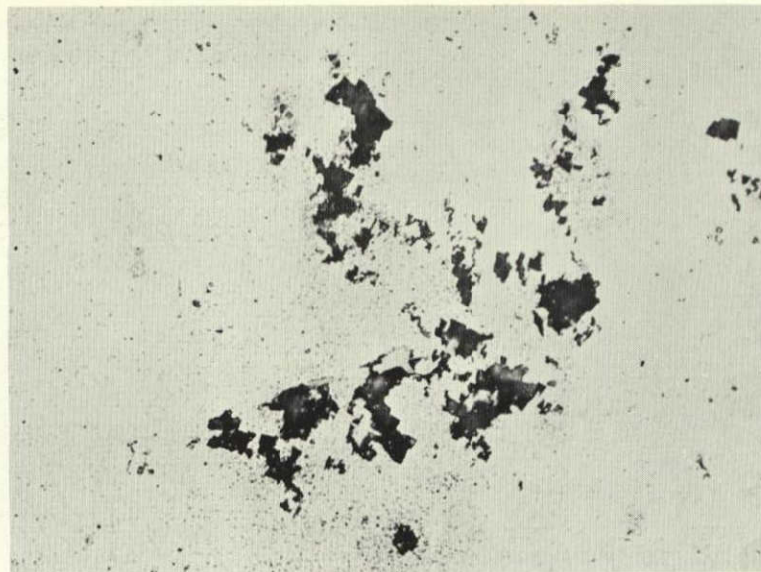


161551  
161553  
161554  
162040

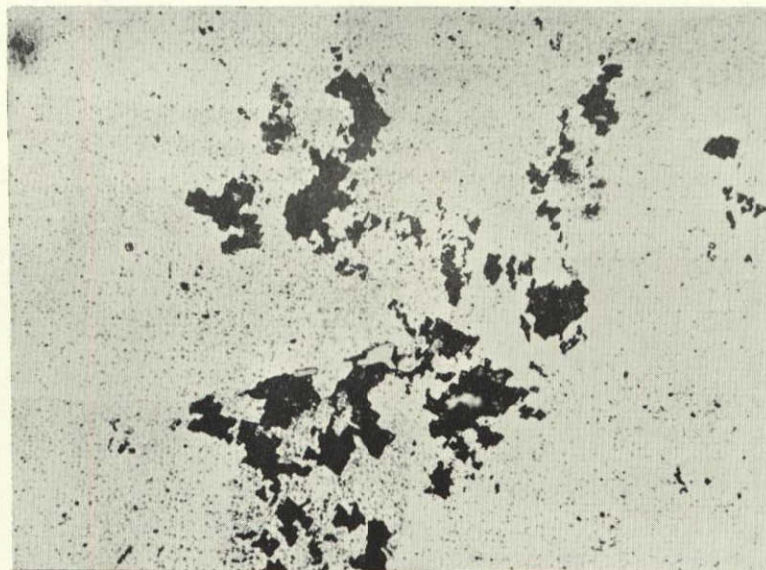
5  
min.



40  
min.



60  
min.



90  
min.  
X-Sect.  
Keller's  
Etch



Cubic pitting in 7075-T73 stressed 75% YS  
in short transverse direction. (X500)

Figure 57

↔ Stress ↔



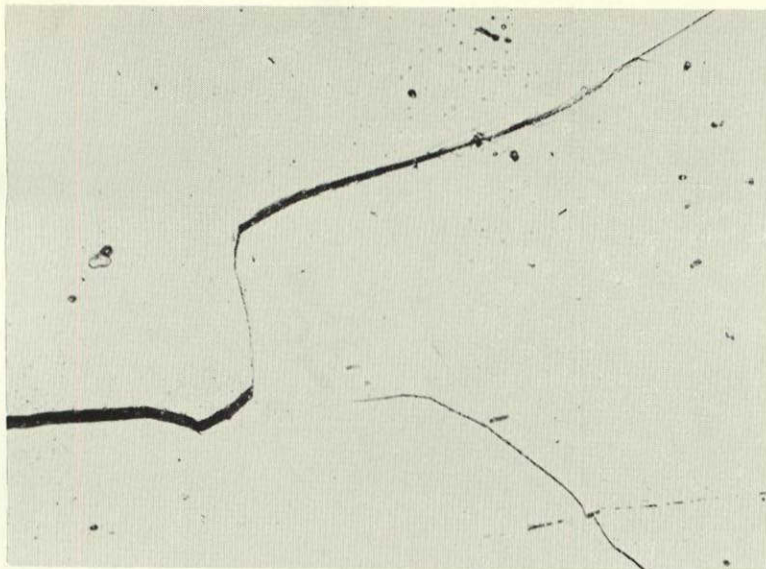
Crack development in X7375-T6 stressed  
to 75% YS short transversely. (X500)

Figure 58

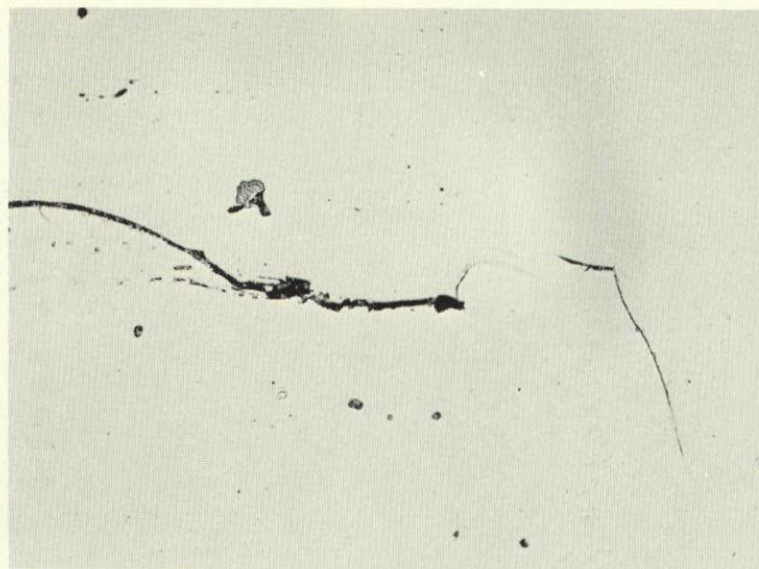


161571  
161570  
161631  
161635

(a)  
12 min.

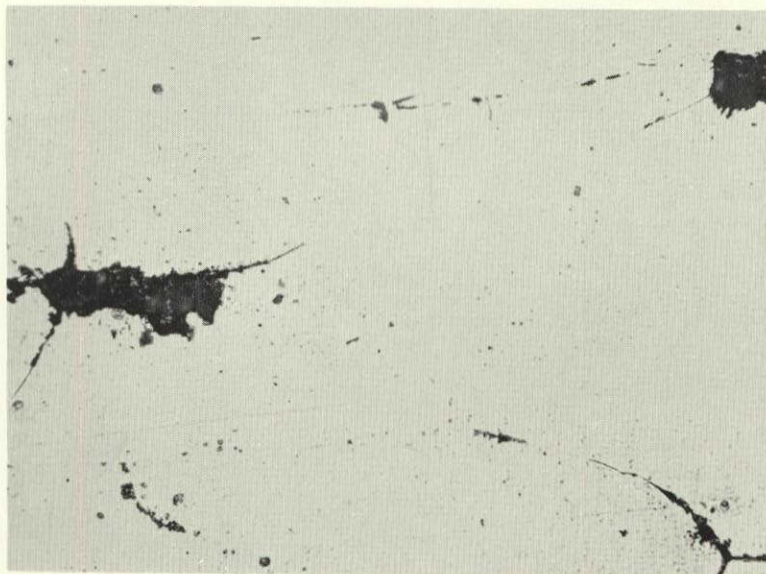


(b)  
12 min.

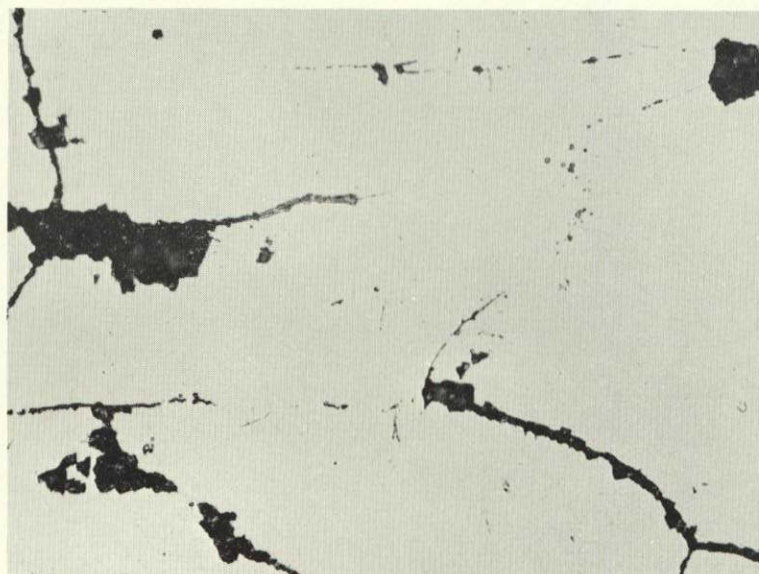


X7375-T6

(c)  
25 min.



(d)  
35 min.



X7375-T73 Type

Initiation of cracks in X7375-T6 and development of intergranular corrosion in X7375-T73 type alloy stressed short transversely to 75% YS.  
(X500)

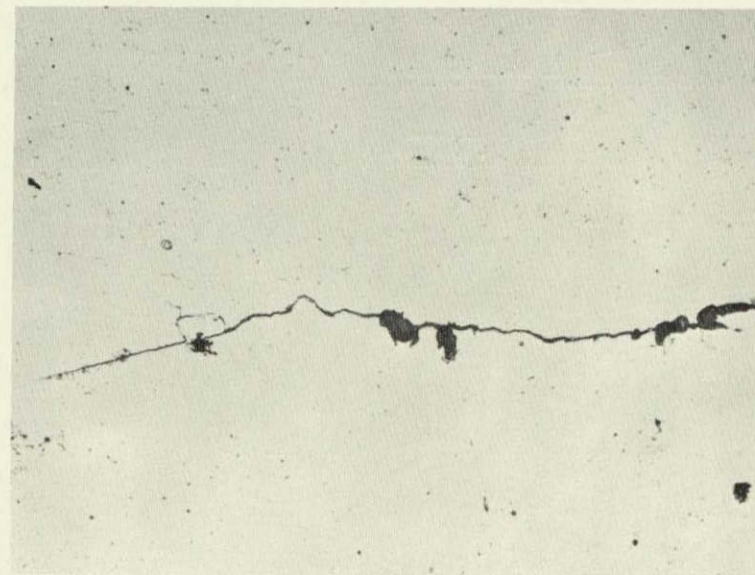
Figure 59

20 min.

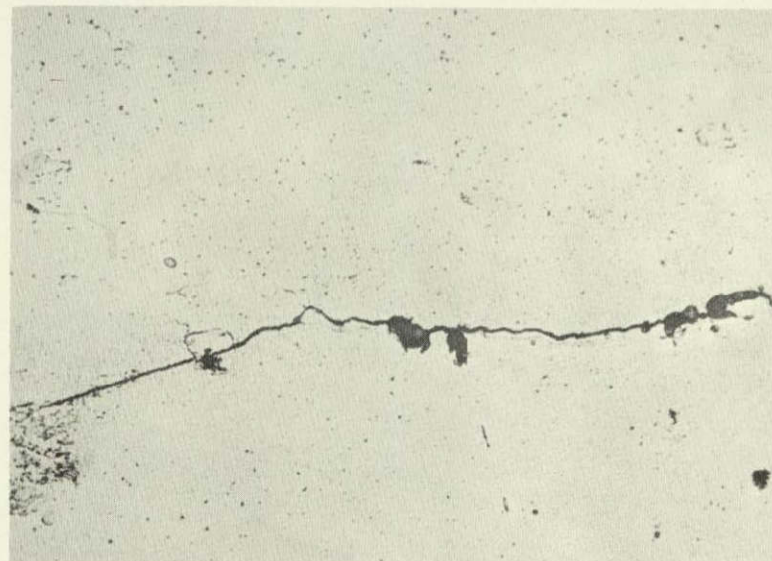
↑  
STRESS  
↓



31 min.



37 min.

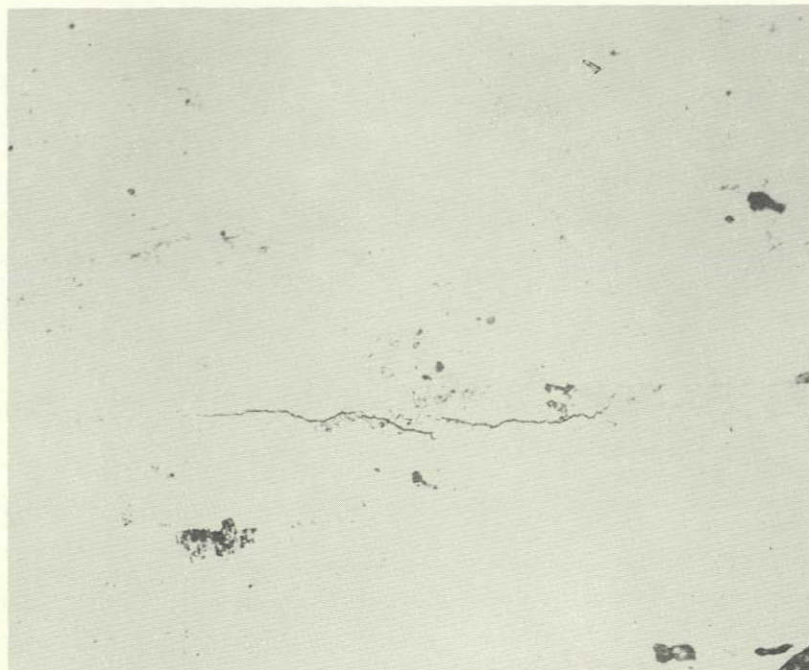


Stress corrosion crack initiation and development in 7079-T6 specimen stressed short transversely to 75% YS and exposed to the pH1 solution. (X500)

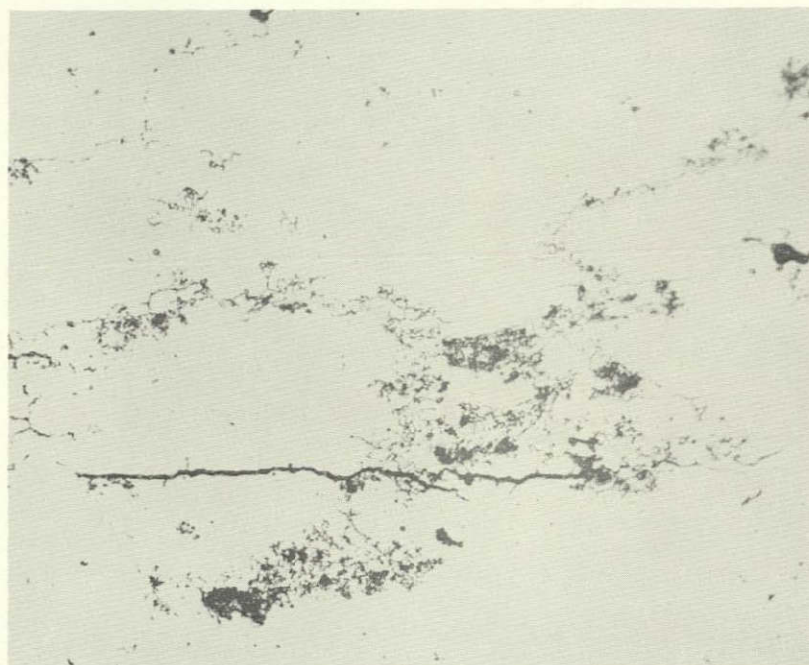
Figure 60



↑  
STRESS  
↓



25 min.

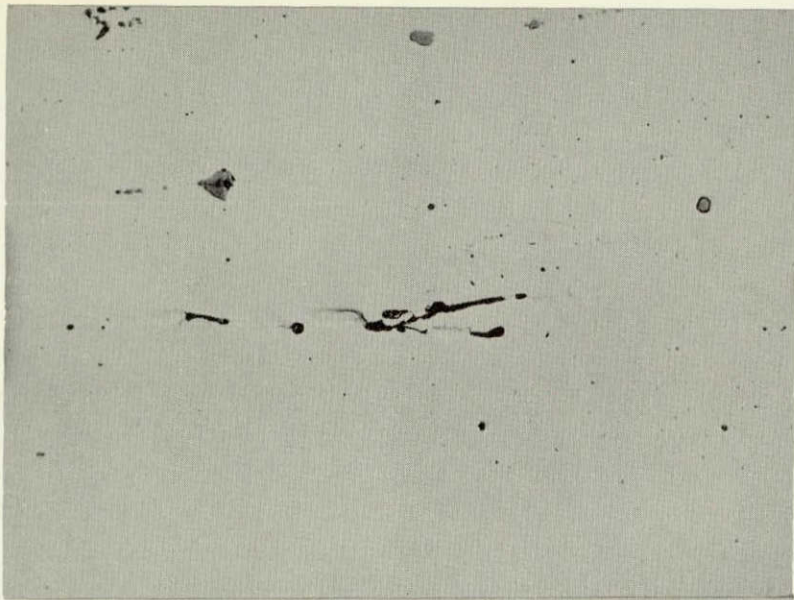


53 min.

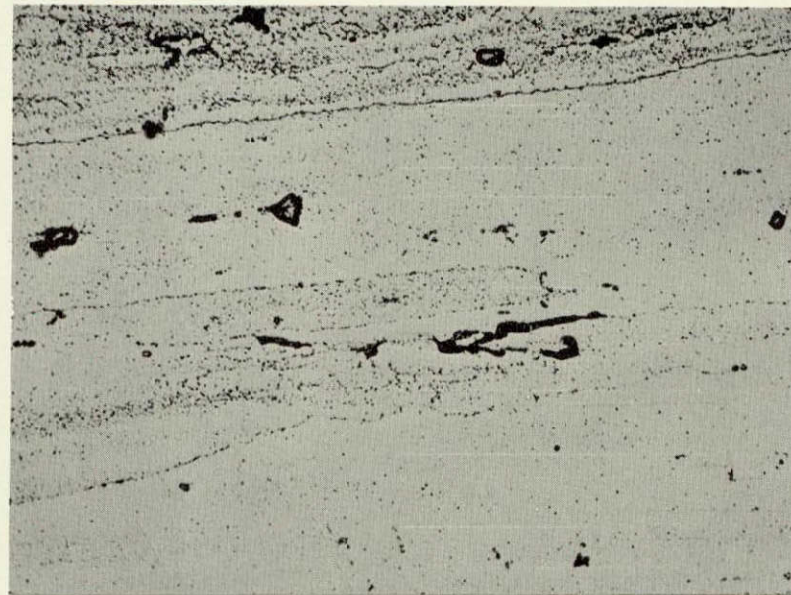
Shows development of interfragmentary attack along sides of a stopped crack in 7079-T6 specimen. Also note interfragmentary fringes along grain boundary. (X500)

Figure 61

As-Exposed

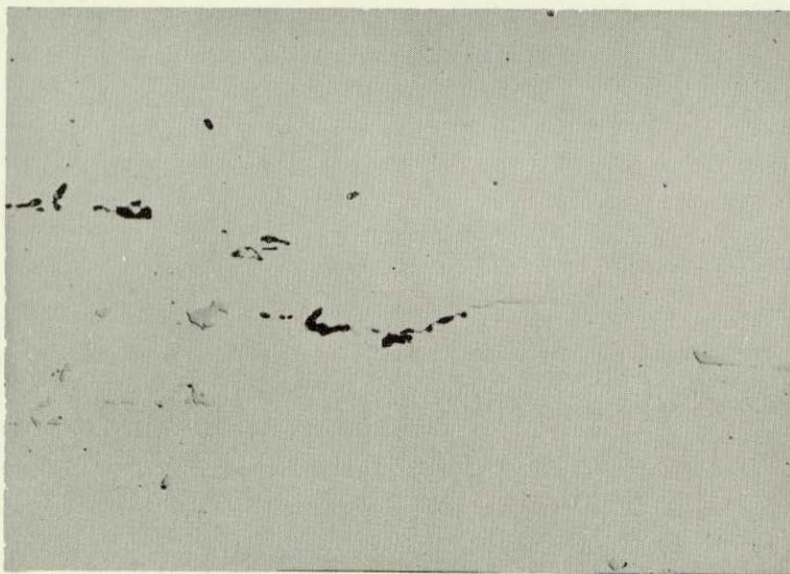


Keller's  
Etch

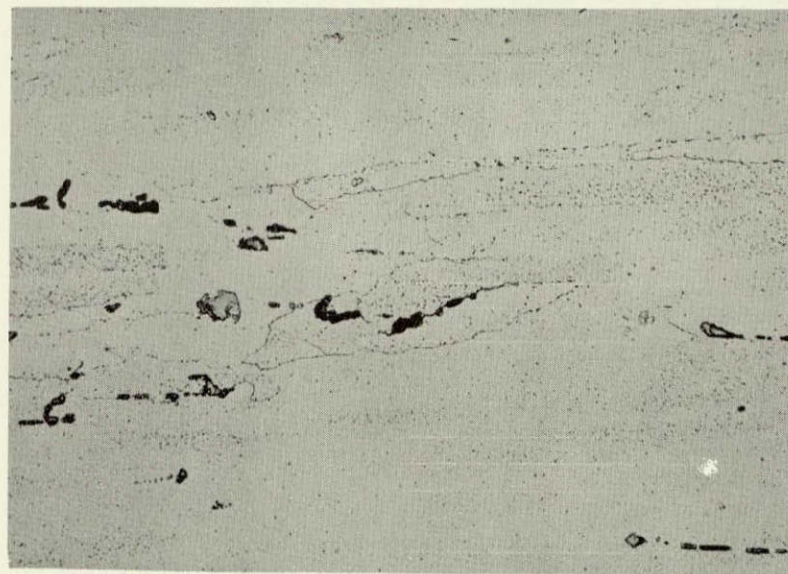


↑  
STRESS  
↓

As-Exposed



Keller's  
Etch



Crack initiation at  $Mg_2Si$  constituent particles in 7039-T6  
stressed short transversely to 75% YS and exposed to 0.5N  
NaCl + 0.5N  $Na_2CrO_4$  solution at pH 2 for 3-1/2 hours. (X500)

Figure 62

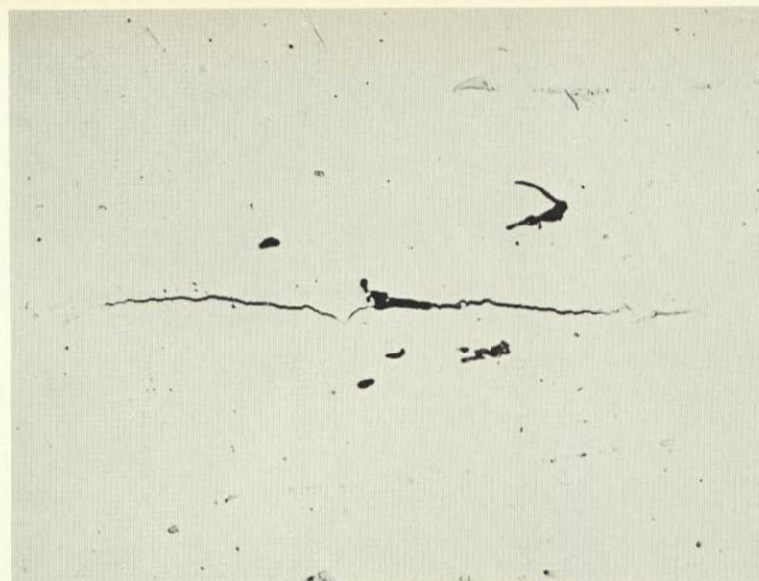


168577  
168579  
168581  
168582

2-1/2 hrs

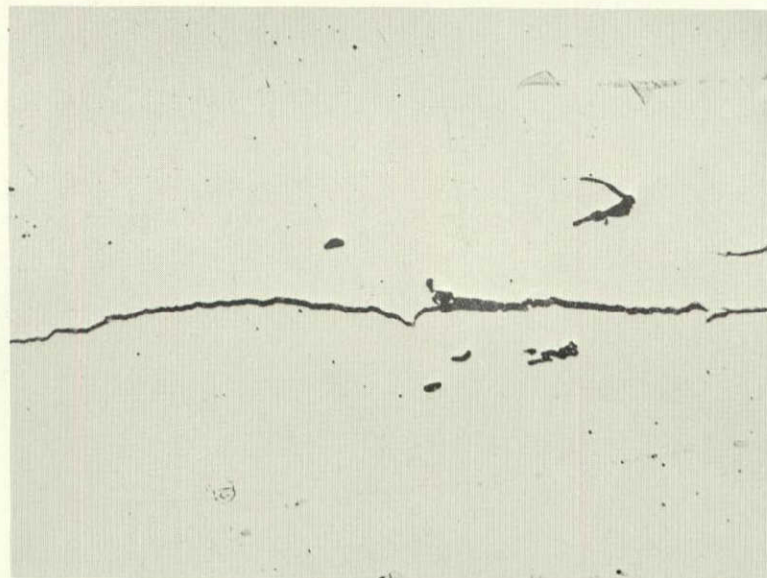


3-1/2 hrs

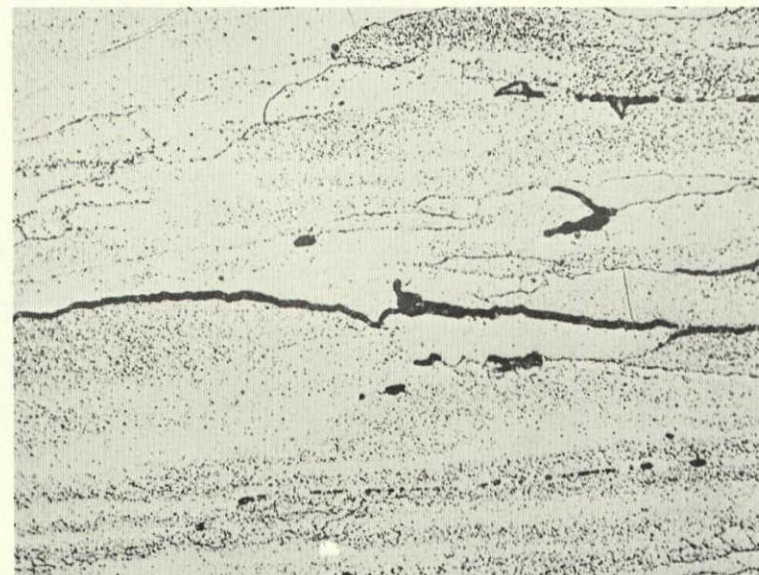


↑  
STRESS  
↓

4 hrs



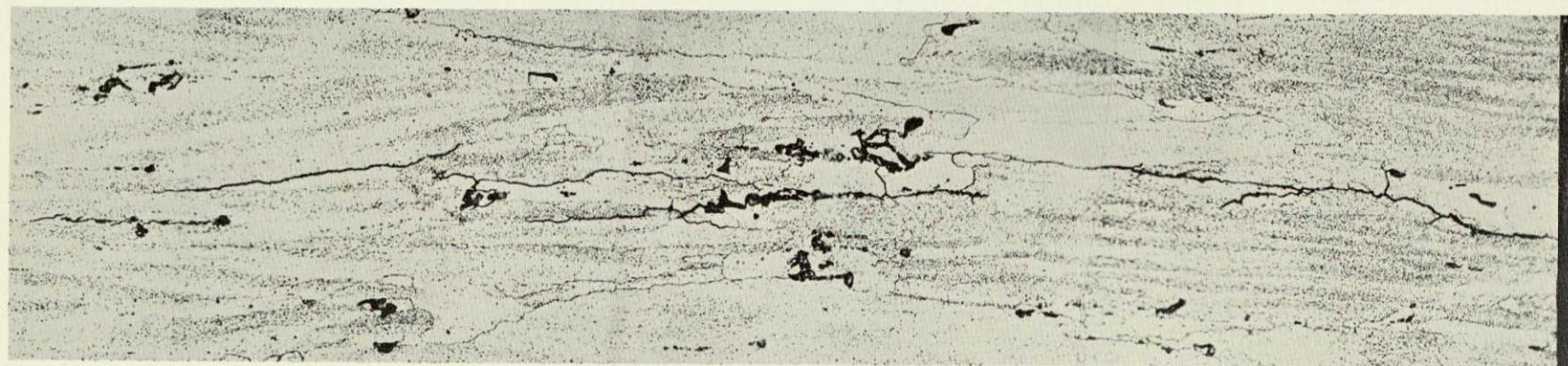
4 hrs  
Keller's  
Etch



Crack initiation and development in 7039-T6 stressed short transversely to 75% YS and exposed to 0.5N NaCl + 0.5N Na<sub>2</sub>CrO<sub>4</sub> solution at pH 2. (X500).

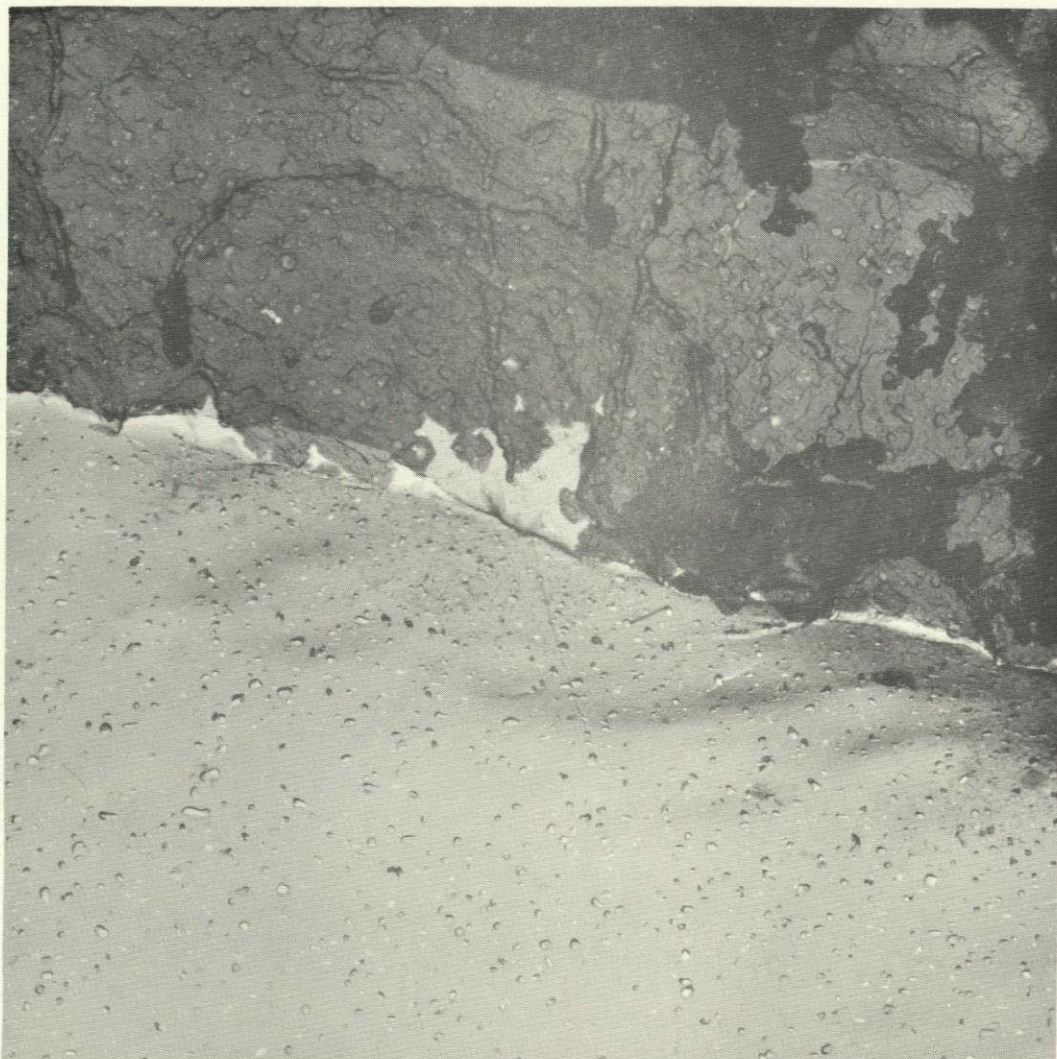
Figure 63





Cross section of sample seen in Fig. 63 showing  
crack development along boundaries. (X500)

Figure 64



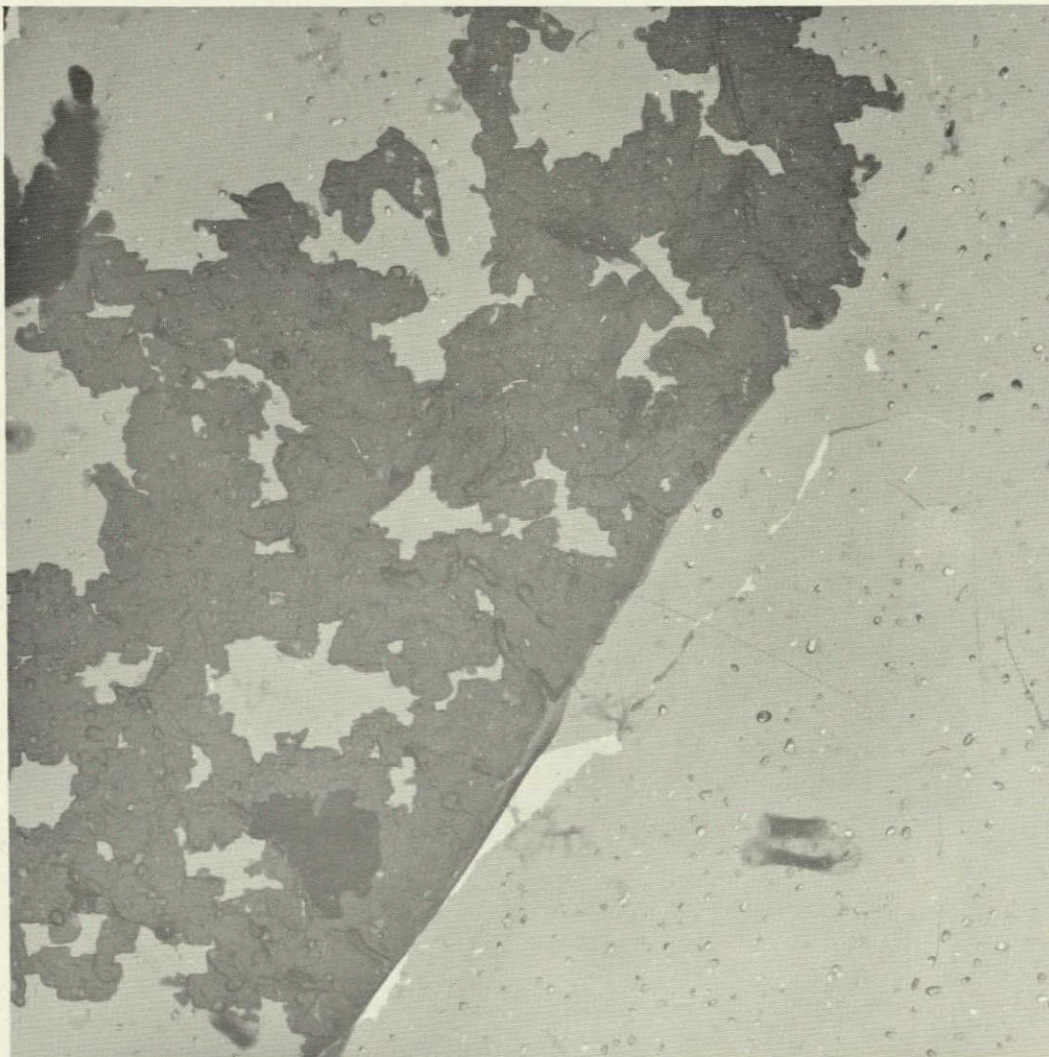
Oxide Replica

5000X

Stress corrosion crack development during 7-minute exposure of 7075-T6 specimen stressed to 75% YS in short transverse direction. Note veining and cubic configurations within crack

Figure 65





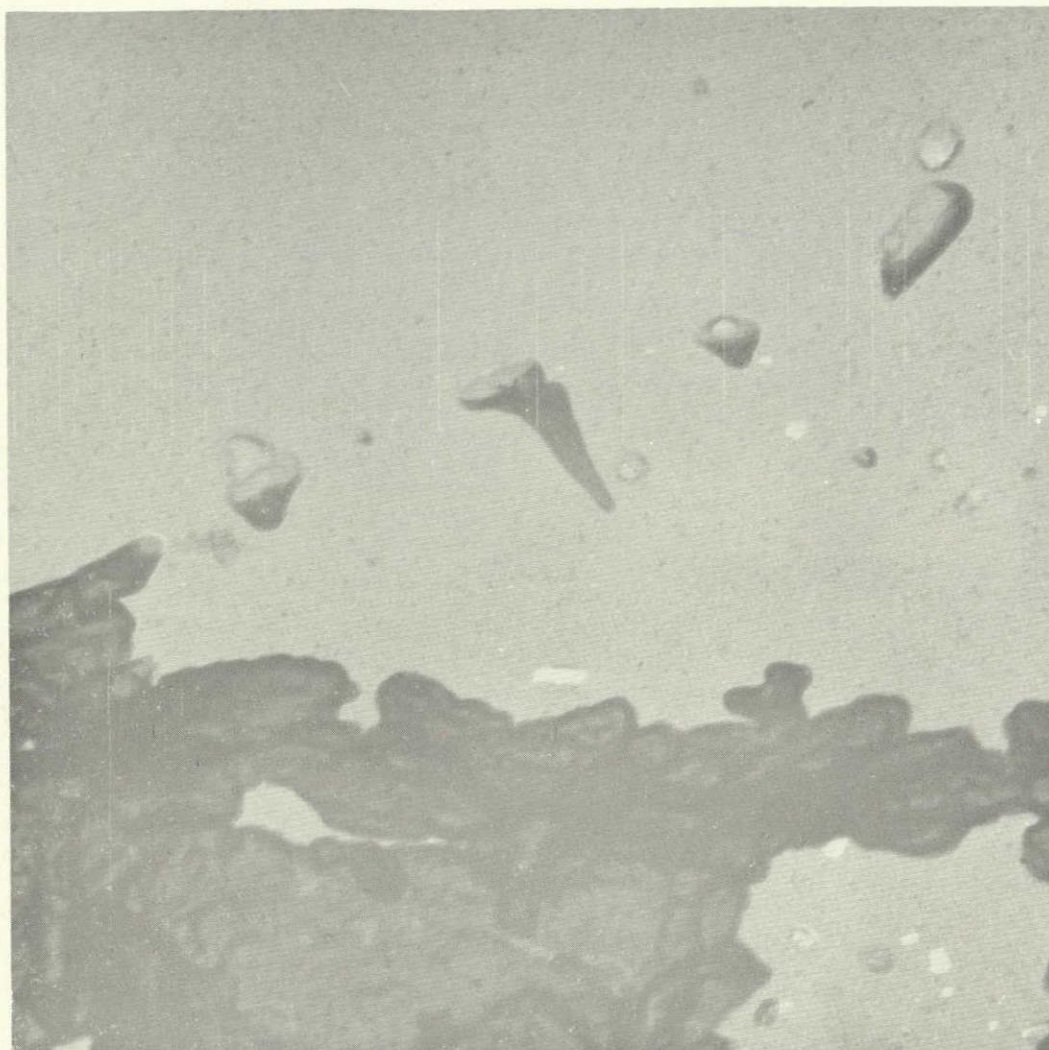
Oxide Replica

5000X

Embryonic cracks in same specimen as Fig. 65.

7075-T6 - 7 minute exposure

Figure 66



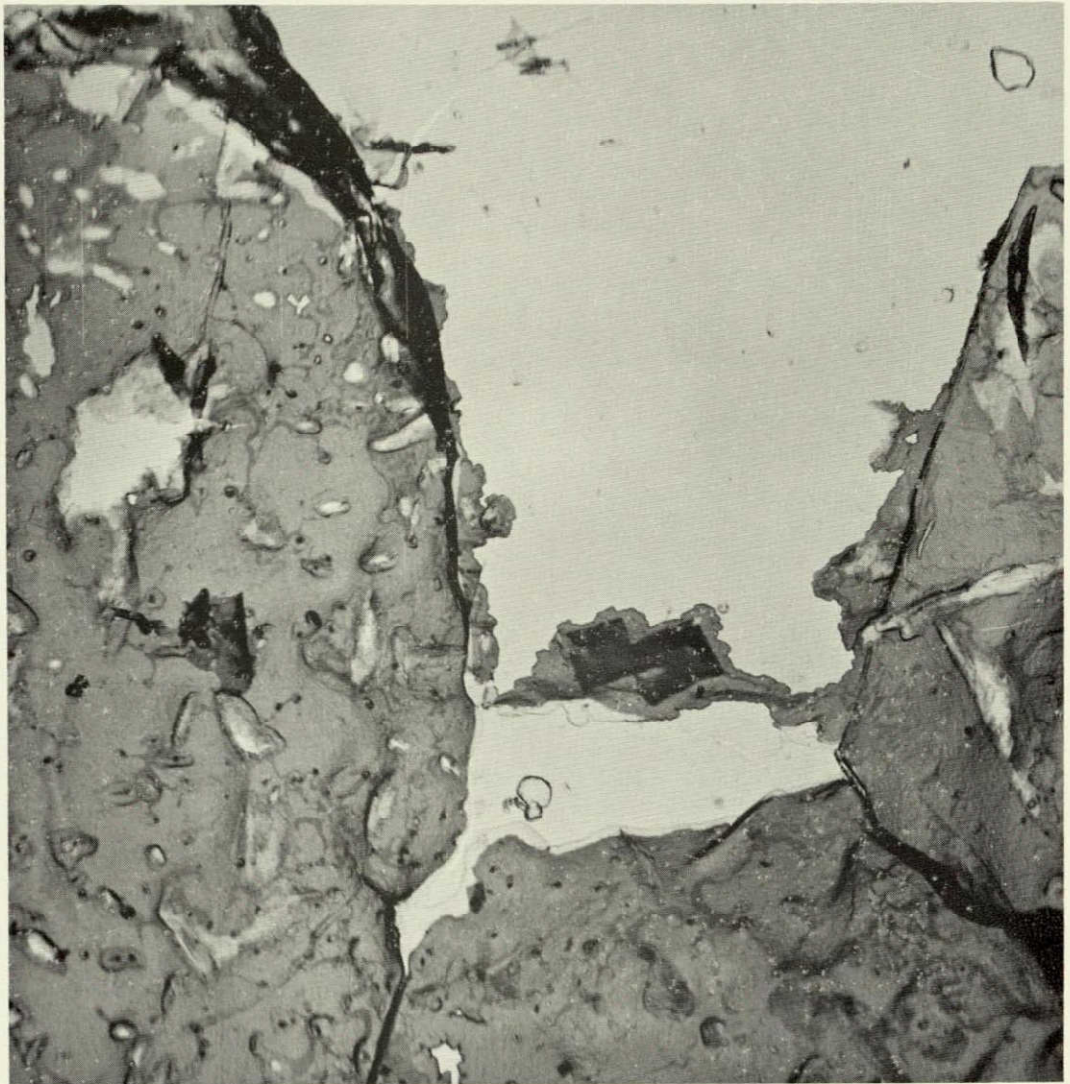
Oxide Replica

50,000X

Penetration at pits along boundary.  
Pits are probably result of attack of  
M-phase particles on boundary.

Figure 67





Oxide Replica

5000X

Crack penetration along boundaries  
of 2219-T351 stressed short transversely  
to 75% Y.S.

Figure 68





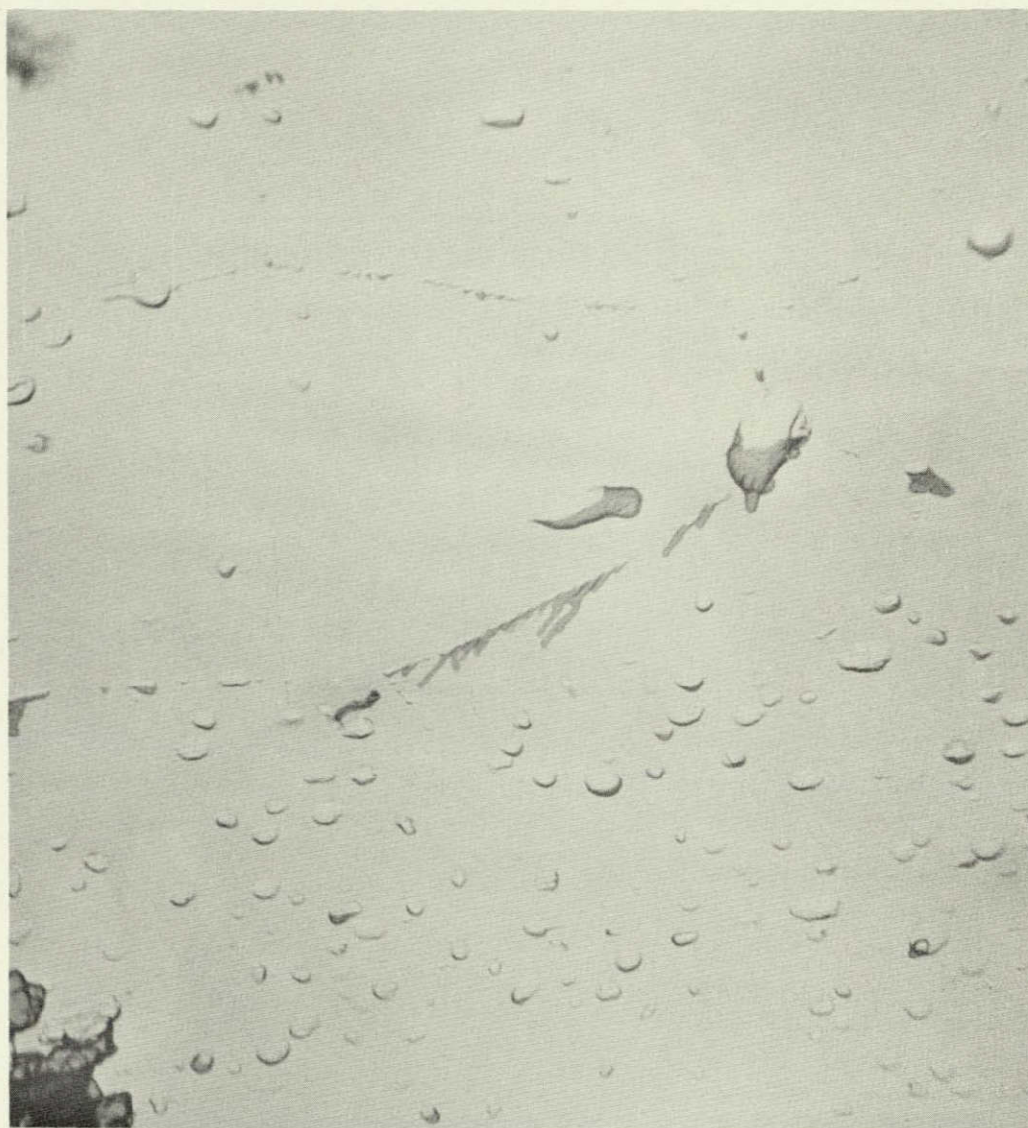
Oxide Replica

20,000X

Cubic penetration along  
boundaries of X7375-T6 stressed  
75% Y.S. short transversely.

Figure 69

↑ STRESS ↓



Oxide Replica

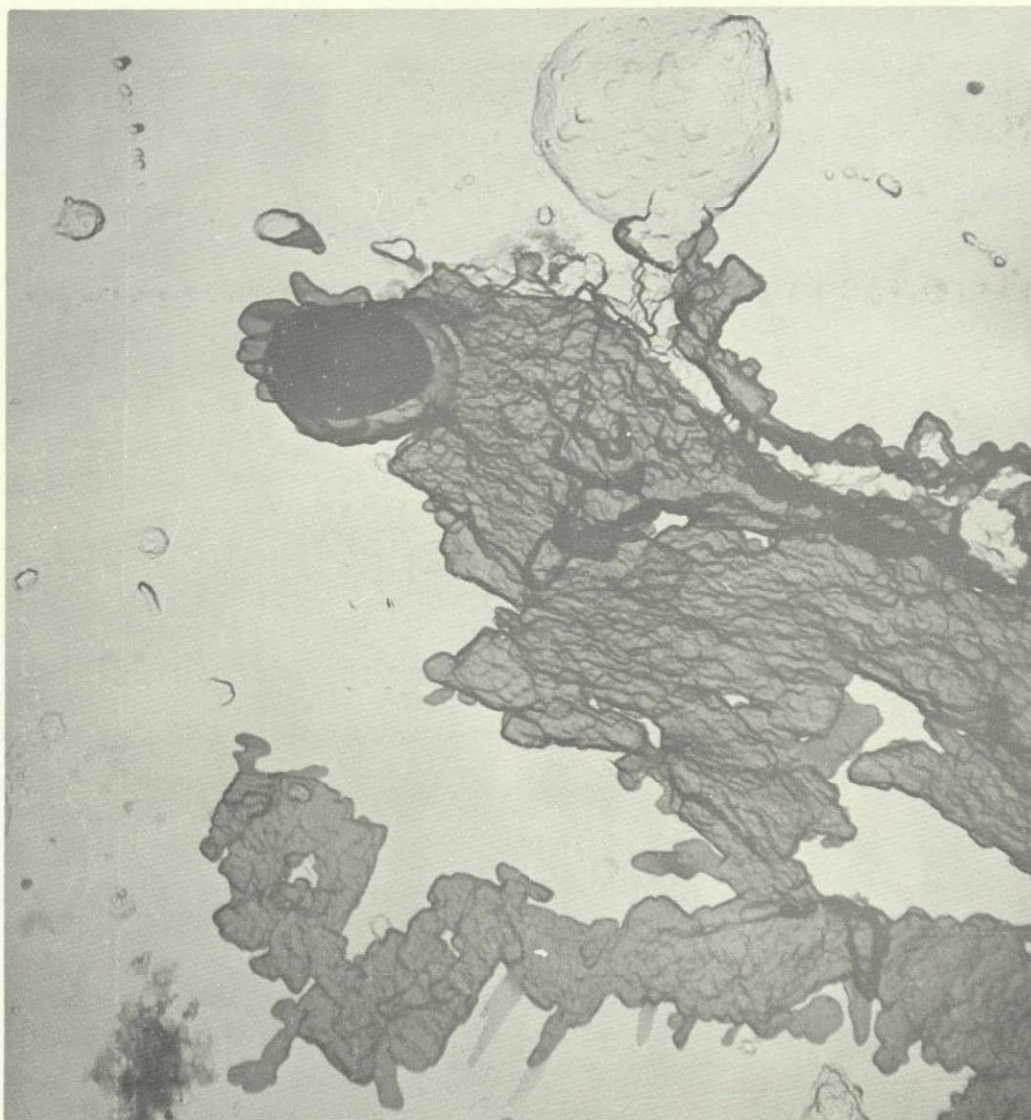
15,000X

**Beginning of a stress-corrosion crack on  
cellular boundary in 7079-T6.**

Figure 70



← STRESS →

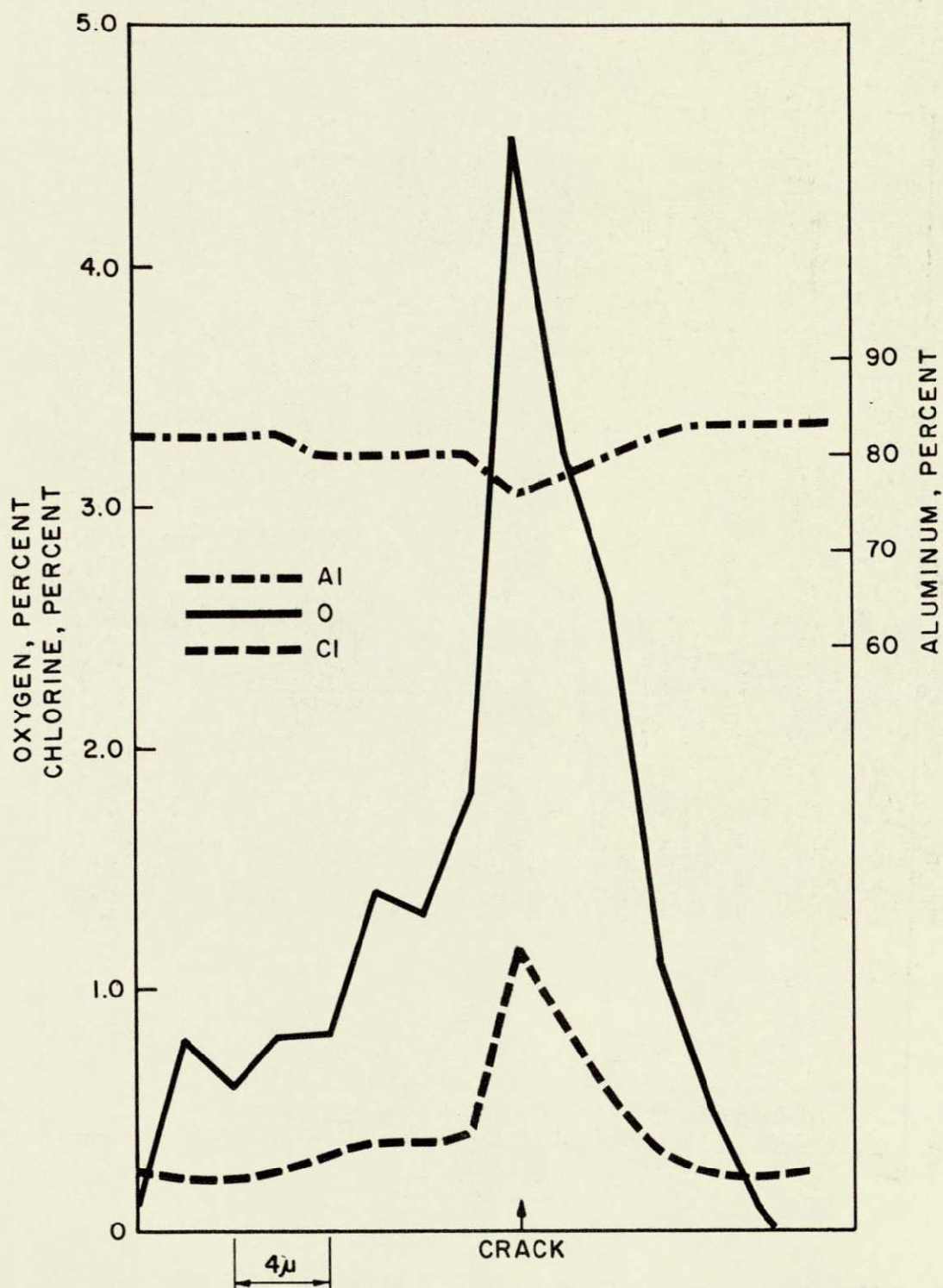


Oxide Replica

15,000X

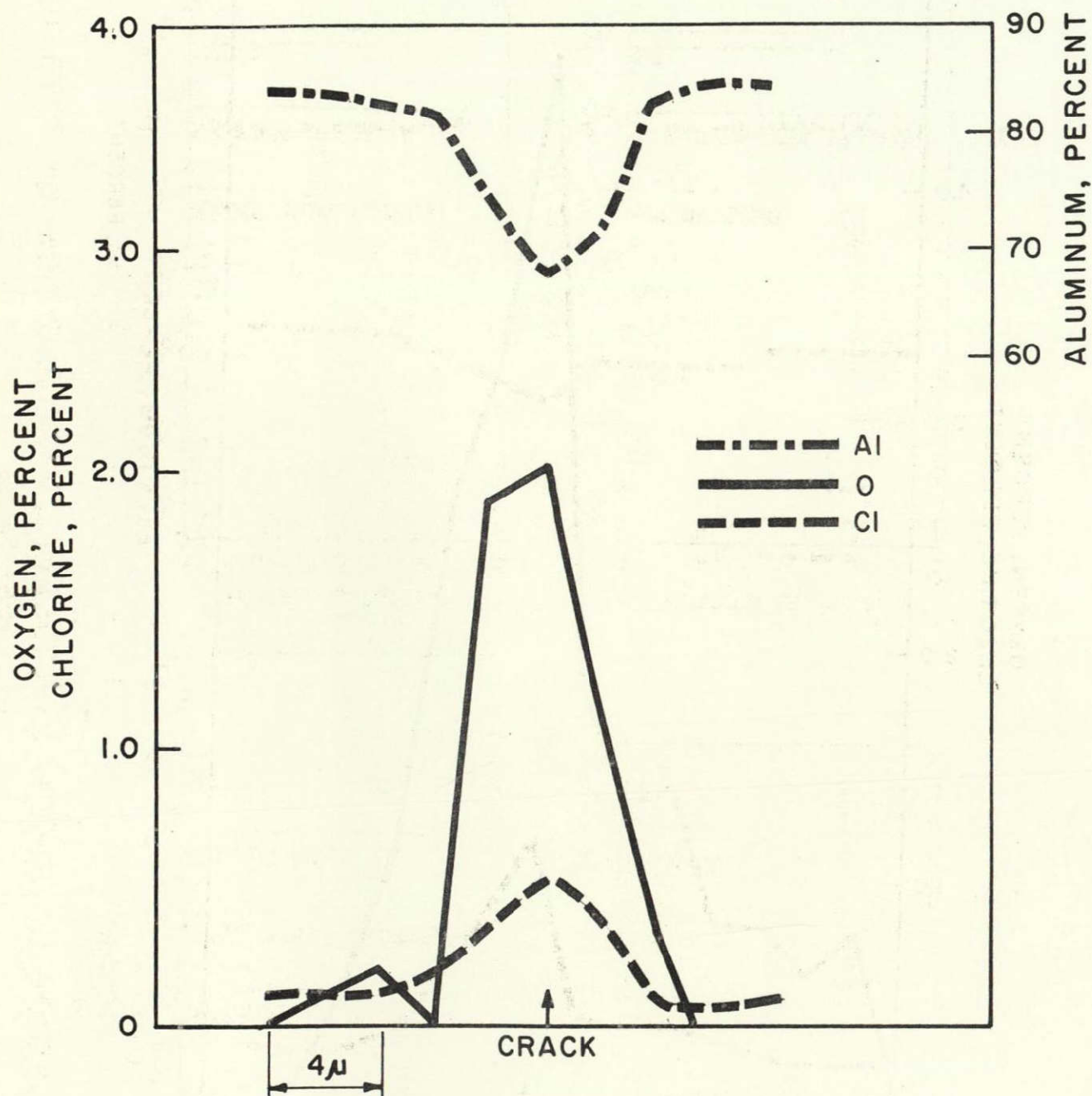
End of a relatively large stress-corrosion crack in 7079-T6. The opening of the crack onto the surface can be seen at the top of the picture and deeper parts of the crack at the bottom.

Figure 71



DISTRIBUTION OF Al, Cl AND O IN VICINITY  
OF STRESS-CORROSION CRACK

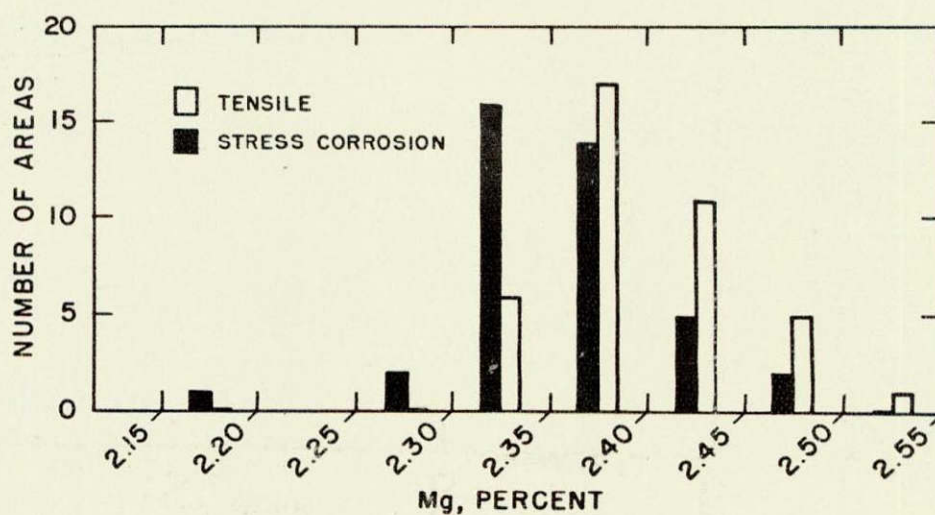
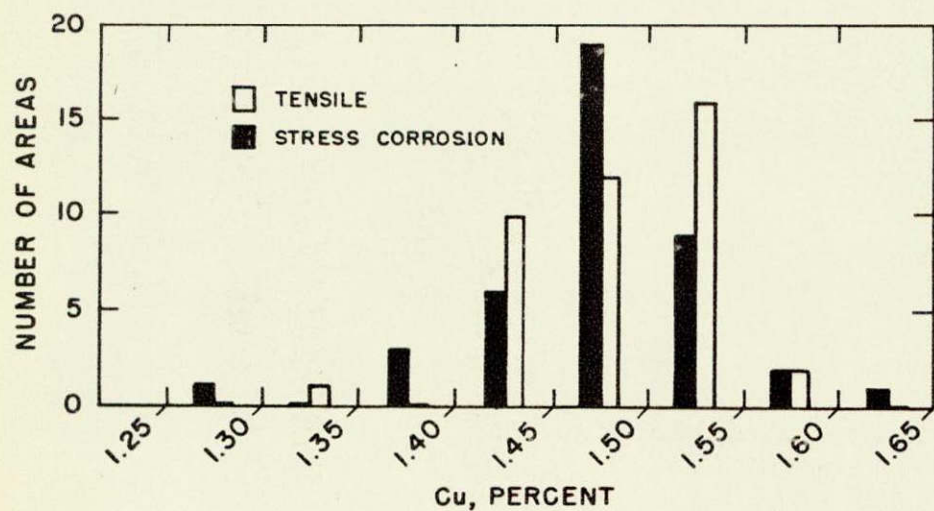
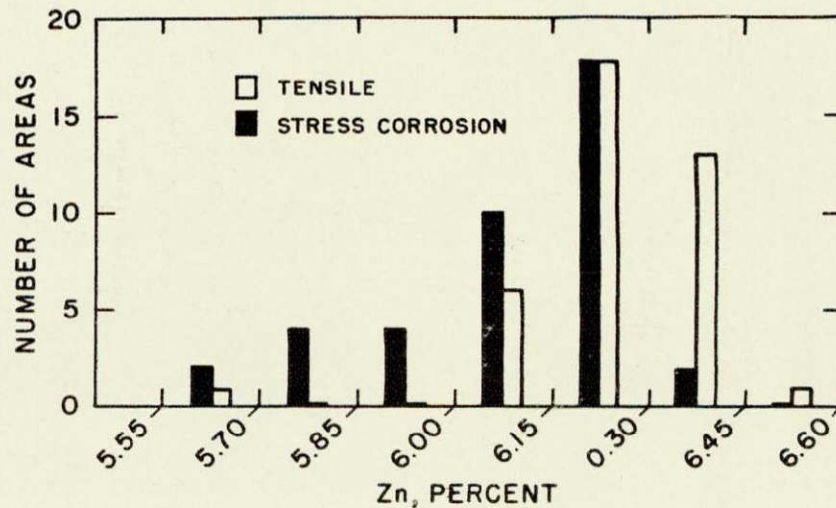
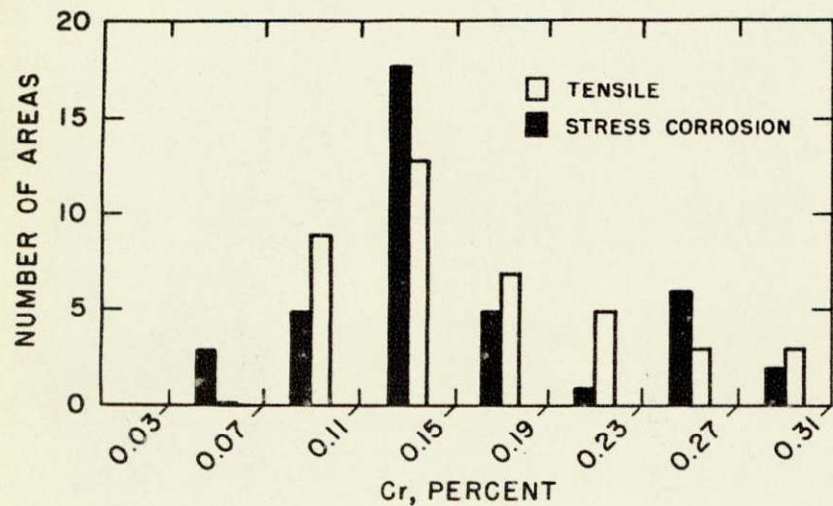
FIGURE 72



DISTRIBUTION OF Al, Cl AND O IN VICINITY  
OF STRESS-CORROSION CRACK

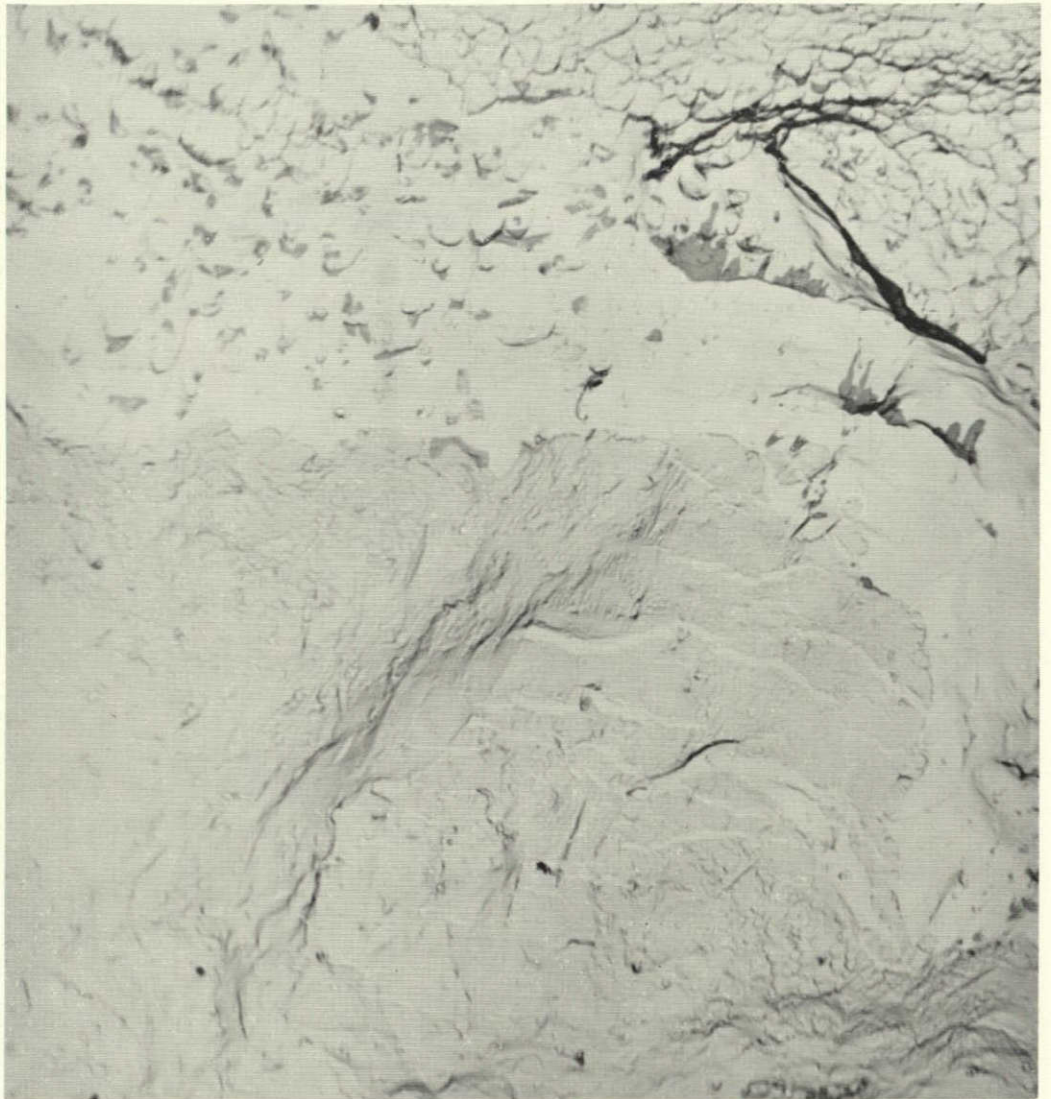
FIGURE 73





COMPOSITION OF STRESS CORROSION CRACK SURFACE OF 7075-T6

FIGURE 74



Double Oxide Replica

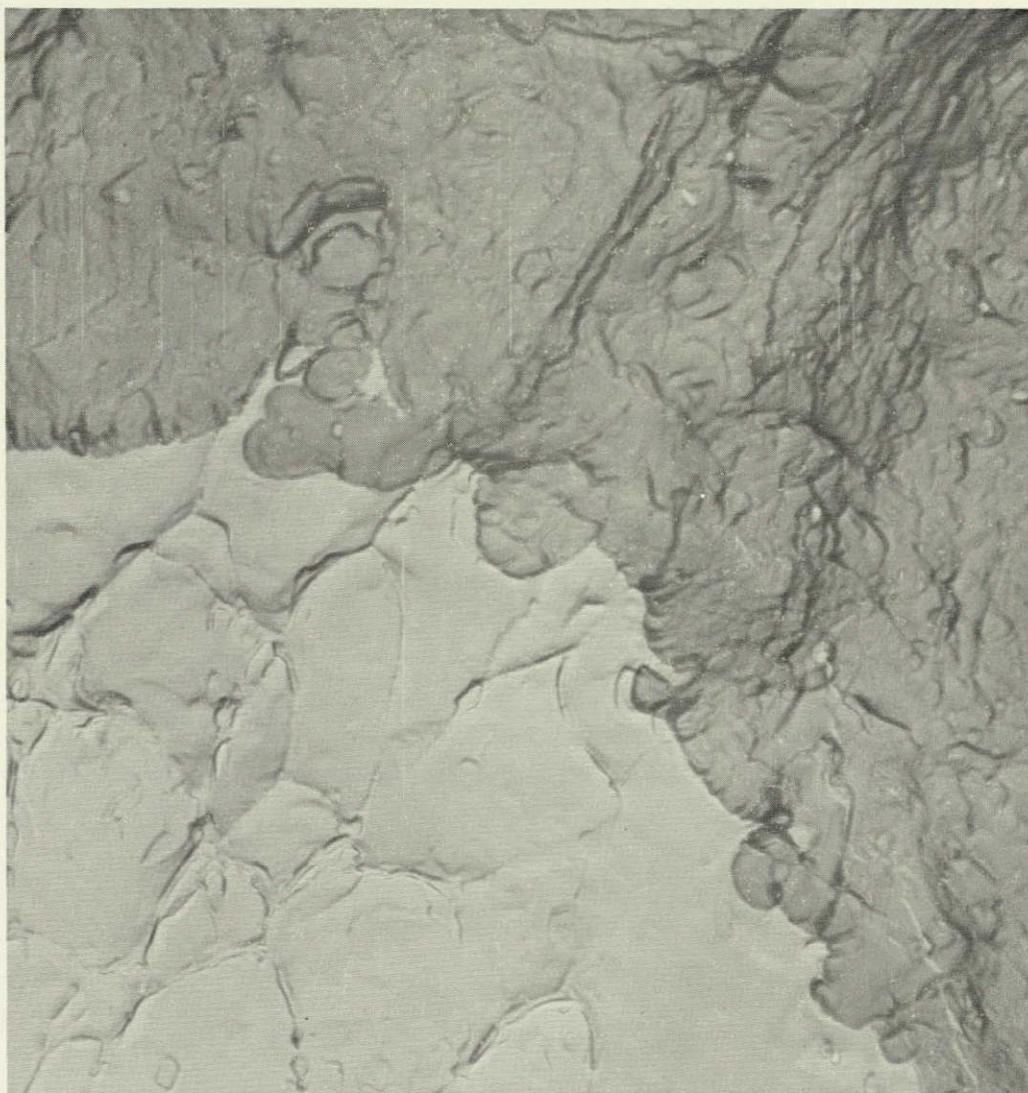
5000X

Transition from a stress corrosion fracture replicated in 22v oxide (lower half) to tensile fracture replicated in 15 v oxide. Note that thick oxide was cracked during the breaking open of the specimen and the cracks were repaired by application of the second oxide.

7075-T6 stressed 75% YS

Figure 75





Oxide-Carbon Replica

20,000X

Transition from a stress corrosion fracture (upper portion) replicated in oxide and carbon to a tensile fracture replicated in carbon alone. 7075-T6 stressed short transversely to 75% YS.

Figure 76



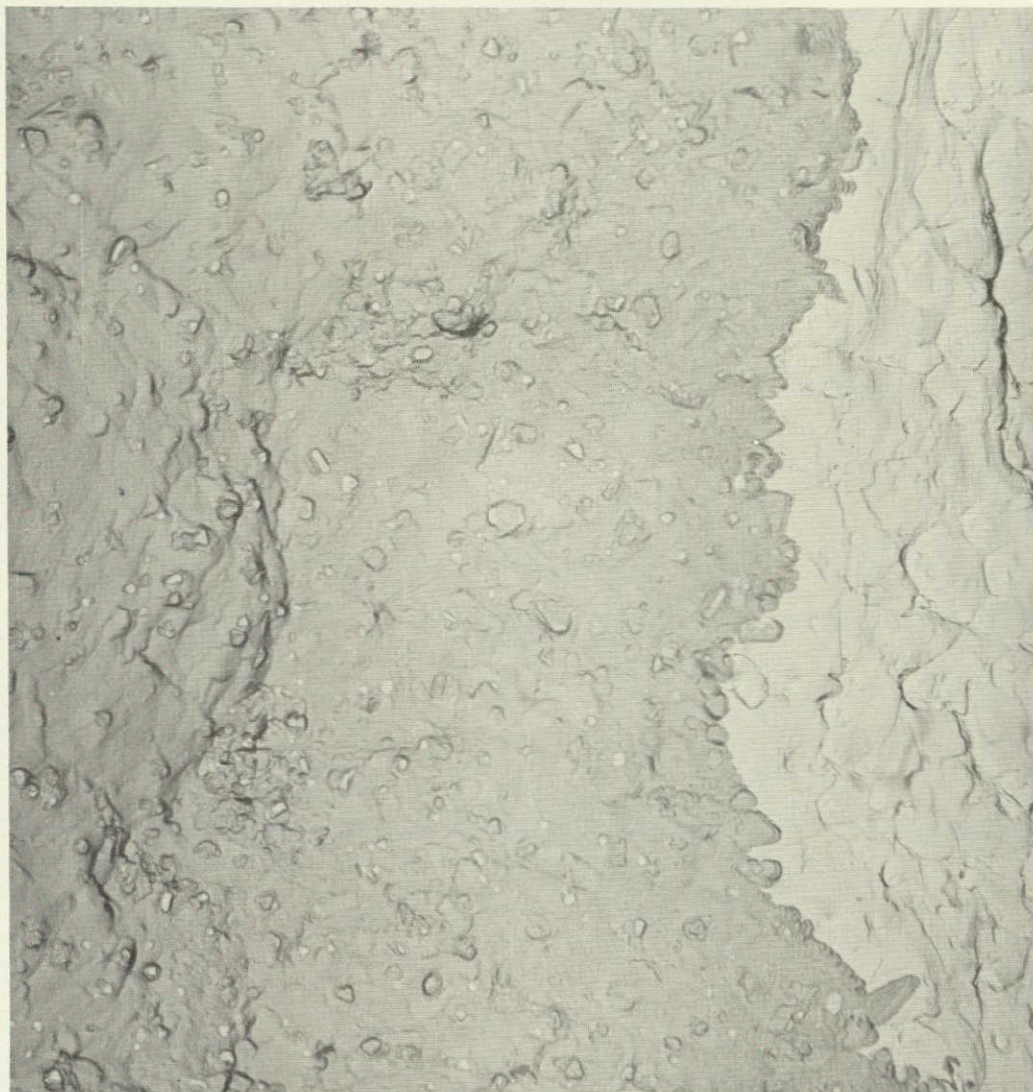
Oxide-Carbon Replica

5000X

Stress corrosion fracture in 7075-T6 stressed to 75% YS. Stress corrosion proceeded from specimen surface seen at lower right, along polygon boundaries. At the top, a small polygon is almost completely surrounded by stress corrosion cracks. Some corrosion product is seen near the surface at right.

Figure 77





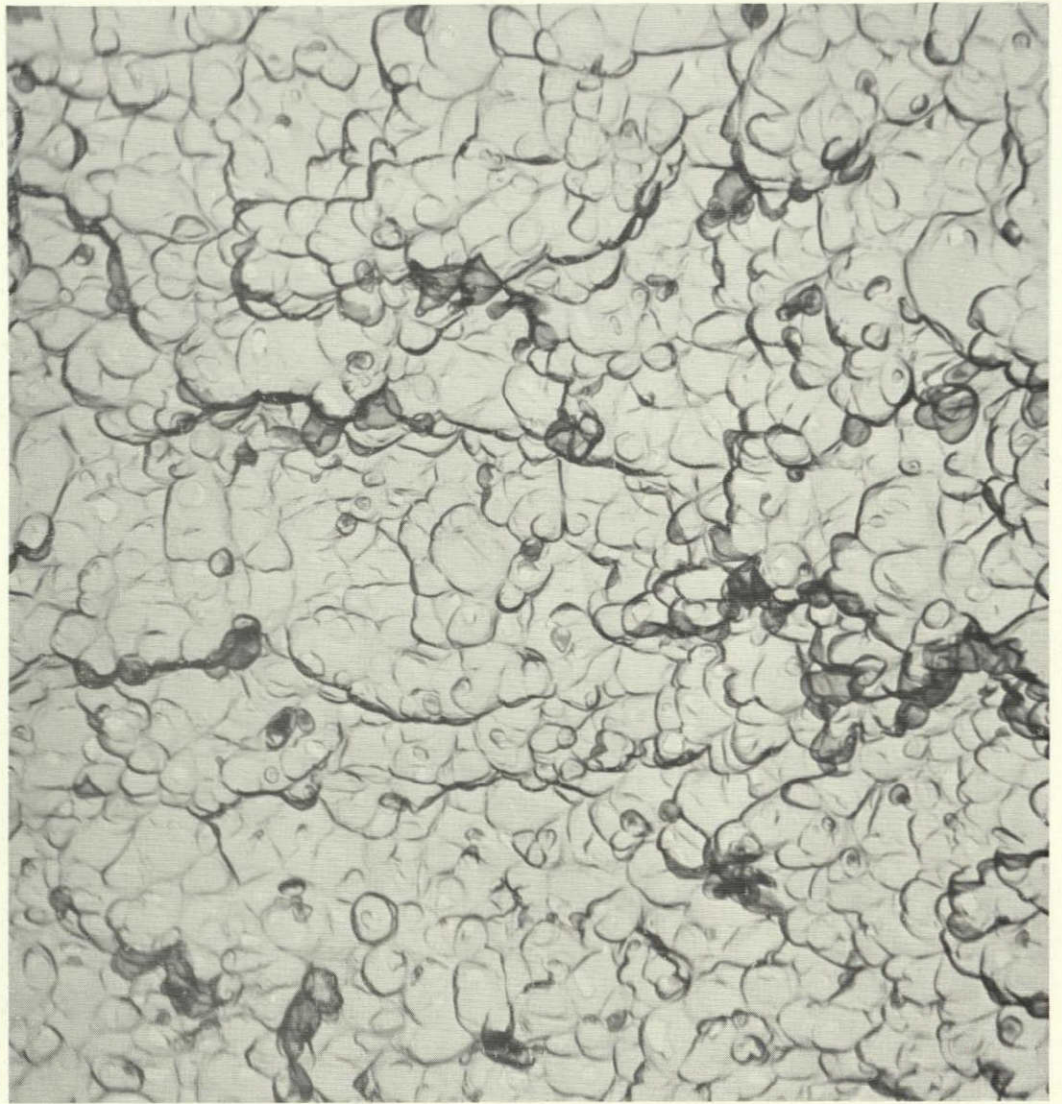
Oxide-Carbon Replica

10,000X

Transition from stress corrosion fracture (left) to tensile fracture showing that tip of stress corrosion crack is irregular. 7075-T6 stressed to 75% YS short transversely.

Figure 78





Oxide Replica

20,000X

Typical tensile fracture in 7075-T6  
showing small particles associated with dimples.

Figure 79



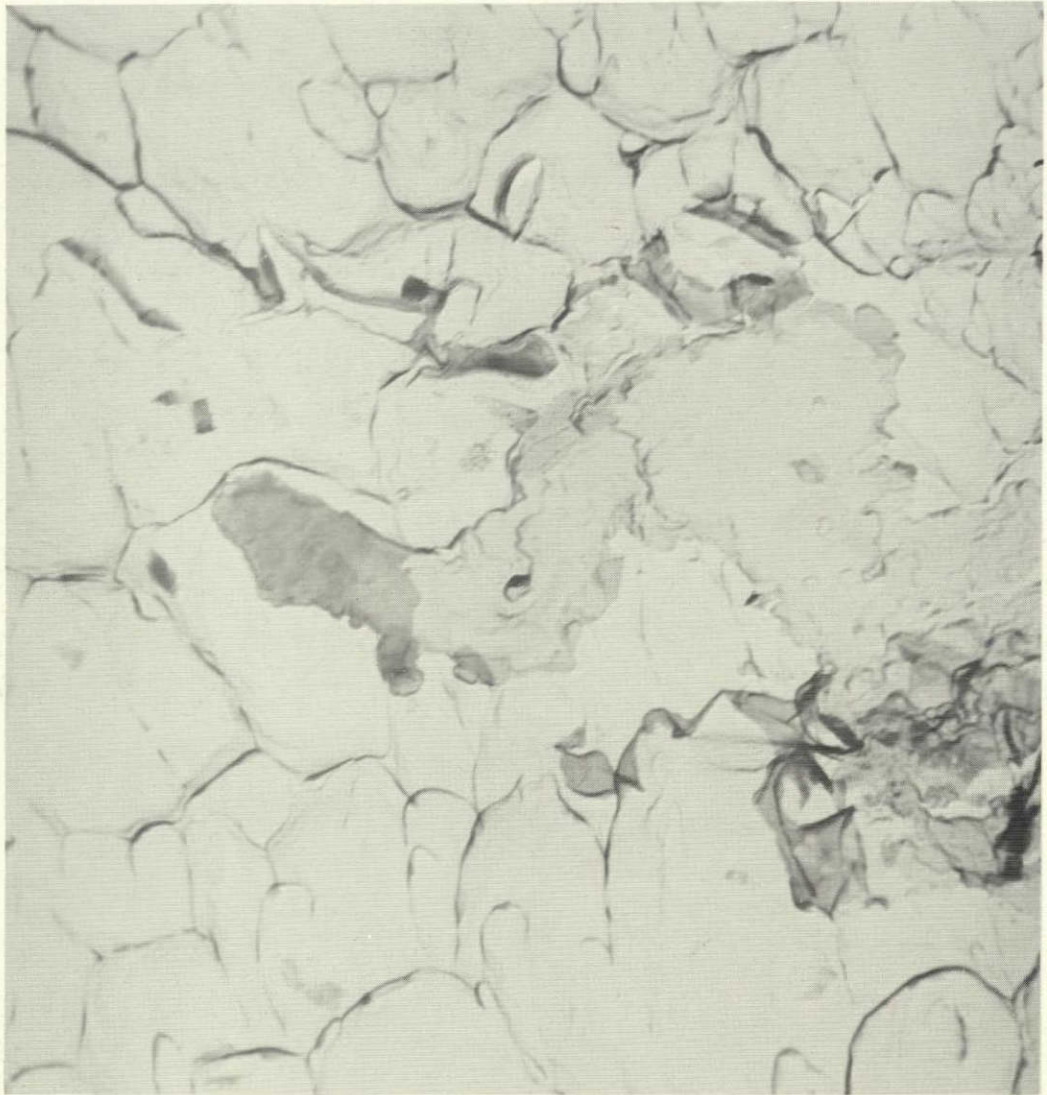
Oxide Replica

20,000X

Parallel markings on stress corrosion fracture which might be indicative of plastic deformation. 2219-T37 with S.T. stress of 75% YS.

Figure 80





Double Oxide Replica

20,000X

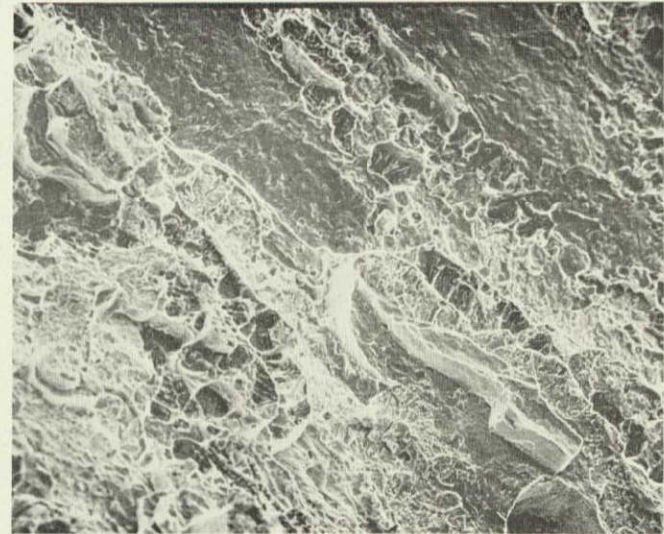
Spade-like tendril of stress corrosion crack which juts out from main stress corrosion crack which is out of view to the right. Specimen surface is above this area and parallel to top edge of photograph. The tip of this stress corrosion tendril is dark because the replicating oxide broke leaving a double thickness at the tip. The stress corrosion tendril is surrounded by tensile fracture both above and below. 2219-T37 with S.T. stress of 75% YS.

Figure 81

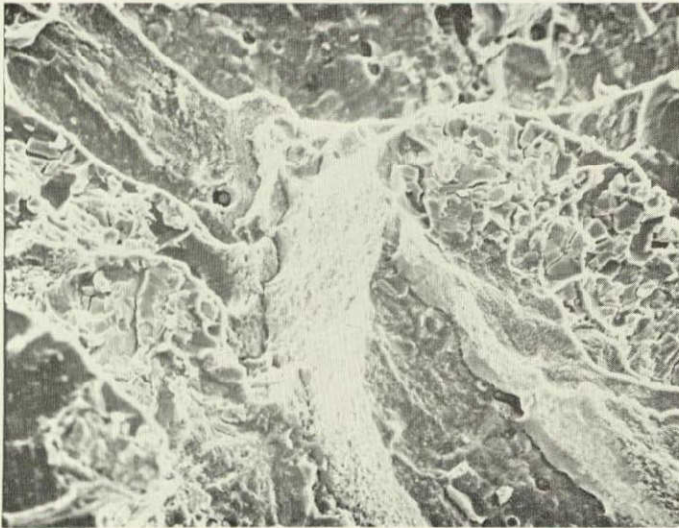




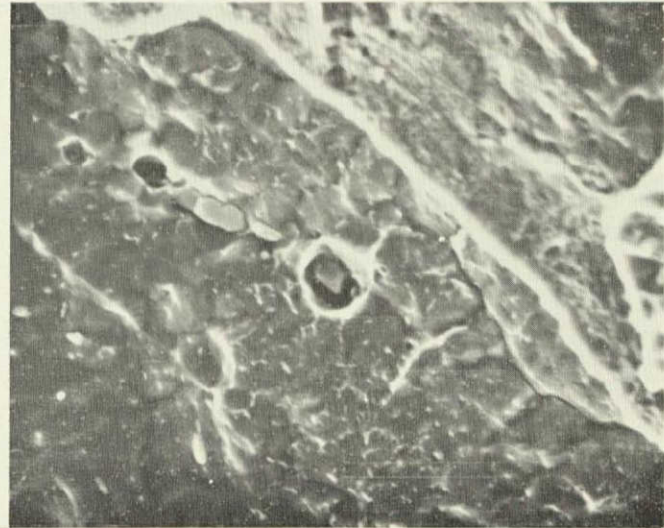
88X



220X



880X



2200X

Stress corrosion fracture in 7075-T6 as seen by scanning electron microscope.

Figure 82



200X



Metal fragment at surface of crack

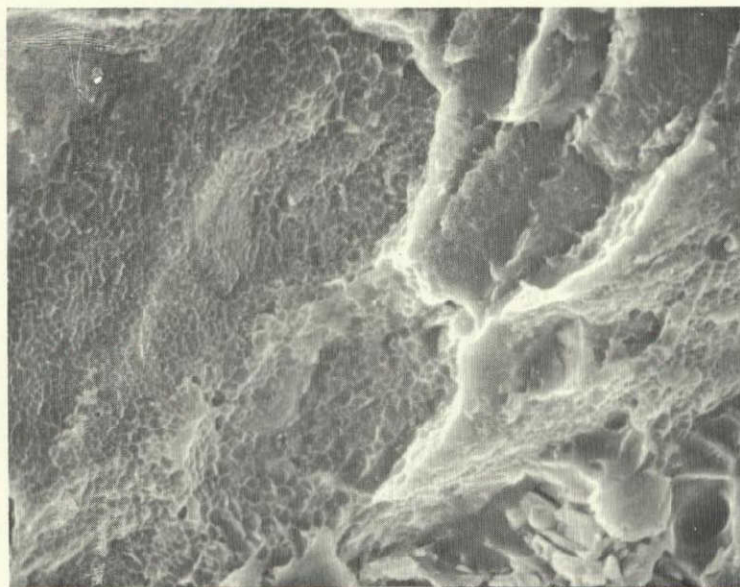
1000X



Detail of metal fragment

NOT REPRODUCIBLE

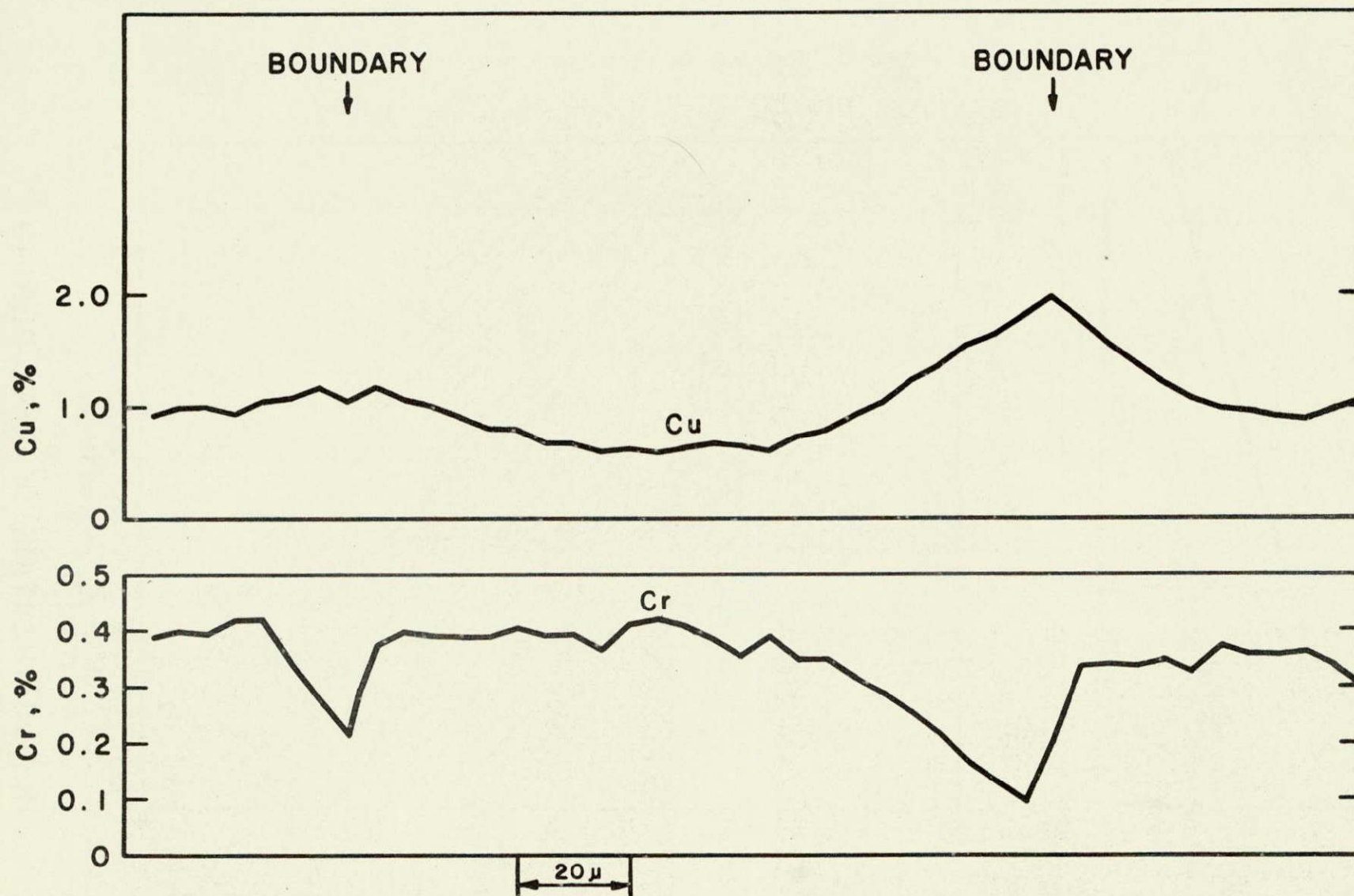
1000X



Dimpled area adjoining crack

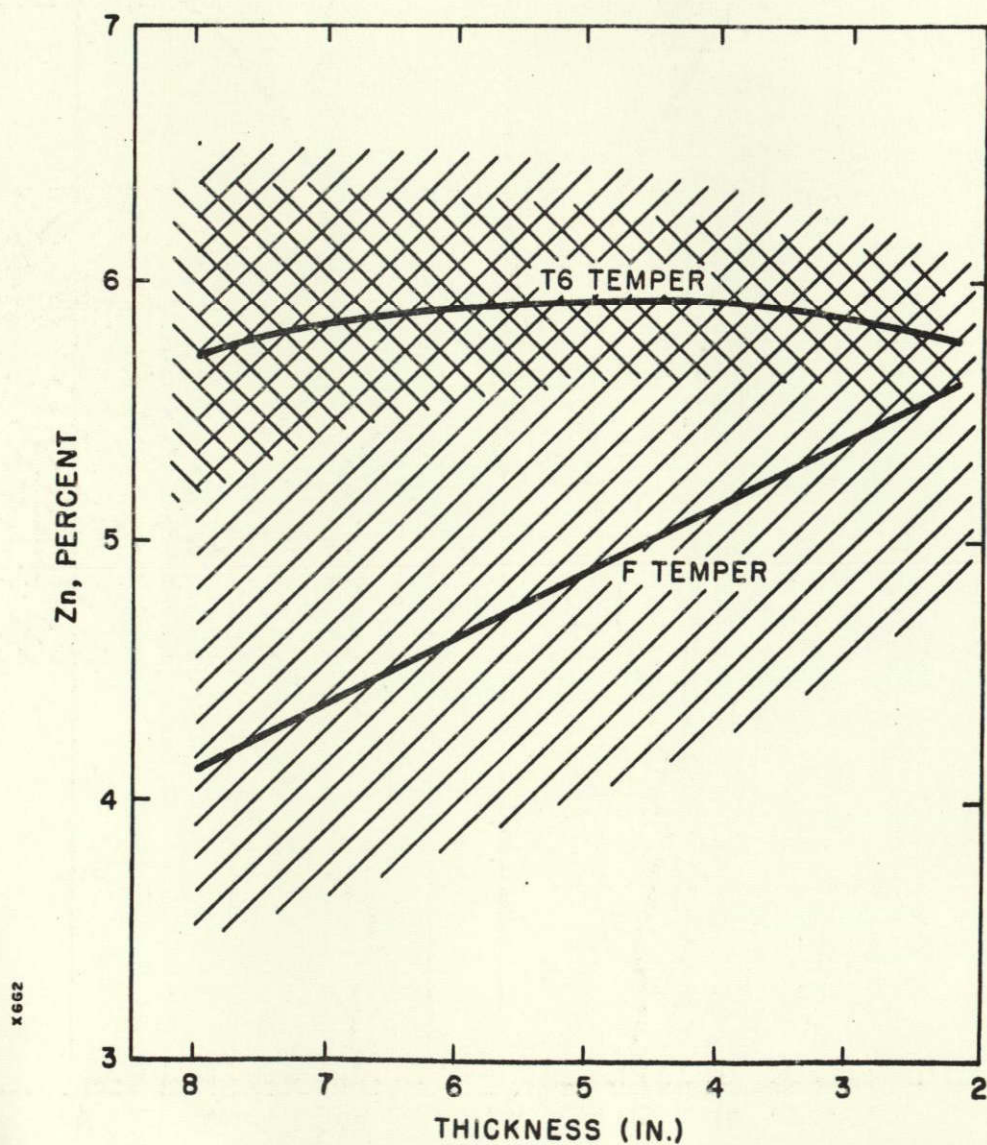
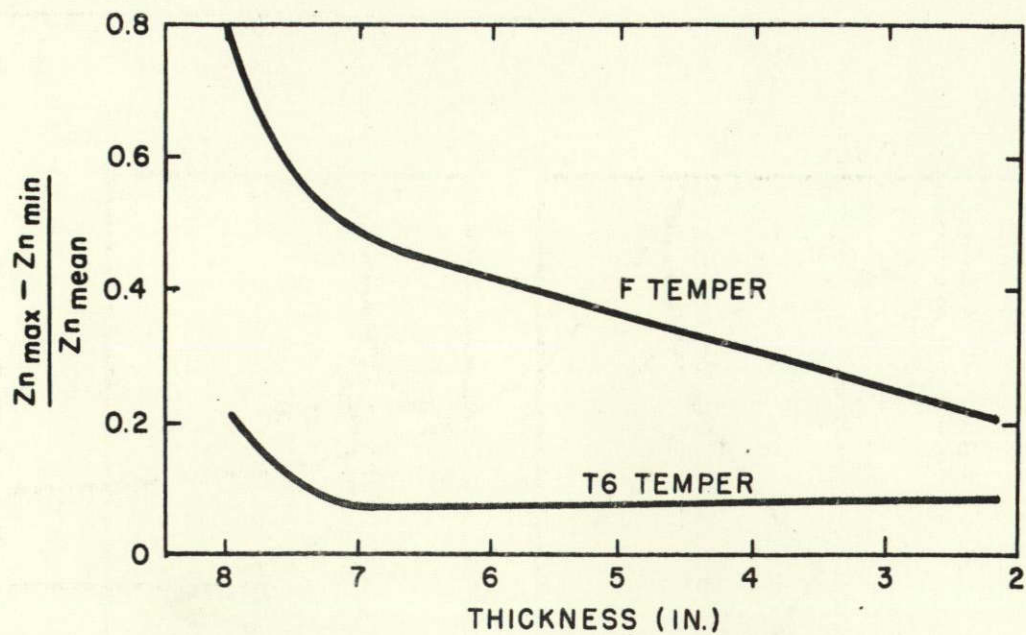
Surface of shallow crack and adjoining area in 2219-T37 as seen by SEM.





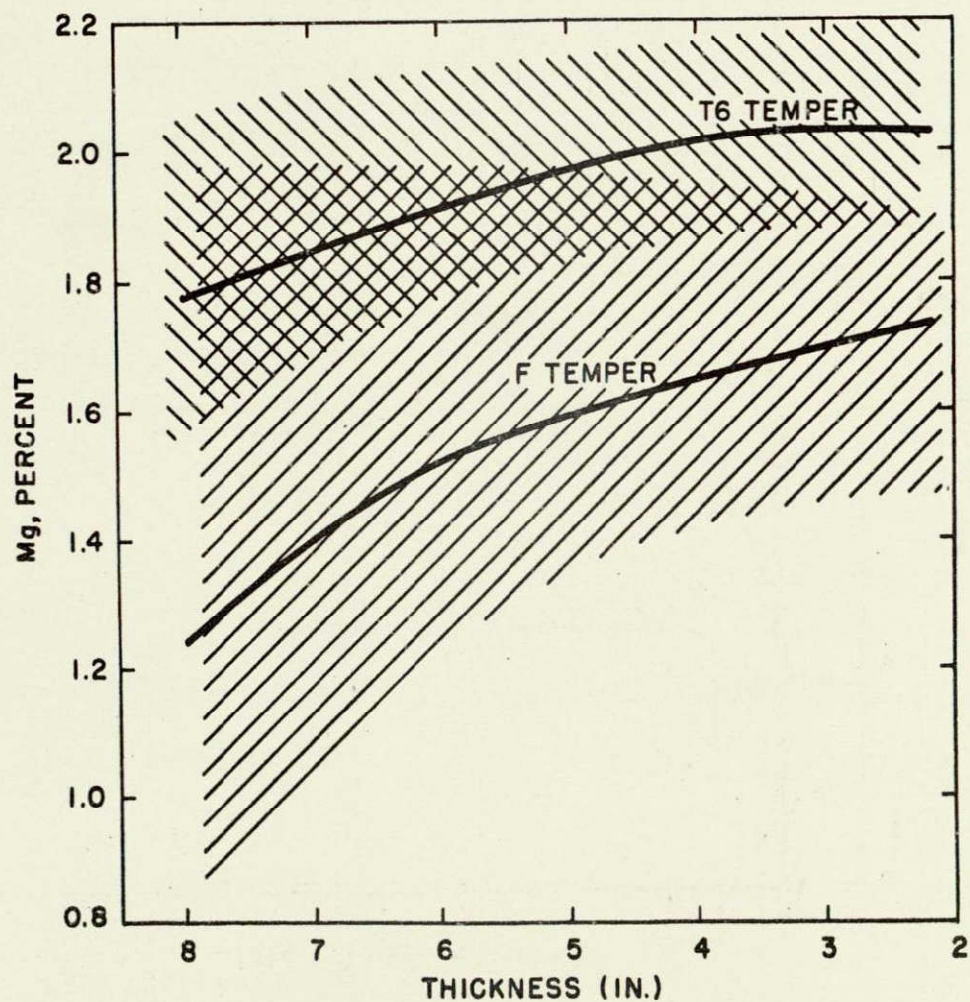
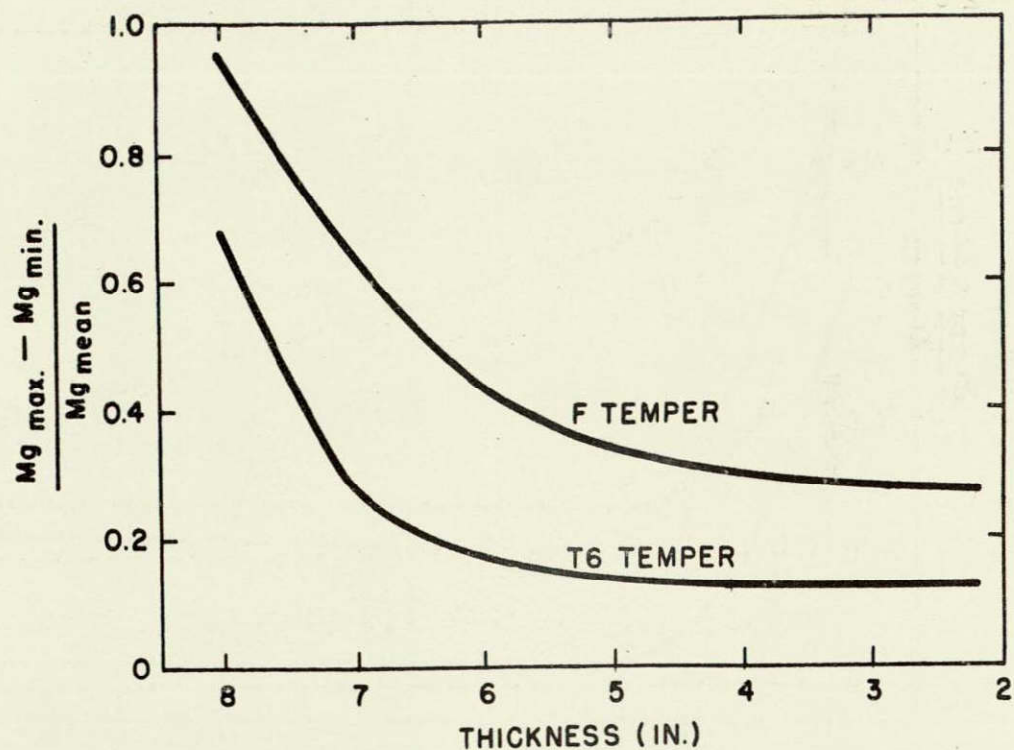
VARIATION OF Cu AND Cr ACROSS A DENDRITE CELL IN 7075 ALLOY INGOT SLICE HEAT TREATED TO THE T6 TEMPER.

FIGURE 84

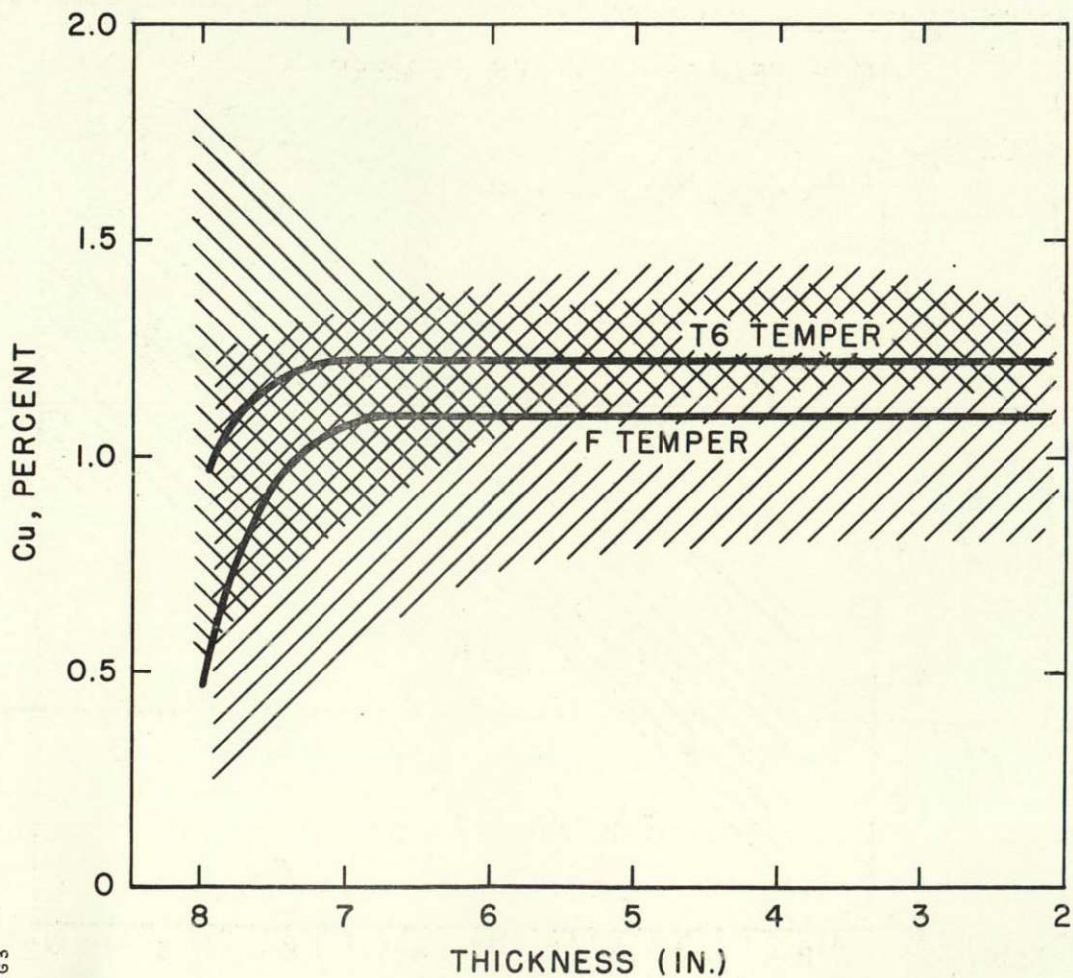
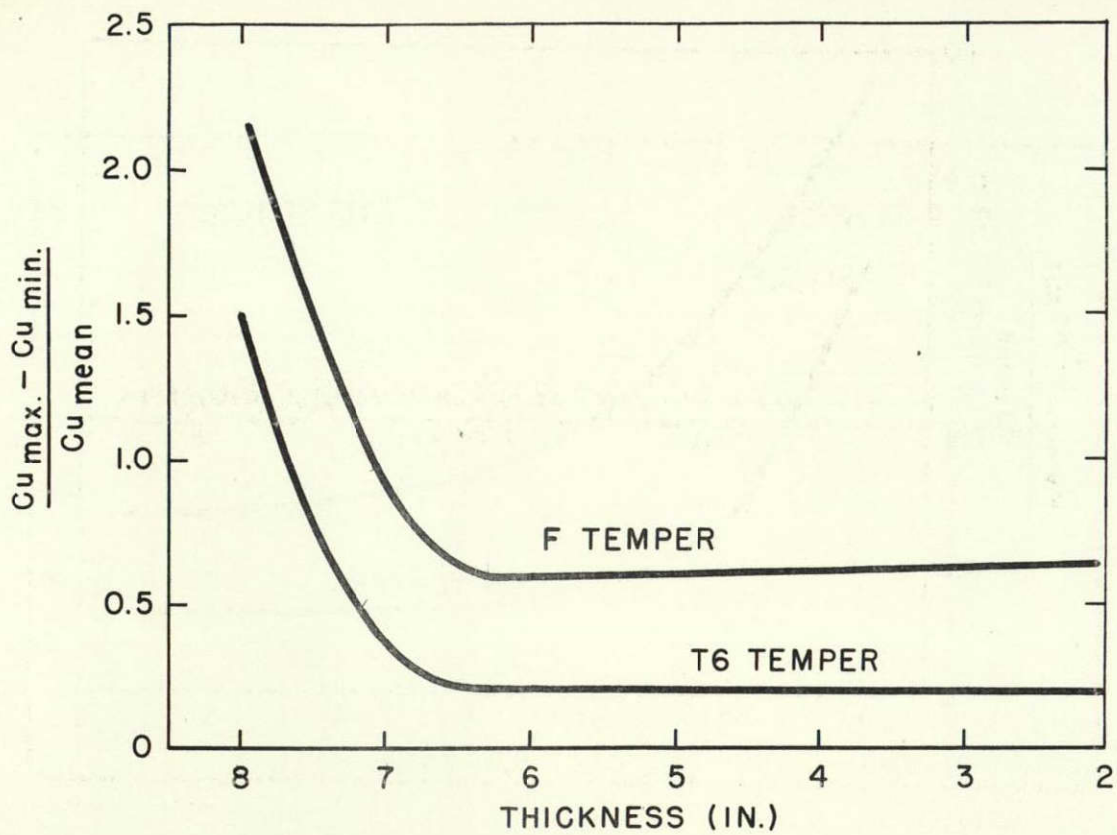


HOMOGENIZATION OF ZINC DURING  
ROLLING OF 7075 INGOT  
FIGURE 85





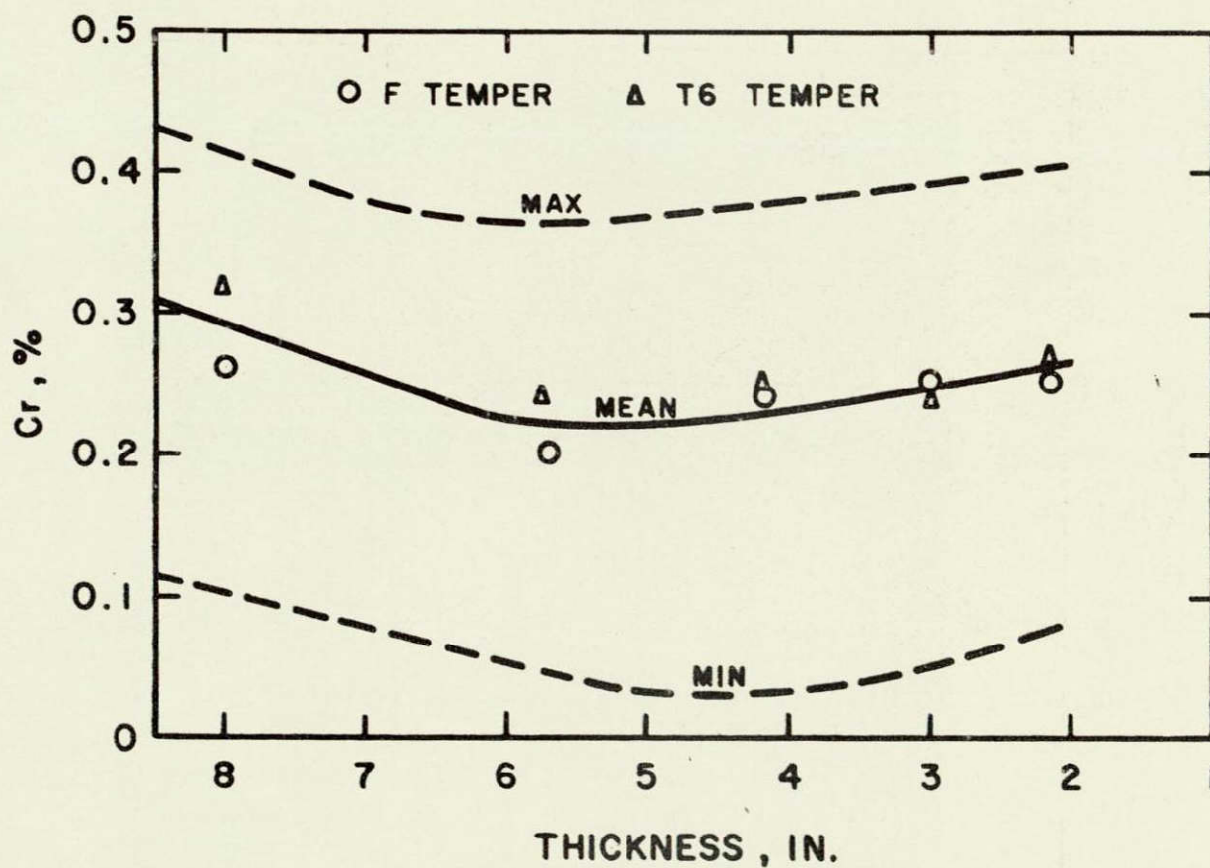
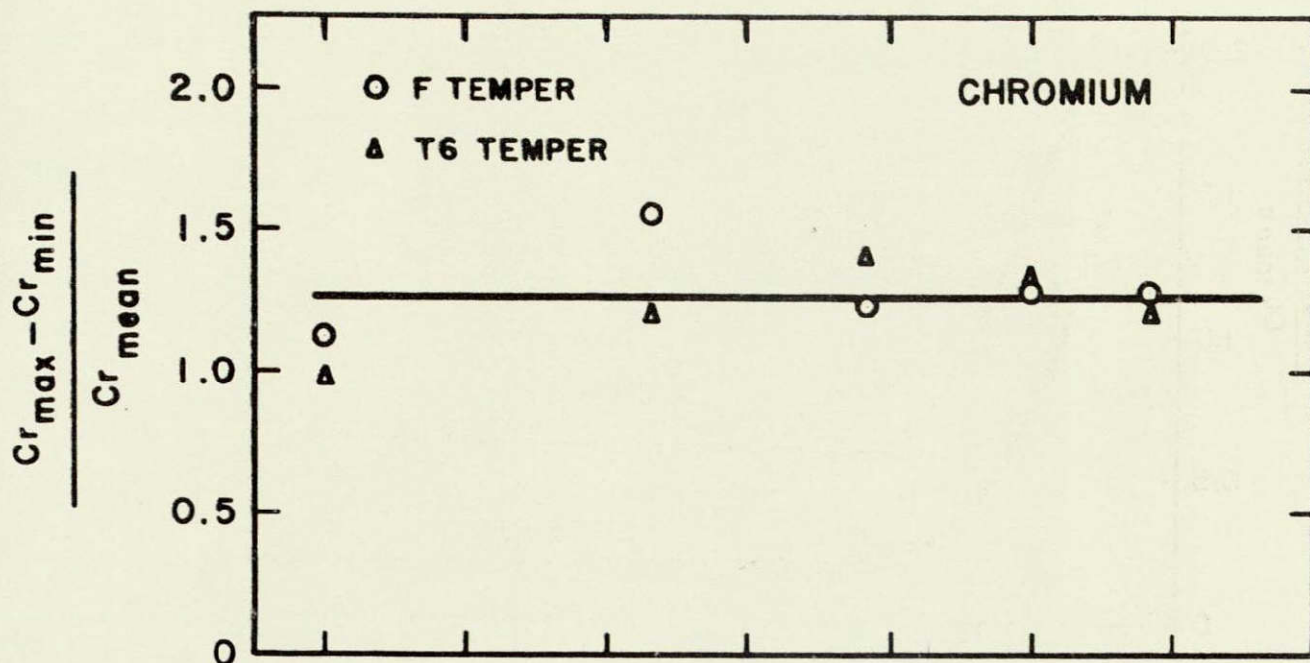
HOMOGENIZATION OF MAGNESIUM DURING  
ROLLING OF 7075 INGOT  
FIGURE 86



XGG3

HOMOGENIZATION OF COPPER DURING  
ROLLING OF 7075 INGOT  
FIGURE 87

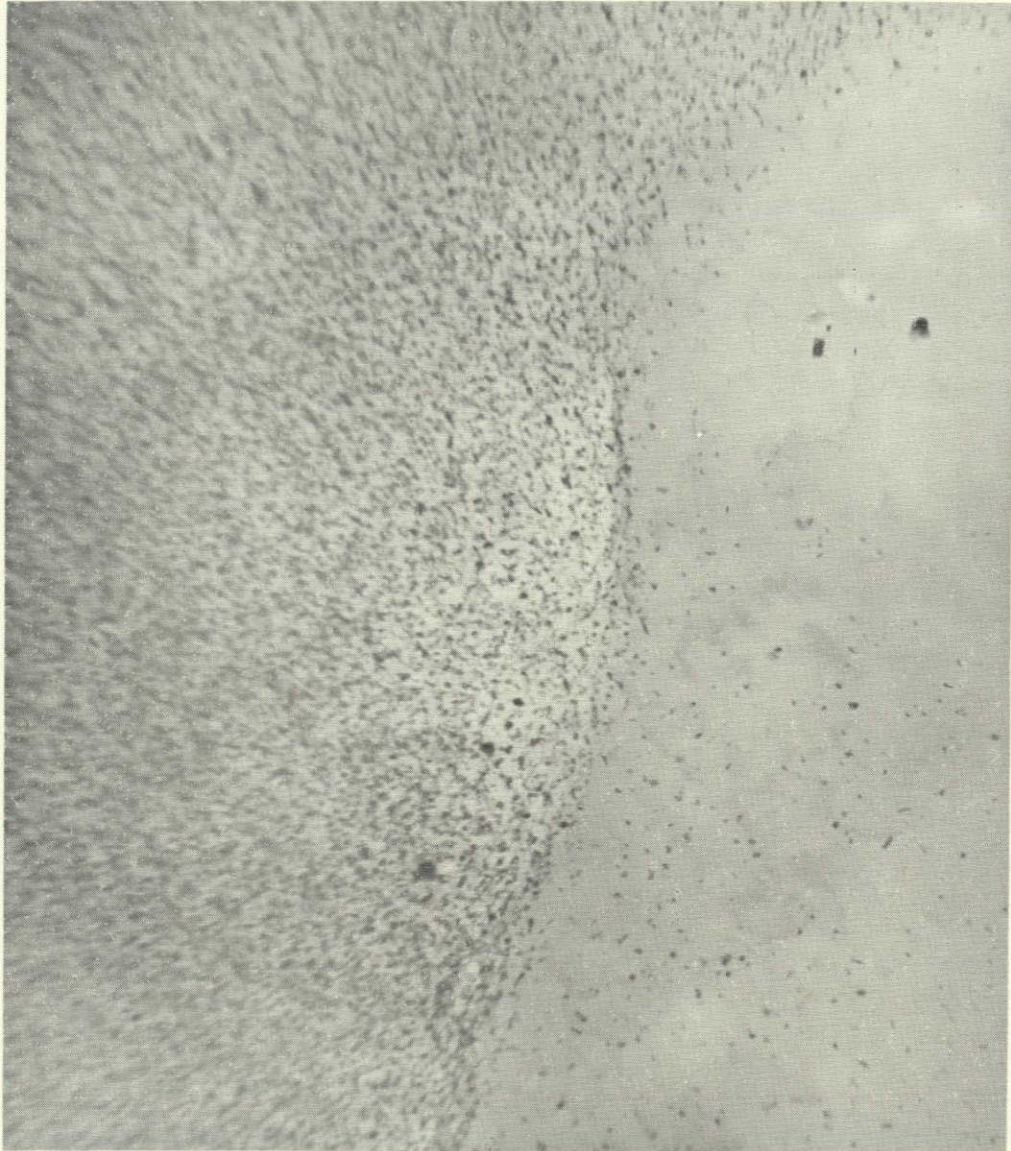




CHROMIUM ANALYSES DURING ROLLING OF 7075 INGOT

FIGURE 88





Thin Foil

15,000X

Variation in dispersoid density in  
7075-T6 which has not been hot rolled.

Figure 89



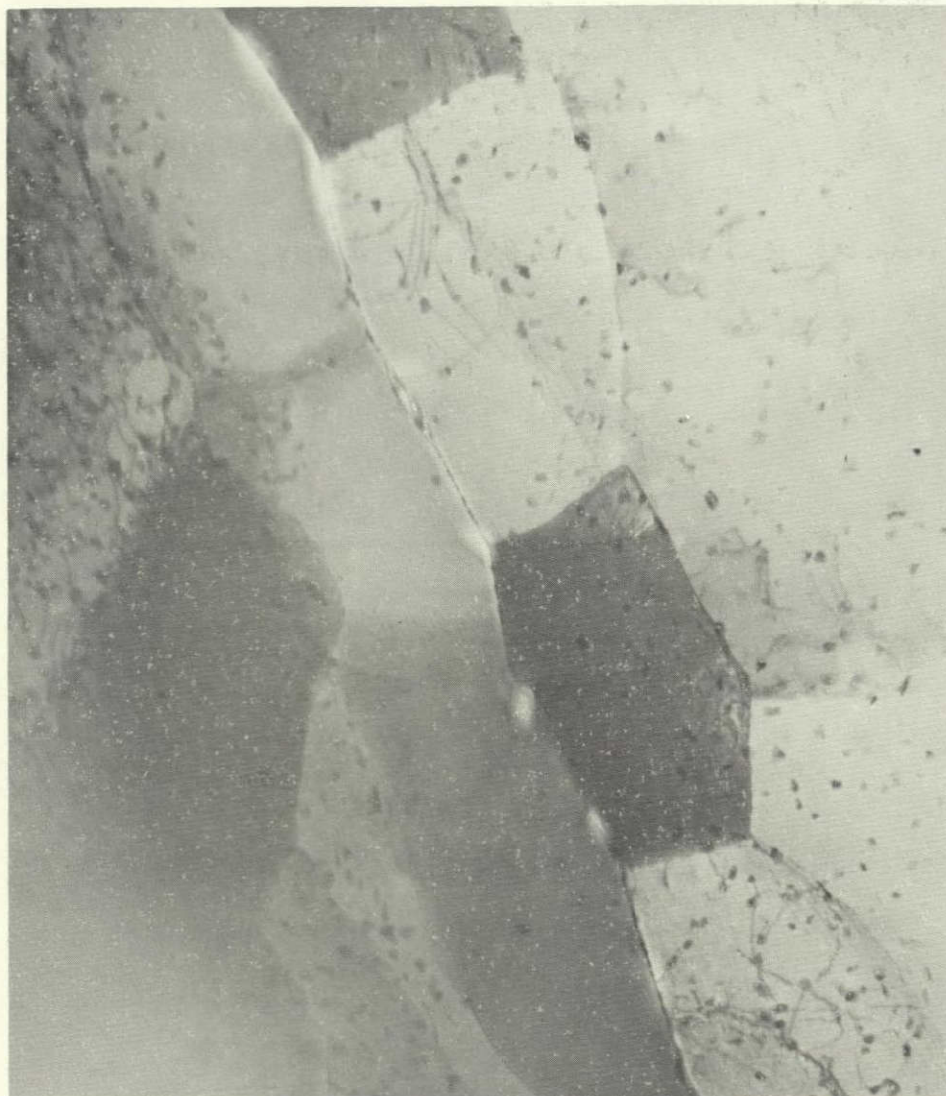
Thin Foil

30,000X

Dislocations interacting with  
dispersoid particles in 7075-T6  
plate reduced 30%.

Figure 90



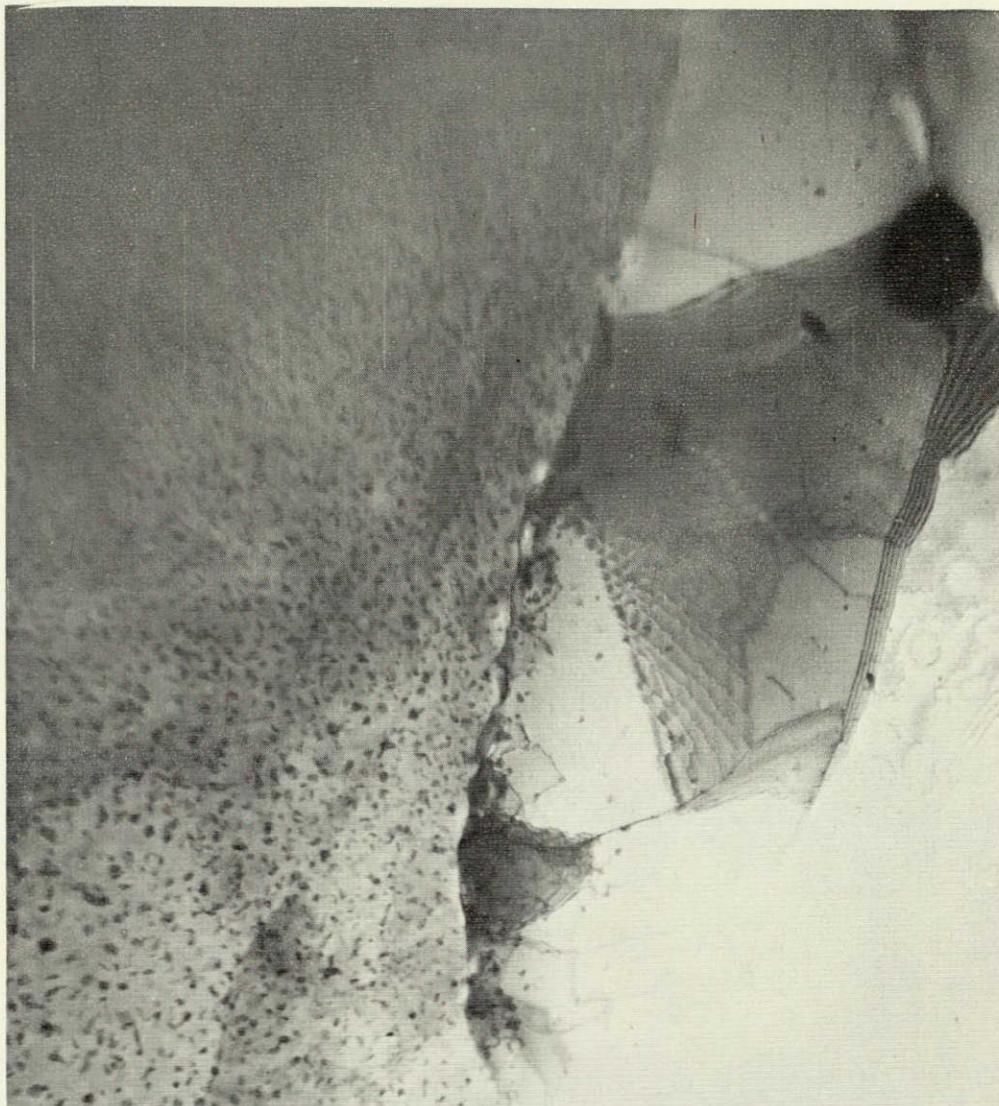


Thin Foil

30,000X

Cellular structure in dispersoid  
free regions at boundary in 7075-T6  
plate reduced 60%.

Figure 91



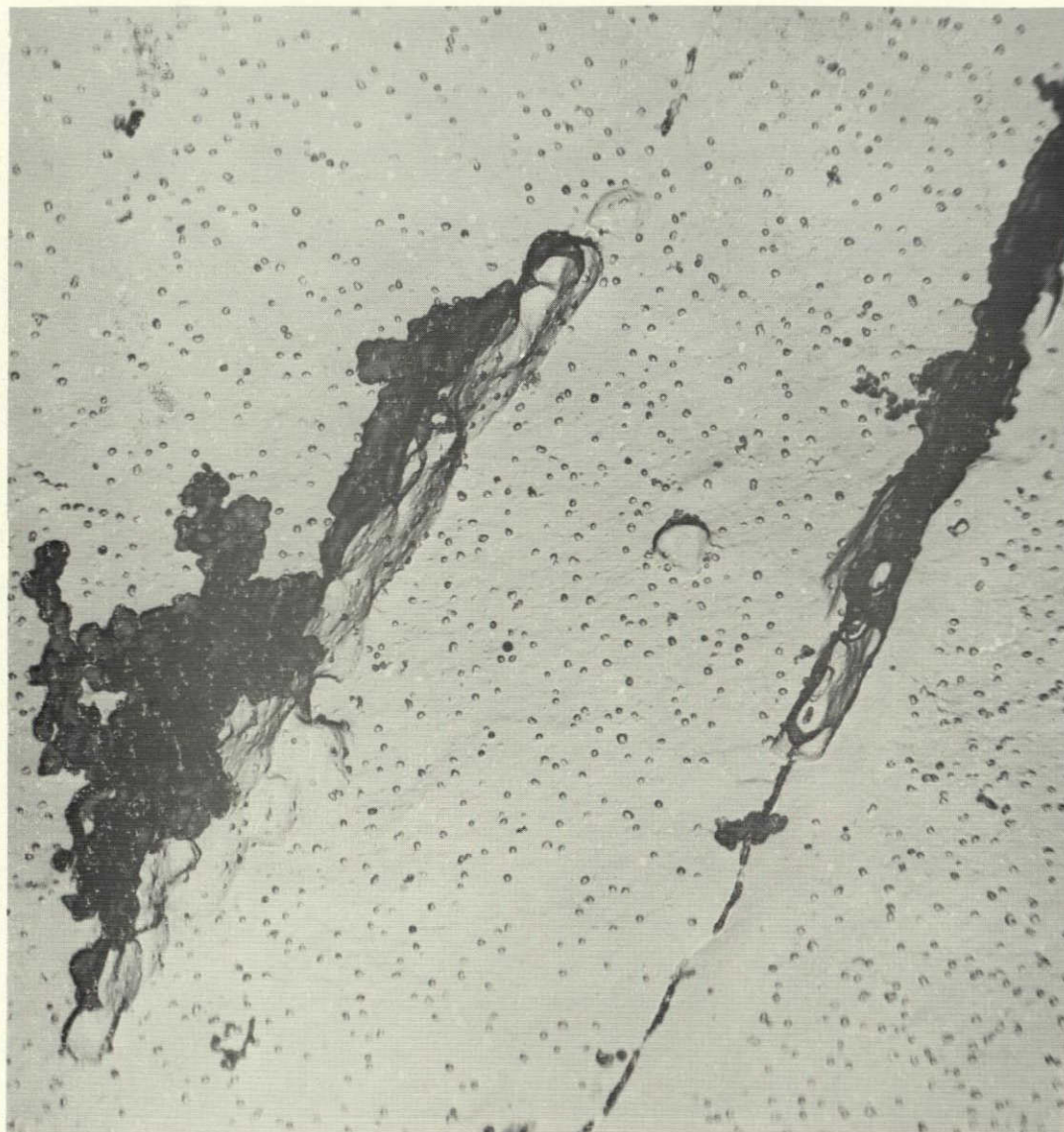
Thin Foil

20,000X

Cellular structure in dispersoid free  
regions at grain boundaries in 7075-T6 plate  
reduced 70%.

Figure 92



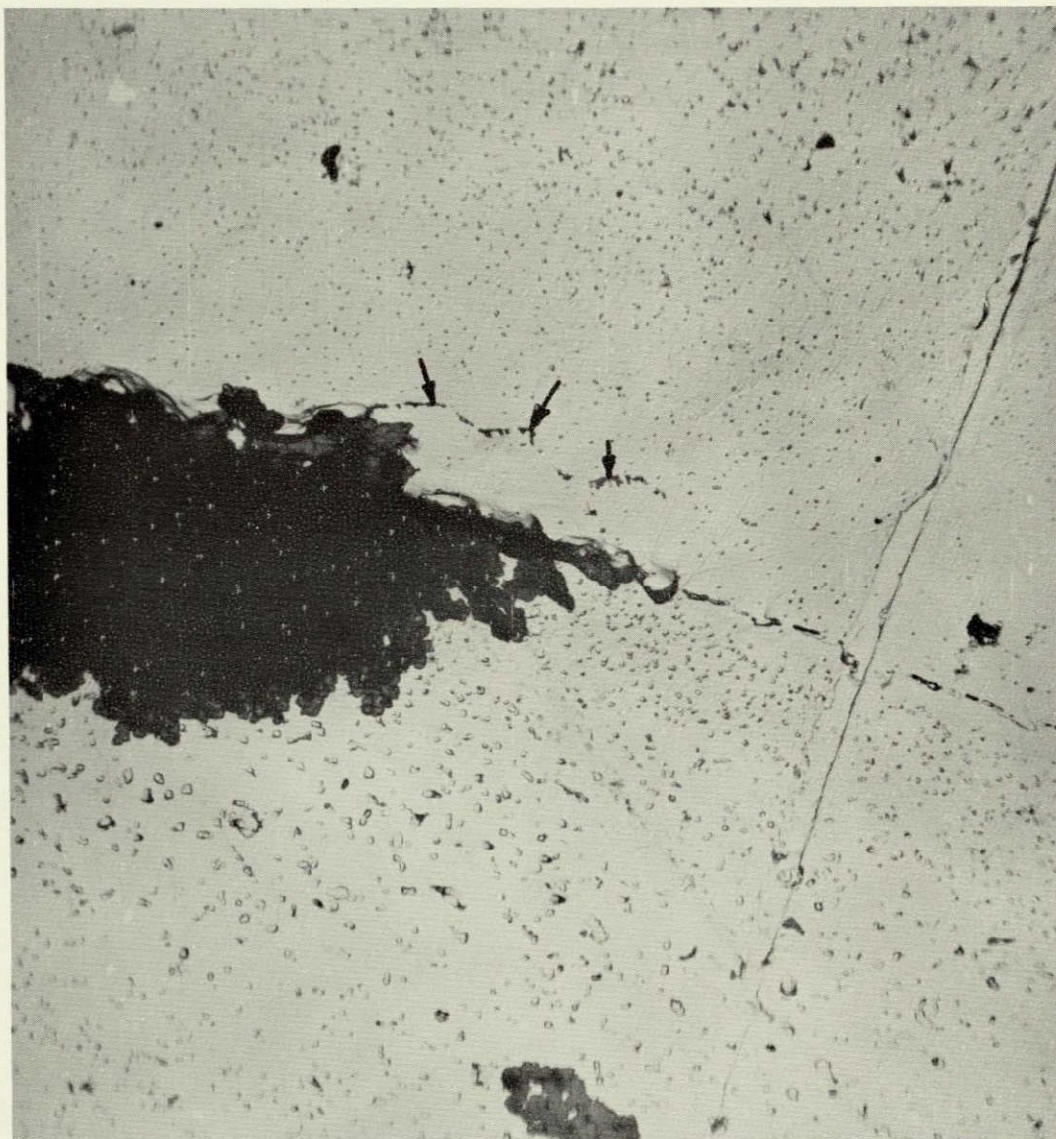


Oxide Replica

7500X

Crack initiation on straight, non-cellular boundaries in 7075-T6 plate reduced 25%.

Figure 93



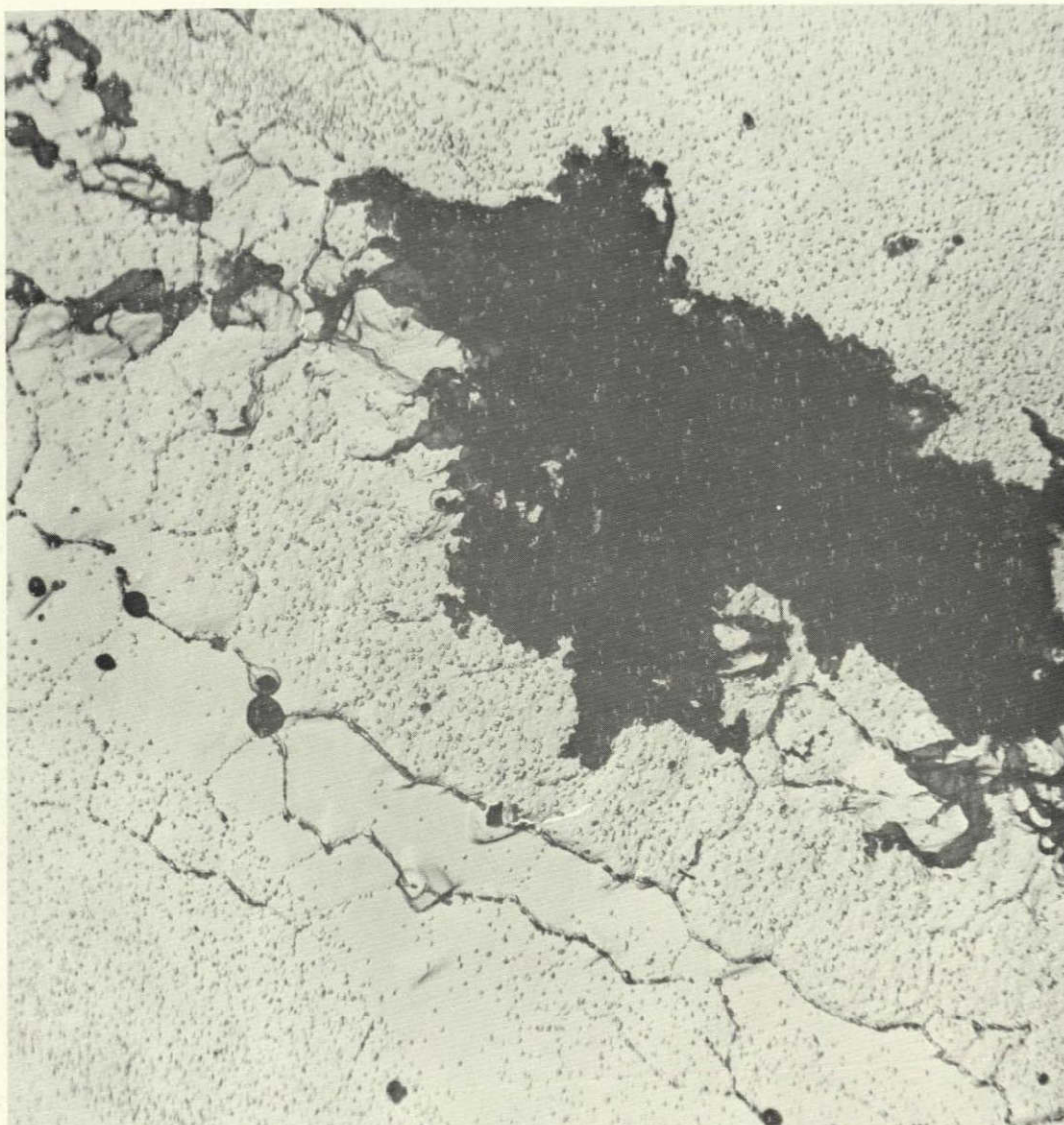
Oxide Replica

5,000X

Beginning of cell formation on boundary  
of 7075-T6 reduced 35%, and crack initiation  
on grain and cell boundaries.

Figure 94





Oxide Replica

5,000X

Widespread cell formation within  
dispersoid-lean regions on boundaries in  
7075-T6 plate reduced 45%, and preferential  
attack of all boundaries.

Figure 95



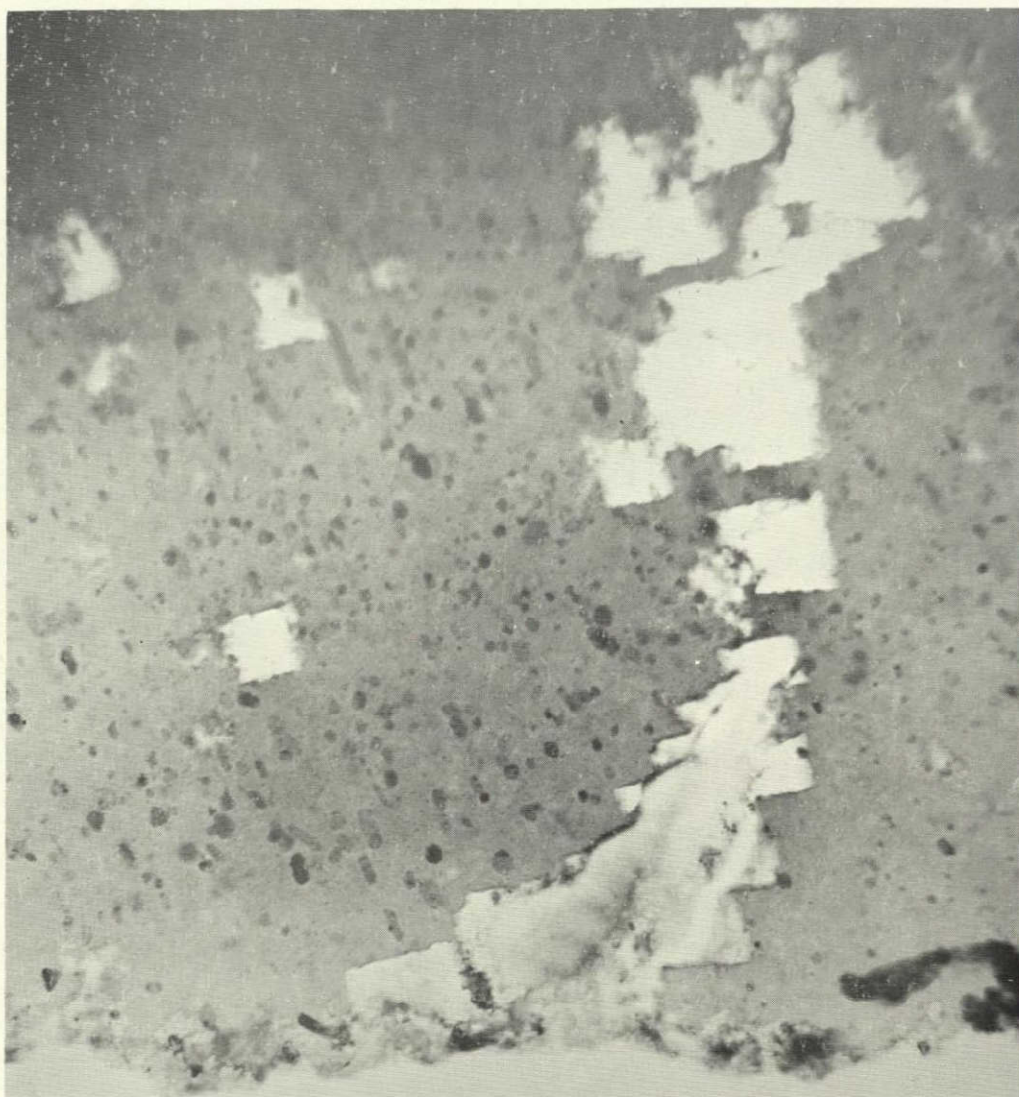
Oxide Replica

5,000X

Cellular boundaries in 7075-T6 plate  
reduced 80% with crack initiation on boundaries.

Figure 96



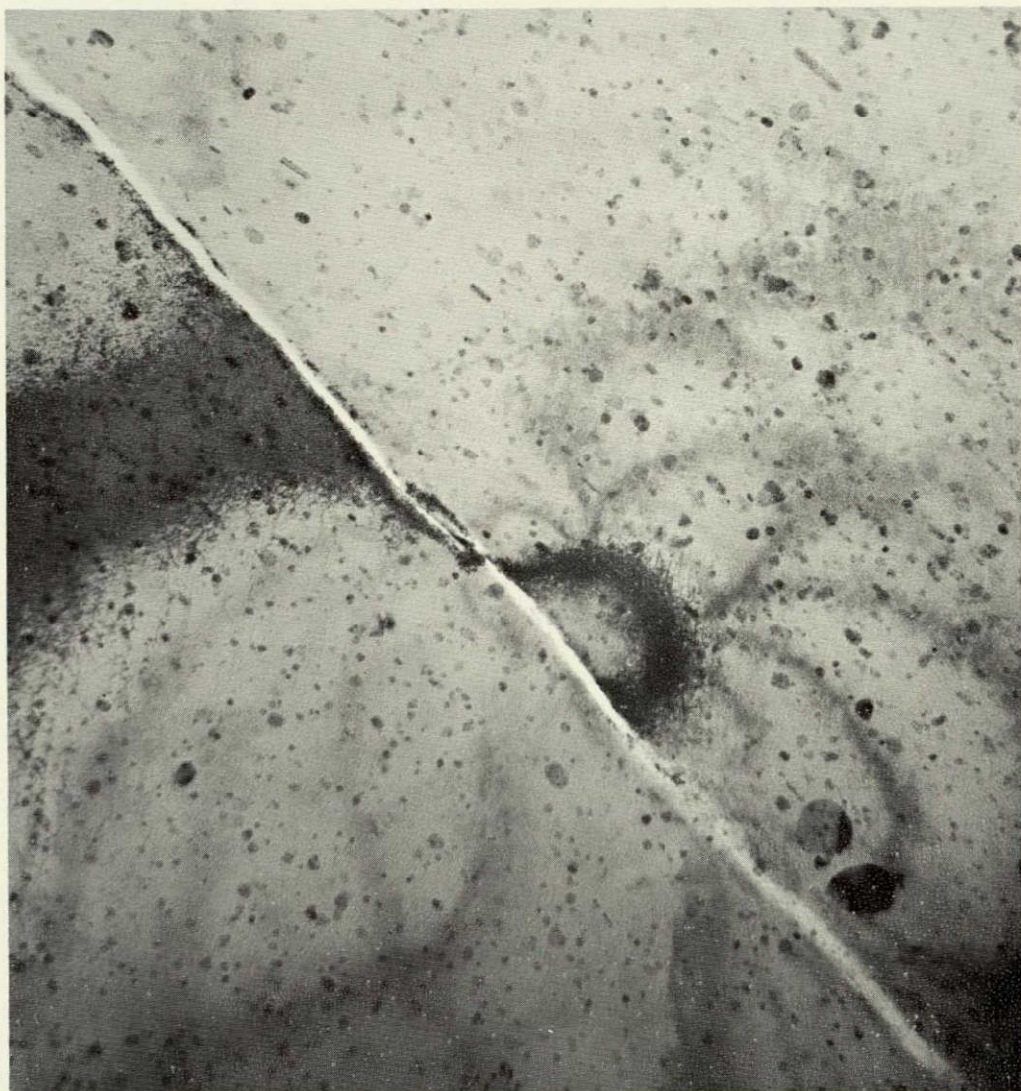


Electron Transmission

30,000X

Pitting corrosion of 7075-T6 exposed  
unstressed to NaCl-AlCl<sub>3</sub> solution at pH 1.

Figure 97



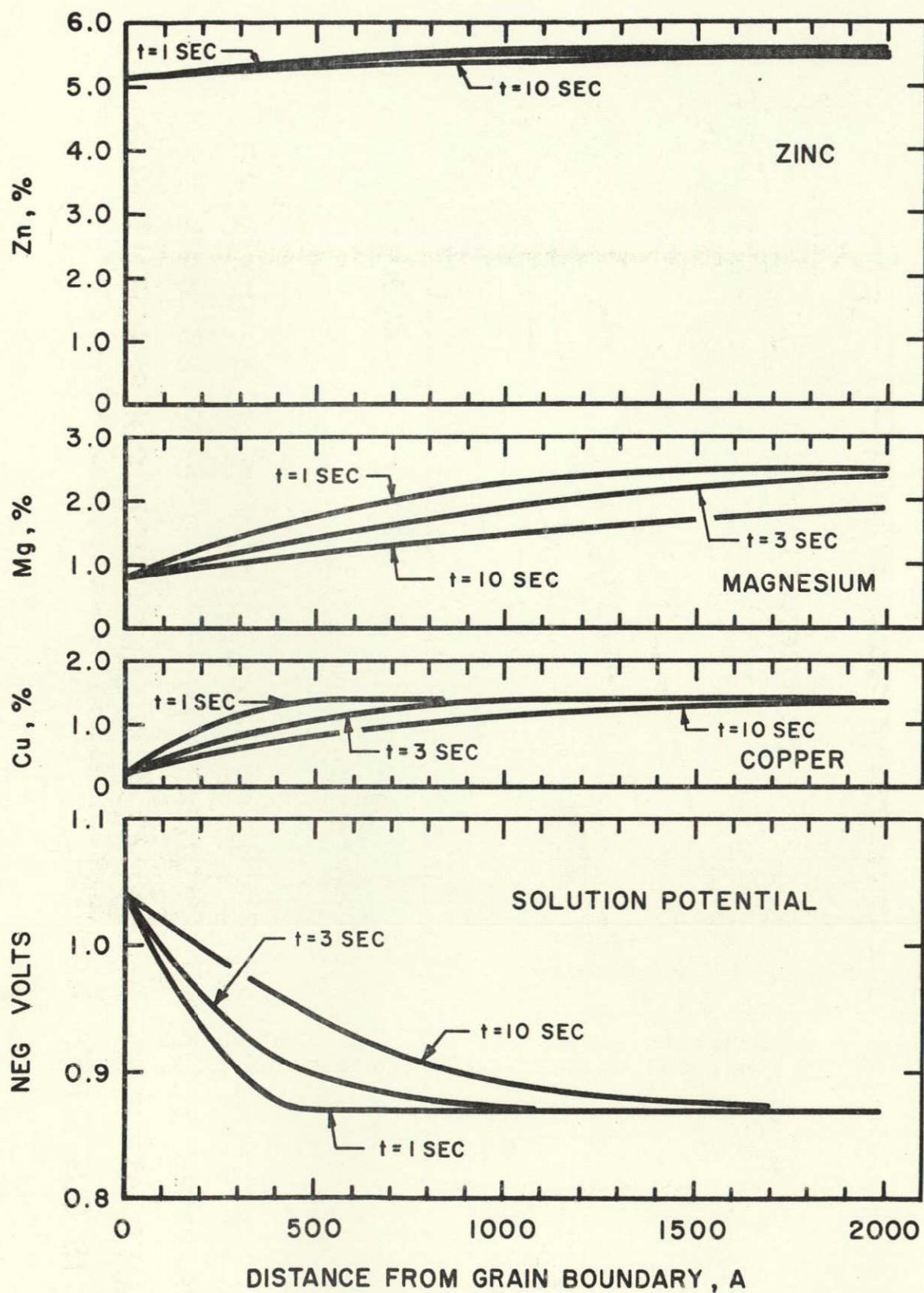
Electron Transmission

20,000X

Crack initiation in 7075-T6 stressed and  
exposed to NaCl-AlCl<sub>3</sub> solution at pH 1.

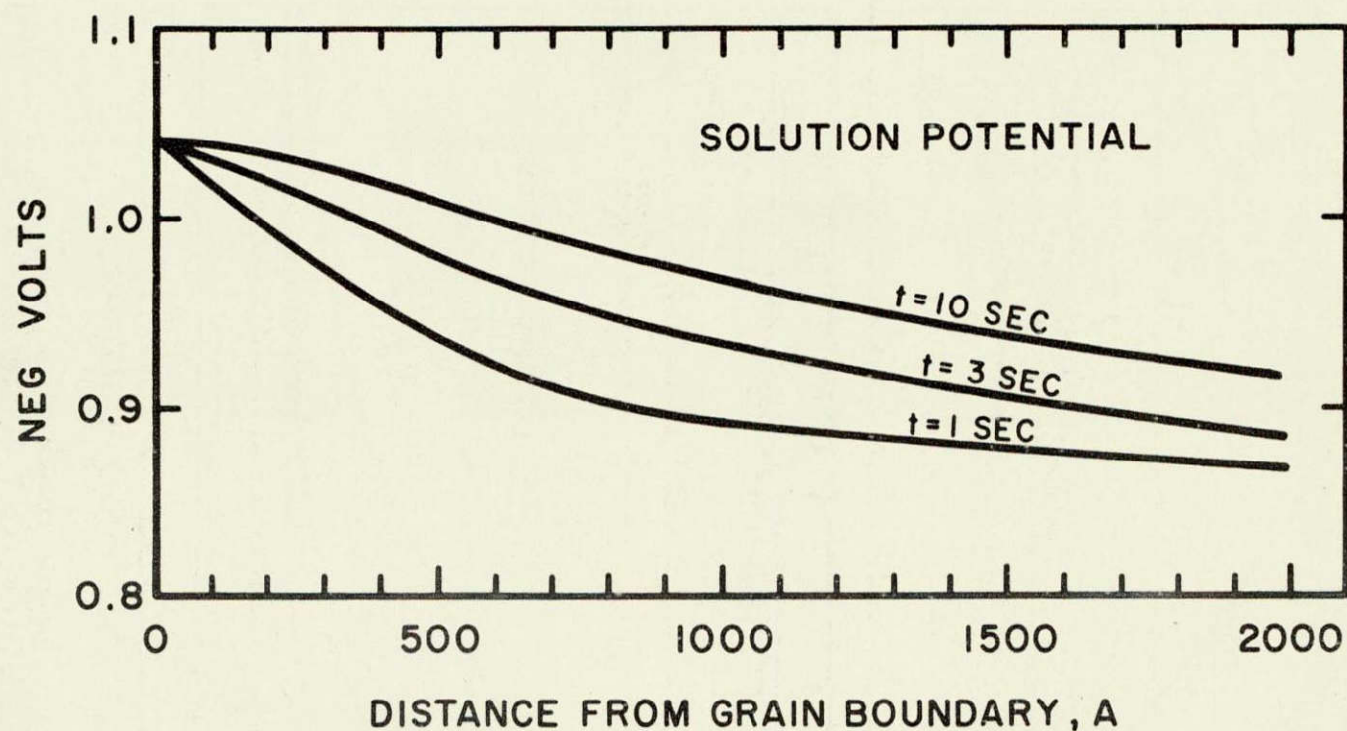
Figure 98





CALCULATED GRAIN BOUNDARY GRADIENTS FOR 7075 ALLOY  
 ASSUMING ALLOYING ELEMENT CONTENTS AT BOUNDARY ARE  
 SOLID SOLUBILITIES AT 680 F.

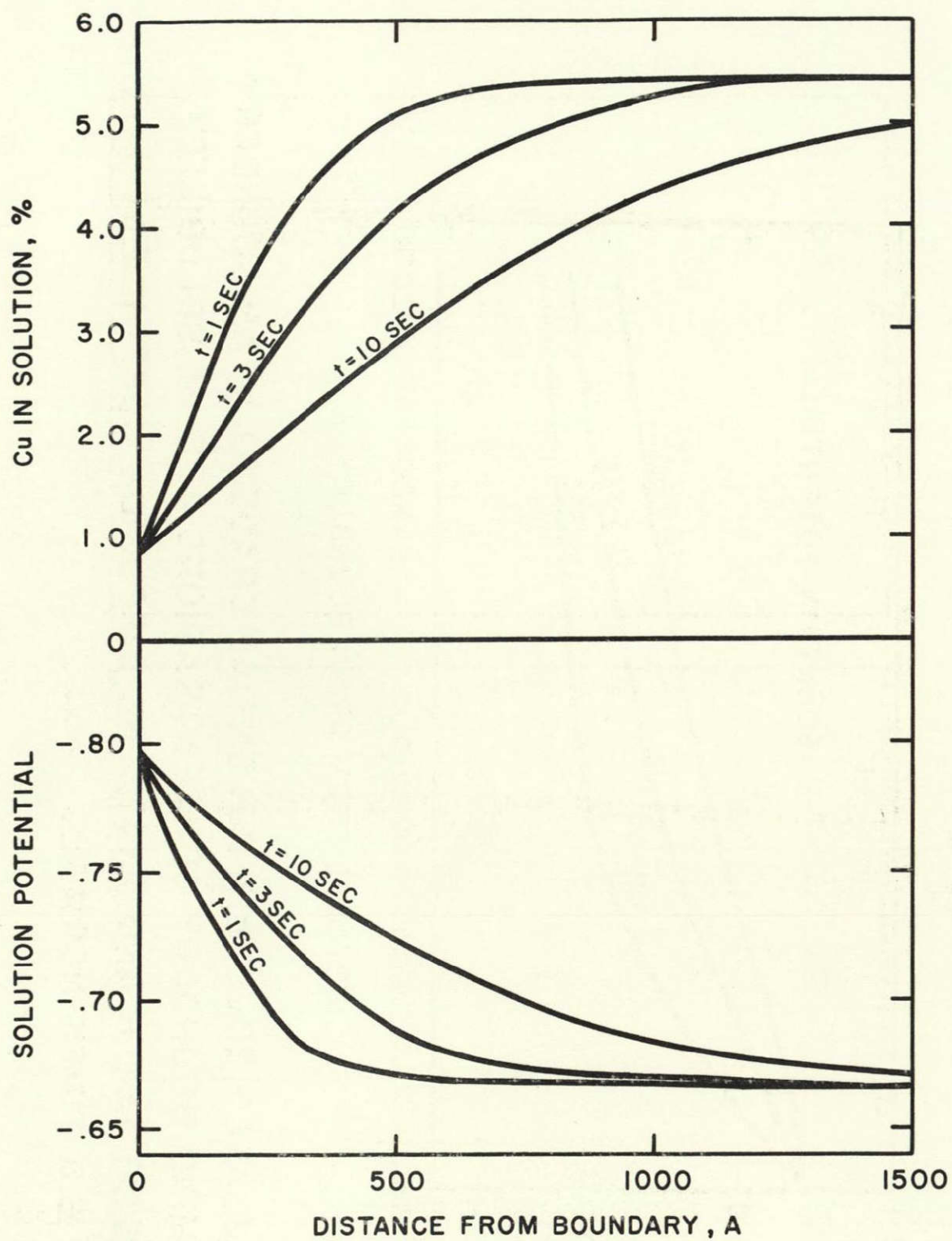
FIGURE 99



CALCULATED SOLUTION POTENTIAL GRADIENT NEAR BOUNDARY  
ASSUMING BOUNDARY CONCENTRATIONS ARE AT SOLUBILITY  
LIMITS AT 680 F AND THAT THE DIFFUSION COEFFICIENT FOR  
Cu IS 6.8 TIMES NORMAL.

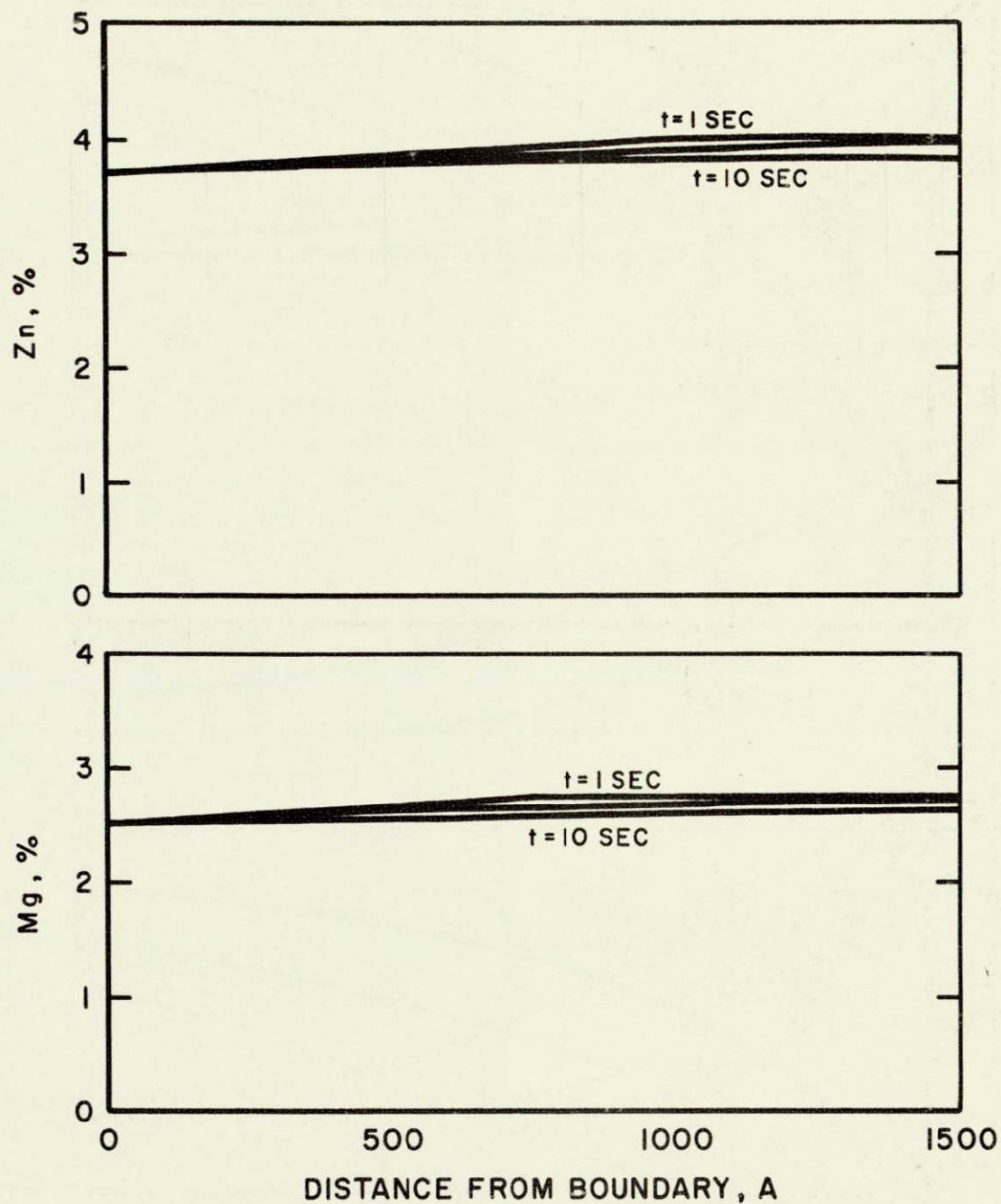
FIGURE 100





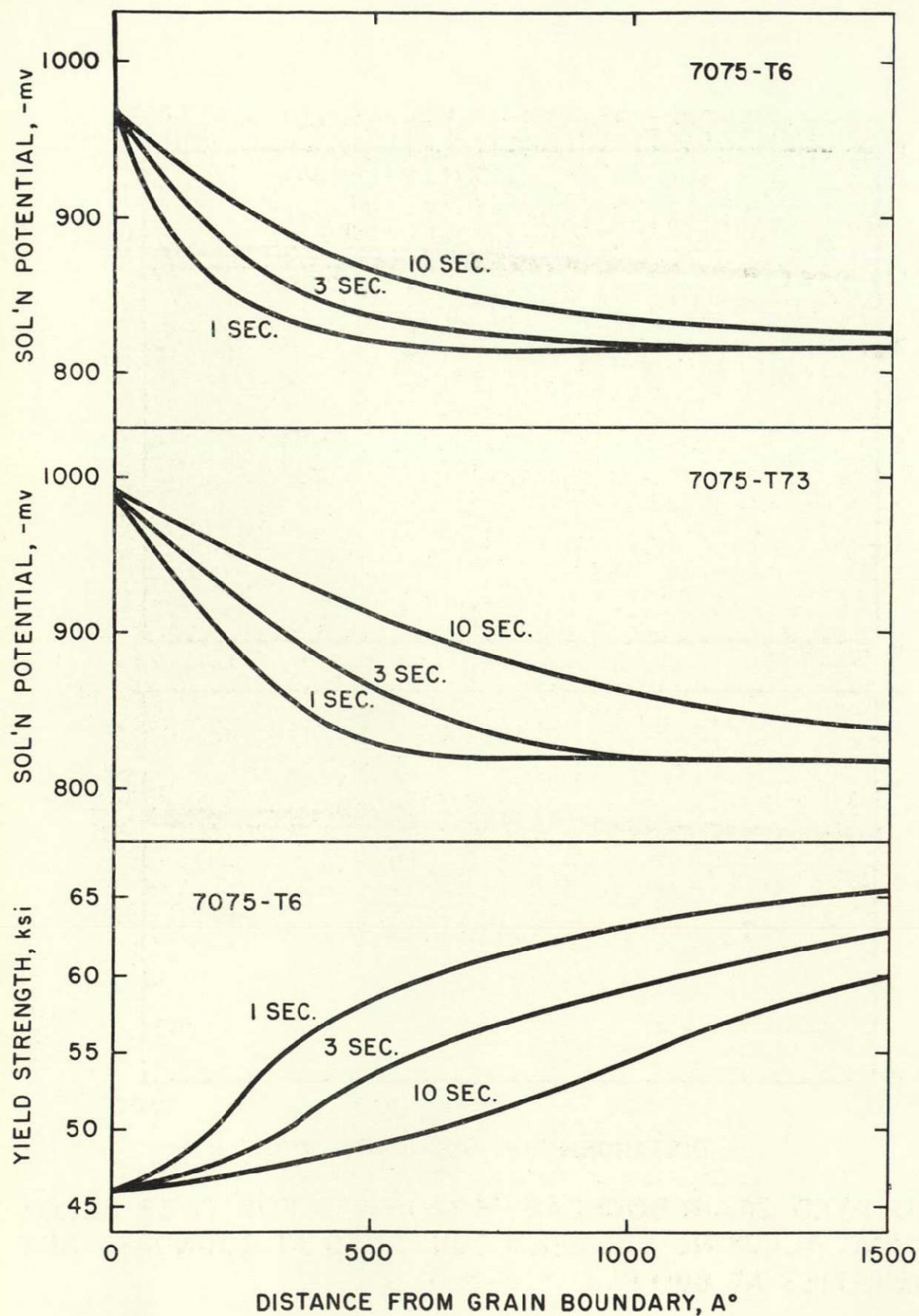
CALCULATED GRAIN BOUNDARY GRADIENTS FOR 2219 ALLOY  
ASSUMING ALLOYING ELEMENT CONTENTS AT BOUNDARY ARE  
SOLUBILITIES AT 680 F.

FIGURE 101



CALCULATED GRAIN BOUNDARY GRADIENTS FOR 7039 ALLOY  
ASSUMING ALLOYING ELEMENT CONTENTS AT BOUNDARY ARE  
SOLUBILITIES AT 680 F.

FIGURE 102



CALCULATED SOLUTION POTENTIALS AND STRENGTHS IN THE VICINITY OF A GRAIN BOUNDARY IN 7075 ALLOY.

FIGURE 103





Oxide Replica

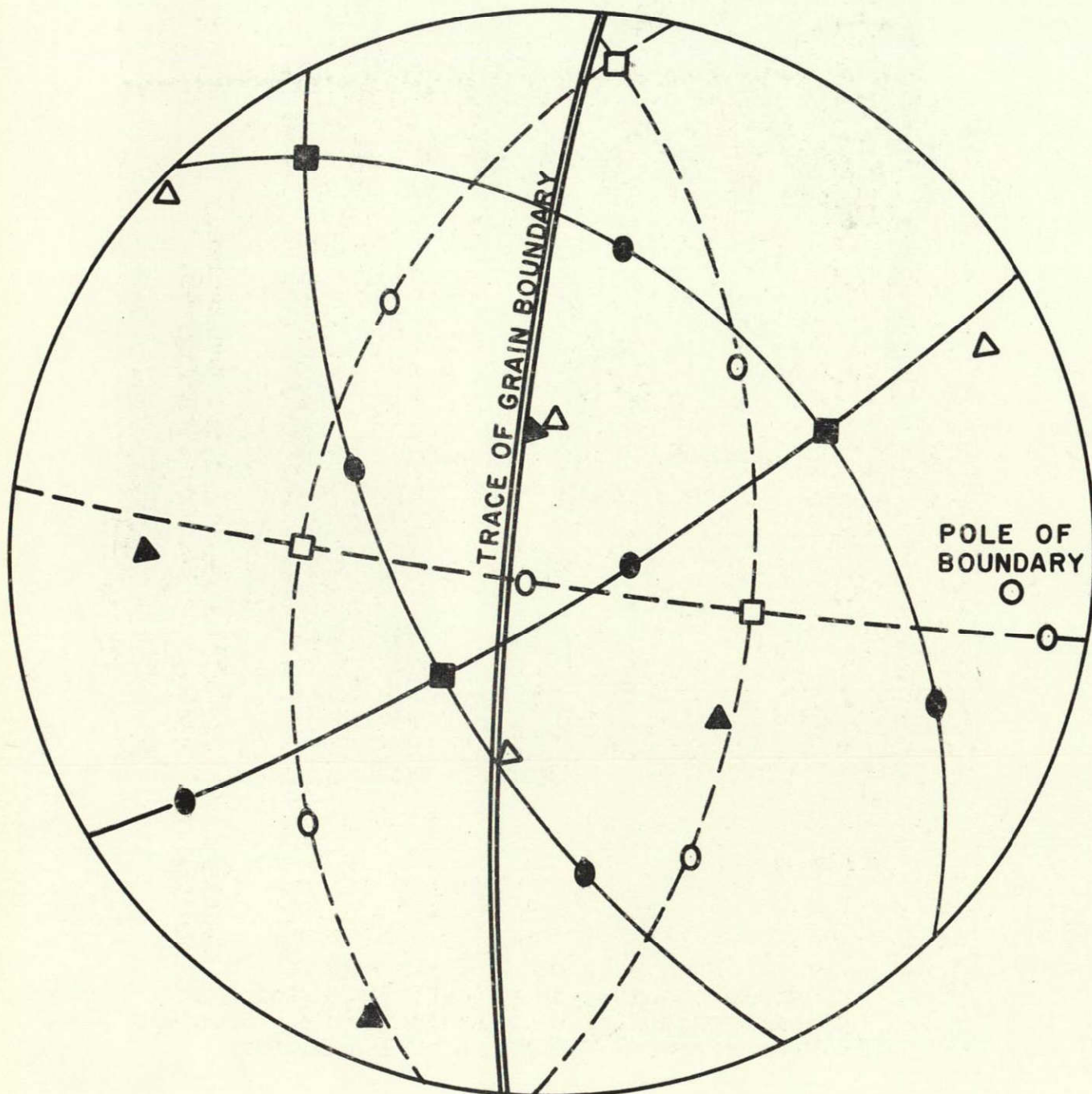
10,000X

Etch pits on opposite sides of a grain boundary in 2219-T37 containing an embryonic stress-corrosion crack. Specimen was stressed 75% YS in pH 1 solution.

Figure 104



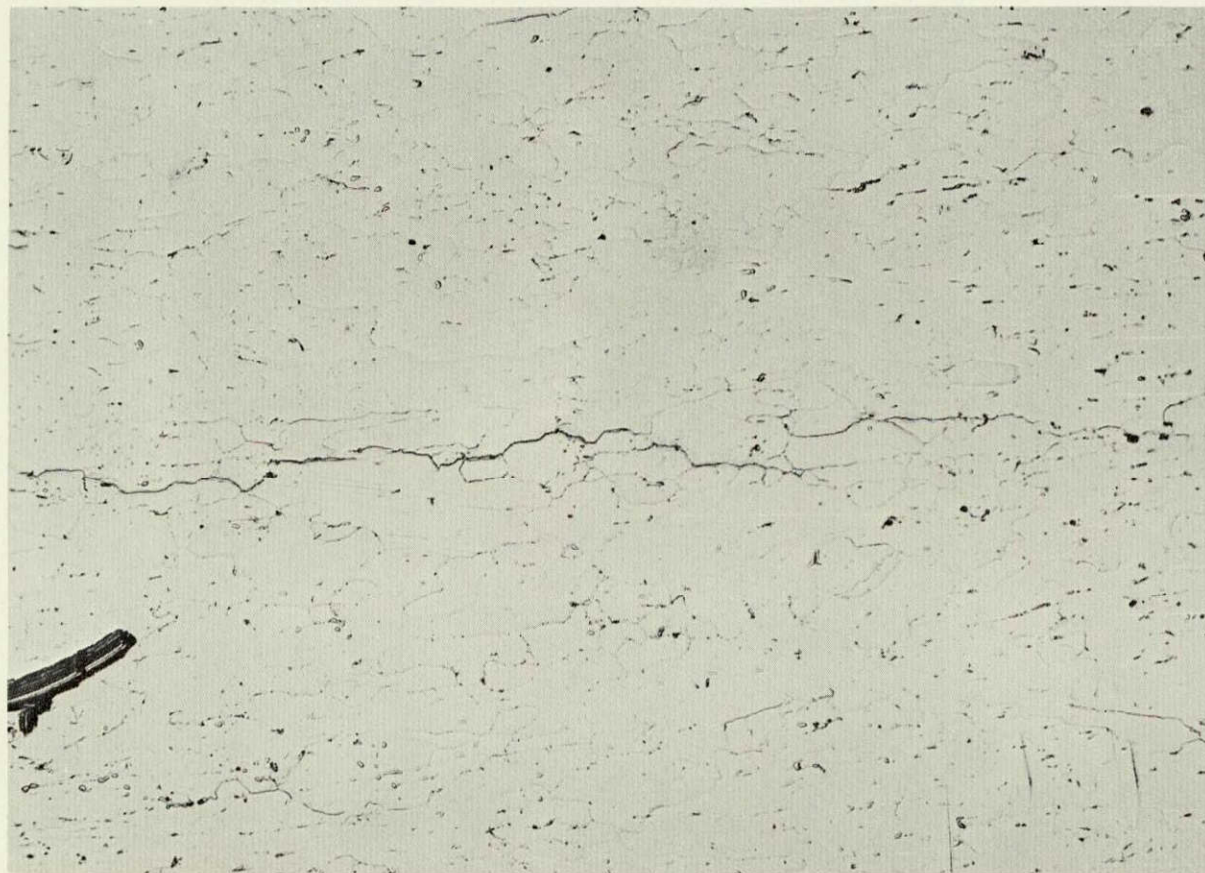
□ OPEN SYMBOLS - LEFT GRAIN  
 ■ SOLID SYMBOLS - RIGHT GRAIN



STEREOGRAPHIC PROJECTION OF PRINCIPAL CRYSTALLOGRAPHIC POLES OF THE TWO GRAINS IN FIG. 104

FIGURE 105

↑ Stress ↓



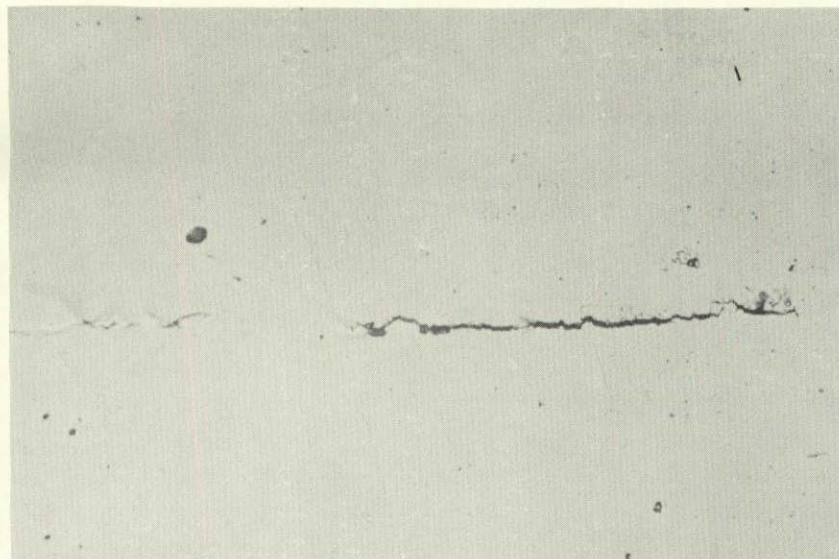
Cracking in 2219-T351 stressed short transversely  
to 90% YS. (X100) Compare with Fig. 46.

Figure 106



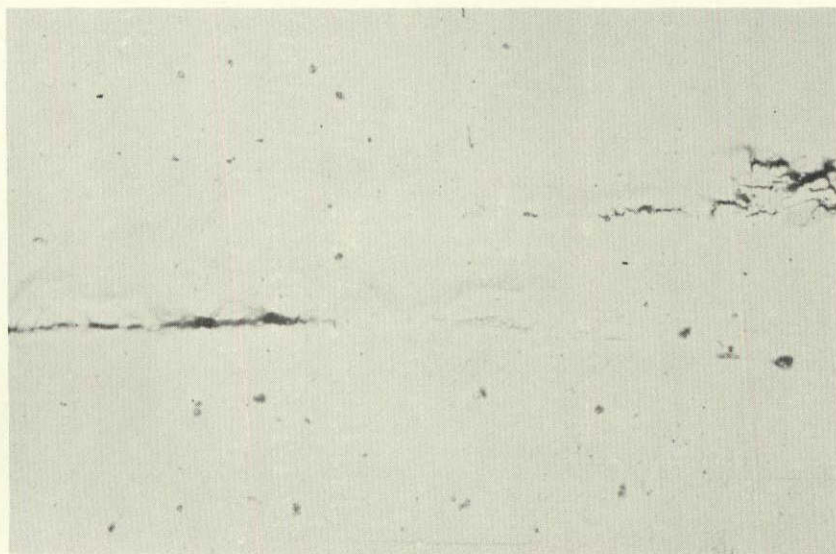
161980  
161981  
161982  
161984

(a)

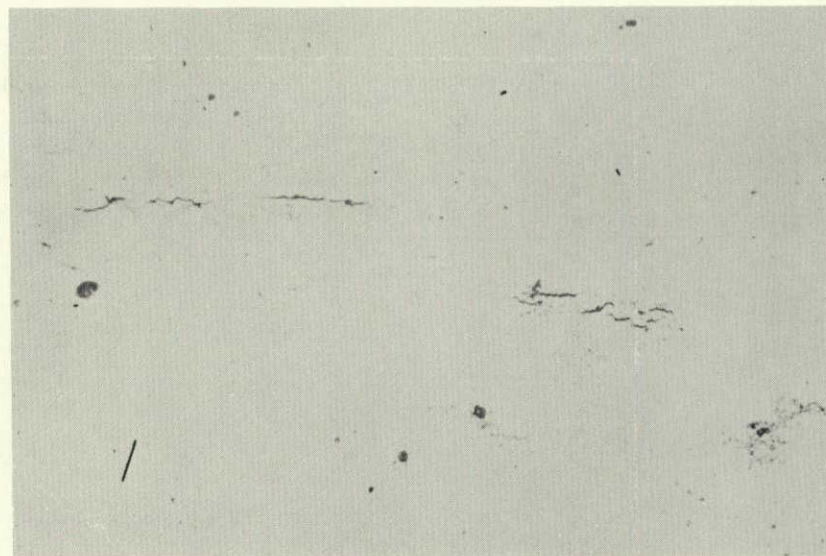


↑  
STRESS  
↓

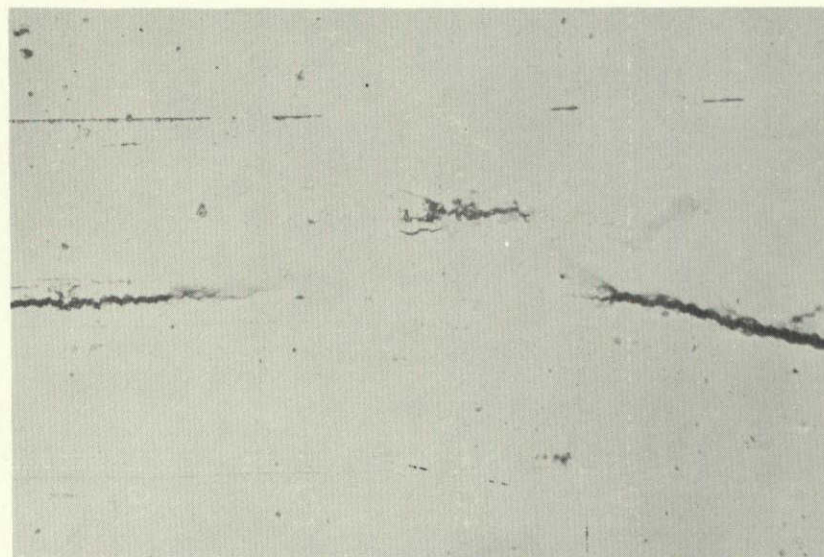
(c)



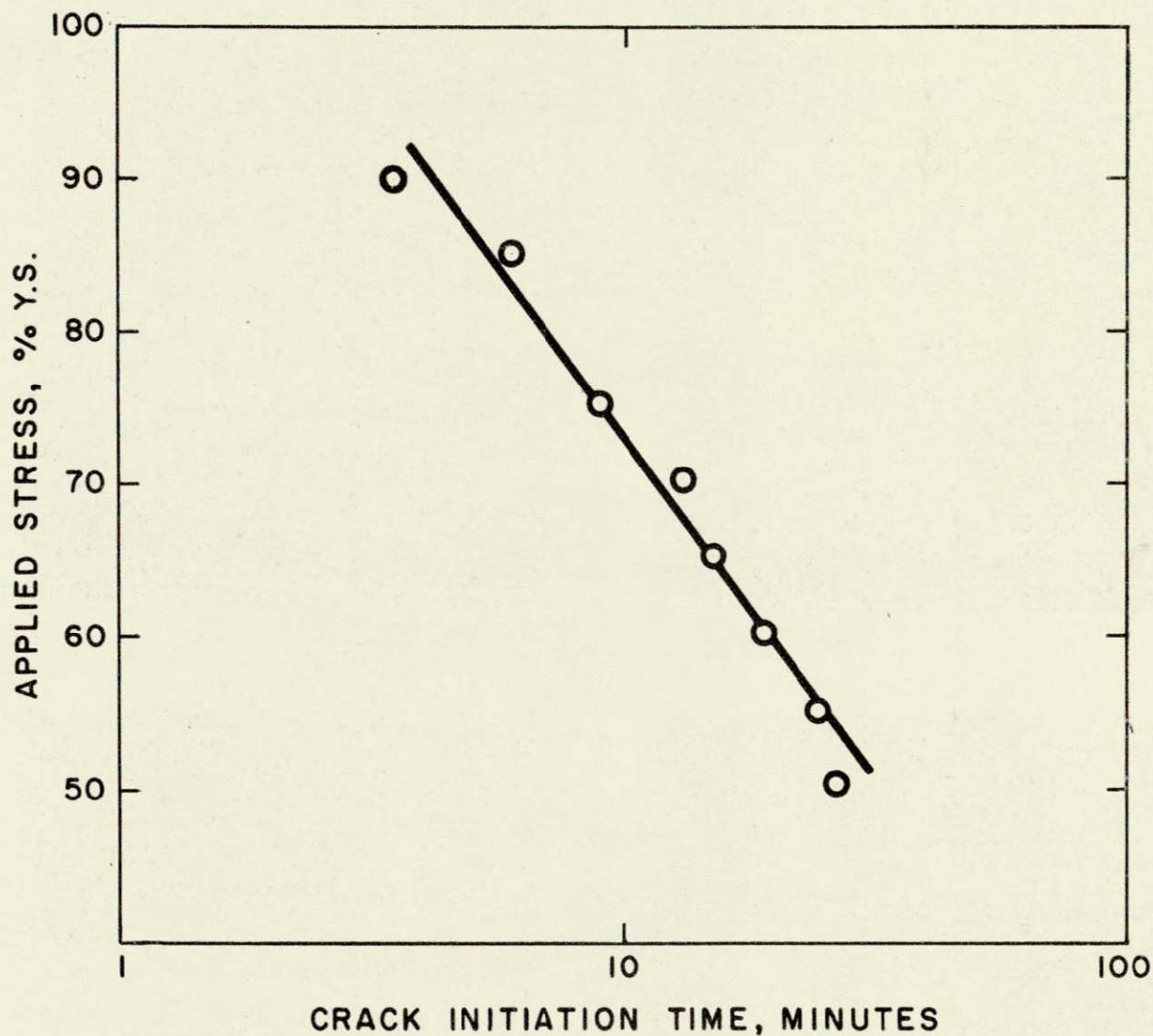
(b)



(d)



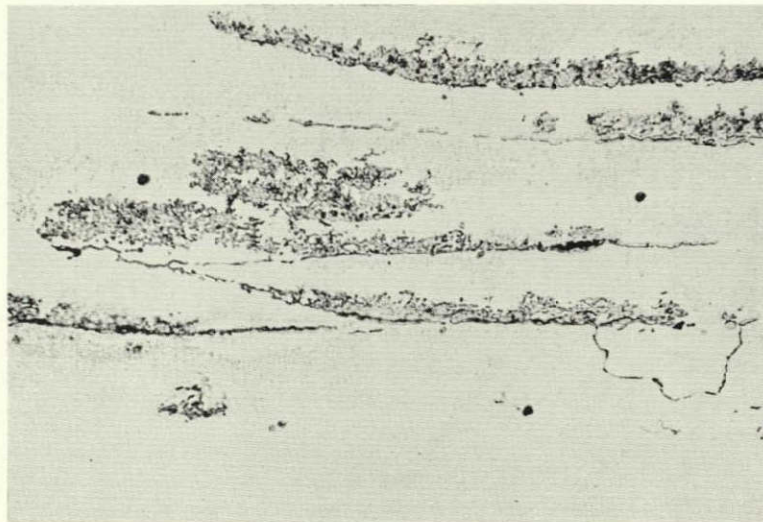
Stress corrosion crack initiation on surface of 7075-T6 specimen stressed to 90% YS in short transverse direction and exposed ten minutes (X500)



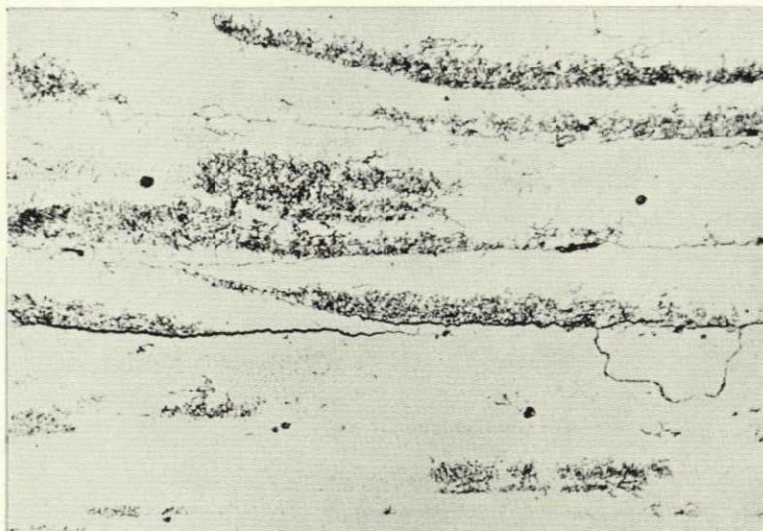
RELATION BETWEEN APPLIED STRESS AND CRACK INITIATION TIME WITH 7075-T6 STRESSED SHORT-TRANVERSELY TO 75% Y.S. AND EXPOSED TO  $\text{NaCl}-\text{AlCl}_3$  SOLUTION.

FIGURE 108

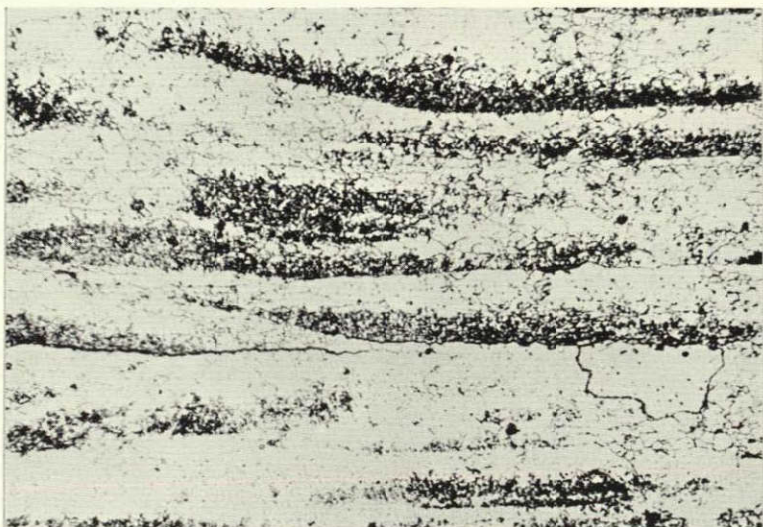




15 min.



60 min.



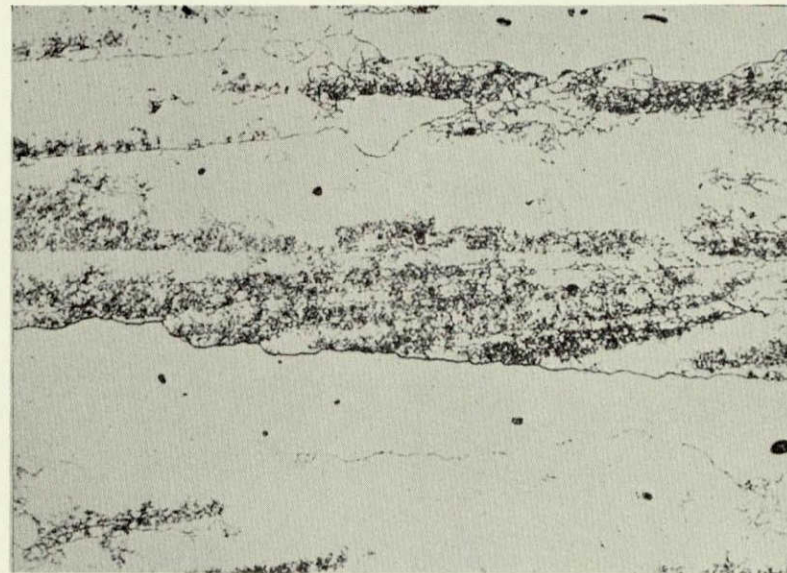
120 min.

STRESS

Crack development in 7075-T6 stressed short transversely to 15% YS. (X500)

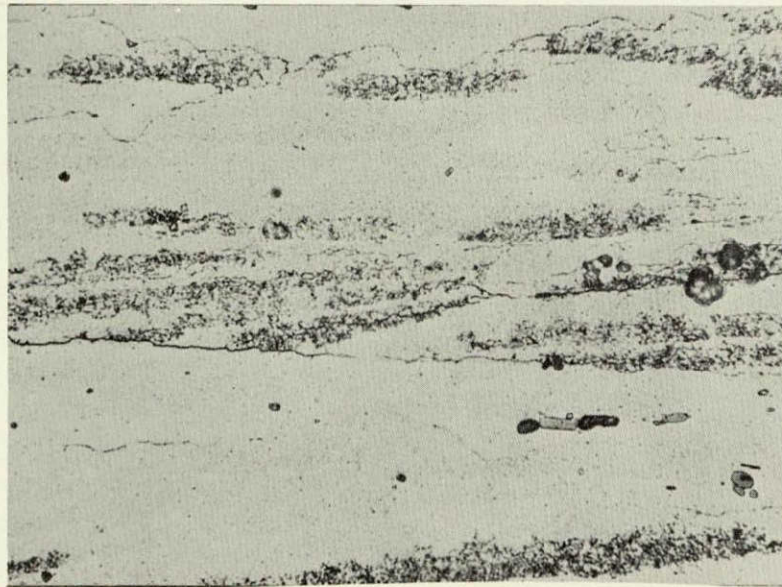
Figure 109



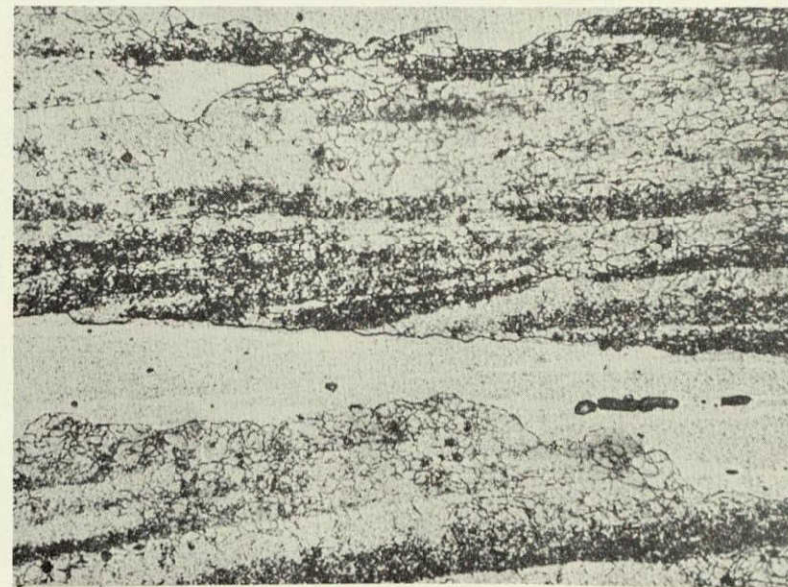


30 min.

↑  
STRESS  
↓



60 min.



120 min.

Crack development in 7075-T6 stressed short transversely to 10% YS. (X500)

Figure 110



← STRESS →



20% YS



15% YS



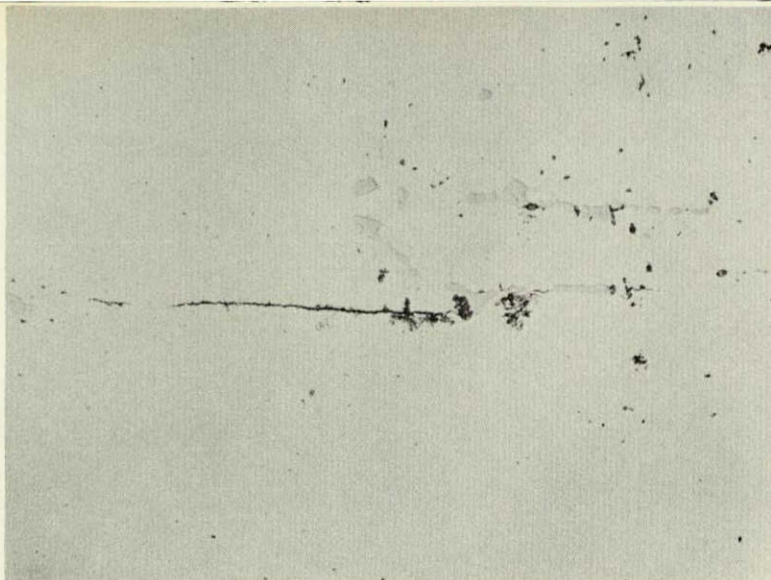
10% YS

Crack development in 7075-T6 at low levels of short transverse stress.

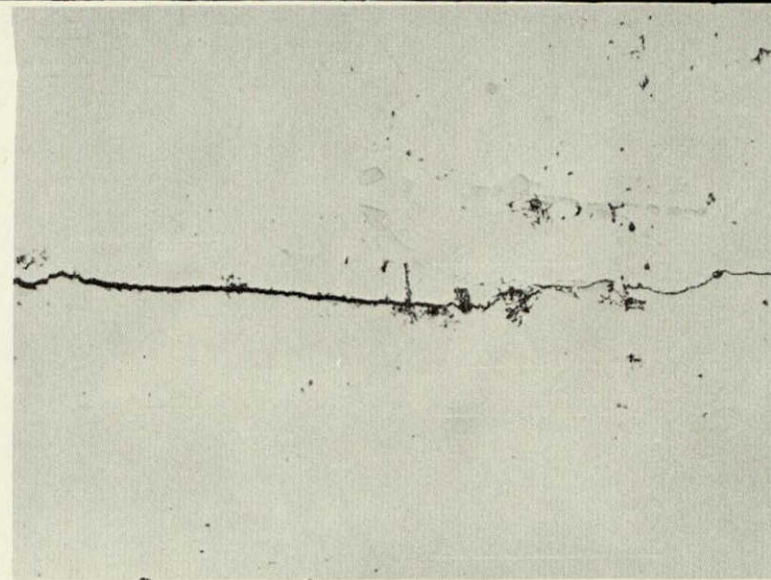
Figure 111



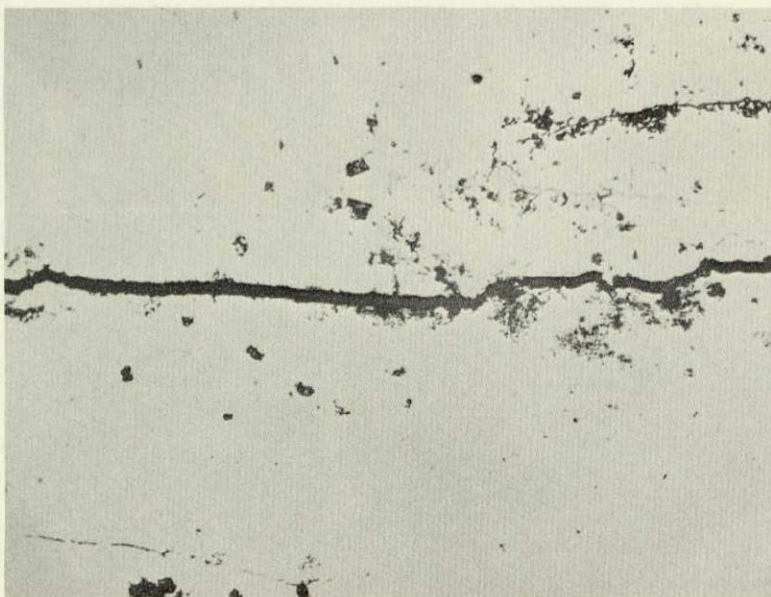
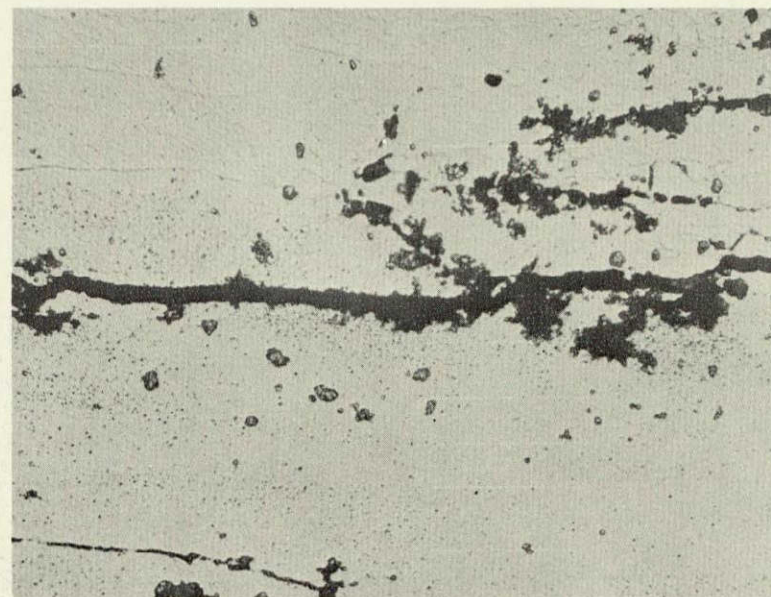
8 min.



11 min.

STRESS  
↑  
↓

26 min.

26 min.  
Keller's  
Etch

Crack initiation and development in 7079-T6 stressed short transversely  
to 90% YS and exposed to pH 1 NaCl-AlCl<sub>3</sub> solution (X500).

Figure 112



← STRESS →

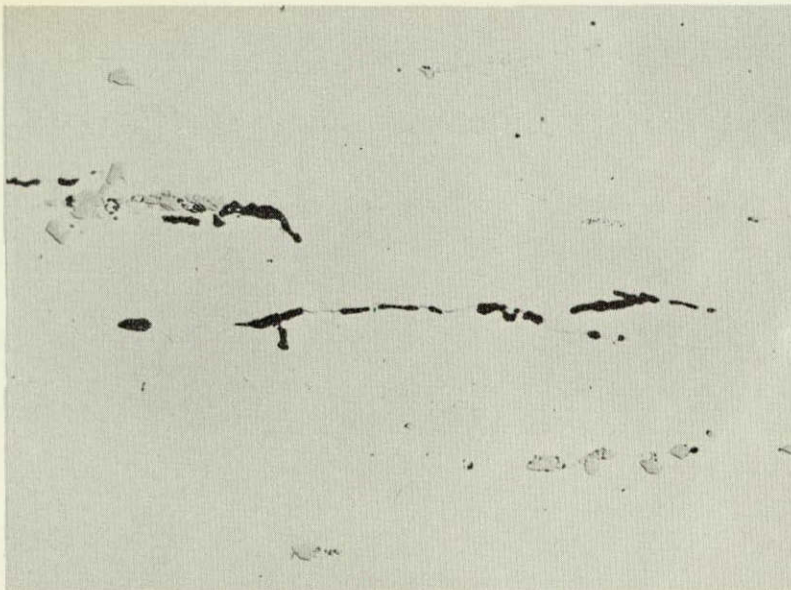


Cross section of sample in Fig. 112  
showing cracks along boundaries. (X500)

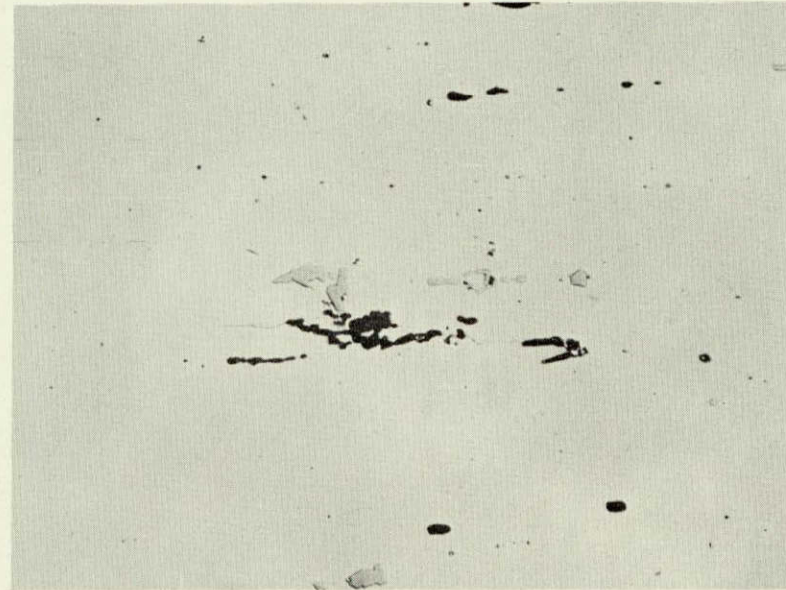
Figure 113



As  
Exposed



As  
Exposed

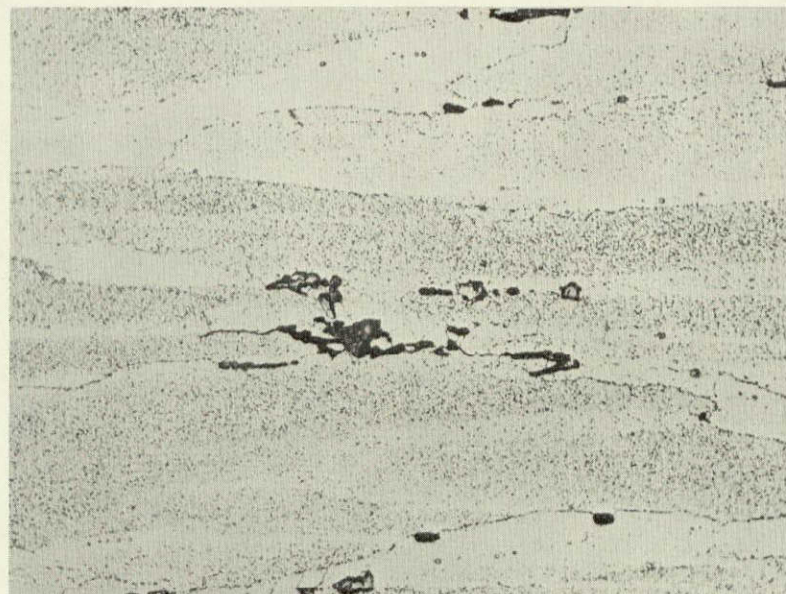


↑  
STRESS  
↓

Keller's  
Etch



Keller's  
Etch



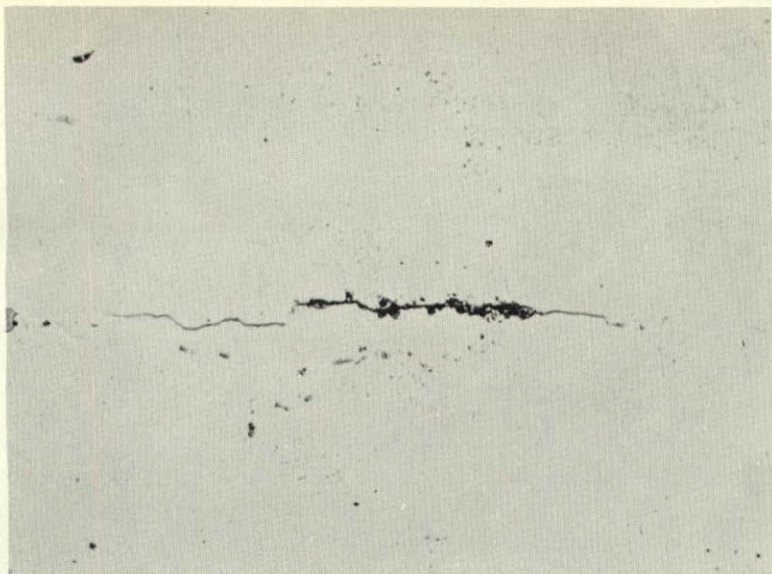
Crack initiation sites at  $Mg_2Si$  particles in 7039-T6 stressed to 90% YS S.T. and exposed to  $NaCl-Na_2CrO_4$  solution at pH 2 for five hours. (X500)

Figure 114

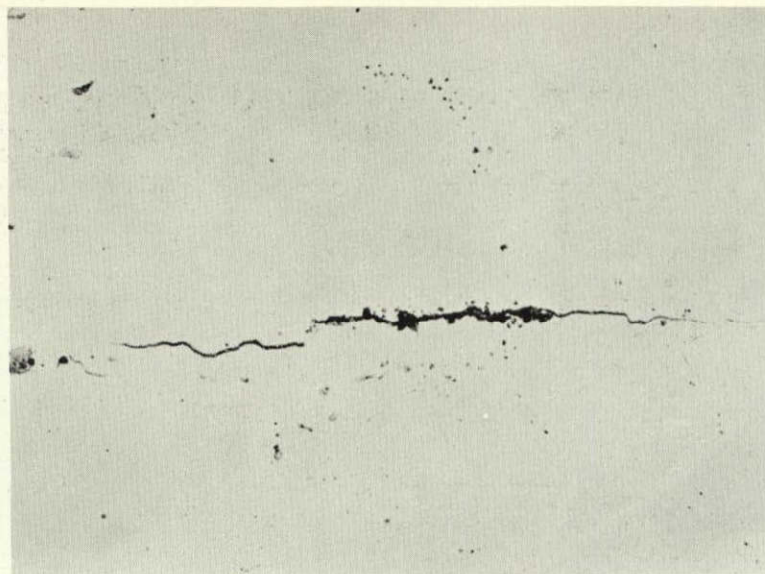


168964-5  
168971-2

3 min.



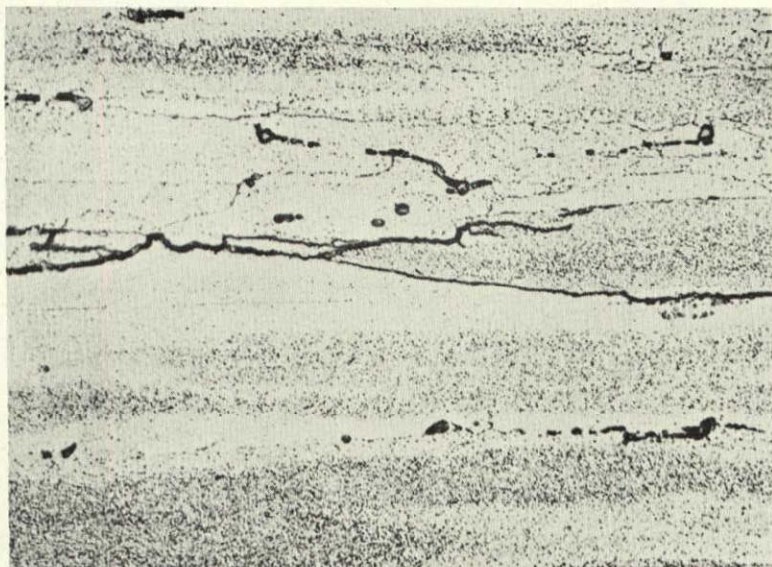
↑  
STRESS  
↓



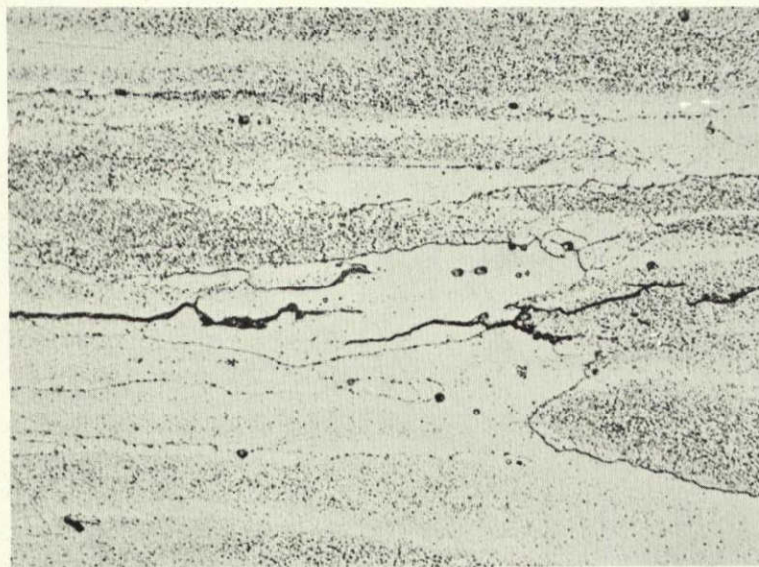
43 min.

Crack initiation at constituent particles

103 min.  
Keller's  
Etch



↑  
STRESS  
↓



103 min.  
Keller's  
Etch

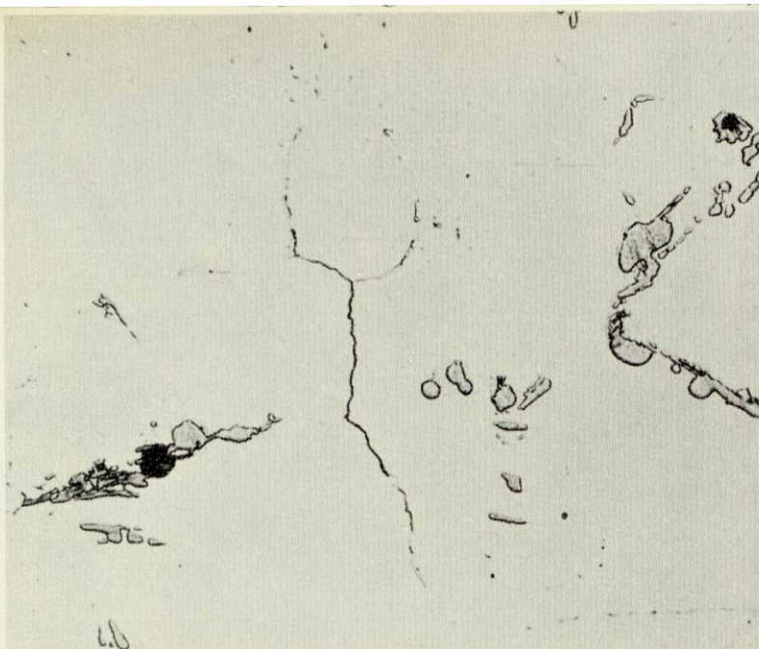
Interfragmentary or transgranular stringers at ends of long cracks

7039-T6 at 90% YS S.T. stress in NaCl-Na<sub>2</sub>CrO<sub>4</sub> solution at pH 2 (X500).



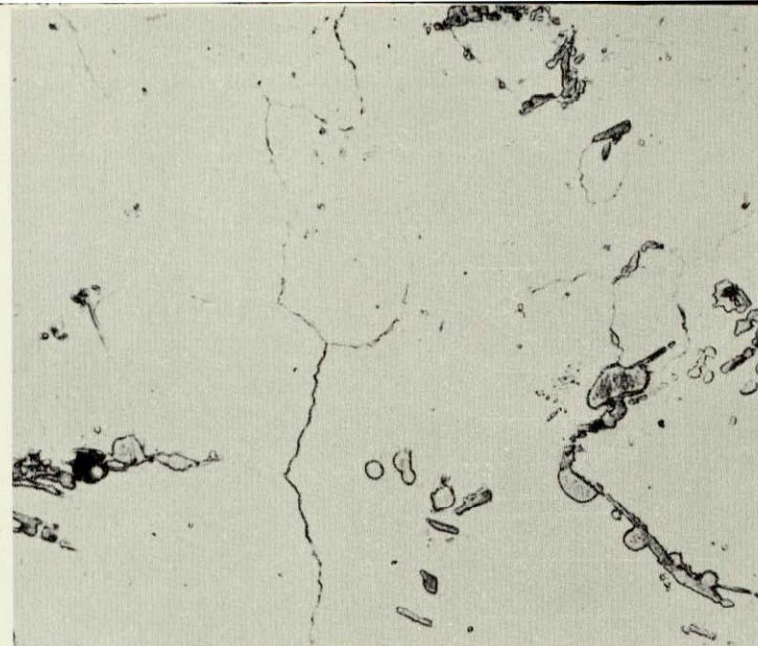
(a)

5 Min.



(b)

18 min.



← STRESS →

(c)

30 min.



(d)

60 min.



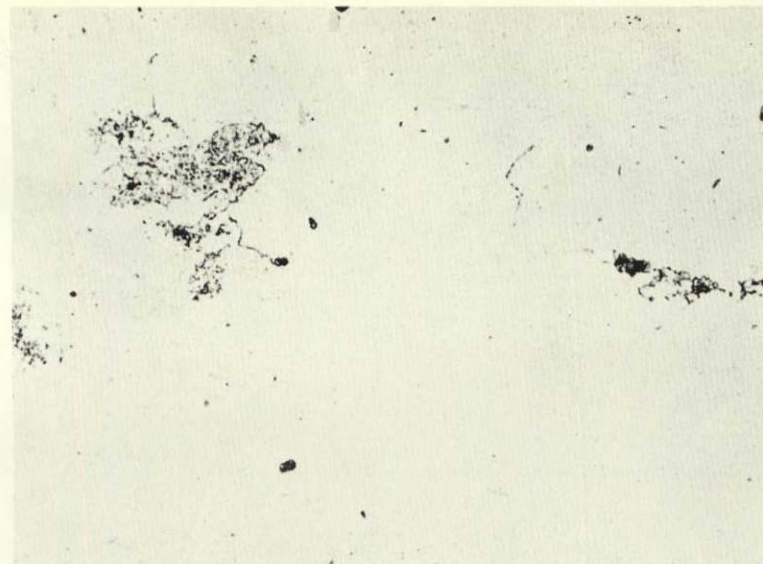
Stress corrosion cracking on surface of 2219-T351 stressed to 75% YS in longitudinal direction (X500)

Figure 116

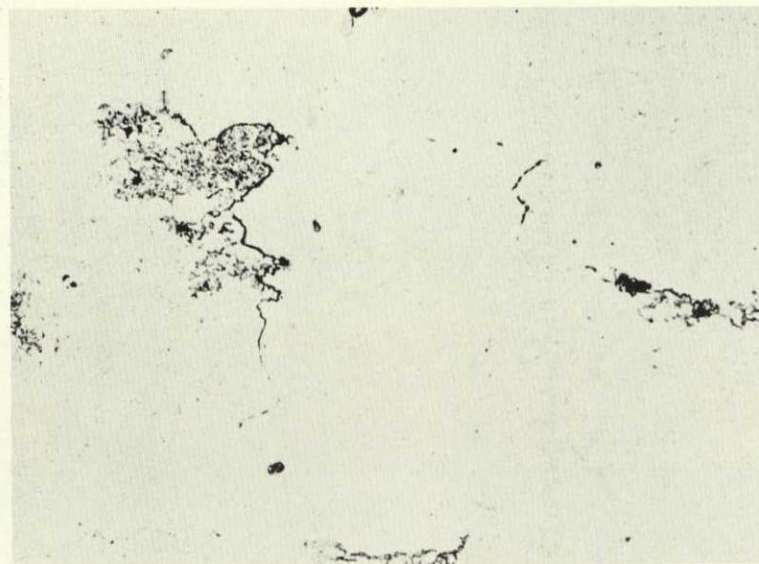


161962  
161963  
161964  
161965

12 min.

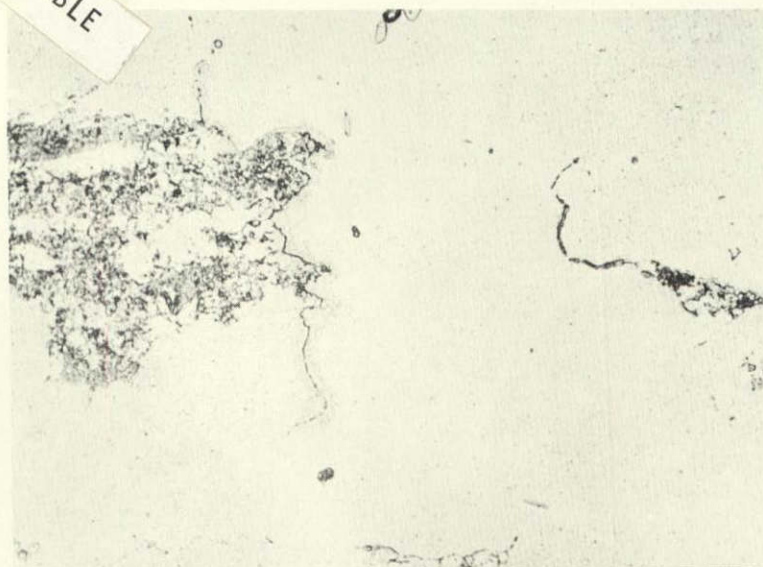


20 min.

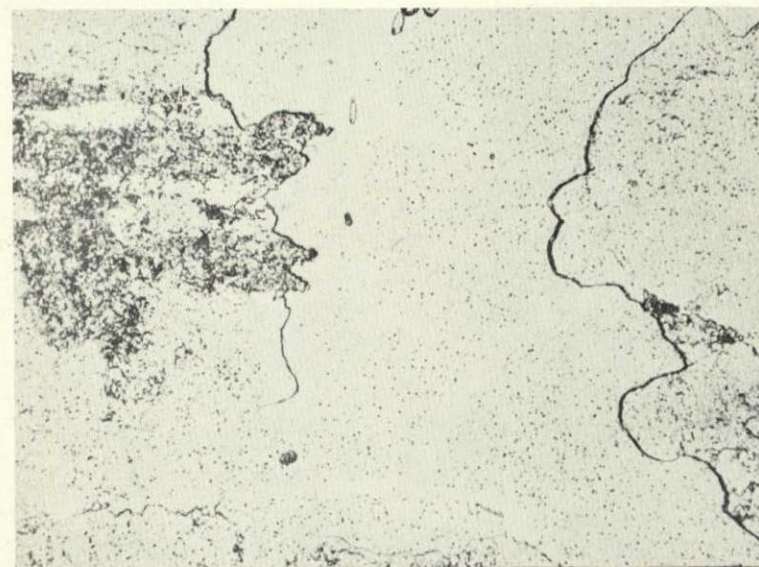


← STRESS →

60 min.



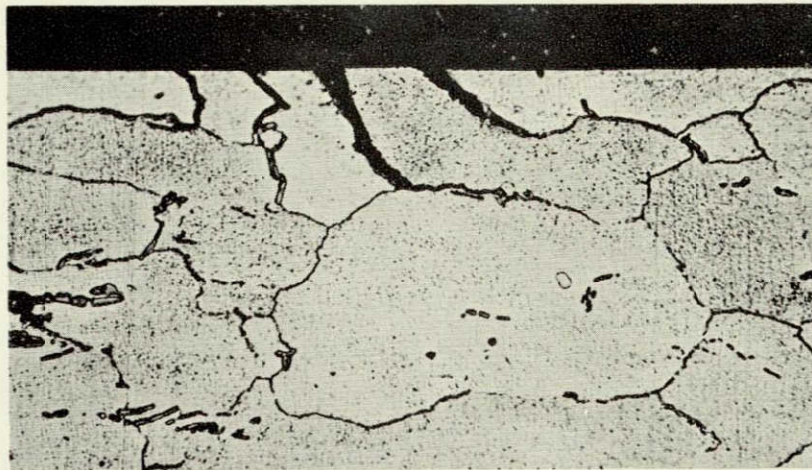
105 min.



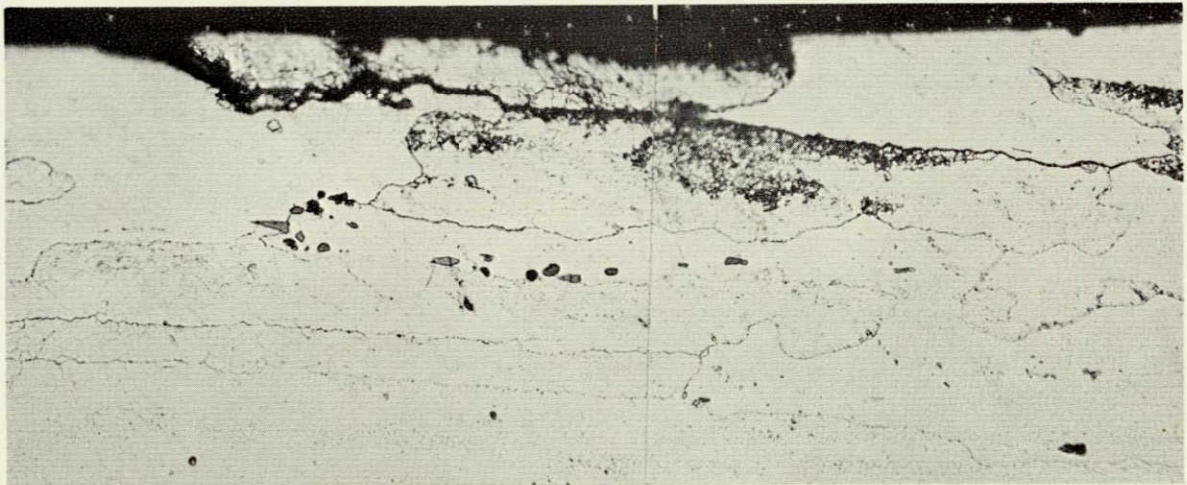
Development of stress corrosion cracks on surface of  
7075-T6 specimen stressed longitudinally to 75% YS. (X500)

Figure 117

← Stress →



2219-T37



7075-T6

Unfavorable boundary orientation beneath surface  
of longitudinally stressed specimens. (X500)

Figure 118



← Stress →



Crack development in 2219-T37 stressed 75% YS  
short transversely (X100). Compare to Fig. 120.

Figure 119



← Stress →



Stress corrosion cracks developed in 25-minute exposure on surface of 2219-T37 specimen stressed longitudinally to 75% YS (X100). Compare to Fig. 119.

Figure 120



← Stress →

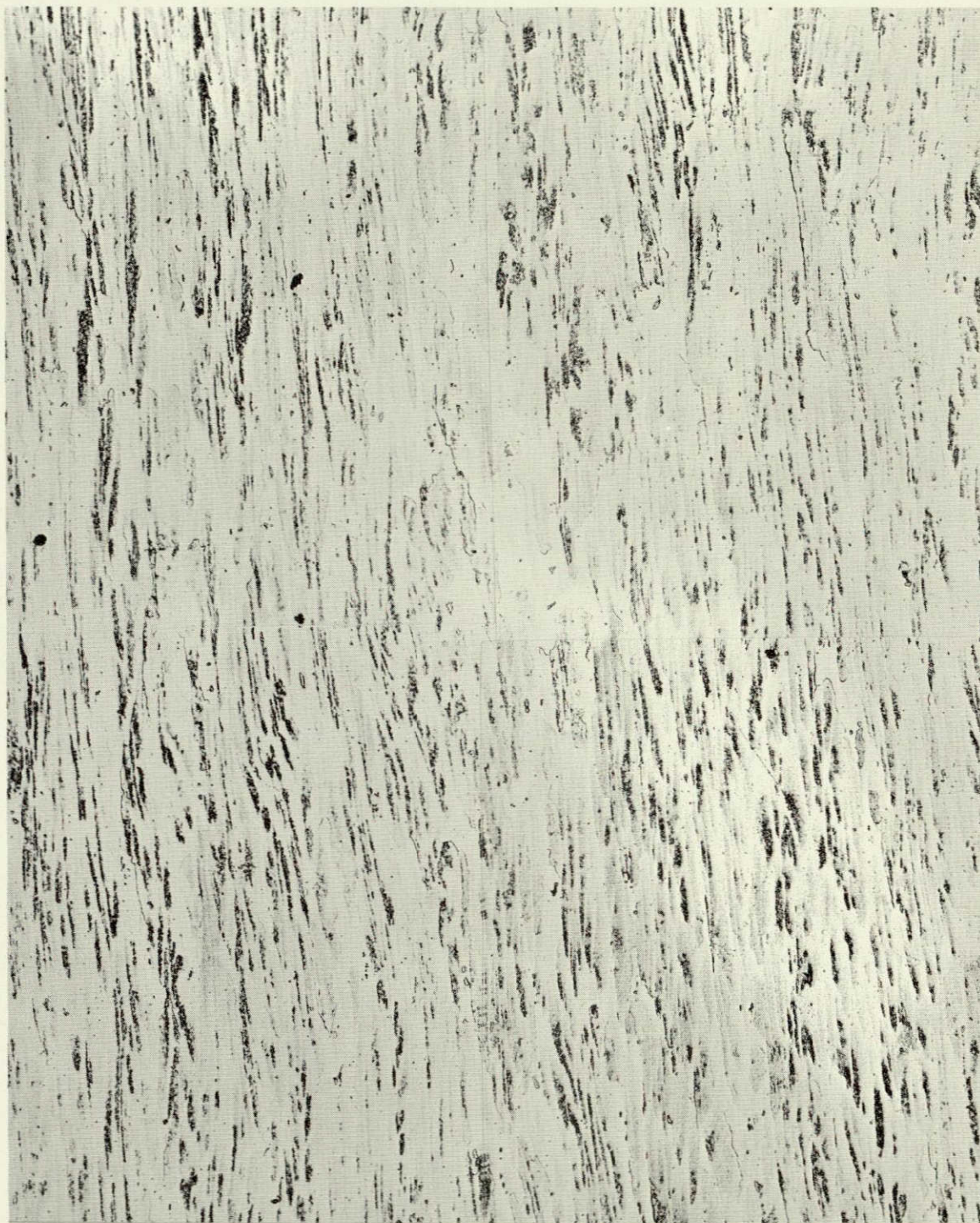


Cracks developed in 7075-T6 stressed 75% YS short  
transversely (100X). Compare to Fig. 122.

Figure 121



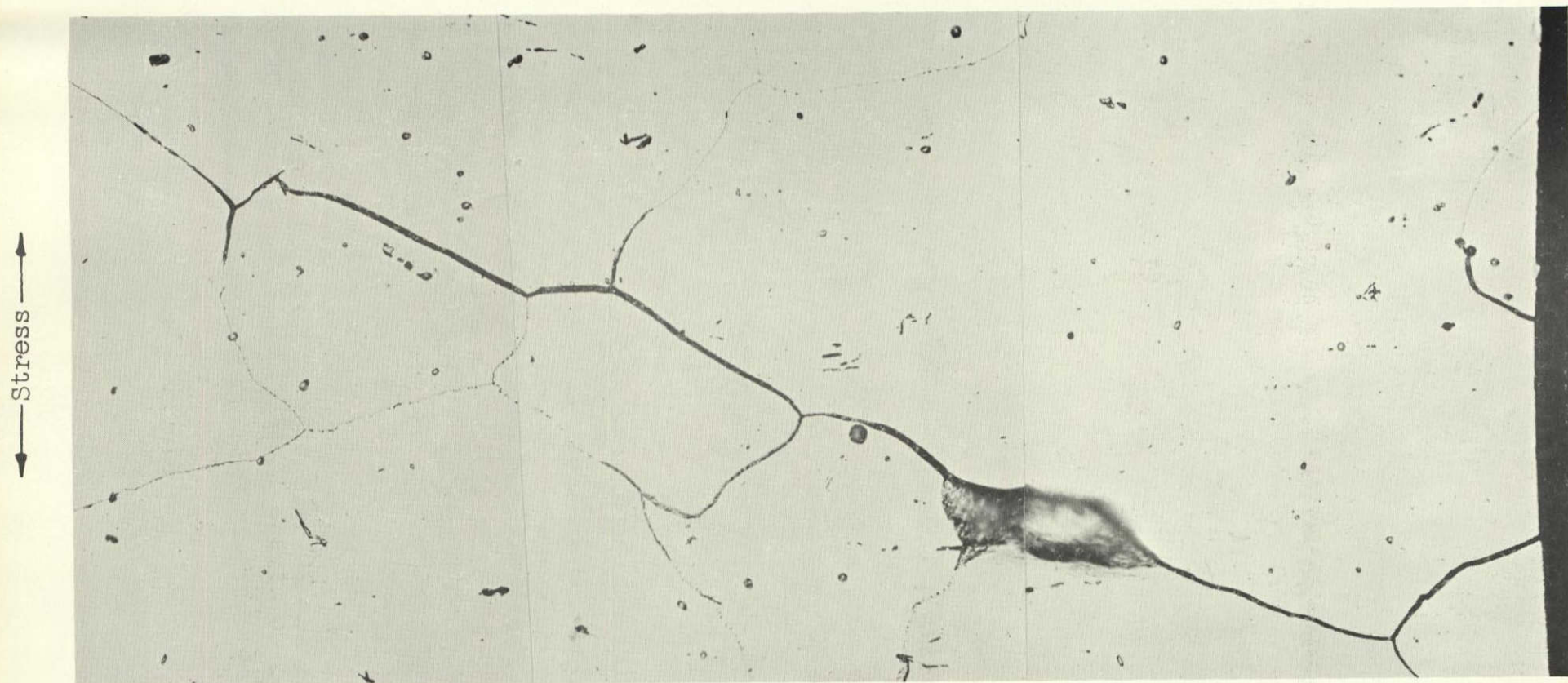
← Stress →



Cracks developed in 7075-T6 stressed 75% YS longitudinally (100X).  
Cracks parallel to stress caused by biaxial stress in specimen.  
Compare with Fig. 121.

Figure 122

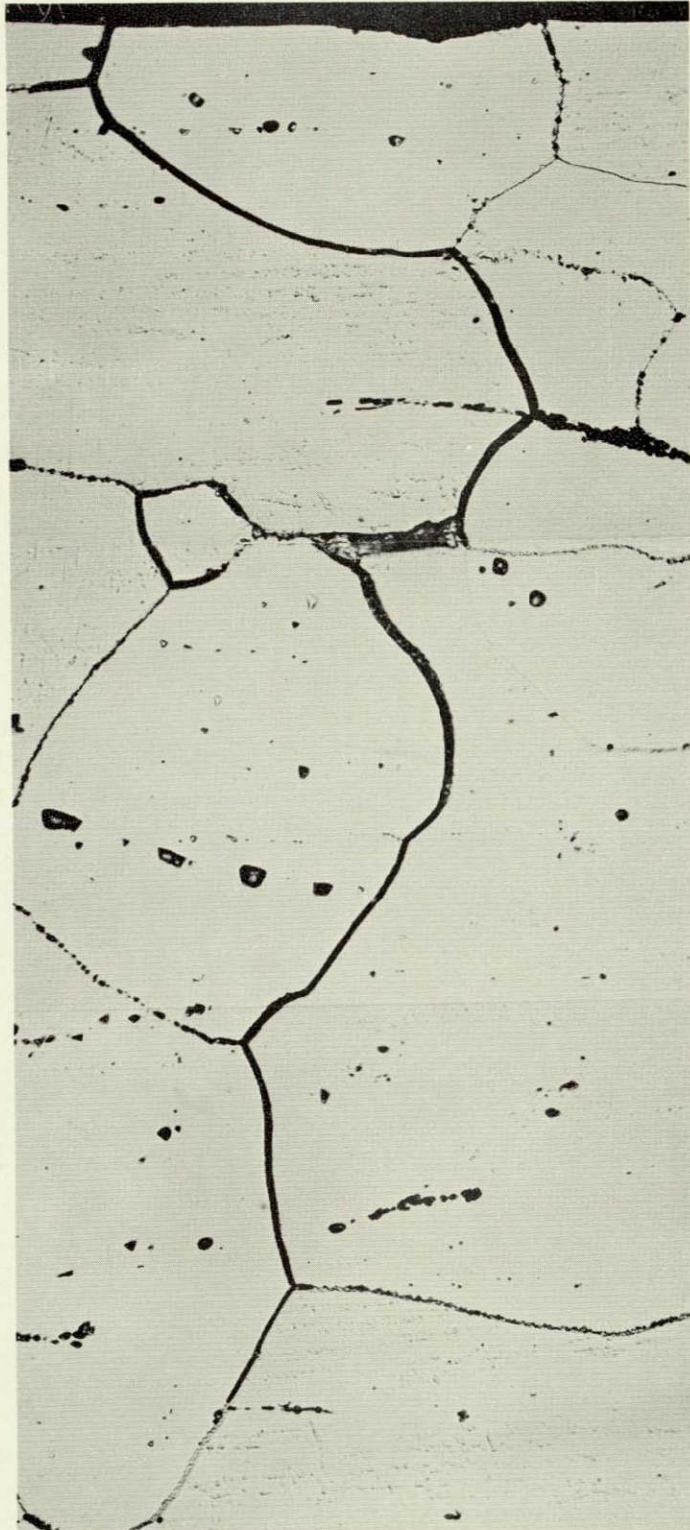




Crack development in X7375-T6 stressed to 75% YS  
short transversely (X500). Compare with Fig. 124.

Figure 123

← Stress →



Crack development in X7375-T6 stressed to 75% YS  
longitudinally (X500). Compare with Fig. 123.

Figure 124



← Stress →



Oxide Replica

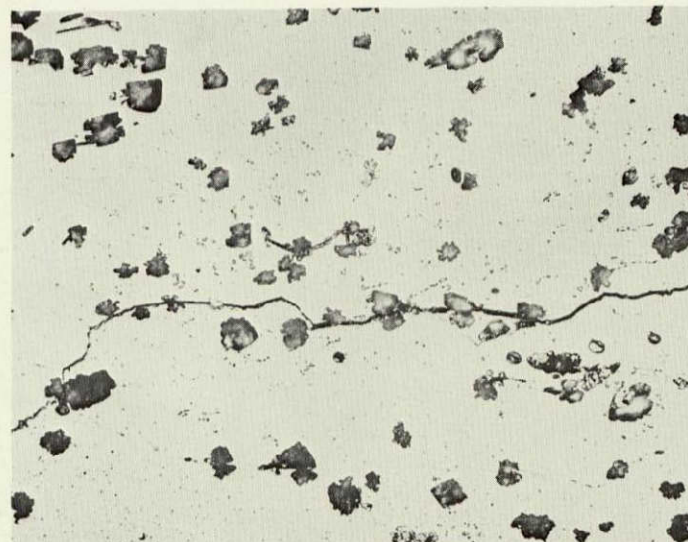
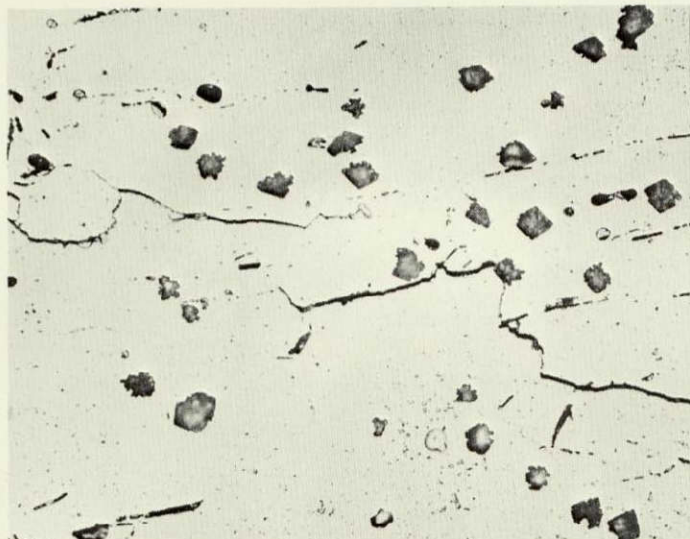
20,000X.

Cracks initiating at low angle to stress in 7075-T6 stressed longitudinally to 75% YS.

Figure 125

As  
Corroded

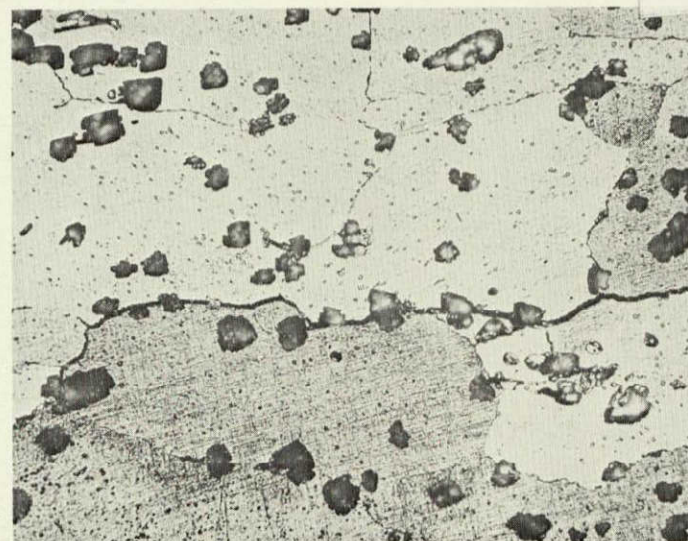
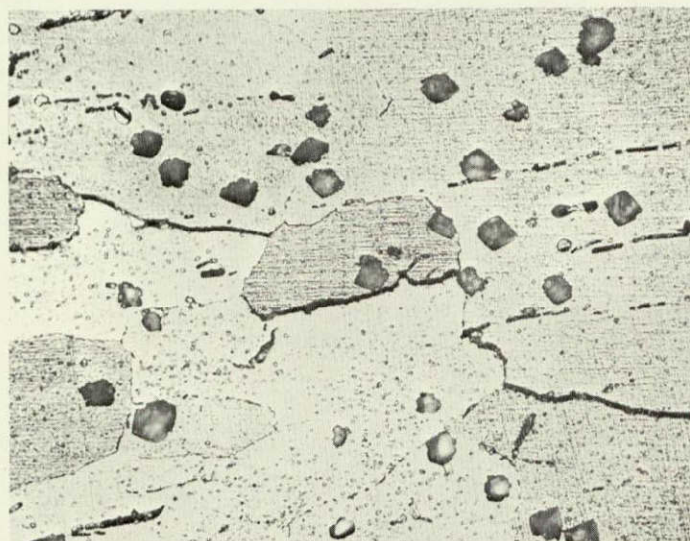
↑  
Stress  
↓



As  
Corroded

NOT REPRODUCIBLE

Keller's  
Etch



Keller's  
Etch

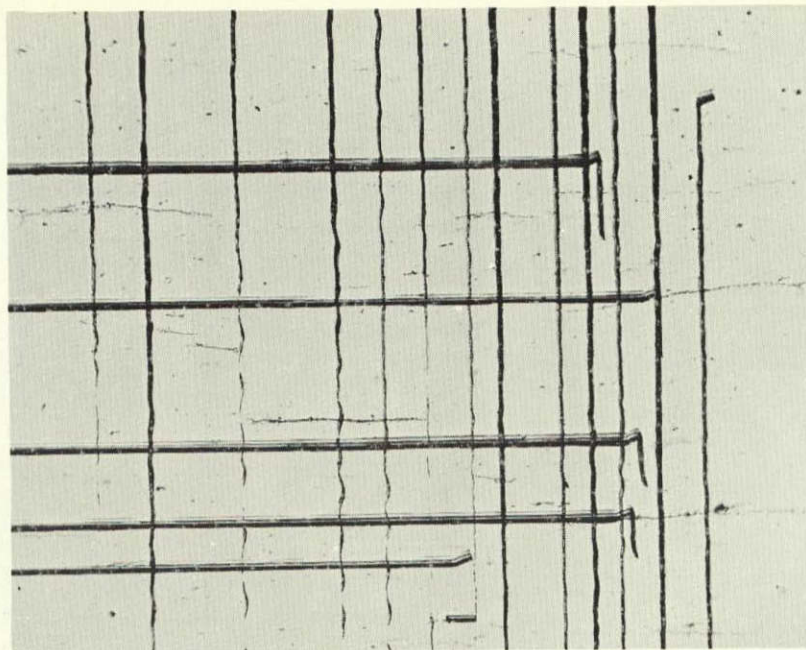
Crack development in pre-pitted specimen of 2219-T37  
stressed 75% Y.S. short transversely (X500).

Figure 126

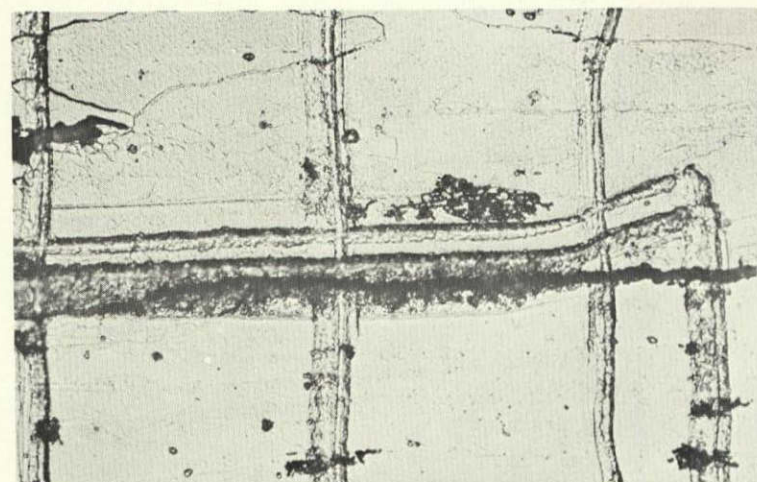
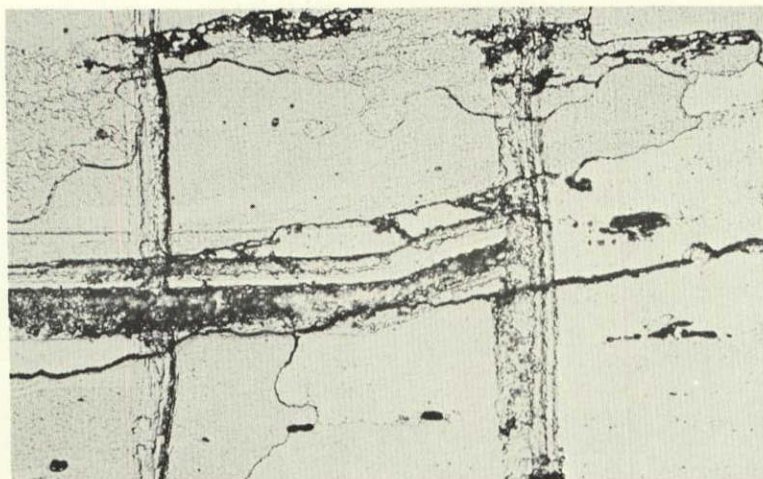


163031  
163045  
163048

↑ Stress ↓



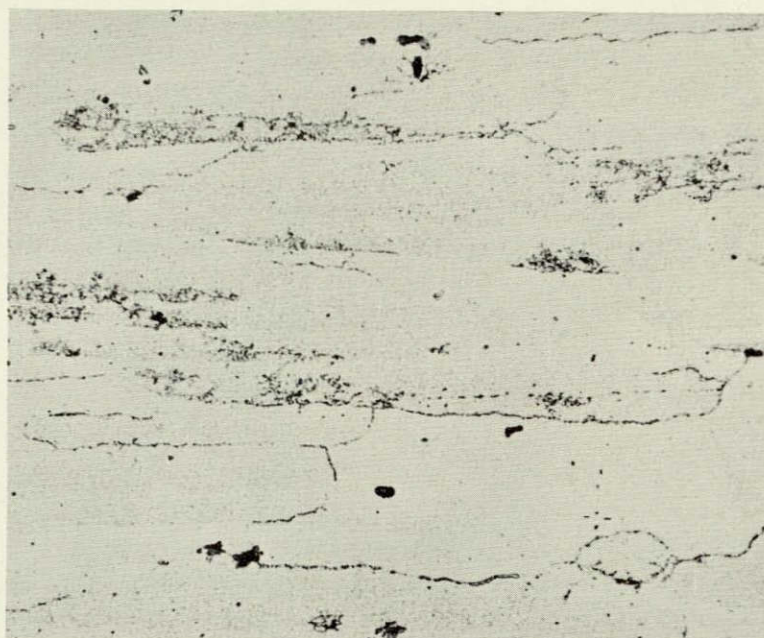
As Corroded  
50X



Keller's  
Etch  
500X

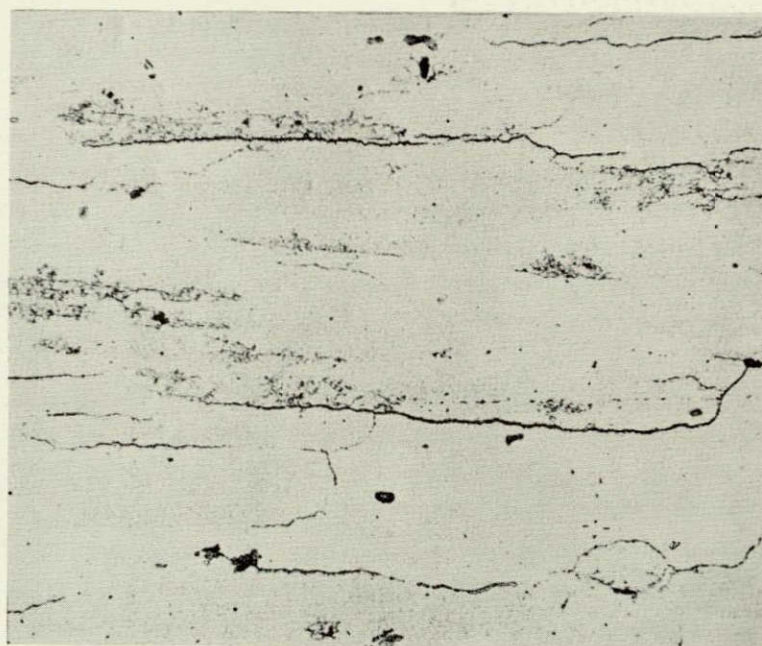
Crack initiation in relation to scratches.  
7075-T6 stressed 75% Y.S. short transversely.

Figure 127



As-corroded

↑ Stress ↓



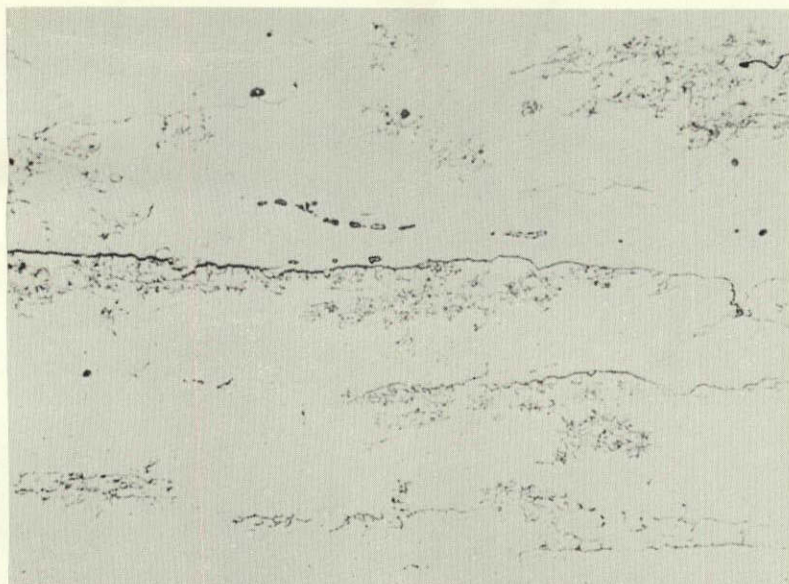
Stressed

Widening of corrosion crevices  
in 7075-T6 corroded and then stressed  
short transversely to 90% YS. (X500)

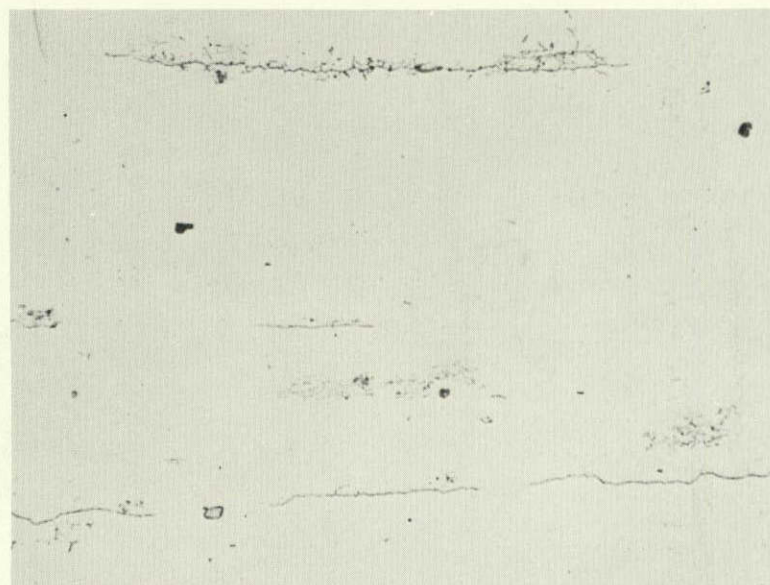
Figure 128



Area A

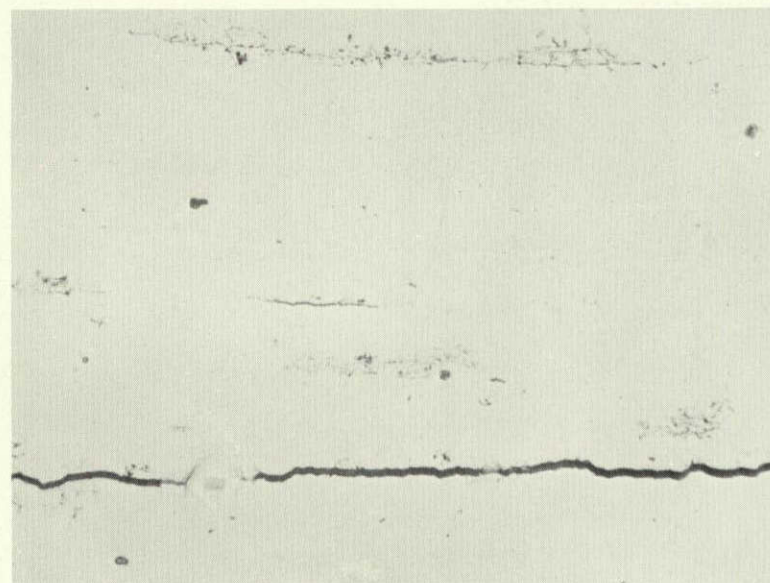
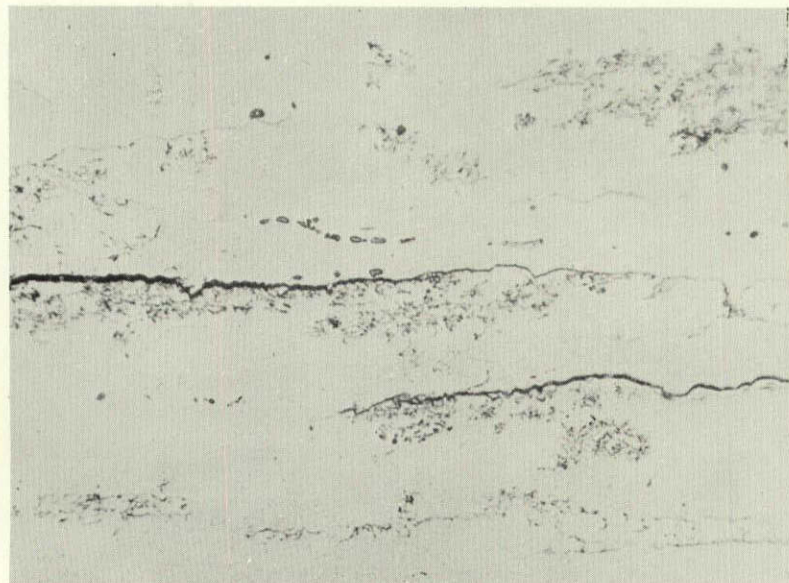


Area B



Corroded  
20 min.,  
then stressed  
S.T. to 75% YS

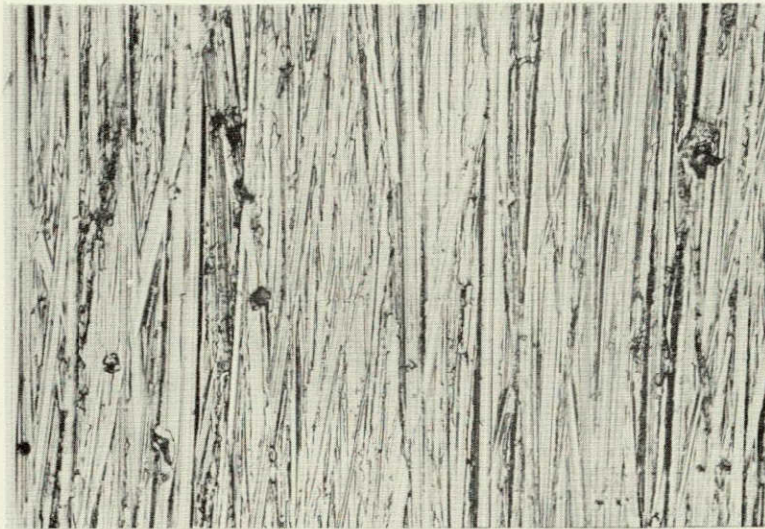
↑  
STRESS  
↓



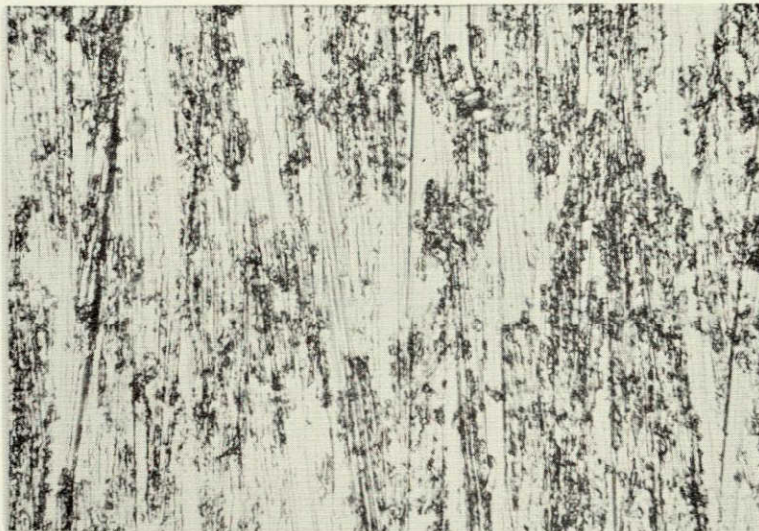
Above after  
additional  
15 min.  
exposure

Stress corrosion crack initiation in pre-corroded specimen of 7075-T6. (X500)

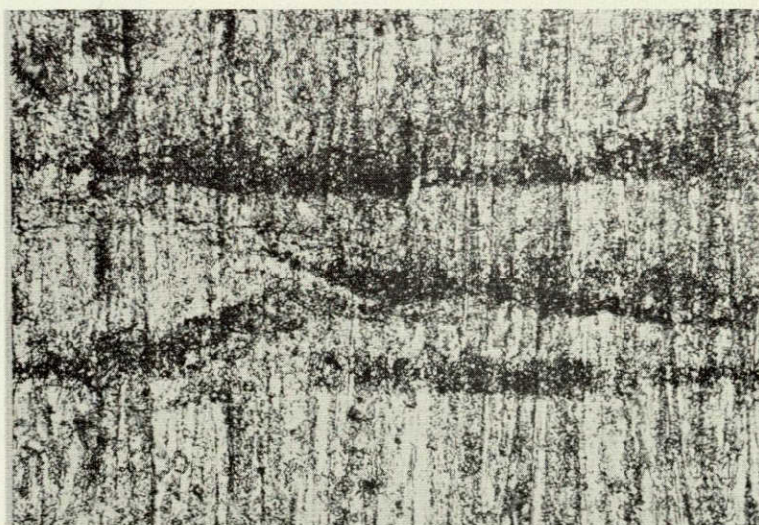




Not corroded



10 min.



60 min.

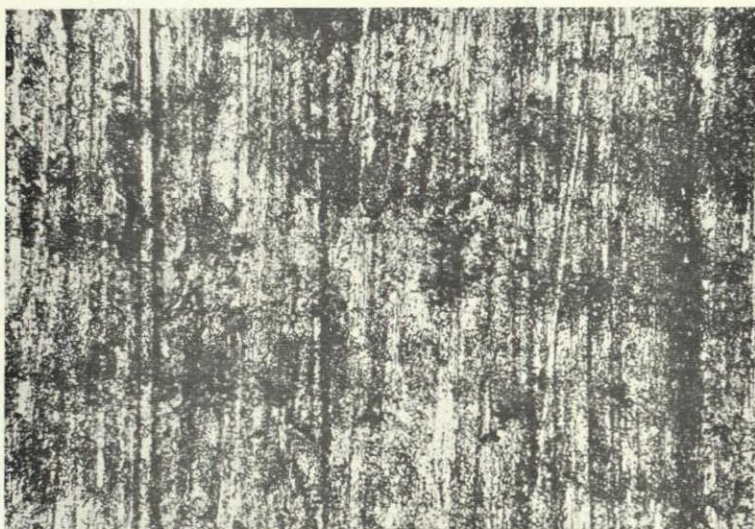
Progress of corrosion of unstressed 7075-T6  
with 3-0 metallographic paper finish. (X500)

Figure 130

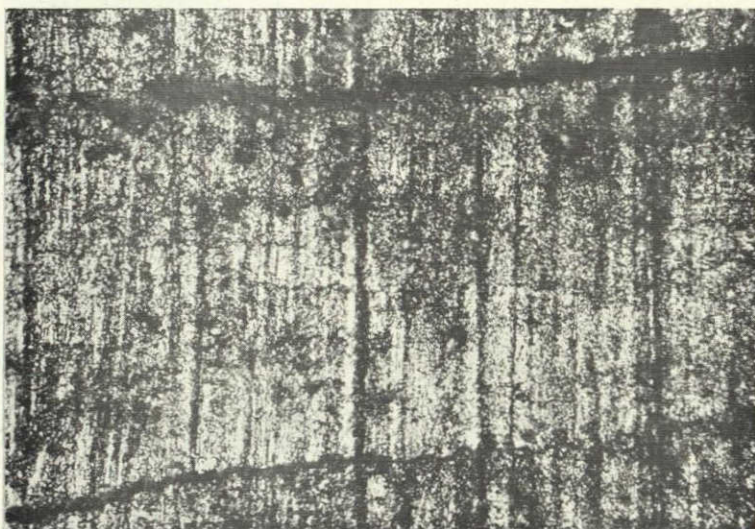




15 min.



30 min.



90 min.

↑ Stress ↓

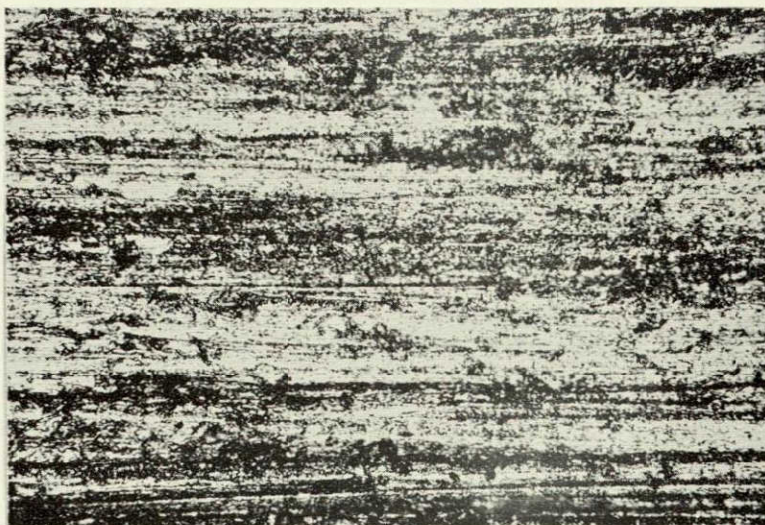
Crack development in 7075-T6  
given 3-0 metallographic paper finish,  
stressed to 75% YS short transversely  
and exposed to pH1 solution. Abrasion  
marks in short transverse direction.

(X500)

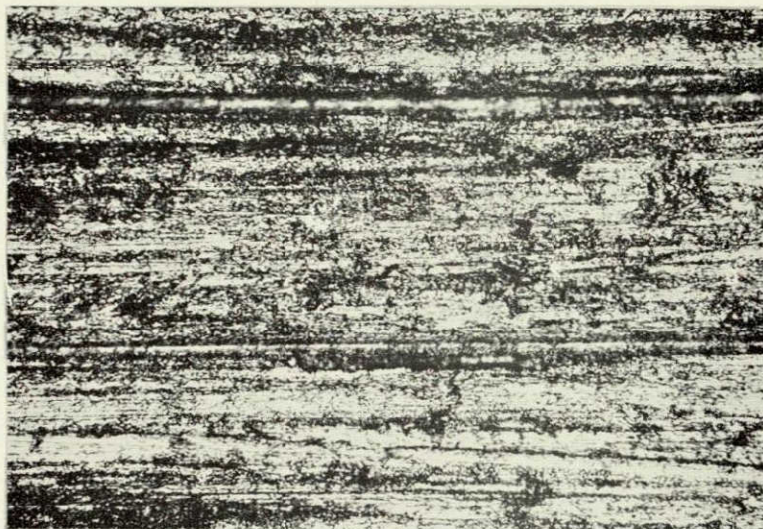
Figure 131

164321  
164322  
164361





15 min.



30 min.



90 min.

↑  
Stress  
↓

NOT REPRODUCIBLE

Same as Fig. 131 but abrasion  
marks longitudinal. (X500)

Figure 132



← STRESS →



Cross section of crack seen in Fig. 132 (X500).

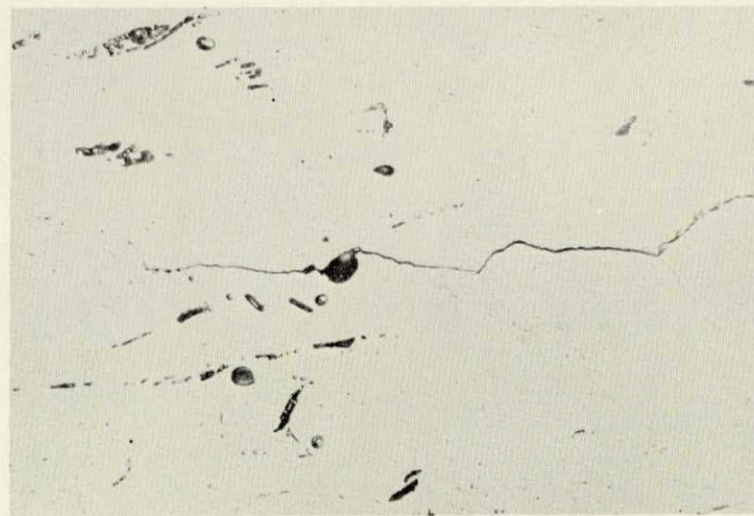
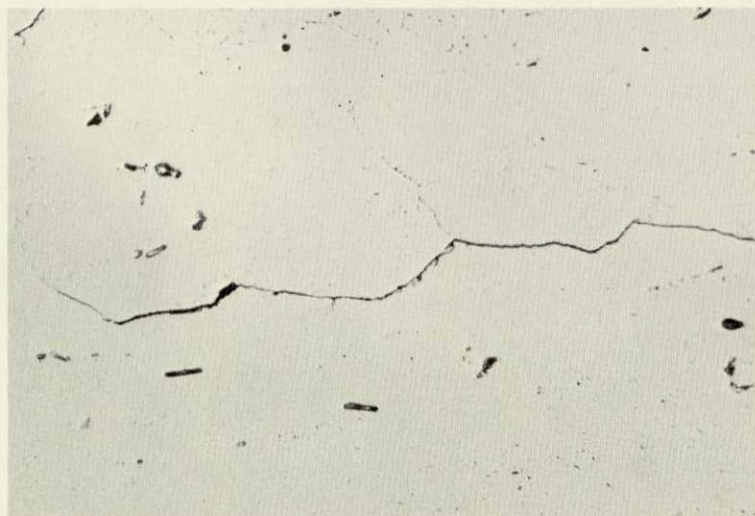
Figure 133

164075-77



As-coated

↕ Stress ↗

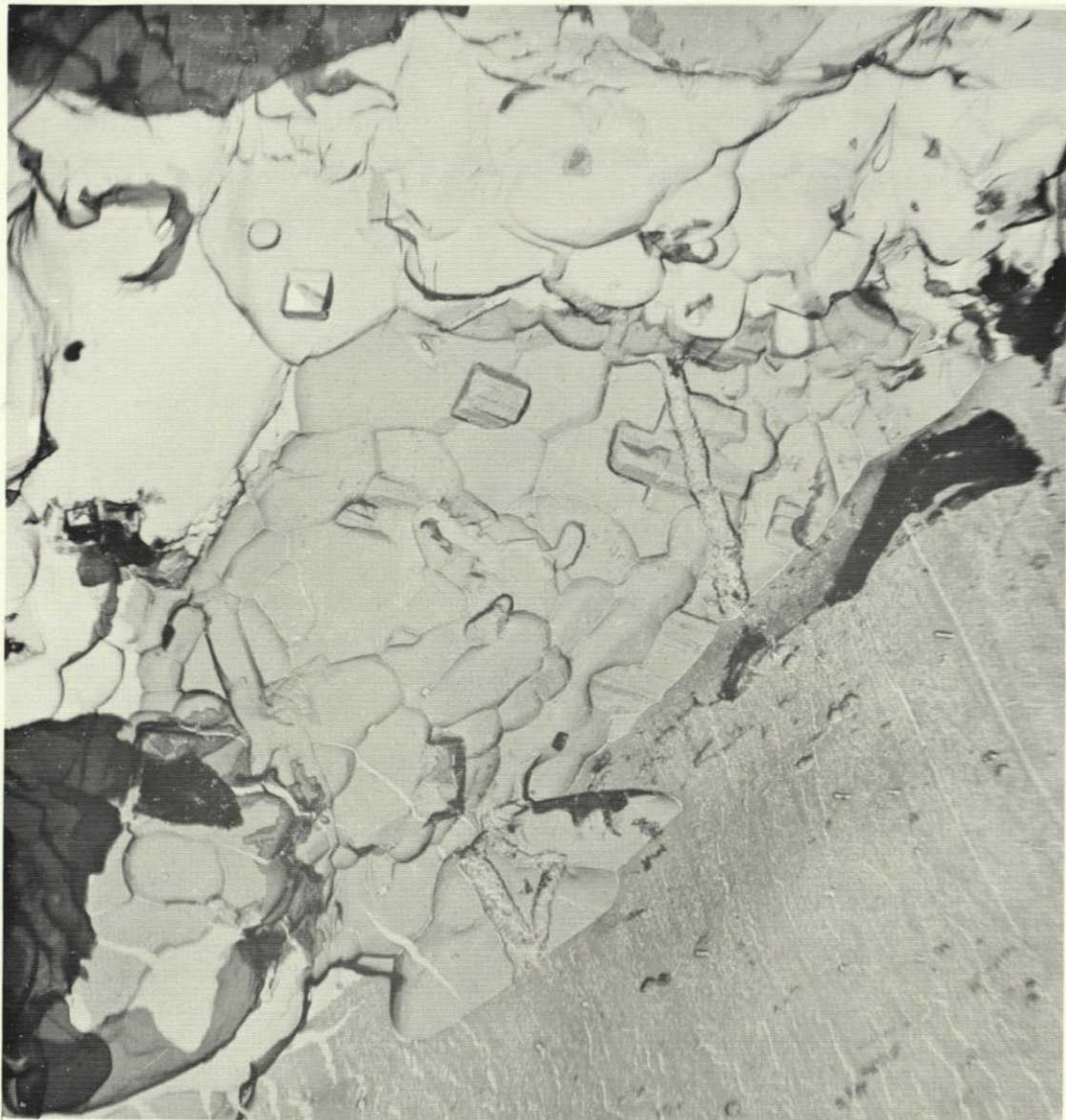


Exposed  
10 minutes

Crack initiation in 2219-T37 given 18V barrier oxide coating and stressed short transversely to 75% YS. (X500)

Figure 134





Dual-Oxide Replica

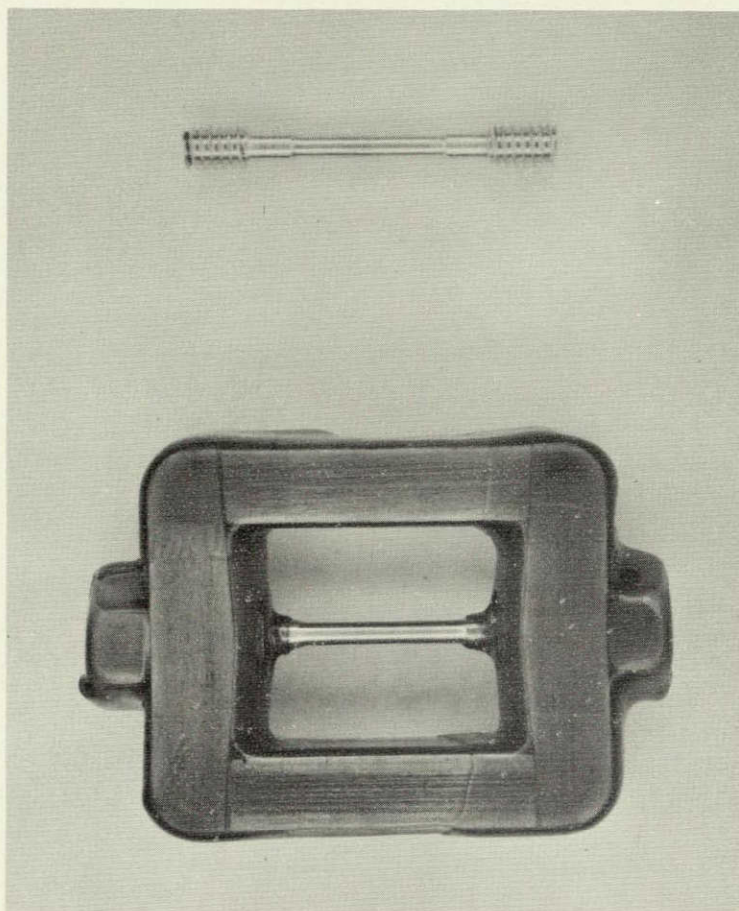
2219-T37

7,500X

A small stress-corrosion crack which was replicated in the thick oxide of the surface seen at the lower right. The extension of this crack during the second immersion is replicated in thinner oxide.

Figure 135



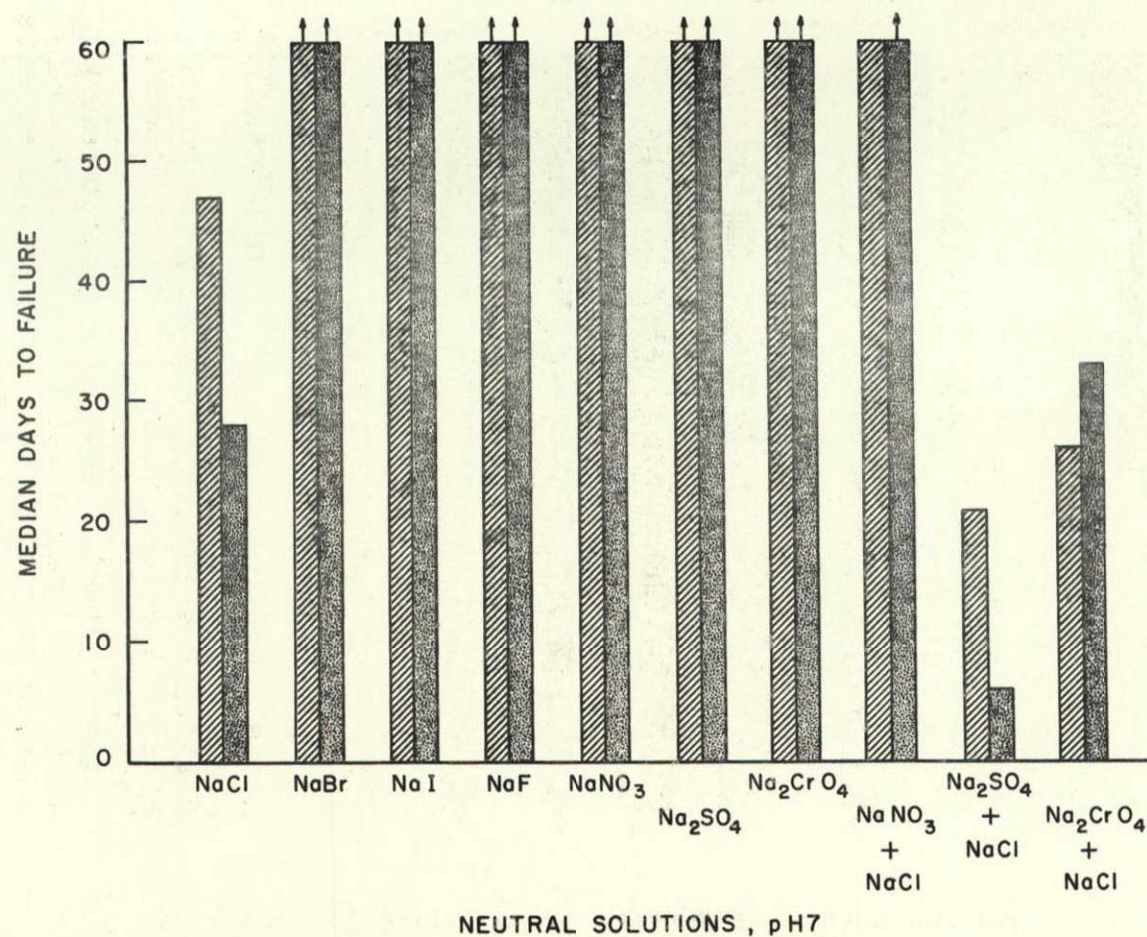


Actual size photograph of an 0.125 in. diameter x 2 in. long threaded-end tension specimen (top) together with a similar specimen assembled in an Alcoa "constant deformation" type stressing frame (bottom). The latter was covered with a strippable cellulose acetate coating to prevent electrochemical effects between specimen and frame.

Figure 136

0.125 IN. DIA , SHORT TRANSVERSE TENSILE SPECIMENS - STRESSED 75% Y.S.

 7075-T651   
  2219-T37   
 ↑ SPECIMENS (3) DID NOT FAIL



EFFECT OF ENVIRONMENT ON RESISTANCE TO STRESS-CORROSION CRACKING  
FIGURE 137

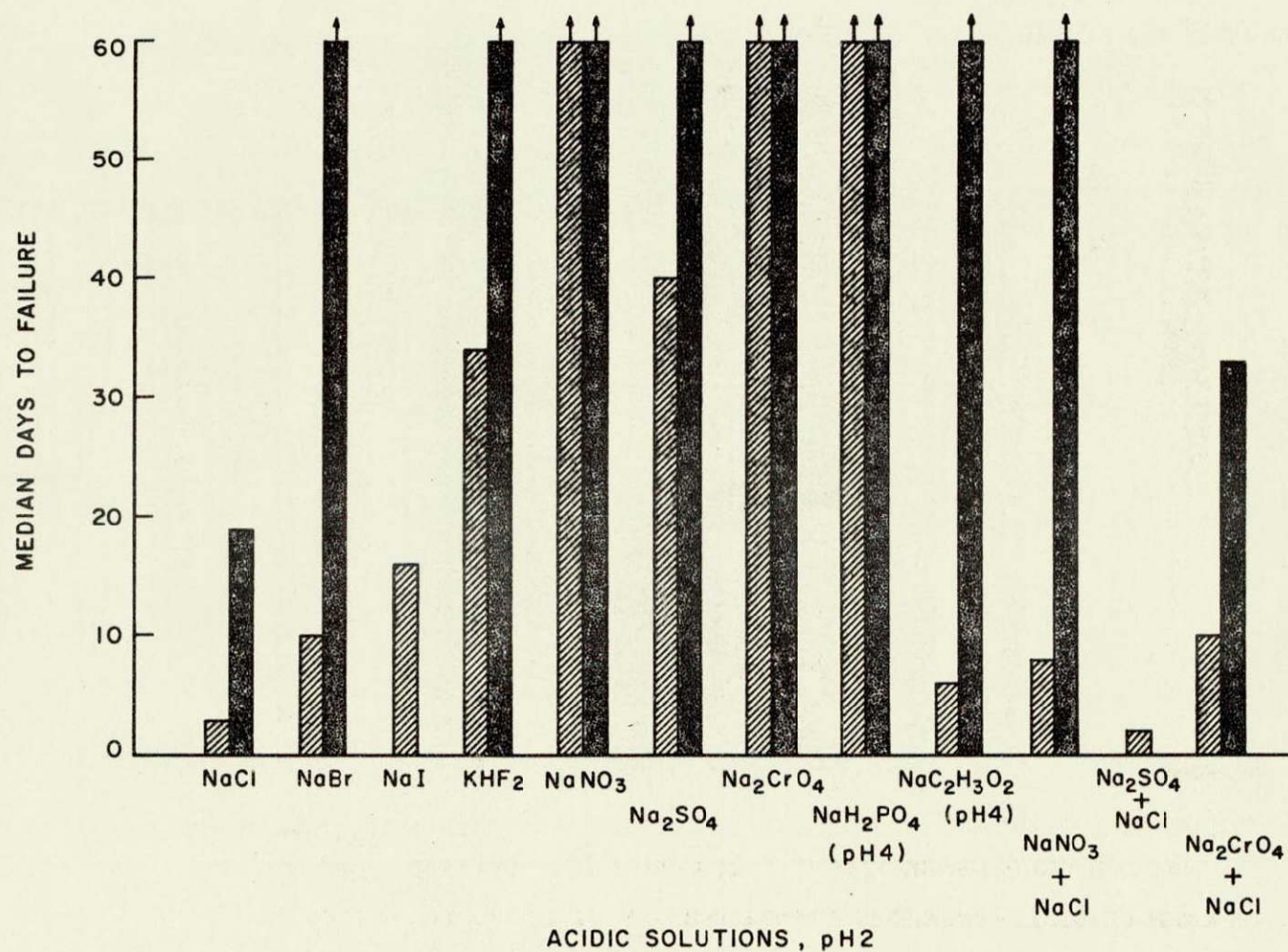


O.125 IN. DIA , SHORT TRANSVERSE TENSILE SPECIMENS - STRESSED 75% Y.S.

7075 - T651

2219 - T37

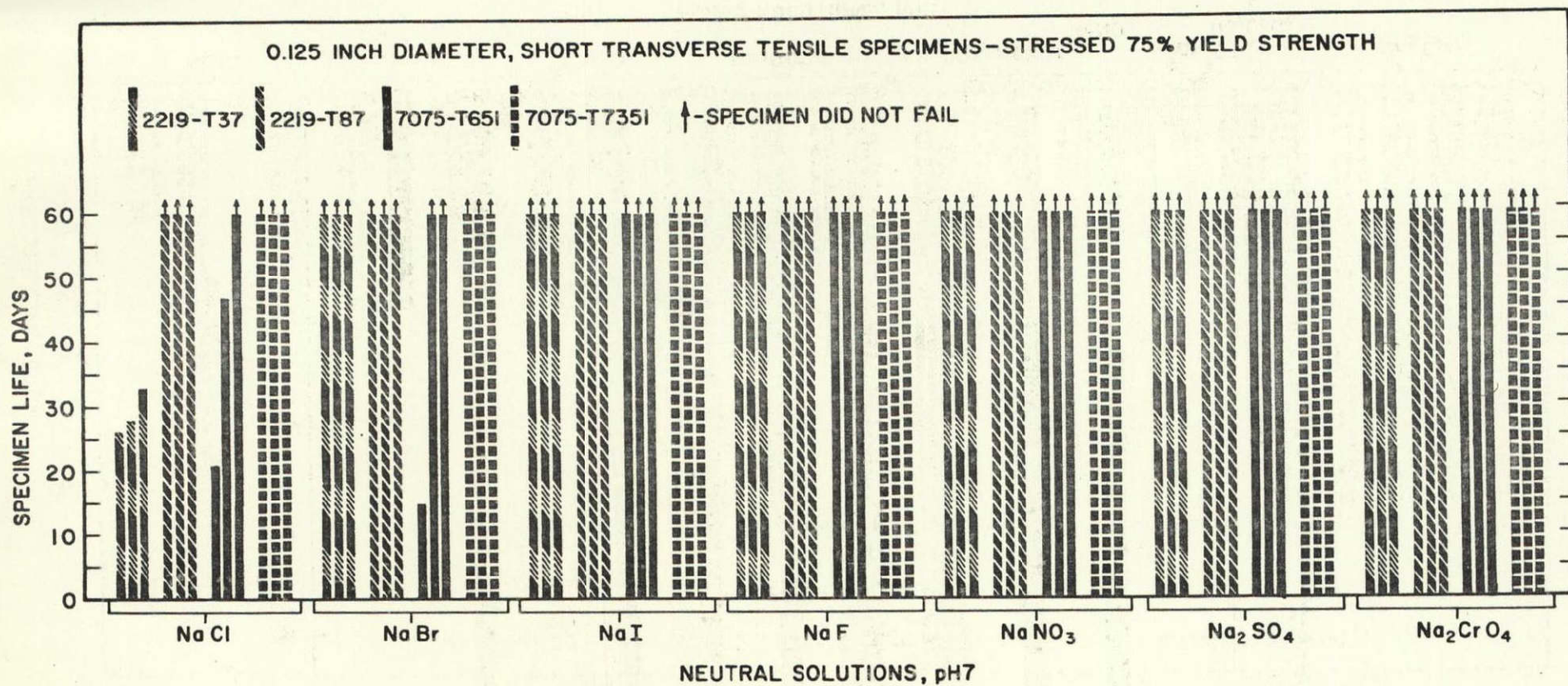
SPECIMENS (3) DID NOT FAIL



EFFECT OF ENVIRONMENT ON RESISTANCE TO STRESS-CORROSION CRACKING

FIGURE 138

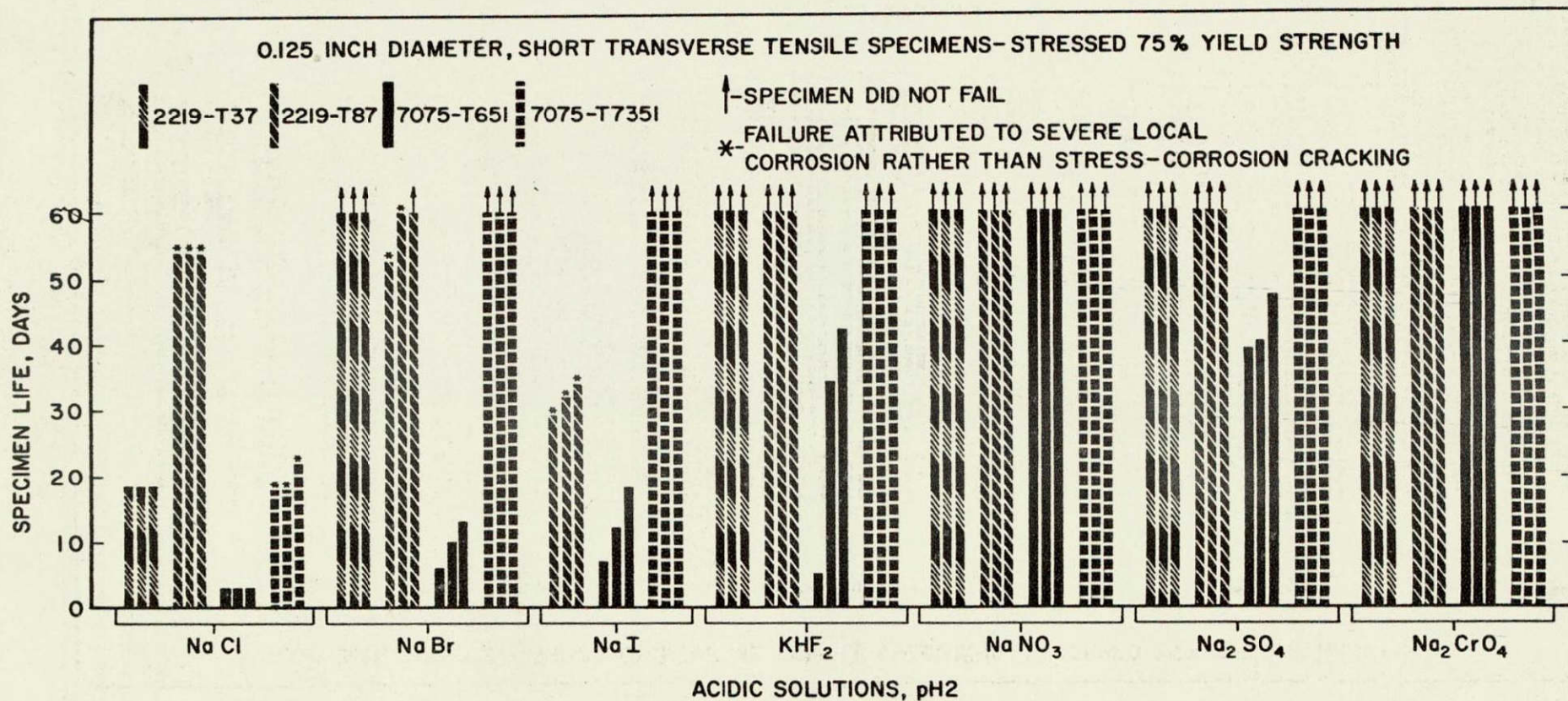




EFFECT OF ENVIRONMENT ON RESISTANCE TO STRESS—CORROSION CRACKING

FIGURE 139

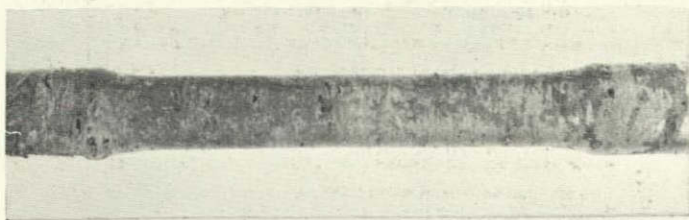




EFFECT OF ENVIRONMENT ON RESISTANCE TO STRESS-CORROSION CRACKING

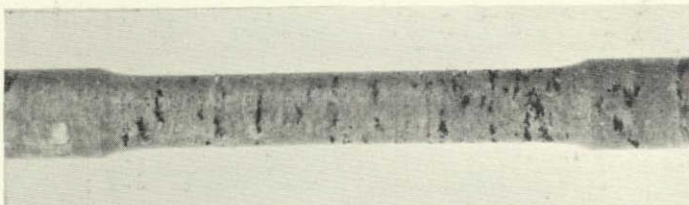
FIGURE 140





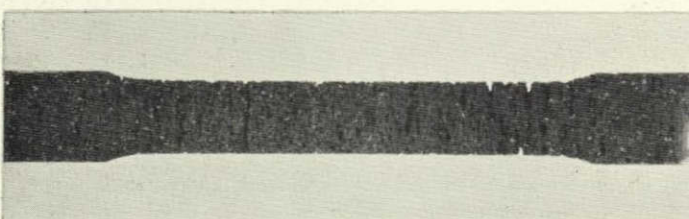
0.5N NaCl + 0.5N Na<sub>2</sub>SO<sub>4</sub>  
(H<sub>2</sub>SO<sub>4</sub>)

Visual Rating - Negligible  
Exposure Period - 4 days  
Percent Loss in T.S. - 55



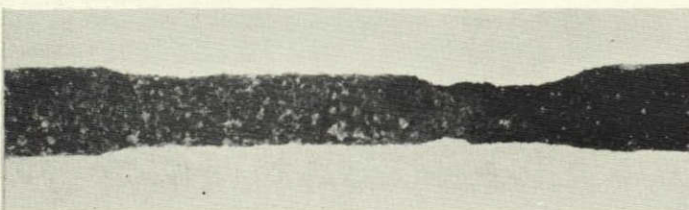
1N NaCl (HNO<sub>3</sub>)

Visual Rating - Mild, directional  
Exposure Period - 7 days  
Percent Loss in T.S. - 49



1N NaCl + 1N AlCl<sub>3</sub>  
(HCl)

Visual Rating - Severe, directional  
Exposure Period - 10 days  
Percent Loss in T.S. - 82



4N NaCl + 0.5N KNO<sub>3</sub>  
(HNO<sub>3</sub>)

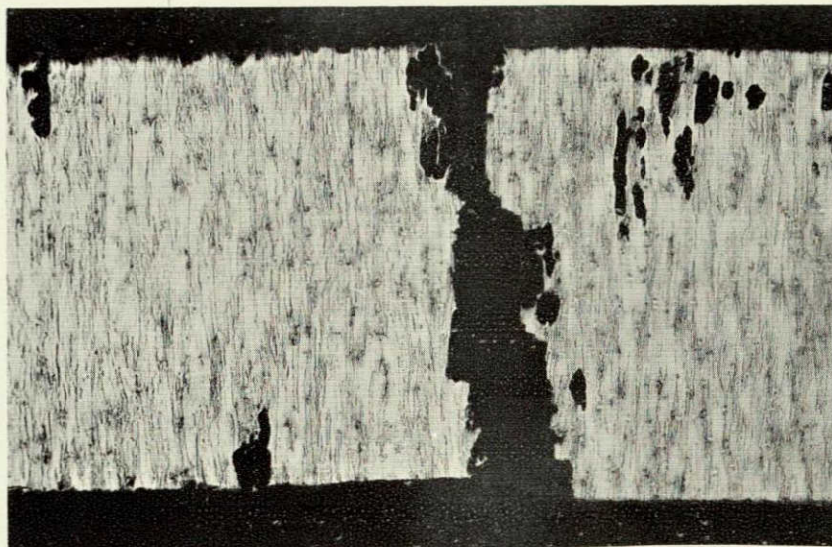
Visual Rating - Severe, random  
Exposure Period - 19 days  
Percent Loss in T.S. - 68

Illustrates the varied corrosion patterns of 7075-T7351 alloy in acidified solutions containing sodium chloride. The specimens shown were exposed unstressed, and were removed from test at times corresponding to the failure of stressed specimens.

(Mag. 3X)

Figure 141





Etch: Keller's

Mag. 20X

Stressed 75% Y.S. - Failed 4 days



Etch: Keller's

Mag. 100X

Unstressed - 4 days



Etch: Keller's

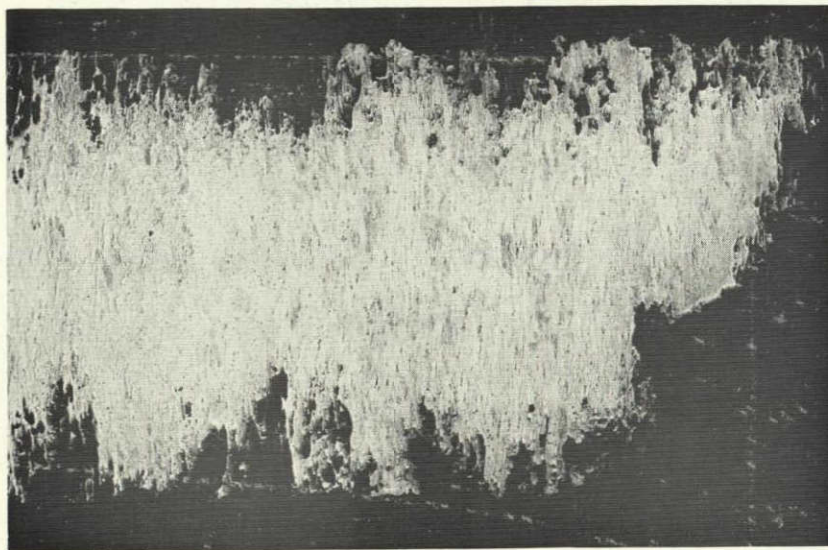
Mag. 100X

Stressed 75% Y.S. - F 4 days

7075-T7351 exposed to 0.5N NaCl + 0.5N Na<sub>2</sub>SO<sub>4</sub>  
pH2 (H<sub>2</sub>SO<sub>4</sub>). Sections through corrosion pits in  
specimens which visually showed negligible attack.

Figure 142





Etch: Keller's

Mag. 20X

Stressed 75% Y.S. - Failed 6 days



Etch: Keller's

Mag. 100X

Unstressed - 6 days



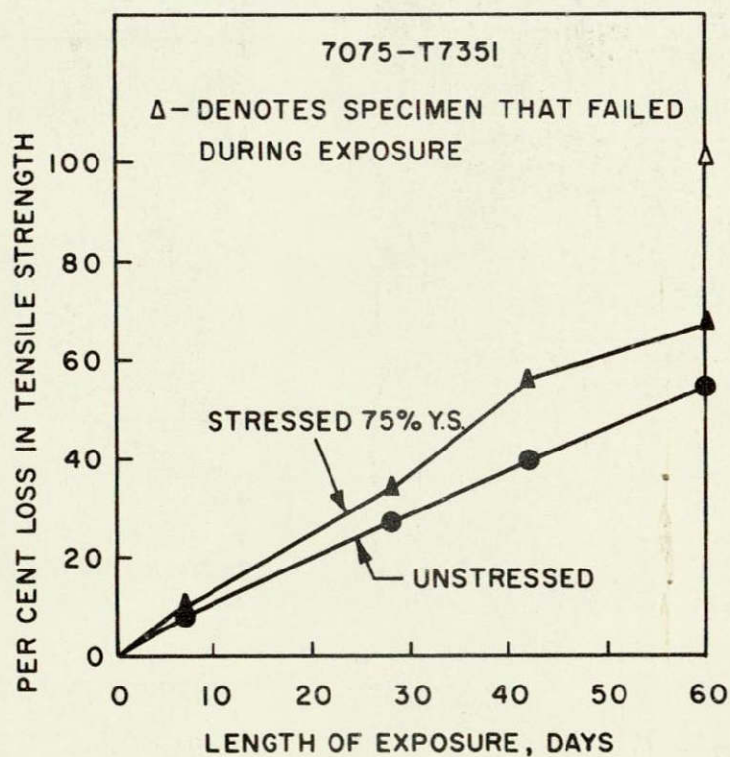
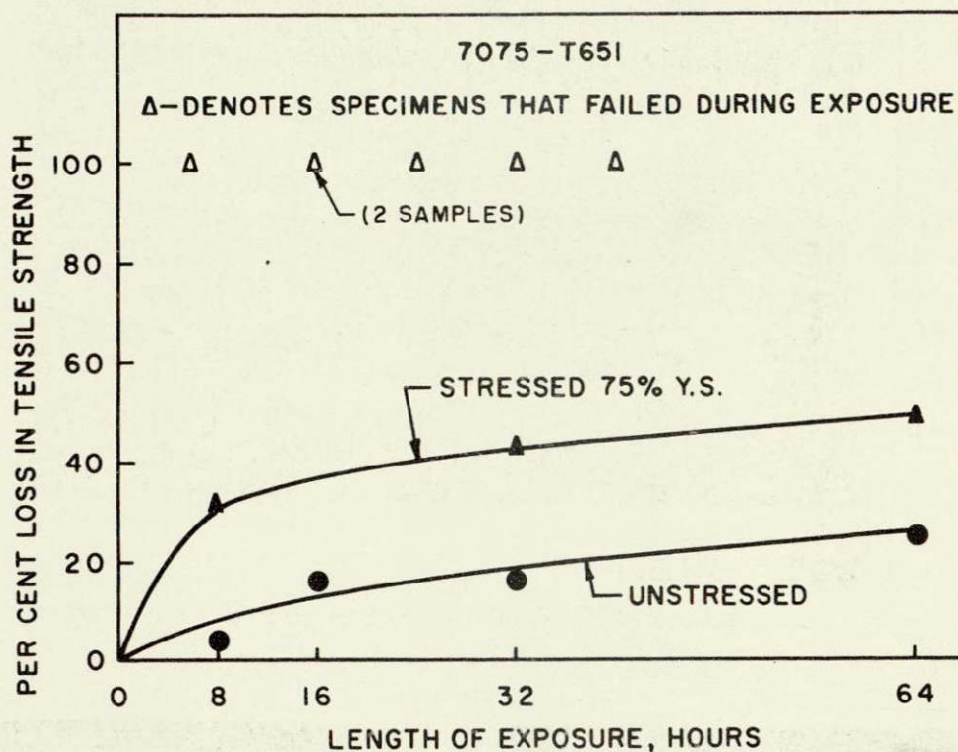
Etch: Keller's

Mag. 100X

Stressed 75% Y.S. - F 6 days

Sections through corrosion pits in 7075-T7351 specimens with a visual corrosion rating of severe, random.

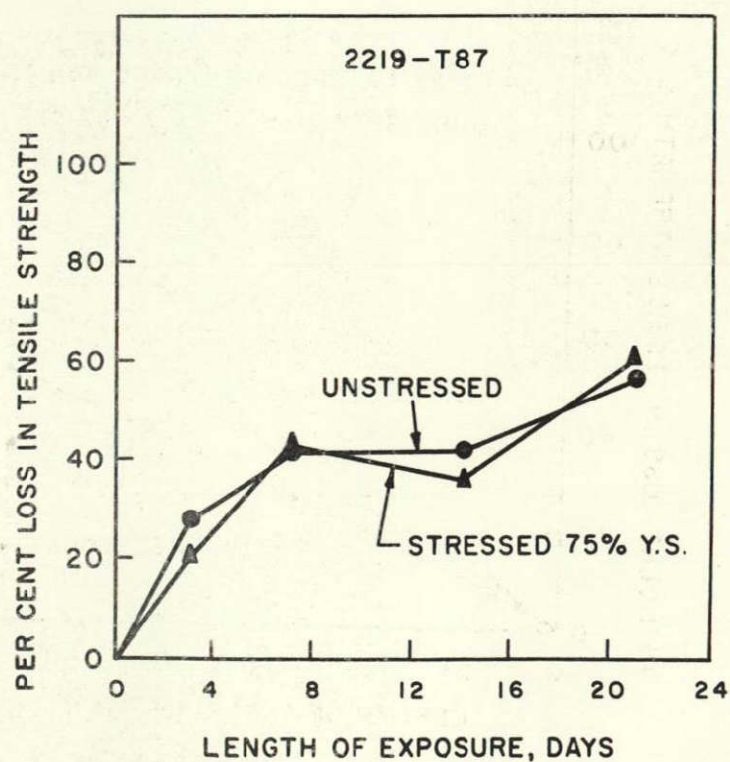
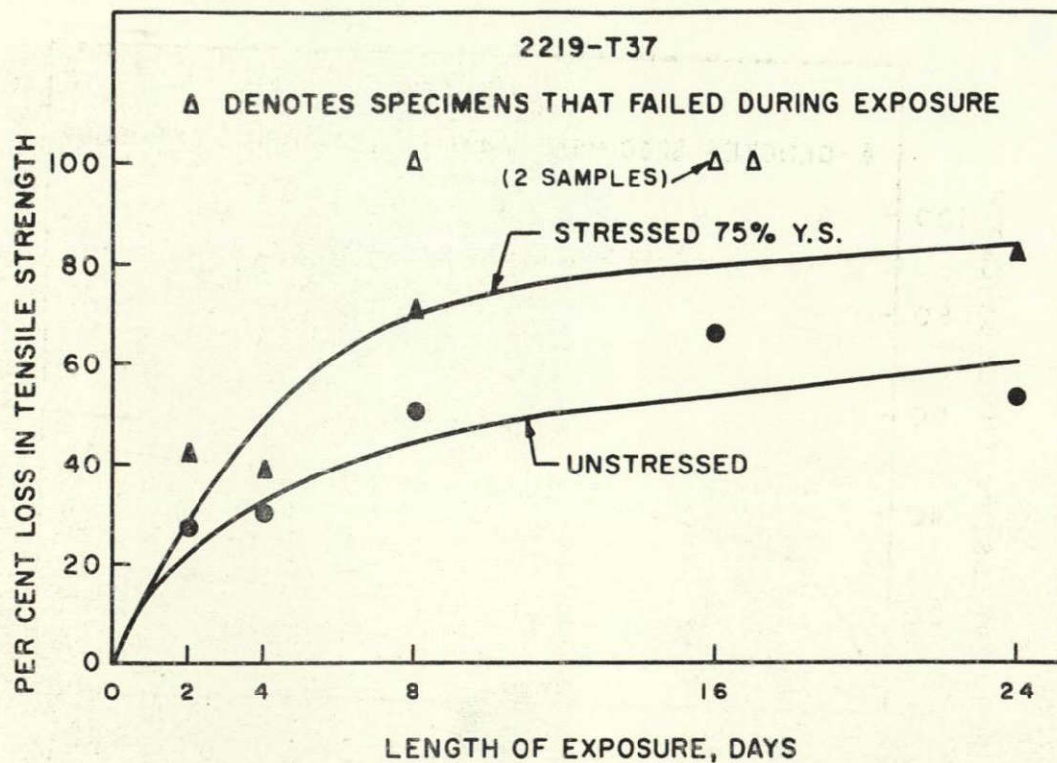
Figure 143



EFFECT OF STRESS ON CORROSION RATE OF 7075 ALLOY IN ACIDIFIED  
NaCl (pH2)

FIGURE 144

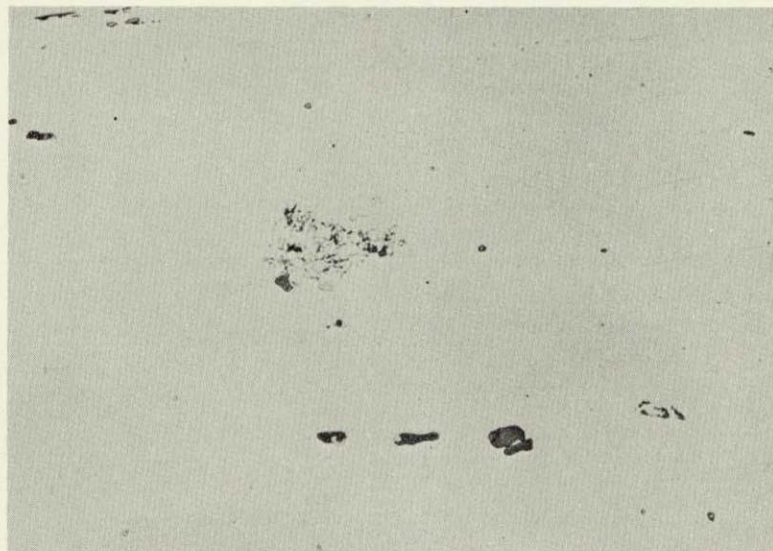




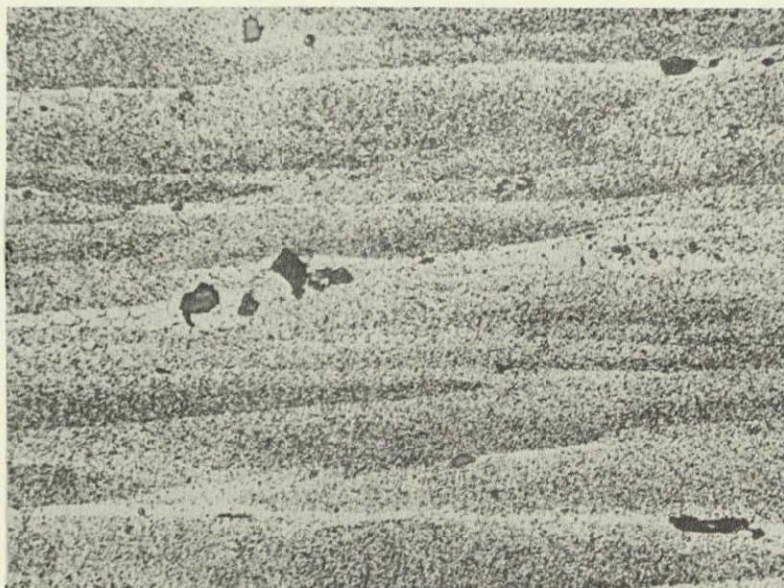
EFFECT OF STRESS ON CORROSION RATE OF 2219 ALLOY IN ACIDIFIED  
NaCl (pH2)

FIGURE 145

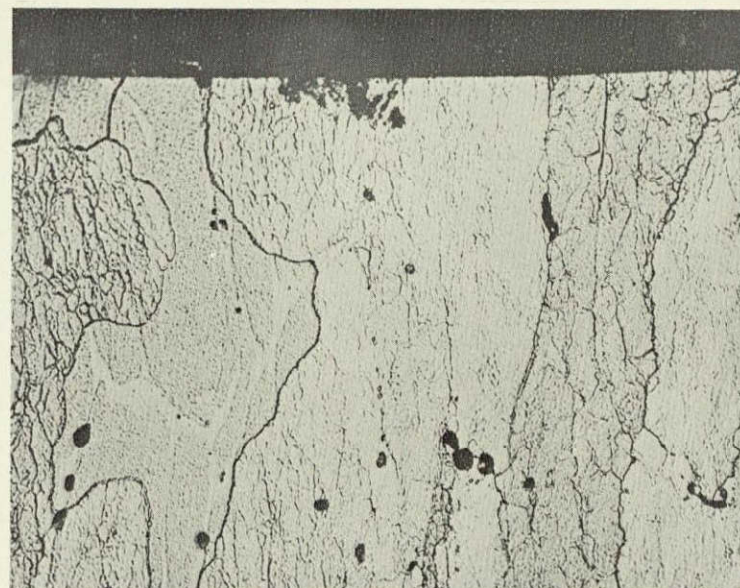
164020  
168090  
168091



Unstressed  
16 hrs



59 hrs  
stressed  
75% YS. S.T.  
surface



59 hrs  
stressed  
X-Sect.  
Keller's  
Etch

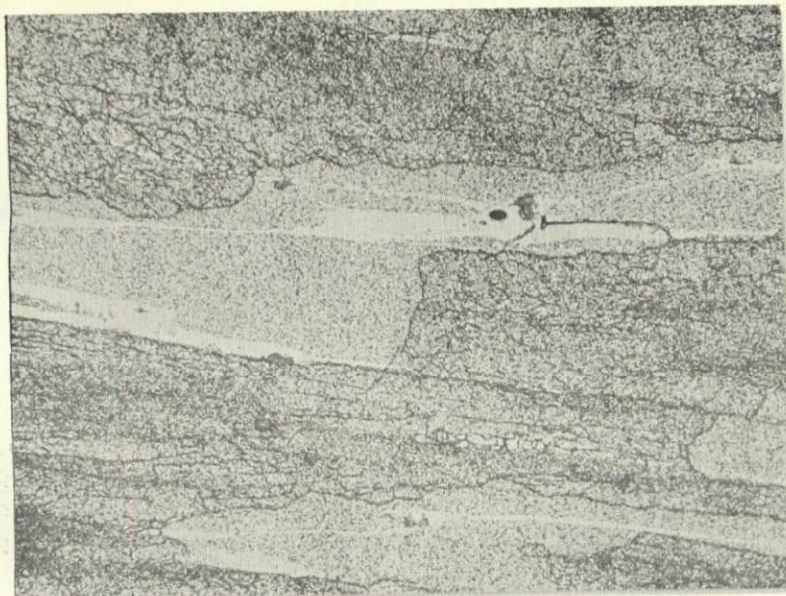
Development of pitting attack in 7075-T6 exposed to 1N NaAc solution at pH4.  
(X500)

Figure 146

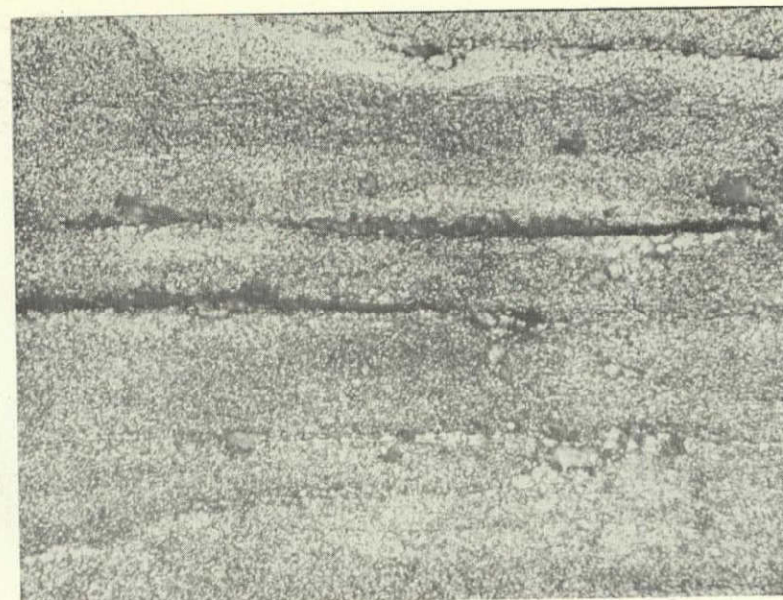


168076  
168077  
168078

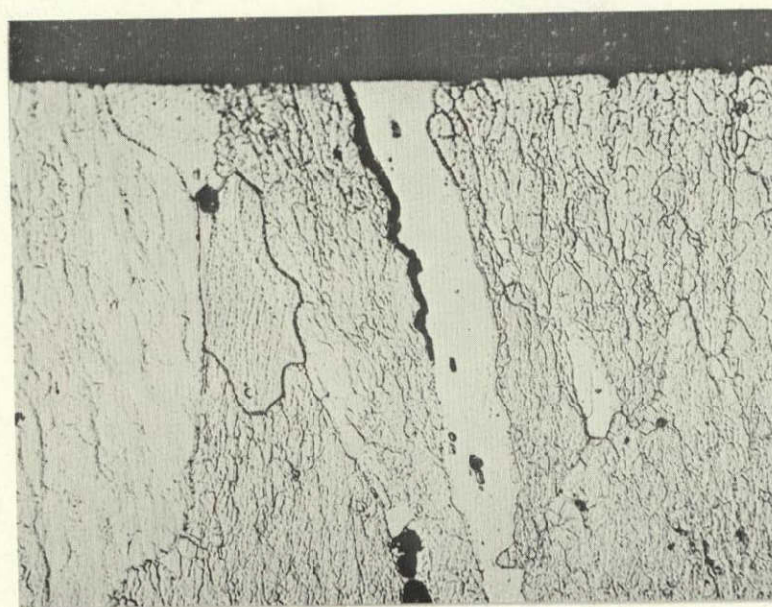
45 min.



↑  
STRESS  
↓



67 hrs



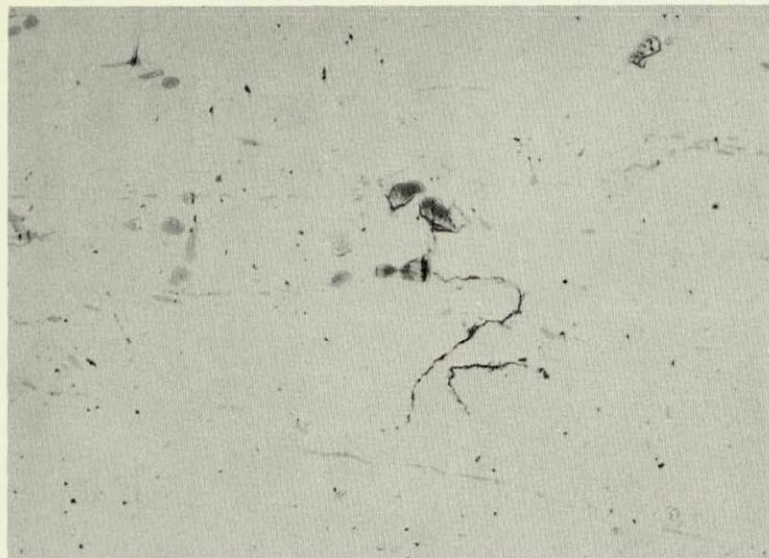
67 hrs  
X-Sect.  
Keller's  
Etch

Crack initiation in 7075-T6 stressed to 75% YS  
S.T. and exposed to 1N Na<sub>2</sub>SO<sub>4</sub> solution at pH2 (X500).

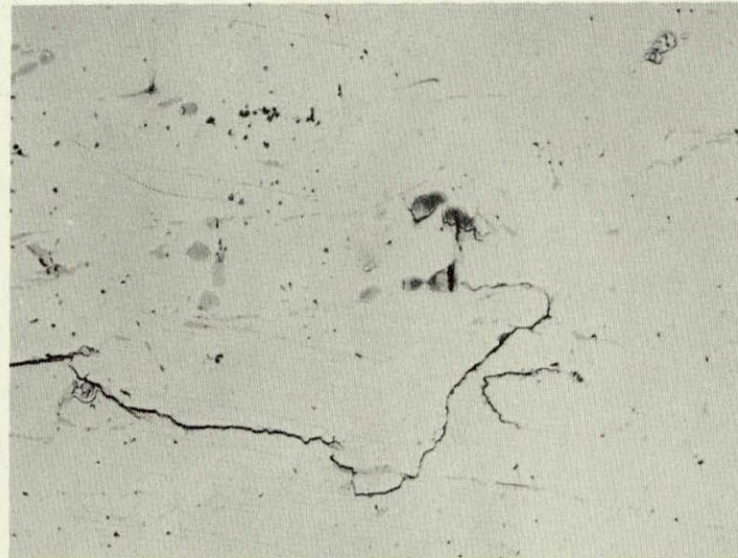
Figure 147



6 min.

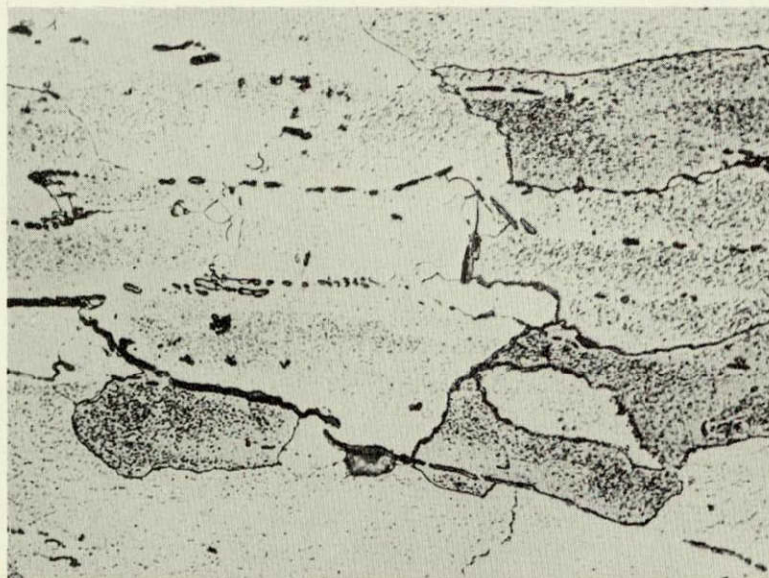


16 min.

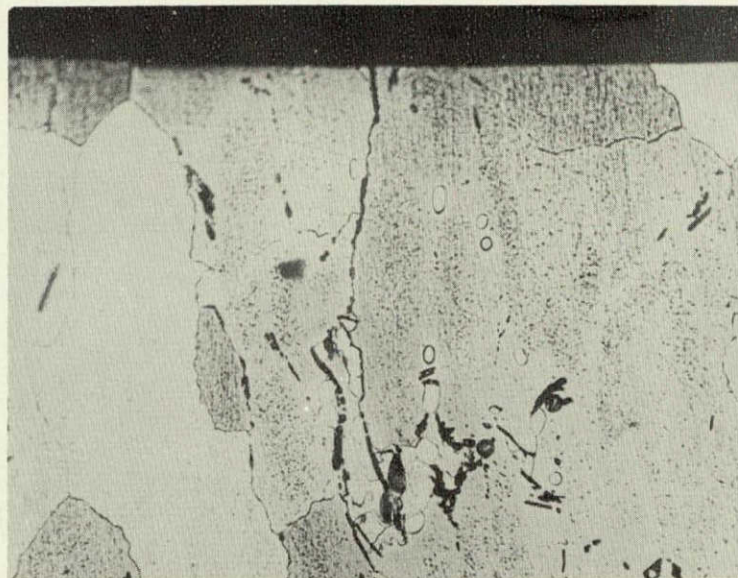


Stress  
↑  
↓

16 min.  
Keller's  
Etch



16 min.  
X-Sect.  
Keller's  
Etch



Tuning fork specimen of 2219-T37 stressed short transversely to 75% YS and exposed to 0.5N NaCl + 0.5N Na<sub>2</sub>CrO<sub>4</sub> solution at pH2. (X500)

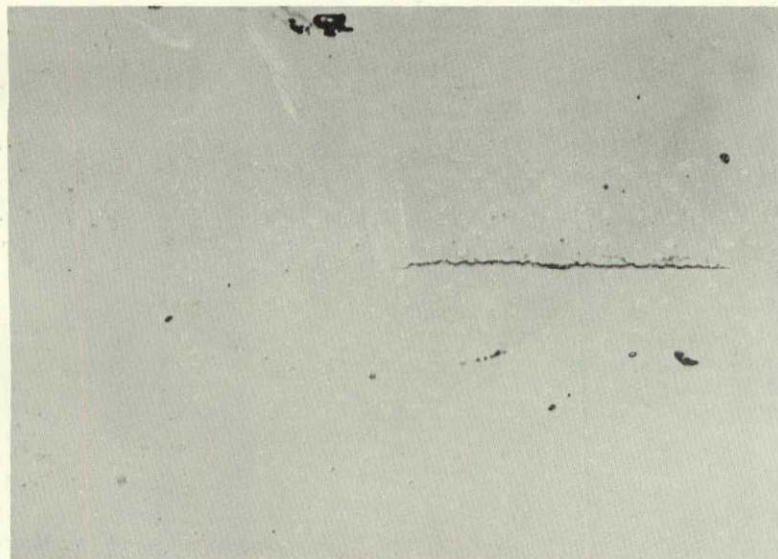
Figure 148



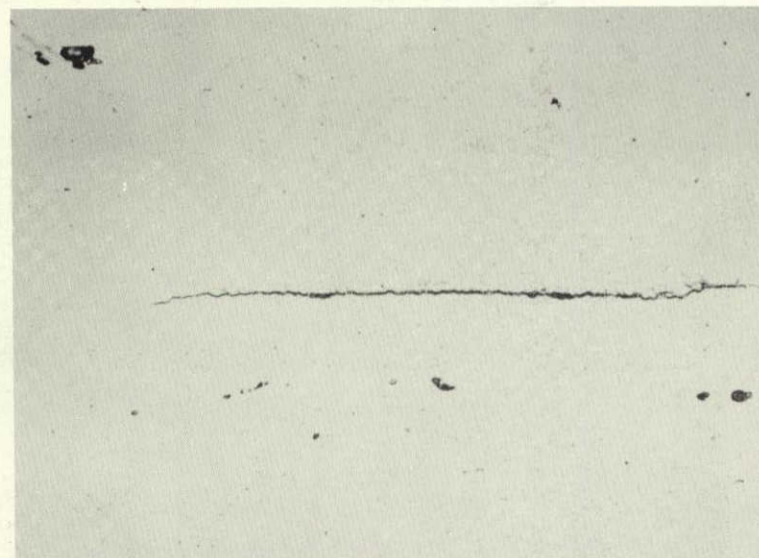
165911  
165913-14  
166219

30 sec.

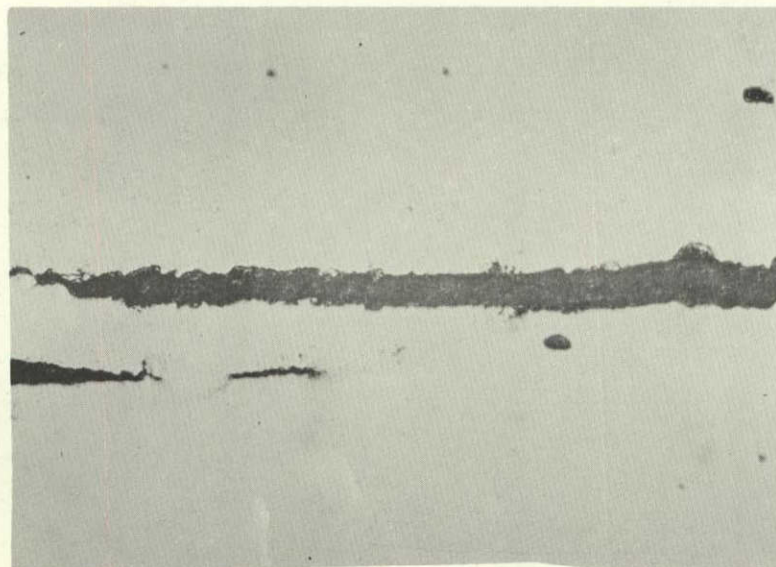
↑  
STRESS  
↓



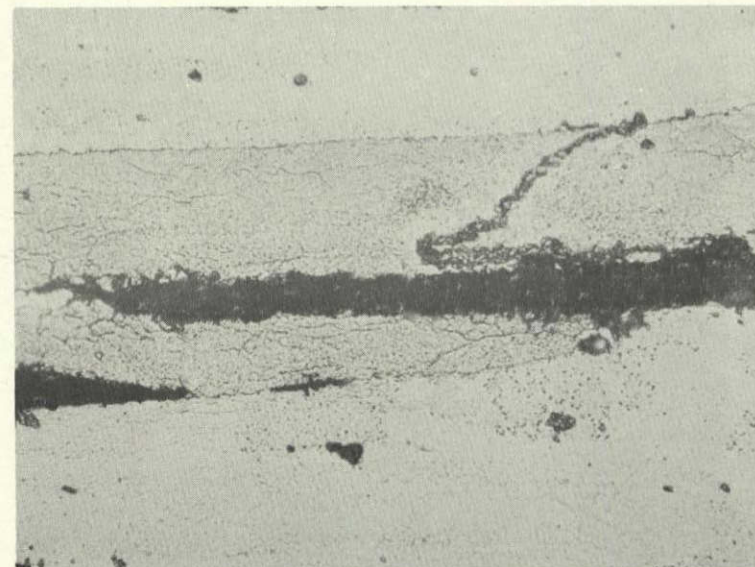
60 sec.



120 sec.



120 sec.  
Keller's  
etch



Crack development in 7075-T6 stressed short transversely to  
75% YS and exposed in 4N NaCl + 0.5N KNO<sub>3</sub> solution at pH 0.4. (X500)

Figure 149

← STRESS →



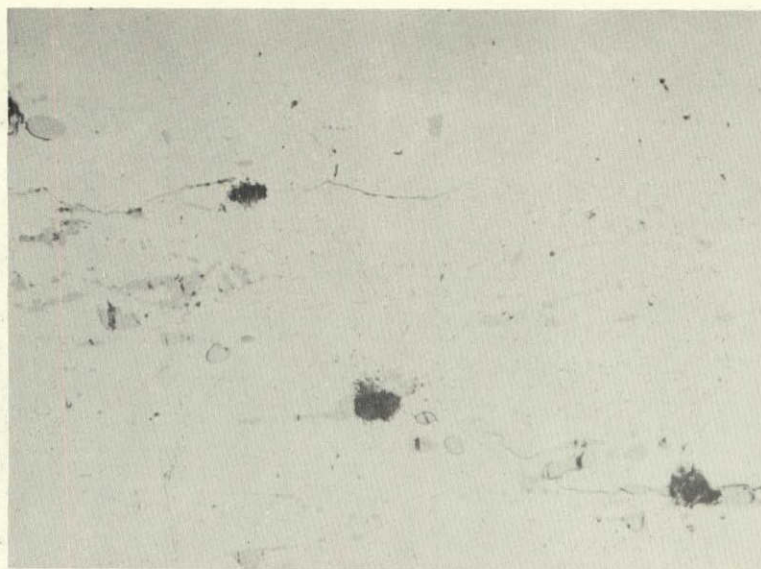
Cross section of specimen in Fig. 149 (X500)

Figure 150

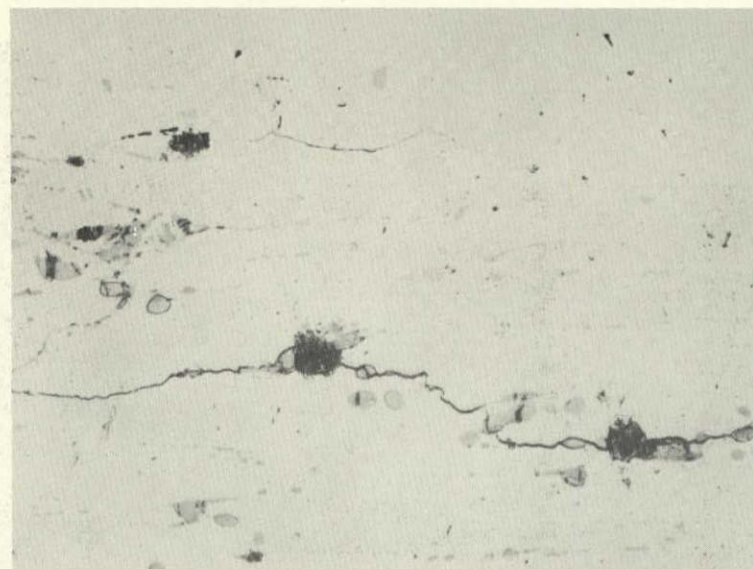


166334-35  
166337  
166791

1 min.

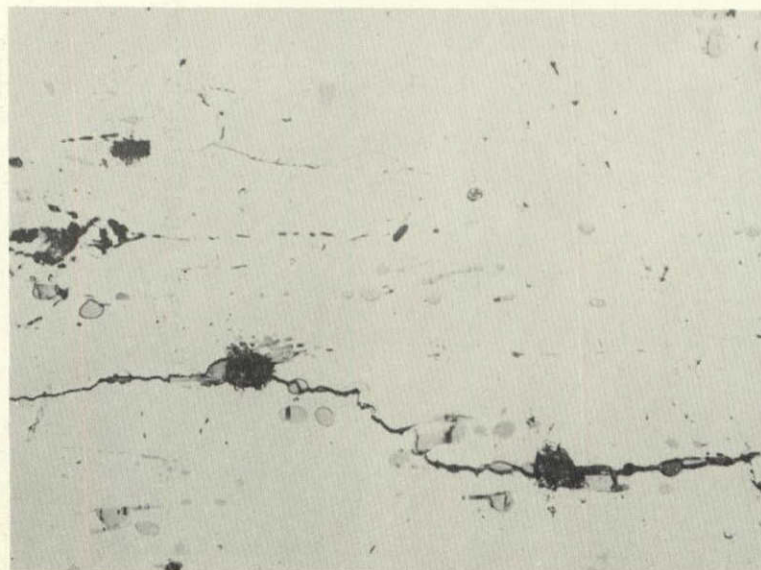


3 min.

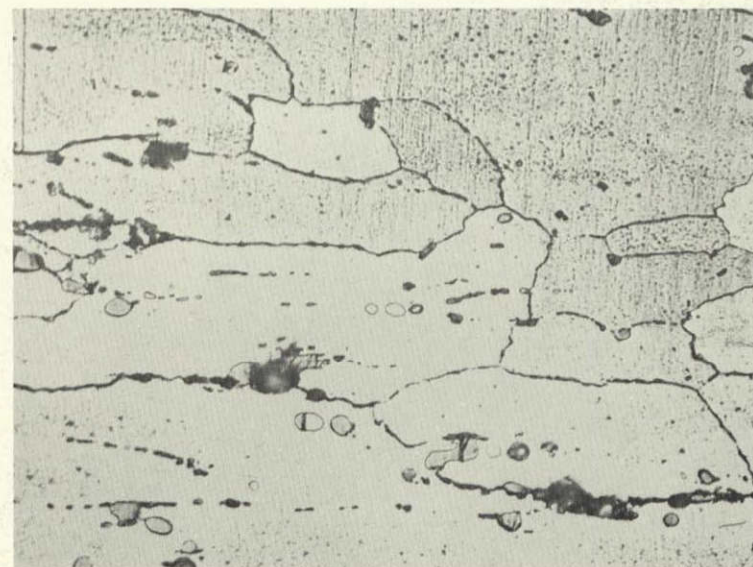


↑  
STRESS  
↓

6 min.



6 min.  
Keller's  
etch



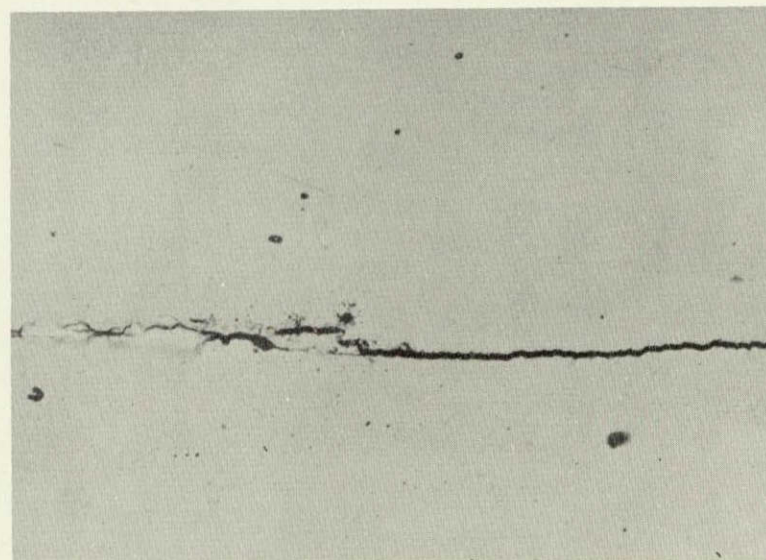
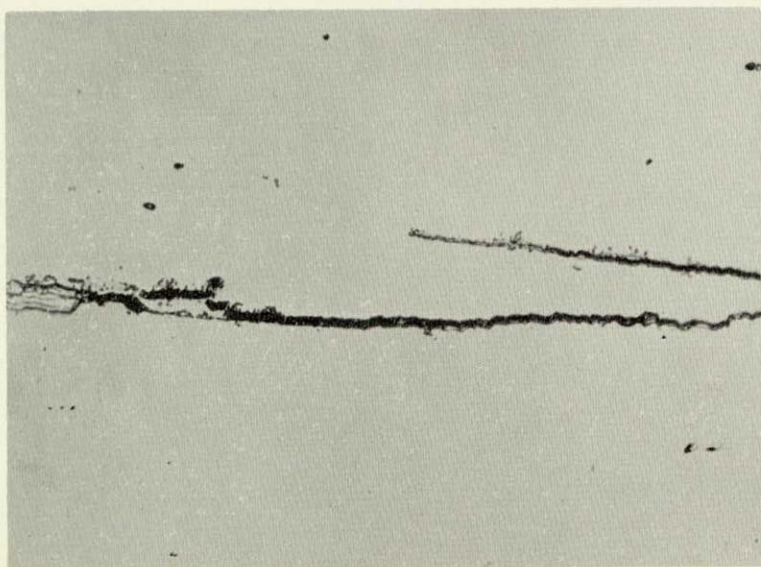
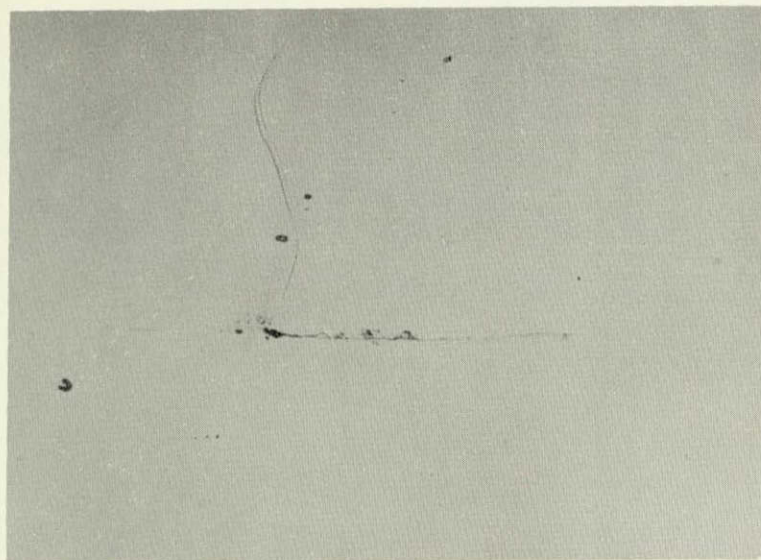
Crack initiation and development in 2219-T37 tuning-fork specimen stressed to 75% YS in short transverse direction and exposed to 4N NaCl + 0.5N KNO<sub>3</sub> solution at pH 0.4. (X500)



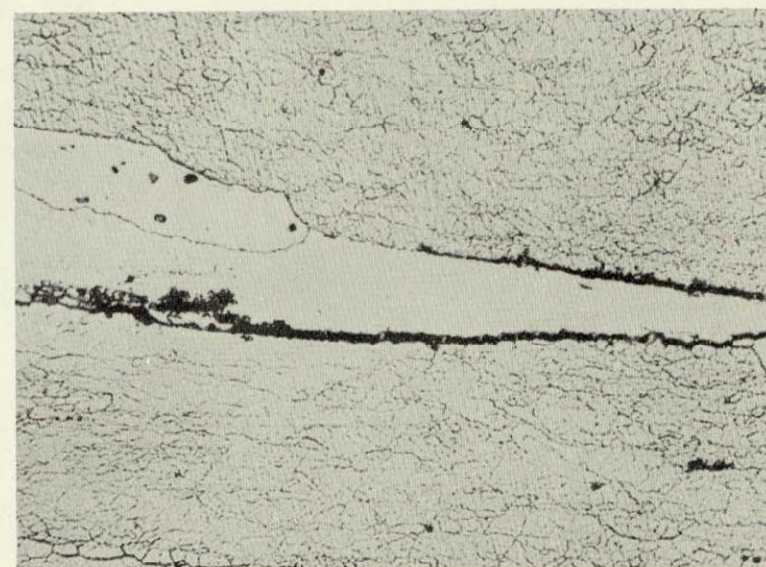
30 sec.

↑  
STRESS  
↓

26-1/2  
min.



16-1/2  
min.



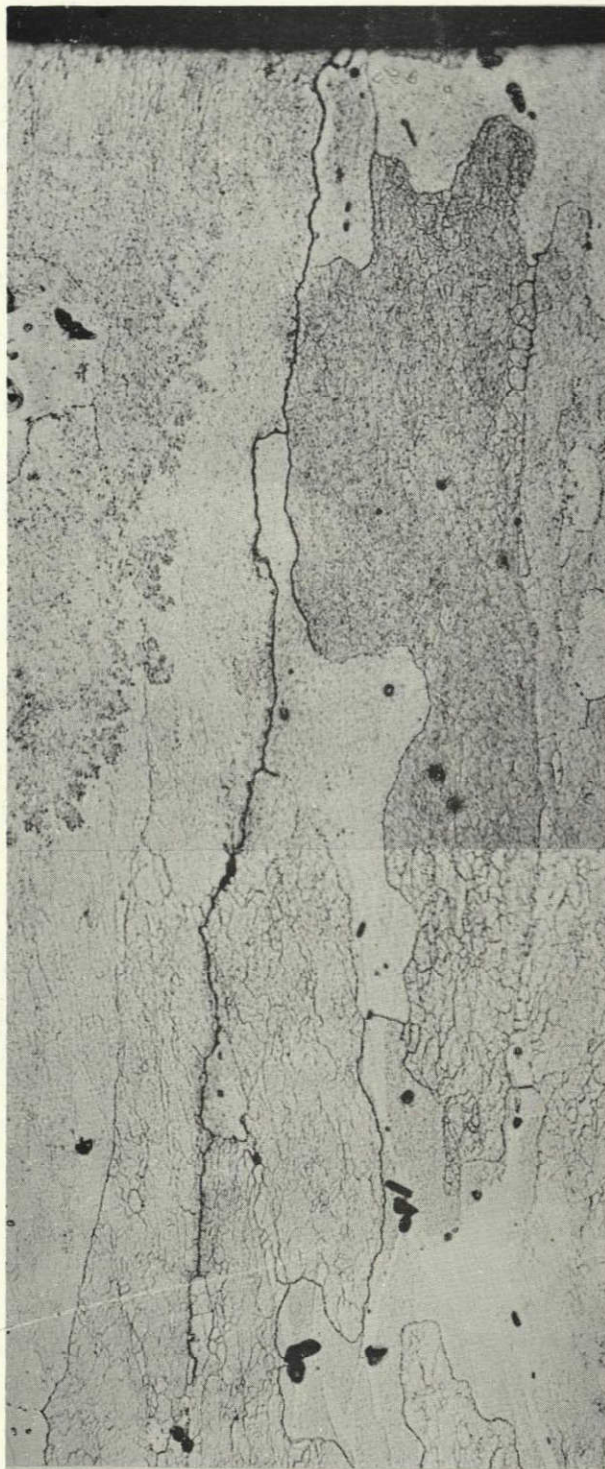
26-1/2,  
min.  
Keller's  
etch

Crack initiation and development in 7075-T6 stressed short transversely to 75% YS and exposed to 0.5 NaCl + 0.5 Na<sub>2</sub>SO<sub>4</sub> solution at pH2. (X500)

Figure 152



← STRESS →

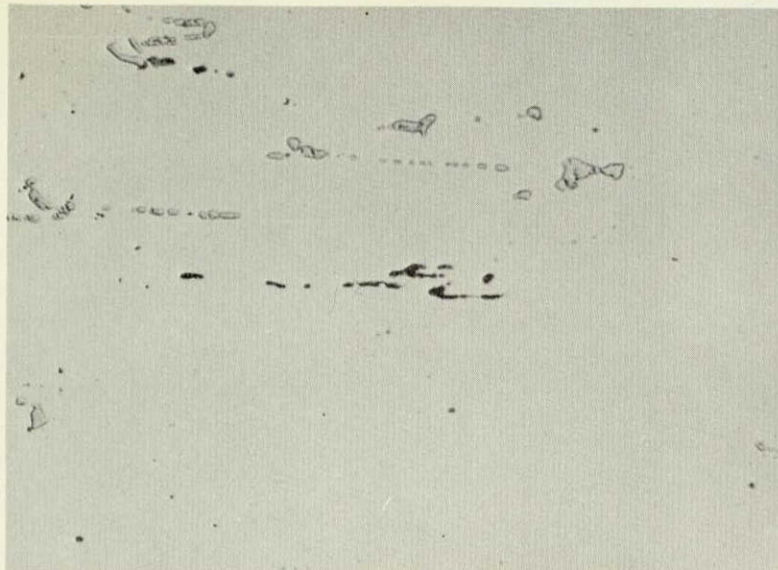


Cross section of sample in Fig. 152 (X500).

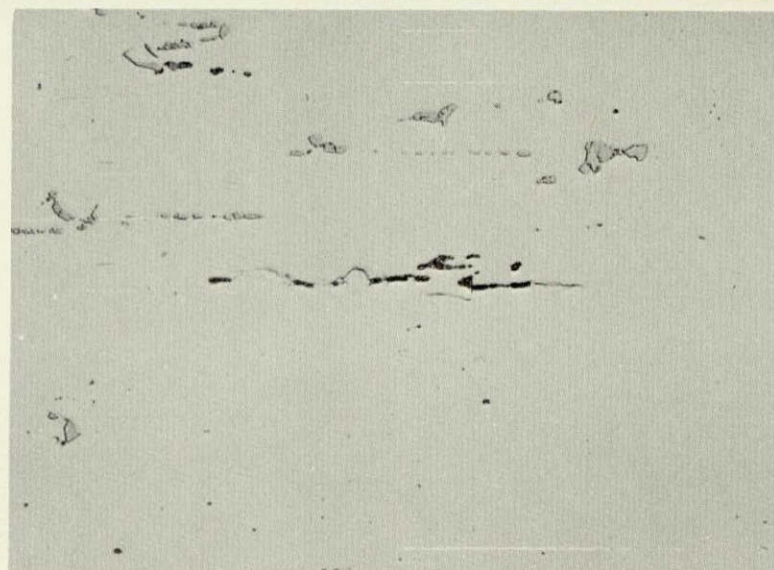
Figure 153



5 days



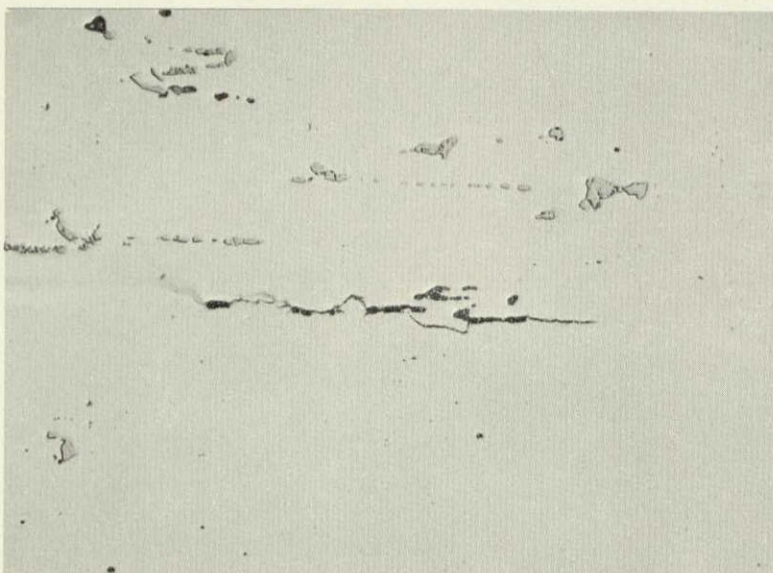
7 days



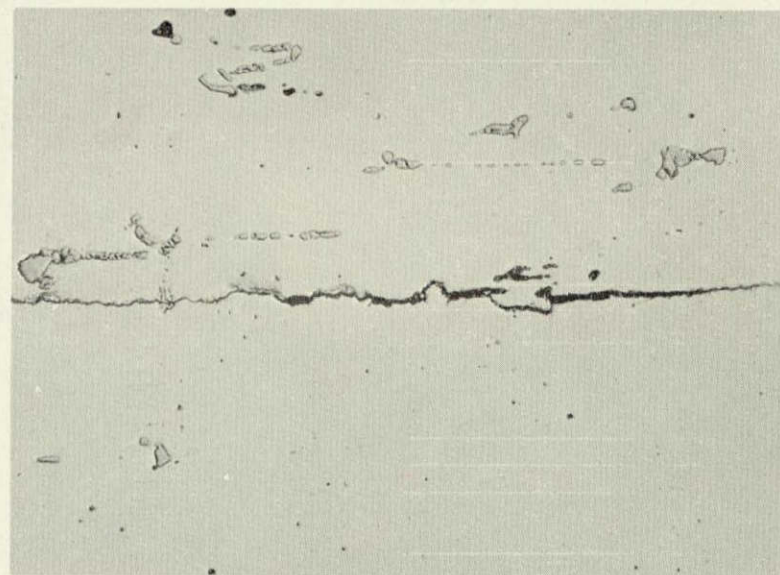
NOT REPRODUCIBLE

↑  
STRESS  
↓

8 days



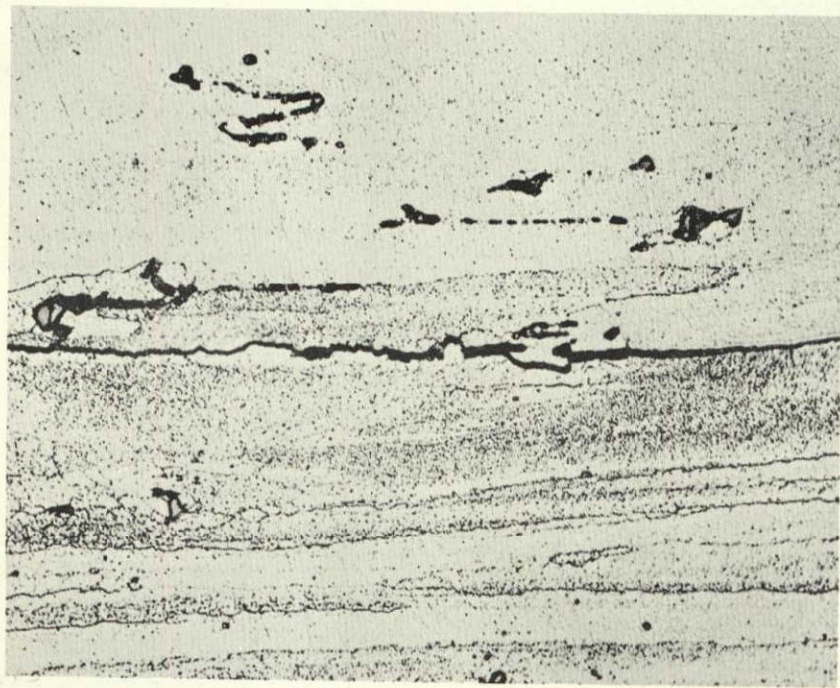
9 days



Crack initiation in 7039-T6 stressed short transversely  
to 75% YS and exposed to laboratory atmosphere (X500).

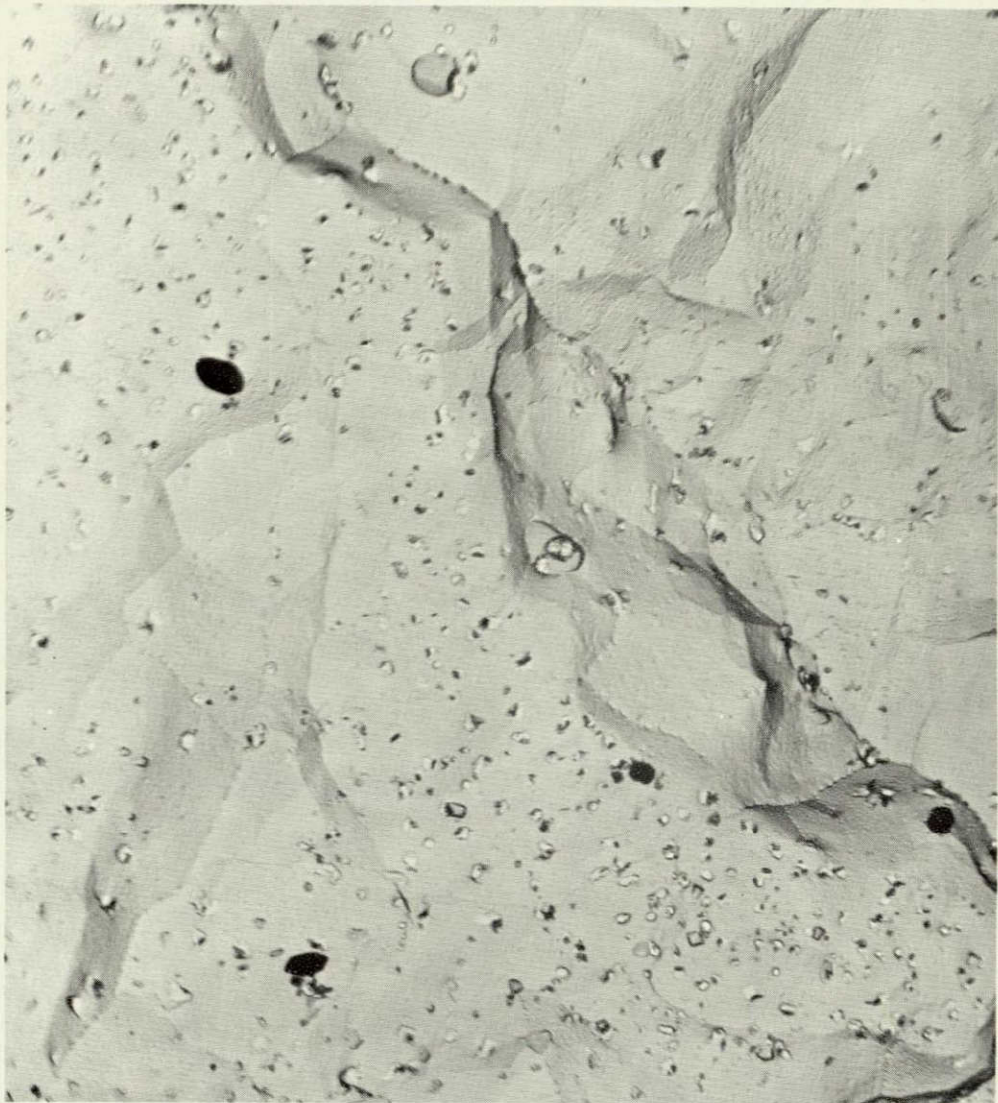
Figure 154





Boundary path of cracks in Fig. 154 as seen on surface  
(left) and in cross section (right). Keller's Etch. (X500)





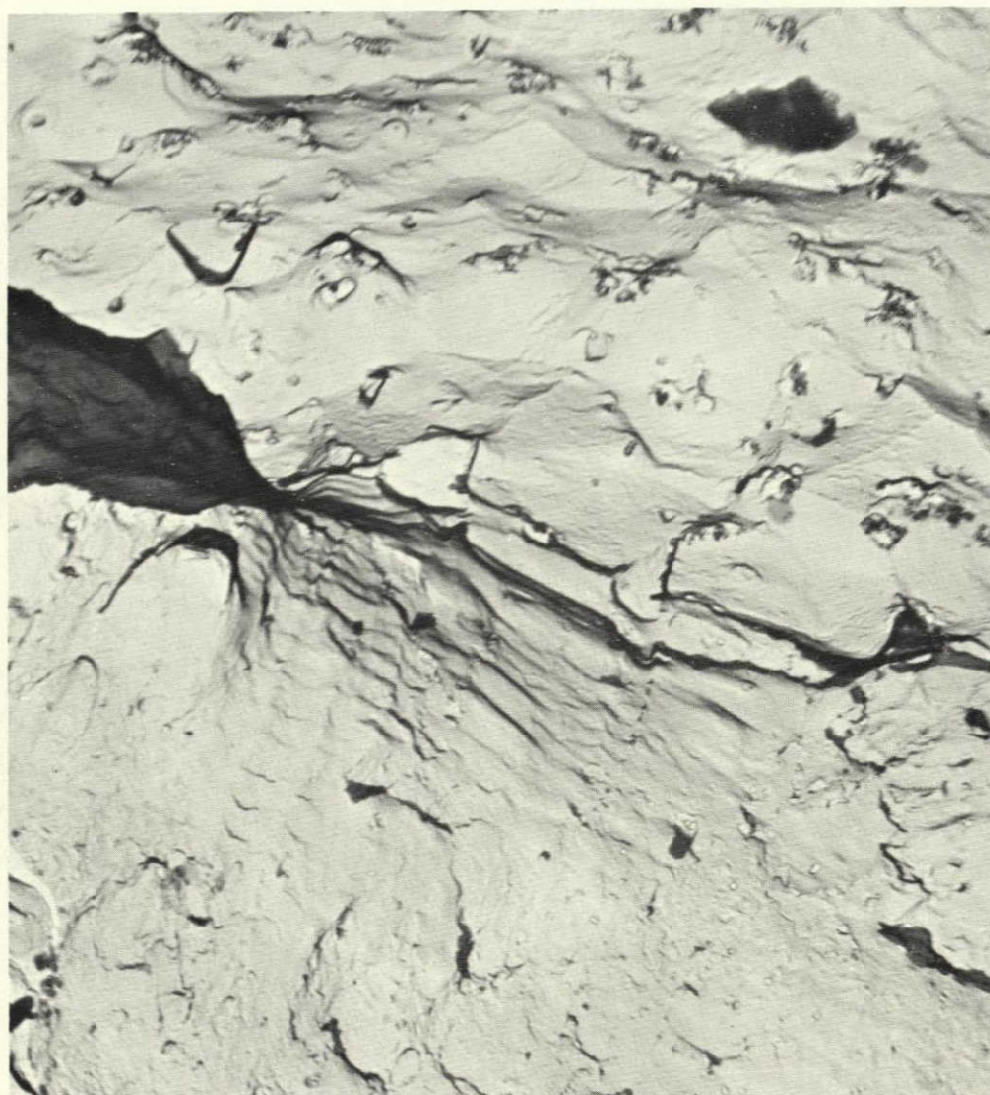
Oxide Replica

5000X

Surface of stress-corrosion fracture at 75% YS in 7039-T6 in laboratory air. Facets are the surfaces of polygonized cells and occur largely in dispersoid-free regions.

Figure 156





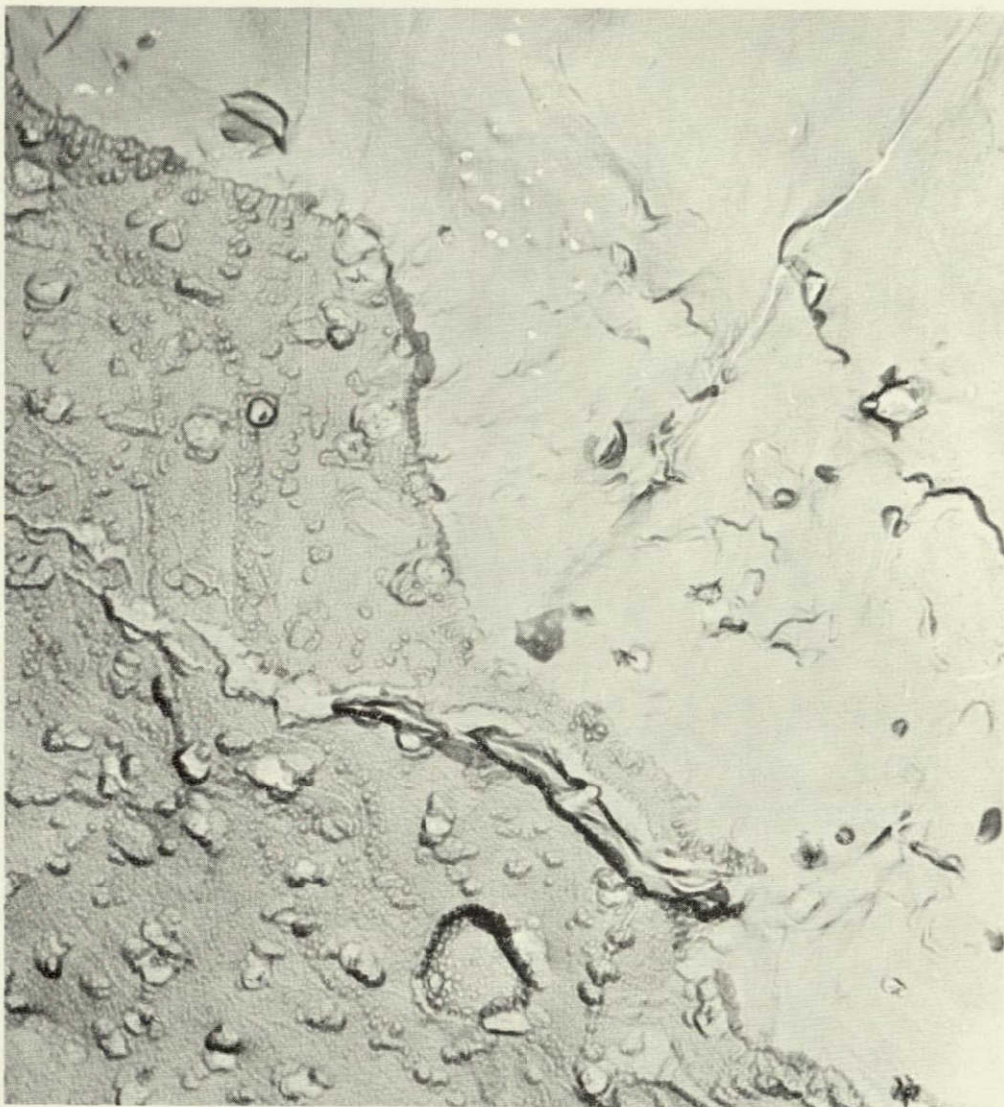
Oxide Replica

5000X

Extreme evidence of plastic  
deformation on the surface of a  
stress-corrosion fracture in  
7039-T6 developed in laboratory air.

Figure 157

NOT REPRODUCIBLE



Double Oxide Replica

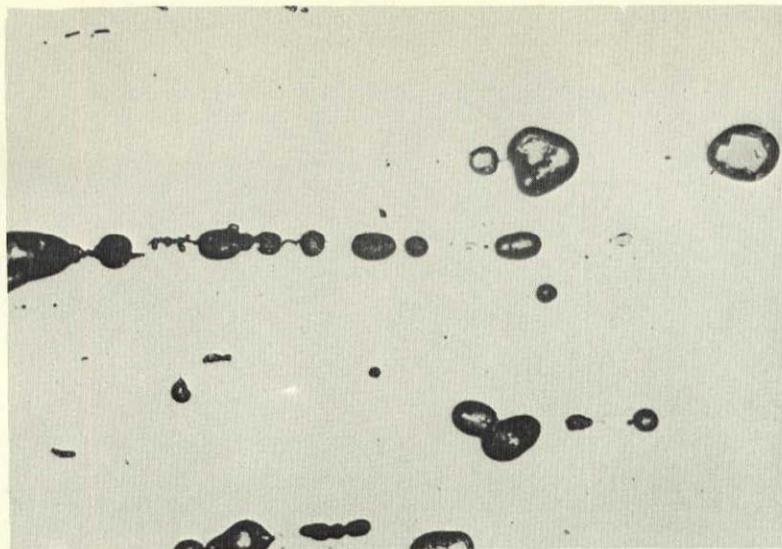
30,000X

Bottom of stress-corrosion crack  
(lower left) in 7039-T6 which has been  
exposed by intentionally fracturing the  
sample. Fine scallops of crack tip are  
reproduced in several lines at lesser depths.

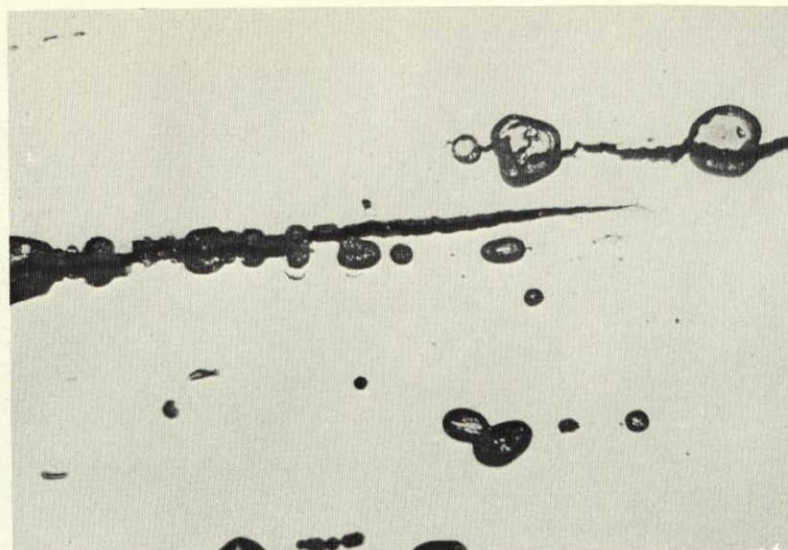
Figure 158



6 hrs

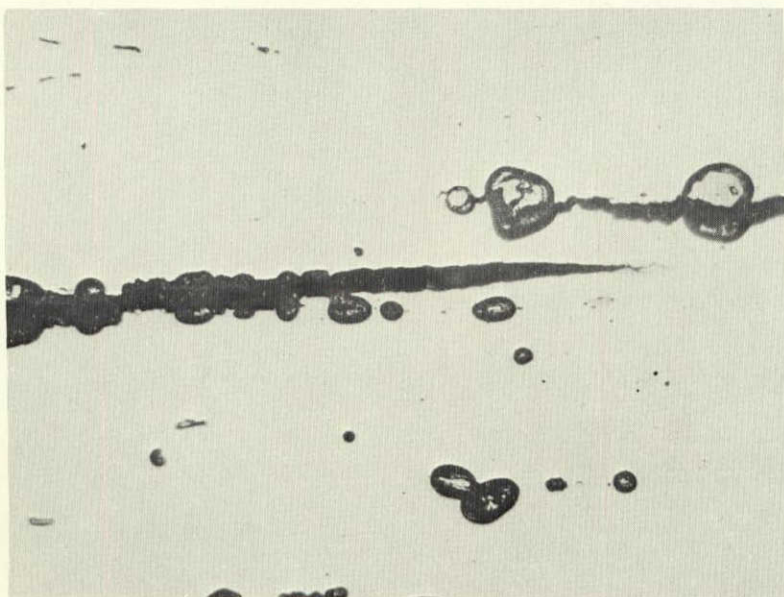


7 hrs

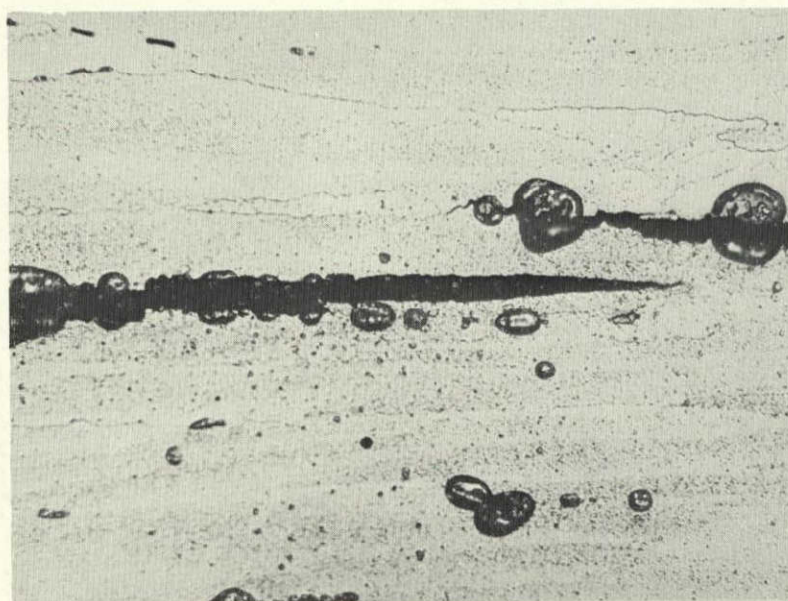


↑  
STRESS  
↓

7-1/2 hrs



7-1/2 hrs  
Keller's  
Etch

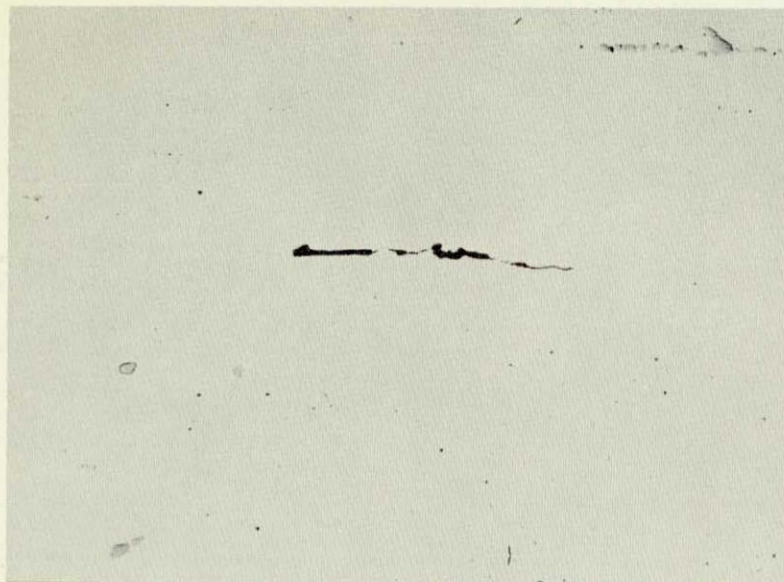


Crack initiation in 7039-T6 stressed short transversely to 75% YS  
and exposed to atmosphere at 125 F and 100% relative humidity. (X500)

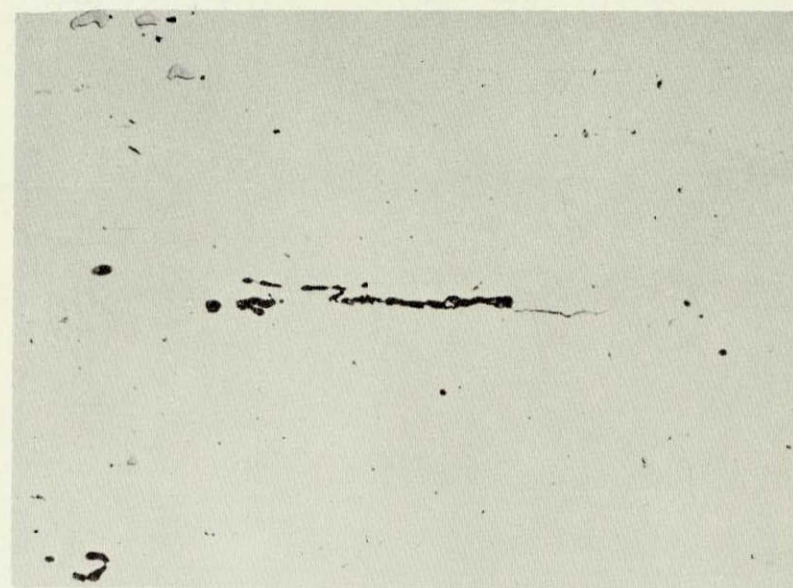


171828  
171830  
171982  
171988

As  
Exposed

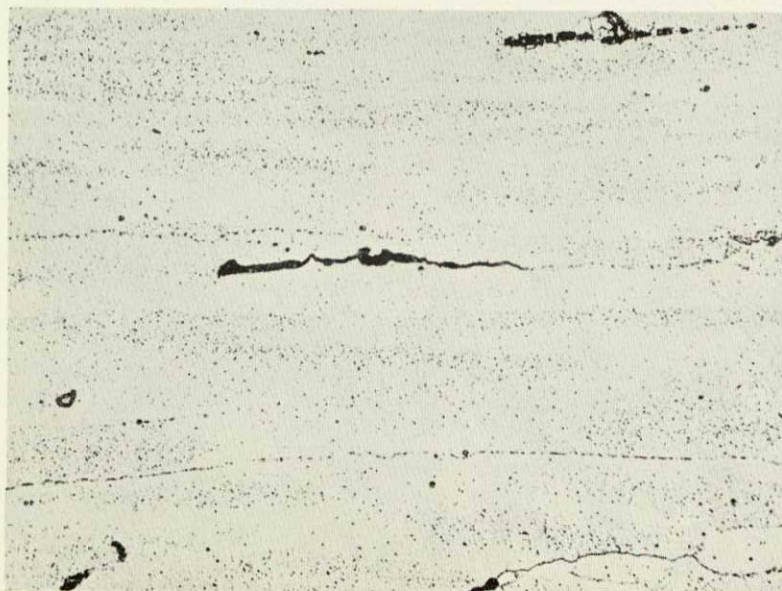


As  
Exposed

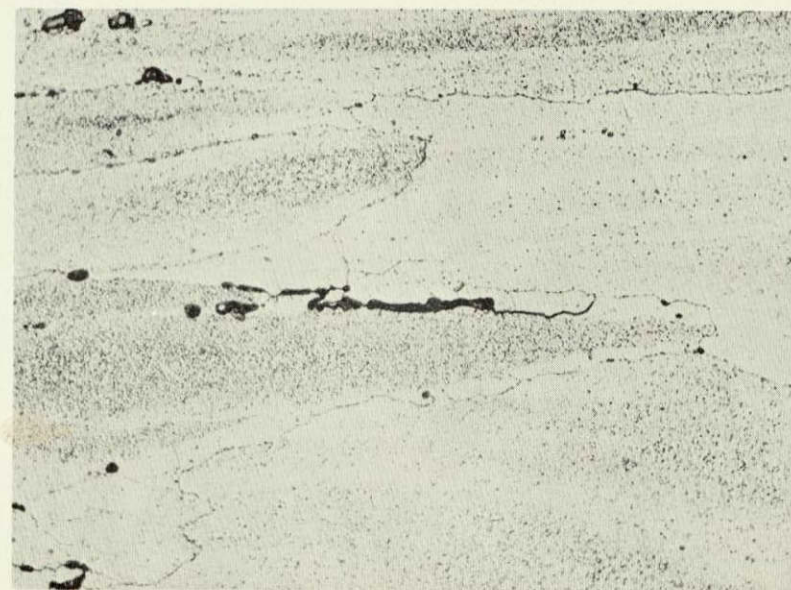


↑  
STRESS  
↓

Keller's  
Etch

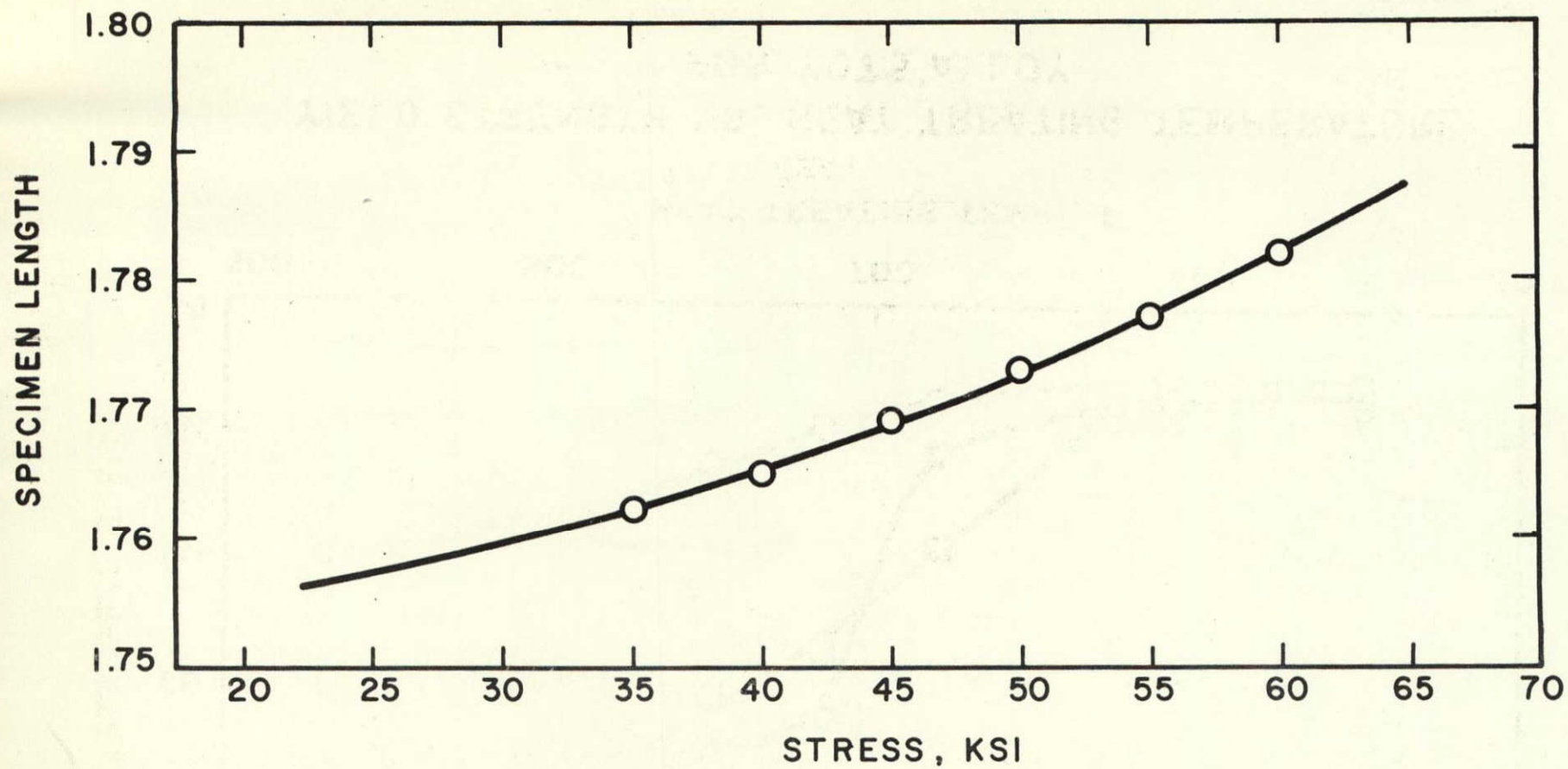


Kellers  
Etch



Crack initiation sites in 7039-T6 stressed to 75% YS short transversely  
and exposed to atmosphere at 100 F and 90% R.H. for ten hours (X500).

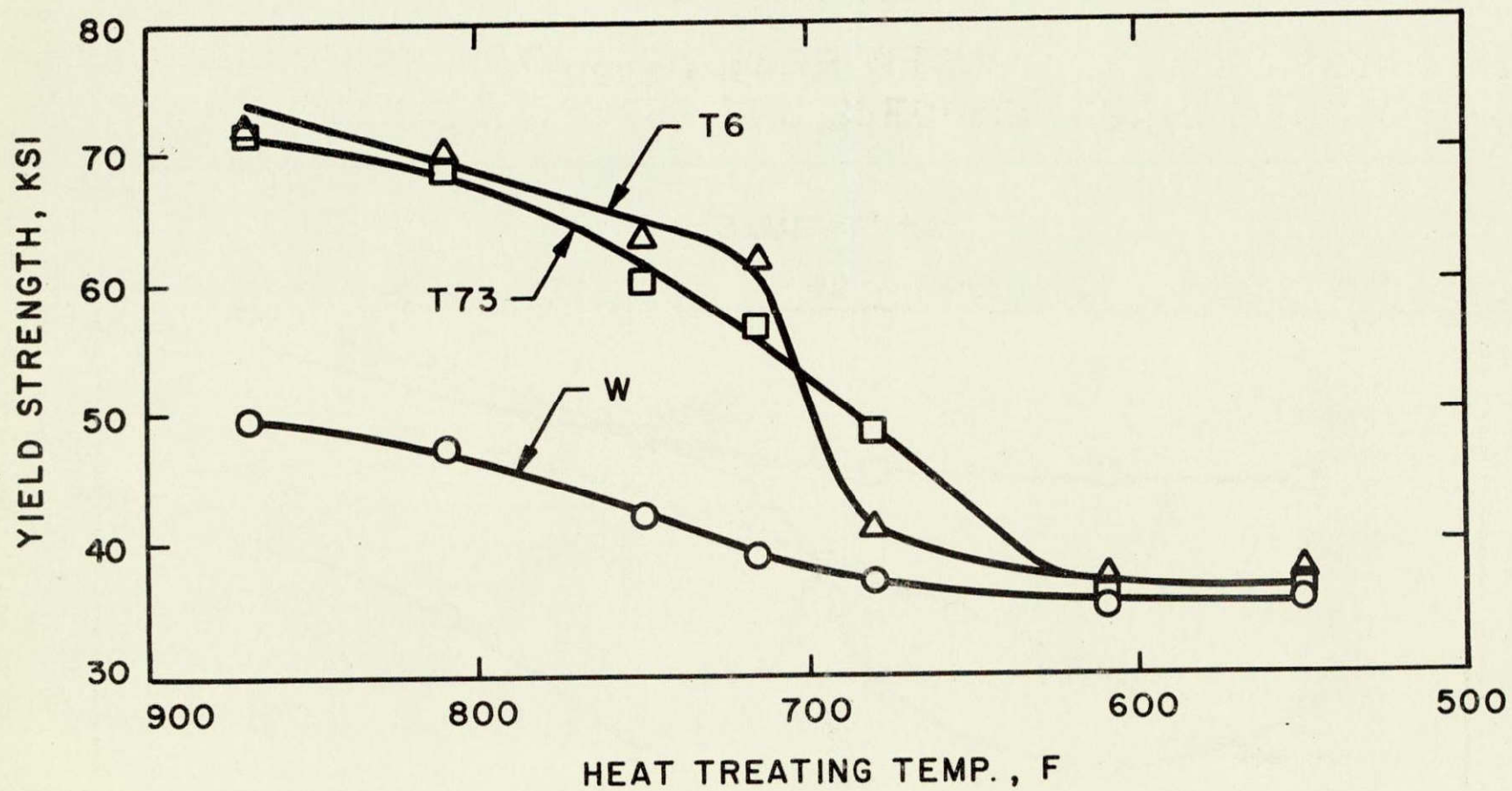
Figure 160



RELATION BETWEEN STRESS AND SPECIMEN LENGTH FOR 0.25 IN.  
SHEET SPECIMENS OF 7075 AND 7039 ALLOYS IN 1.75 IN. SPAN FIXTURE

FIGURE 161

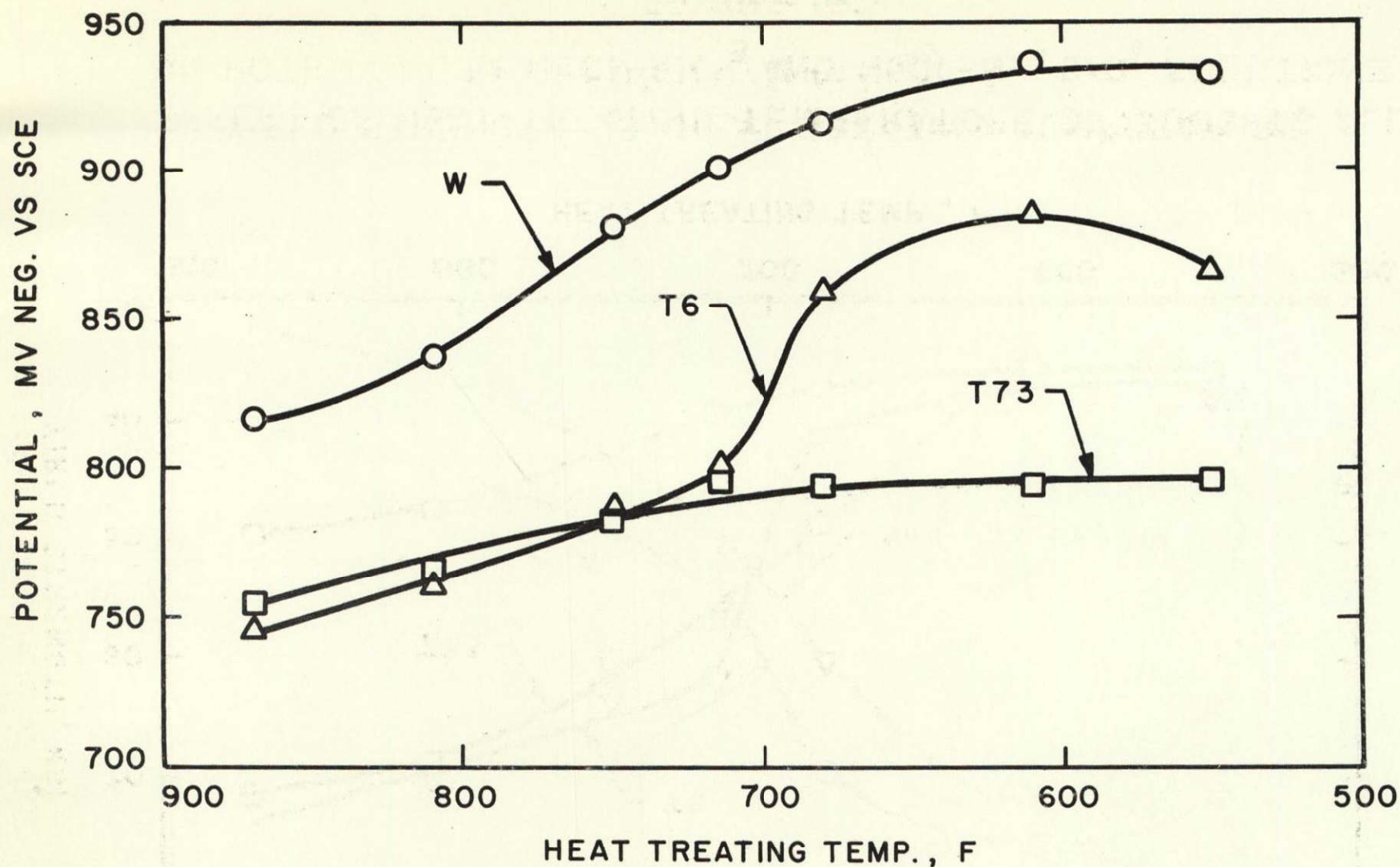




YIELD STRENGTH VS. HEAT TREATING TEMPERATURE  
FOR 7075 ALLOY

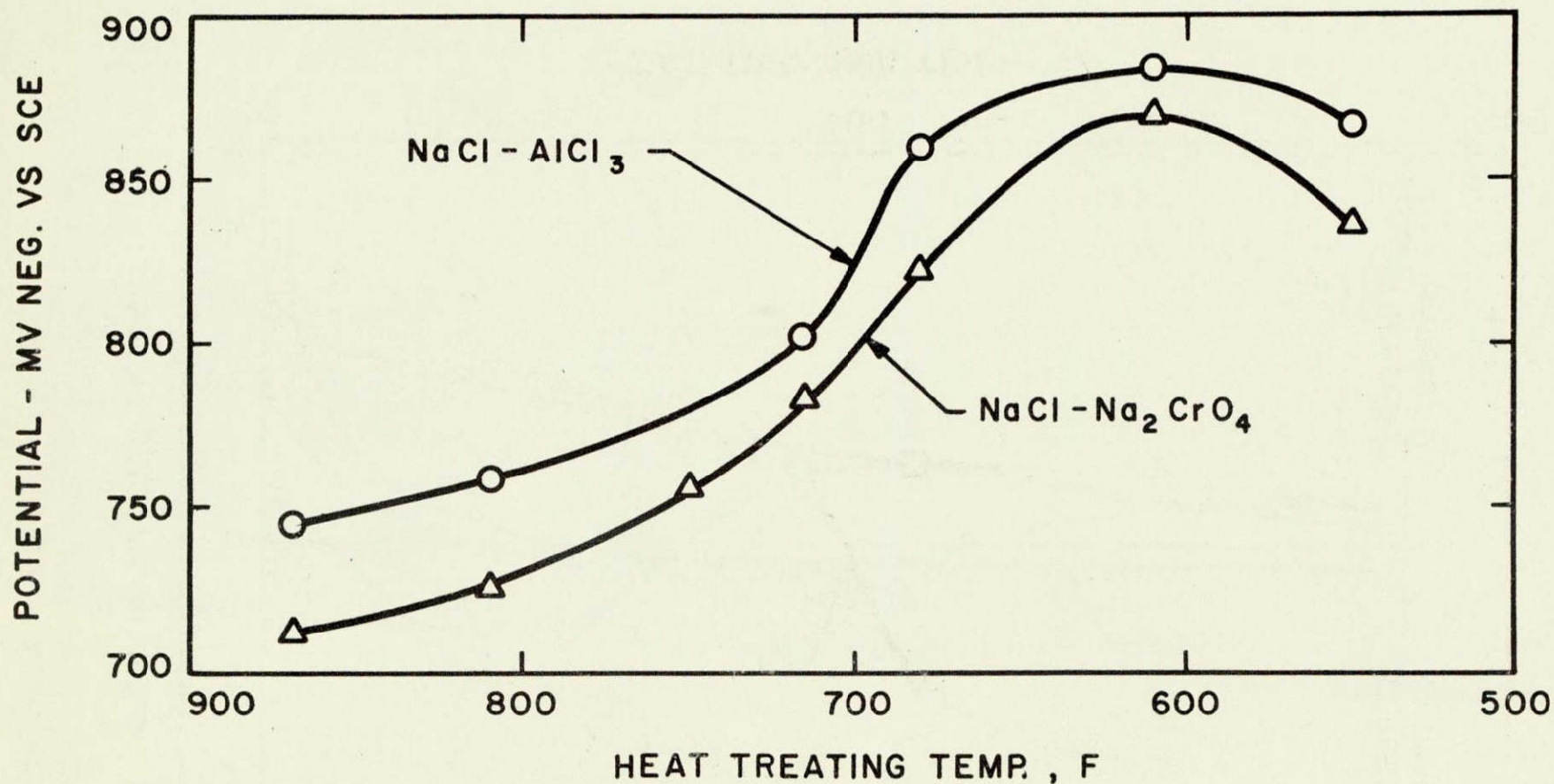
FIGURE 162





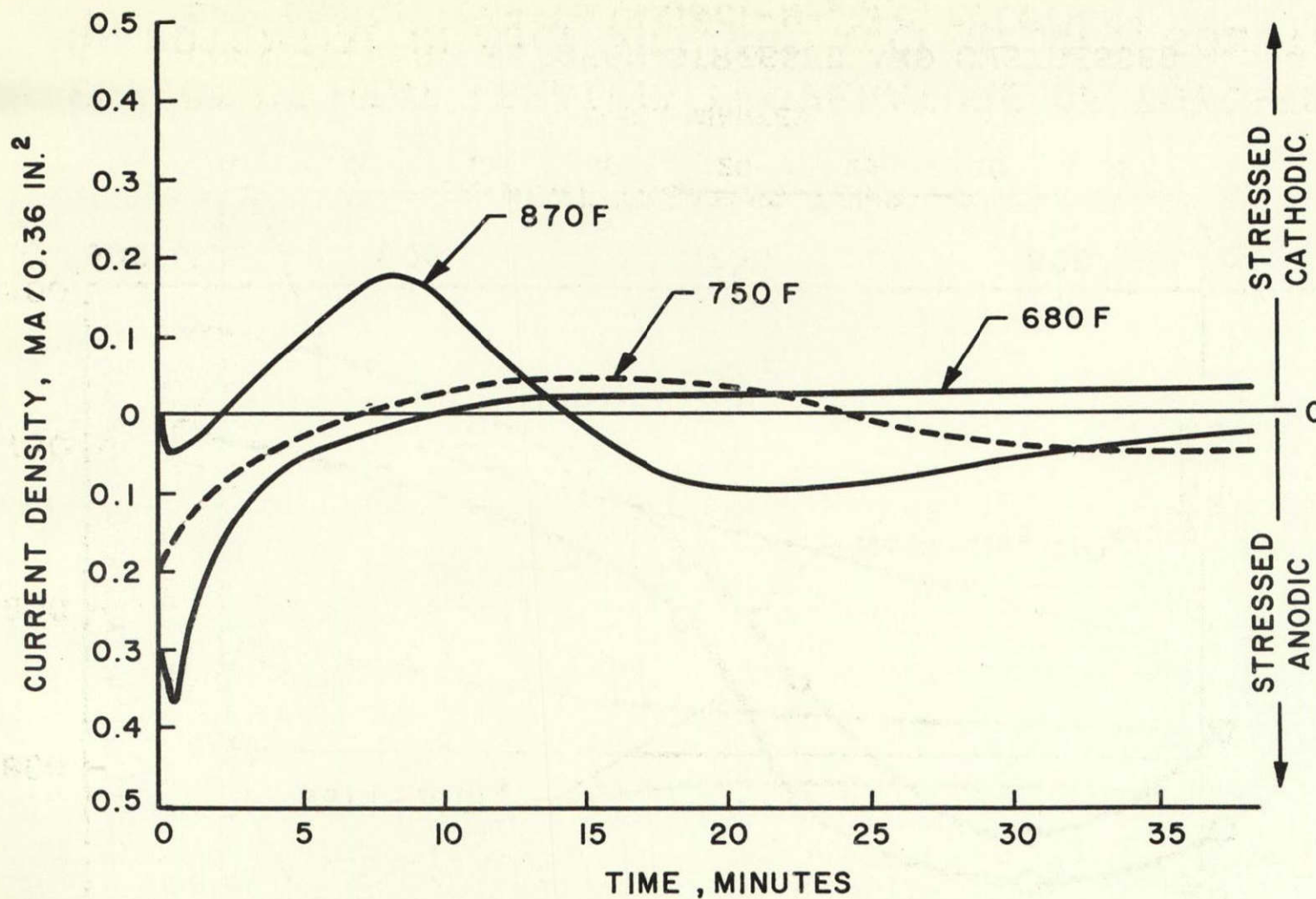
EFFECT OF HEAT TREATING TEMPERATURE ON POTENTIAL OF  
7075 ALLOY IN  $\text{NaCl} - \text{AlCl}_3$  SOLUTION AT pH 1

FIGURE 163



EFFECT OF HEAT TREATING TEMPERATURE OF 7075-T6 ALLOY  
ON POTENTIAL IN NaCl-AlCl<sub>3</sub> AND NaCl-Na<sub>2</sub>CrO<sub>4</sub> SOLUTIONS

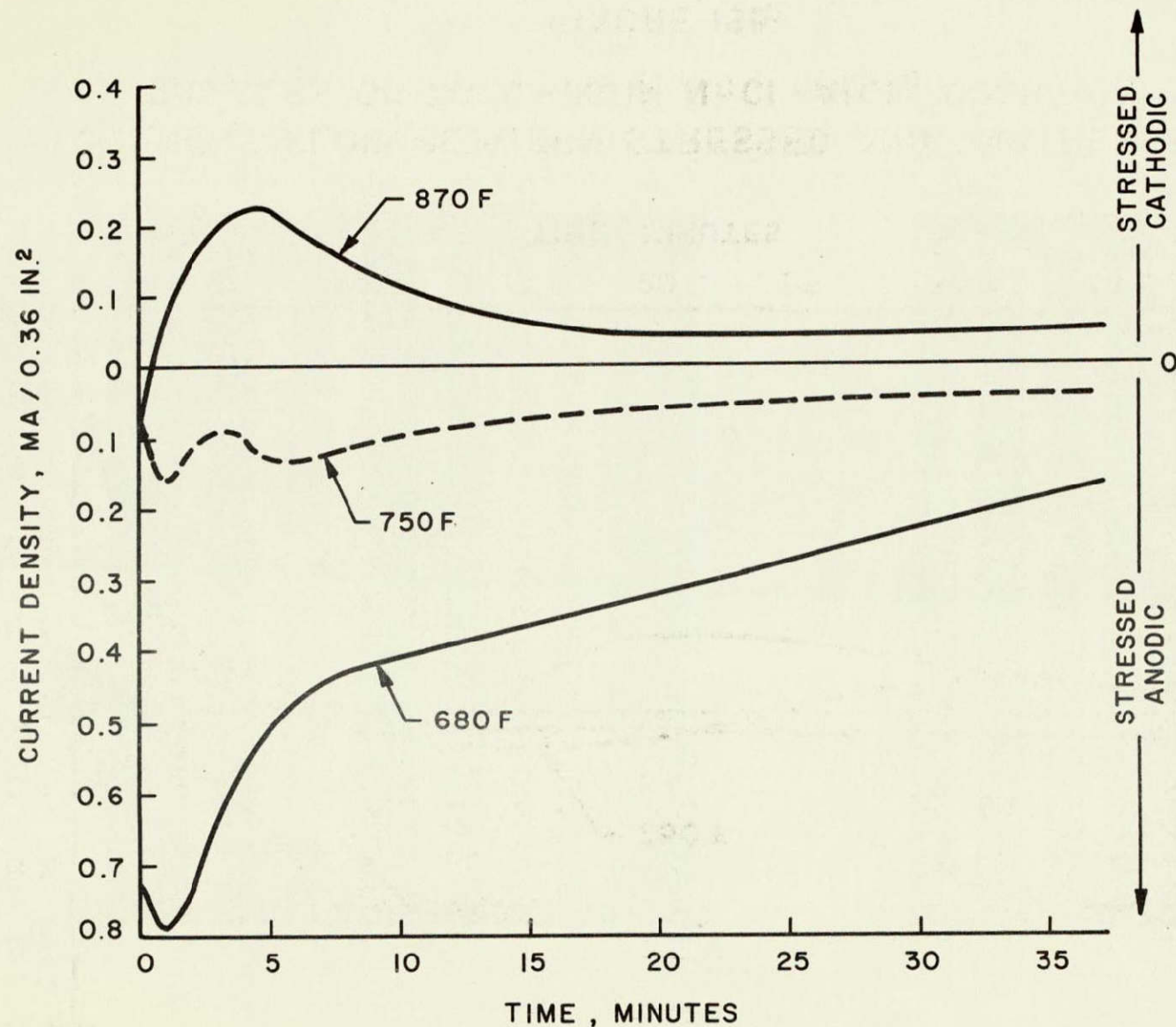
FIGURE 164



CURRENT FLOW BETWEEN STRESSED AND UNSTRESSED  
SAMPLES OF 7075-T6 IN NaCl-AlCl<sub>3</sub> SOLUTION

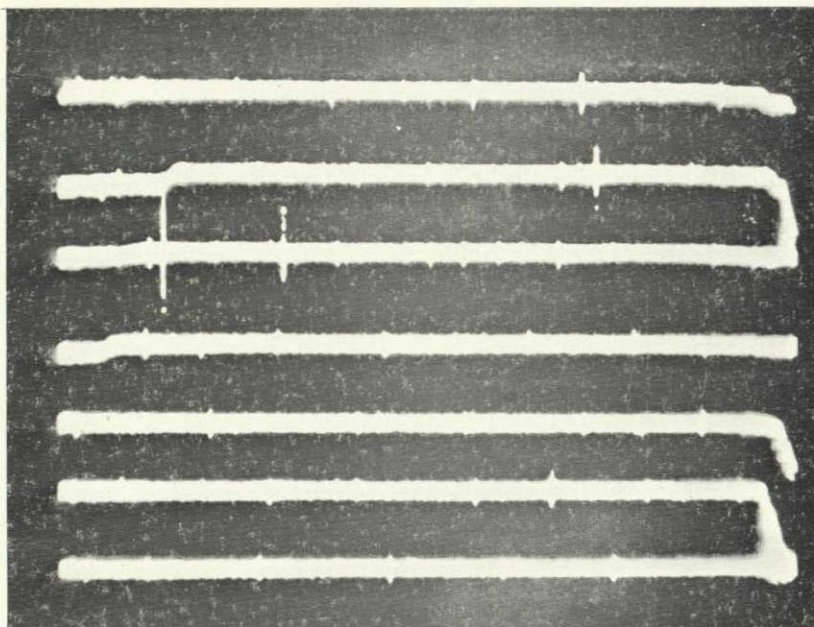
FIGURE 165



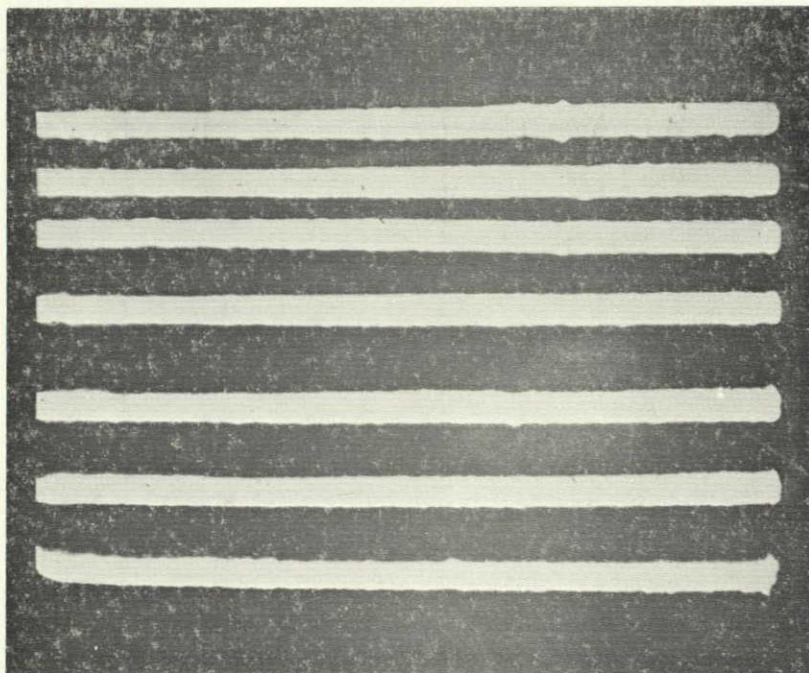


CURRENT FLOW BETWEEN STRESSED AND UNSTRESSED  
SAMPLES OF 7039-T6 IN  $\text{NaCl} - \text{Na}_2\text{CrO}_4$  SOLUTION.

FIGURE I66



7075-T6



7039-T6

Acoustic emission during stress-corrosion cracking.

Figure 167